AGARD-R-784

AGARD-R-784

AGARD

ADVISORY GROUP FOR AEROSPACE RESEARCH & DEVELOPMENT
7 RUE ANCELLE 92200 NEUILLY SUR SEINE FRANCE

AGARD REPORT 784

Integrated Design Analysis and Optimisation of Aircraft Structures

(L'Analyse pour la Conception Intégrée et l'Optimisation des Structures d'Aéronefs)

Papers presented at the 72nd Meeting of the AGARD Structures and Materials Panel, held in Bath, United Kingdom 29th April—3rd May 1991.

NORTH ATLANTIC TREATY ORGANIZATION

Published February 1992

Distribution and Availability on Back Cover

40th Anniversary Year

AGARD

ADVISORY GROUP FOR AEROSPACE RESEARCH & DEVELOPMENT

7 RUE ANCELLE 92200 NEUILLY SUR SEINE FRANCE

AGARD REPORT 784

Integrated Design Analysis and Optimisation of Aircraft Structures

(L'Analyse pour la Conception Intégrée et l'Optimisation des Structures d'Aéronefs)

Papers presented at the 72nd Meeting of the AGARD Structures and Materials Panel, held in Bath, United Kingdom 29th April—3rd May 1991.

North Atlantic Treaty Organization
Organisation du Traité de l'Atlantique Nord

The Mission of AGARD

According to its Charter, the mission of AGARD is to bring together the leading personalities of the NATO nations in the fields of science and technology relating to aerospace for the following purposes:

- Recommending effective ways for the member nations to use their research and development capabilities for the common benefit of the NATO community;
- Providing scientific and technical advice and assistance to the Military Committee in the field of aerospace research and development (with particular regard to its military application);
- Continuously stimulating advances in the aerospace sciences relevant to strengthening the common defence posture;
- Improving the co-operation among member nations in aerospace research and development;
- Exchange of scientific and technical information;
- Providing assistance to member nations for the purpose of increasing their scientific and technical potential;
- Rendering scientific and technical assistance, as requested, to other NATO bodies and to member nations in connection with research and development problems in the aerospace field.

The highest authority within AGARD is the National Delegates Board consisting of officially appointed senior representatives from each member nation. The mission of AGARD is carried out through the Panels which are composed of experts appointed by the National Delegates, the Consultant and Exchange Programme and the Aerospace Applications Studies Programme. The results of AGARD work are reported to the member nations and the NATO Authorities through the AGARD series of publications of which this is one.

Participation in AGARD activities is by invitation only and is normally limited to citizens of the NATO nations.

Published February 1992

ISBN 92-835-0653-7

Printed by Specialised Printing Services Limited
40 Chigwell Lane, Loughton, Essex IG10 3TZ

Abstract

At its 72nd Meeting, the Structures and Materials Panel held a Workshop to address the role of integrated design analysis and optimisation of aircraft structures in order to review and evaluate modern computer codes, and the methodologies for their use.

The Workshop provided a very useful forum for the exchange of information which is reflected in the papers presented in this Report.

Papers presented at the 72nd Meeting of the Structures and Materials Panel held in Bath, United Kingdom, 29th April—3rd May 1991.

Abrégé

Lors de sa 72ème réunion, le Panel AGARD des structures et matériaux a organisé un atelier avec pour objectif d'examiner le rôle de l'analyse pour la conception intégrée et l'optimisation des structures d'avion. Les participants ont passé en revue et évalué les codes machine modernes et les méthodologies y associées.

L'atelier a servi de forum pour un échange d'informations très fructueux dont les grandes lignes sont développées par les communications présentées dans ce rapport.

Ces communications ont été presentées lors de la 72ème réunion du Panel AGARD des structures et materiaux, à Bath, United Kingdom du 29 Avril au 3 Mai 1991.

Structures and Materials Panel

Chairman: Mr Samuel L. Venneri
Director, Materials & Structures
Division (Code RM)
Office of Aeronautics & Space Technology
NASA Hq
Washington DC 20546
United States

Deputy Chairman: Mr Roger Labourdette
Directeur Scientifique des Structures
ONERA
29 ave de la Division Leclerc
92320 Châtillon
France

SUB-COMMITTEE MEMBERS

Chairman: Dipl. Ing. Otto Sensburg
Chief Engineer for Structures
MBB Flugzeuge/FE2
Postfach 80 11 60
8000 Munich 80
Germany

Members:

D. Chaumette	FR
G. Cunningham	UK
M. Doruk	TU
E.H. Dowell	US
W. Elber	US
H. Foersching	GE
R. Freymann	LU
E. Fuente	SP
V. Giavotto	IT
M.A. Hogge	BE
J.J. Kacprzynski	CA
M.L. Minges	US
H.H. Ottens	NL
R. Potter	UK
M. Rother	GE
A. Salvetti	IT
N. Sandsmark	NO
A.F. Tovar de Lemos	PO
S.L. Venneri	US
A.P. Ward	UK
R.J. Zwaan	NL

PANEL EXECUTIVE

Mr Murray C. McConneli, United Kingdom

Mail from Europe:
AGARD—OTAN
Attn: SMP Executive
7, rue Ancelle
92200 Neuilly-sur-Seine
France

Mail from US and Canada:
AGARD—NATO
Attn: SMP Executive
Unit 21551
APO AE 09777

Tel: 33 (1) 47 38 57 90 & 57 92
Telex: 610176 (France)
Telefax: 33 (1) 47 38 57 99

Preface

The past 15 years have seen major developments in the power and applicability of structural optimisation computer codes. These can perform complex sizing exercises minimising structural weight subject to the satisfaction of behavioural constraints.

Clearly there is a wide availability of structural optimisation programmes and this has resulted in the extensive use of this capability in the Aerospace Industry. No new military fixed-wing aircraft is designed without the use of a minimum weight structural optimisation programme. The growing popularity of optimsation as a major design tool has been matched by an ever increasing breadth of applicability. A decade ago minimum weight designs could only be realistically generated for structures subject to static strength and stiffness constraints for isotropic structures. Today the scope has increased to the point where aeroelastic factors relating to efficiency, flutter speed limitations, active control aspects etc. are routinely included together with composite material properties. Current developments are focused on increasing the problem scope still further to include performance, avionics aspects and in certain cases shape parameters. In consequence optimisation programmes are being slowly transformed in the direction of becoming genuine multi-disciplinary design systems.

AGARD was one of the prime movers in the early development of usable structural optimisation programmes. Several symposia were organised in the 70s and the 2nd symposium in 1973 saw the first public exposition of the emerging "optimality criteria" methods. Having set the ball rolling AGARD has maintained a watching brief on developments in this area but has not actively participated. At the AGARD Structures and Materials Panel (SMP) meeting in April 1986 in Oslo, Norway, it was decided that a new initiative was required to take account of the world wide use of optimisation programmes, and particularly, to focus on multi-disciplinary design.

After a lengthy gestation period, the activity plans were firmed up in the Spring of 1988 and most of the execution took place in 1989 and 1990. The participating companies and research establishments reported on their results in a set of 14 papers presented at the Workshop held in Bath on May 1st—2nd 1991.

The aims of the activity were threefold:

(i) To assess the capabilities of the existing systems and synthesis tools to optimise problems involving structures, aerodynamics, and active control in aircraft design.

(ii) To stimulate the development of new capabilities where current methods are lacking or inadequate and to provide new reference test problems.

(iii) To depart from existing design studies by determining interaction and synergism of structures, aerodynamics, and active control and to chart directions for improved designs.

Otto Sensburg
Chairman, Sub-Committee on
Integrated Design Analysis and
Optimization of Aircraft Structures

Contents

OVERVIEW

by

Prof. Alan Morris
Cranfield Institute of Technology
Cranfield
United Kingdom

Dr Jaroslaw Sobieski
NASA Langley Research Center
Hampton, Virginia
United States

INTRODUCTION

The past 15 years have seen major developments in the power and applicability of structural optimisation computer codes. These can perform complex sizing exercises minimising structural weight subject to the satisfaction of behavioural constraints. Some codes are an integral part of a commercial finite element program such as the MSC optimiser in NASTRAN, OPTI in the SAMCEF, or OPTISEN in SDRC's IDEAS suite. Alternatively codes are available which can stand outside of a specific system such as the RAE/SCICON STARS programme or the USAF's ASTROS programme but can link with any FE code. In addition to these commercially available systems there are a variety of in-house programmes with equal power to those supplied by vendors. Examples of these are the BAe ECLIPSE programme, MBB's LAGRANGE and Gruman's FASTOP programmes.

Clearly there is a wide availability of structural optimisation programmes and this has resulted in the extensive use of this capability in the Aerospace Industry. No new military fixed-wing aircraft is designed without the use of a minimum weight structural optimisation programme. The growing popularity of optimisation as a major design tool has been matched by an ever increasing breadth of applicability. A decade ago minimum weight designs could only be realistically generated for structures subject to static strength and stiffness constraints for isotropic structures. Today the scope has increased to the point where aeroelastic factors relating to efficiency, flutter speed limitations, active control aspects etc. are routinely included together with composite material properties. Current developments are focused on increasing the problem scope still further to include performance, avionics aspects and in certain cases shape parameters. In consequence optimisation programmes are being slowly transformed in the direction of becoming genuine multi-disciplinary design systems.

AGARD was one of the prime movers in the early development of usable structural optimisation programmes. Several symposia were organised in the 70's and the 2nd symposium in 1973 saw the first public exposition of the power of the emerging "optimality criteria" methods. Having set the ball rolling AGARD has maintained a watching brief on developments in this area but has not actively participated. At the AGARD Structures and Materials Panel (SMP) meeting in April 1986 in Oslo, Norway. it was decided that a new initiative was required to take account of the world wide use of optimisation programmes and, particularly, to focus on multi-disciplinary design.

After a lengthy gestation period, the activity plans were firmed up in the Spring of 1988 and most of the execution took place in 1989 and 1990. The participating companies and research establishments reported on their results in a set of fourteen papers presented at the Workshop held in Bath in May 1-2 1991 and listed, in the order of presentation, in the REFERENCES section at the end of this summary paper.

The aims of the activity were threefold:

(i) To assess the capabilities of the existing systems and synthesis tools to optimise problems involving structures, aerodynamics, and active control in aircraft design including performance.

(ii) To stimulate the development of new capabilities where current methods are lacking or inadequate and to provide new reference test problems.

(iii) To depart from existing design studies by determining interaction and synergism of structures, aerodynamics, and active control and to chart directions for improved designs.

This paper reports on the Bath proceedings and begins with a systematic inventory of topics covered by the Workshop papers and the final Panel Discussion. Next, the paper gives an assessment of the progress shortcomings, common threads, and trends. Finally, the paper discusses inferences drawn from the inventory and from the assessment, formulates a forecast of the future developments, points to the opportunities open to AGARD to influence these developments, and the recommends specific actions.

INVENTORY OF WORKSHOP CONTENT

The Workshop content consisted of a block of fourteen papers and a Panel Discussion. This section provides a summary of the topics covered in these two parts as a prerequisite to an assessment of the results produced by the subject AGARD activity.

Topics Covered in Papers

Table 1 shows the contents of the thirteen papers on the programme of the Bath Workshop (paper (1) was omitted from the table because it was an introductory review of the other papers; paper (10) was included because the U.S. Coordinator was familiar with its substance even through the authors could not attend the meeting). The table is organised by topics, listed in no significant order, each topic is followed by a line of numbers indicating the papers, from the list of references, which included the particular topic. These reference numbers so spaced that each paper occupies its own column in order to emphasize how the content is distributed over the set of topics. That distribution is significant because it carries additional information about each contribution. For example, a paper may be shown under "Aeroelasticity" but not under "Aerodynamics". This is not inconsistent, even though aeroelasticity comprises aerodynamics by definition. It simply means that the aerodynamic data, e.g., a matrix of aerodynamic

influence coefficients, was an external input. It is recommended to reader to scan the entire length of the table, even superficially, before reading the discussion below.

The first line in the table shows that three papers are concerned with the aircraft as a system namely, papers 2, 4 and 11 in the reference list. The implication is that these address the wider optimisation problem posed when design variables are employed which stretch across several disciplines', wing aspect ratio would constitute such a variable. The second line in the table refers to papers where two or more disciplines are taken into account possible through their sensitivity to a specific variable such as a conventional thickness parameter.

A review of the entire table reveals that all the contributions employed some analytical methods usually in the form of a "black box". Because nearly all papers dealt with static and/or dynamic aeroelasticity the most frequently used analytic tools related to predicting the structural and aerodynamic loads and responses. In six of the papers this analysis involved the entire aircraft even though optimisation was applied to a specific part of the structure. For example, this occurred where a wing was optimised subject to flutter constraints employing a vibration analysis of the entire free-free airframe.
Consistent with the scarcity of papers addressing the whole aircraft synthesis, two only included the vehicle performance analysis and one showed results that accounted for propulsion considerations. This same paper was alone in including the effects of heat exchange on aerodynamic flow, probably because no other paper covered the hypersonic speed range.

It is strongly indicative of the present trend that the number of papers reporting applications of composites in structures exceeded the number limited to the metallic construction; opposite to what would have been observed had the workshop been held a decade ago.

Nearly all papers included sensitivity analysis as a tool. Typically, a quasi-analytical method was used for structural sensitivities with finite differencing applied exclusively in the aerodynamics sensitivity analysis, except of one paper (3) in which the aerodynamic sensitivity analysis based on a quasi-analytical approach was used - an important harbinger of things to come.

With the exception of one paper (3) devoted solely to sensitivity analysis in aeroelasticity, all papers were concerned with the optimisation. Nonlinear Mathematical Programming (NLP) was the most often cited tool followed by the Optimality Criteria (OC) approach. This was to be expected in view of the emphasis on aeroelasticity and composite construction - two areas where it is difficult to formulate rigorous OC. However, the Fully Stressed Design and Uniform Strain Energy Distribution methods were successfully applied in a number of reported applications, especially those with a very large number of detailed design variables. A selection technique based on branching was used in (9) as an example of an innovative alternative to NLP or OC.

The dominant focus of the entire activity was on cross-sectional sizing, with few papers discussing the use of the aerodynamic shape variables in optimisation. The papers that did include these variables were - as one would expect - those listed under the "Aircraft as a system..." heading. That strong bias was a result of the aeroelasticity orientation of most of the papers, one paper (11) broke out of that mold and by so doing gained a considerable advantage over all other optimisation results obtained for the MBB fin structure, establishing another important precedent for future developments.

Even though most of the papers were concerned with applications with large dimensionality, three papers brought in decomposition, hierarchic and non-hierarchic as an alternative to an all-in-one approach to optimisation and sensitivity analysis. Two papers devoted attention to overall organisation of the computational process that supports design and the impact of the optimisation and sensitivity analysis on that process.

Although engineering computations often have to be carried out with uncertainties in the data, one paper only, (14), brought this up as an issue.

A distinct majority of eight out of the total of thirteen papers dealt with applications of methods that were already well-established, and only five papers were devoted primarily to the issues of development and introduction of new methods. However, these papers also referred to actual applications as examples and validation cases to establish the new methods they offered, consequently, all papers presented were well-grounded in a strong application base.

Of these papers which considered the airframe and its principal components, a little more than half referred to the wing applications, the remainder being concerned with empennage. Most of the latter resulted from the MBB fin data having been made available as a test case to all the participants in the activity. This fin was originally intended to be the common test case to focus all work on the same artifact but that idea never gained an universal acceptance. However the fin did appear in five papers as the only, or one of a few, test cases.

Three papers considered problems that included fuselage combined with a wing, and one only, (14), presented optimisation of a complete airframe.

A remarkably large majority of 10 papers reported on applications to aircraft that were either in the process of being designed or were actually built. This contrasted with four papers limited to examples created for research purposes. This preponderance of the optimisation applications to actually built aircraft constitutes important, noteworthy, progress since Holt Ashley's well-known survey on optimisation in aerospace published in 1981. The author of that survey had difficulty in finding a single instance of a prototype or production airframe designed with the aid of optimisation, despite hundreds of theoretical publications on the subject.

Not surprisingly, a majority of nine papers in this AGARD-sponsored activity use fighter aircraft as the object of study, and five dealt with large transports. Consistent with that choice, the subsonic and transonic speed regimes were most often considered, extending in a few cases to low supersonic, and to hypersonic and transatmospheric vehicles in one of the papers (2). Generic methodology presented in this paper is applicable to non-aerospace vehicles, and as evidenced by one paper, (6), which used examples of automotive applications.

Even though the AGARD activity originally intended to provide an extensive assessment of analysis tools by comparison of analytical and experimental data, three papers only followed up in that direction, with extensive empirical information being given in (5).

Distribution of the software used in the studies among the three categories listed at the very end of the

table portrays the field as one that has reached maturity and provides engineers with tools routinely available in form of production-level software packages. This development correlates well with the relatively large number of applications to actually built aircraft observed in the foregoing.

Topics Covered in Panel Discussion

This inventory of the Workshop content would be incomplete without a summary of the Panel Discussion held with the audience participation at the end of the Bath meeting.

One of the Panel members was Mr. Norman Harpur who had a key role in the British part of the Concorde design and development. The ringing endorsement he gave to optimisation, sensitivity analysis, and the system approach to aircraft design had a special importance.

It was pointed out by Dr. Venkayya that the design cycle has four main phases; Conceptual, Preliminary, Detail and Final design and whilst optimization is used in all four it finds it's chief application in the latter two. This was demonstrated in the workshop where all the contributions dealing with real structures were concerned with detail design or post service modifications. It is a reflection of current stage of development in the numerical modelling of aircraft structures where it is relatively straightforward to simulate the behaviour by the Finite Element Method and add constraints on loosely coupled behavioural parameters, eg. stresses, frequencies etc. Thus, we can expect to see a continued and extending use of optimization methods in the later stages of the design cycle coupled with an extending range of addressable problem types. The software and system developments associated with these extensions will be undertaken, primarily, by the developers of commercial software.

The following major trends emerged from the discussion:

- The need to postpone freezing of the major configuration design variables until more information from all major disciplines involved is generated and brought to bear on that decision. This should remove the present paradox of the design process whereby the amount of knowledge about the aircraft being designed increases with time while, the freedom to act on that knowledge decreases.

- Four major components emerge as having an influence on the design decision making 1. Human judgment; 2. Analysis that treats the aircraft as a system of interacting parts and physical phenomena and includes sensitivity to design variables; 3. Formal optimisation performed on the basis of the analysis and sensitivity data, and 4. Data base and visualisation supporting the former three components. Among these components, the human judgment is in full control - a radical departure from the past attempts at the "push button" design.

- However, there is a migration of functions from the man to the computer that is a natural result of the progress in theory, the accumulation of experience, and the new computer capabilities. What is regarded today as an art that requires close human monitoring and intervention may become an automated operation tomorrow. For example, redundant structure cutting for analysis purposes was a demanding art in the 50's and, yet, it was superceded by the totally computerised displacement-based finite element methods. Similarly, the detailed cross-sectional sizing of stiffened panels for minimum weight is being delegated completely to optimisation. Extrapolating this implies the process of laying out the aircraft configuration, which currently belongs in the domain of human ingenuity may not remain so indefinitely. But this migration of functions to the computer does not remove the human mind from the design process. It simply gives the human engineer more time to ponder issues of higher order and to consider more alternatives.

An event in the Panel Discussion was the recognition given to MBB for winning an informal contest for the most optimal design of the fin structure. This optimal design demonstrated a significant fin control performance improvement gained by exploiting a sensitivity study involving structures - aerodynamics - weight - control effectiveness trade-offs. It also involved an extended set of design variables, including shape, that influenced several engineering disciplines. In doing this the MBB paper became one of the trend setters at the Workshop.

This result put a spotlight on paper (2) which formulated a generic methodology exploited in the MBB study. The pros and cons of that methodology generated a number of comments from the audience. Among the pros, the generality and applicability of the method to entire aircraft was emphasised. Another significant advantage of the method was its use of sensitivity derivatives as a mathematically rigorous and precise interdisciplinary language that should put the communication among the disciplinary specialists on a rational basis. As one of the most important cons, it was noted that the piece-wise approximation intrinsic to the method may force it to operate within move limits so narrow as to make it impractical. Attention was also directed to another shortcoming of the method: it does not accommodate the existing disciplinary expertise available for suboptimisations of the parts of the problem.

Even though the workshop papers showed that rapid progress has taken place in the use of optimisation methods, the Panel Discussion participants wished to increase the pace. Asking for ways and means to broaden the optimisation use in the profession, an opinion was voiced that the practitioners need training in the use of the existing methods more than they need new methods, and that the greatest benefit would accrue from investing in robustness and user-friendliness of the methods offered for general use.

ASSESSMENT OF WORKSHOP CONTENT

Measuring the achievements of the workshop against the original aims of the activity the results are disappointing. It had been the wish of the organisers that a wide range of methods and programmes would be employed against a specific, complex, problem. In this way the strengths and weaknesses of the various approaches to optimisation and the associated algorithms could be assessed. This objective was only partially achieved, as was the satisfaction of the three main aims listed in the Introduction. There was also an unevenness of application with some contributions putting in a major effort to stretch the available techniques with others making a more 'conference' like contribution. Nevertheless, sufficient results of real importance were presented to allow a partial assessment of the current position and future potential to be made.

The Workshop demonstrates very effectively that a strong core of production-level software packages exists and are being routinely used in airframe optimisation. The use ranges from detailed sizing of

major components, e.g., wings, to entire airframes. It includes static strength as well as static and dynamic aeroelasticity employed in applications that encompass all categories of military and civilian commercial aircraft. The capability covers metallic and composite material types of construction. The aerodynamic analytical support in the form of integrated structural-aerodynamic analysis appears to be adequate with respect to the accuracy of the predicted loads. This is true providing velocity stays in the low supersonic range not moderate angles of attack. The high temperature influence on the airflow at high supersonic/hypersonic speeds and flow separated at high angles of attack, make the aerodynamic loads predictions much less reliable. Reduced accuracy of these predictions and of the flutter critical speed evaluation are also evident near the sonic speed.

Regarding the optimisation methods themselves, it appears that the old feud between OC and NLP methods has been finally put to rest and both types of methods are being used wherever they are most effective. Indeed, judging from the results provided all of the methods employed exhibit a similar rate of performance when used on identical problems. For purely sizing problems it would appear that the algorithms in current use are adequate for the task and are robust.

However, the aerodynamic analysis is woefully inadequate in the computation of derivatives of the flow variables with respect to elastic deformations and variables governing the airfoil and planform changes. This inadequacy forces users into finite differencing whose cost becomes a barrier, and it contrasts starkly with the quasi-analytical sensitivity analysis now routinely available in structures.

In contrast to the above well-established methods for structural optimisation integrated with aerodynamic load analysis, there is a void as far as integration of that methodology with the remainder of the aeronautical disciplines is concerned. Despite this fact a few papers presented convincing examples of the beneficial potential hidden in such an integration. A truly multidisciplinary optimisation involving trade-off between the wing weight and drag both, influenced by the airfoil height-to-chord ratio, is still far from being as routine as the wing structural sizing. The decades old practice of setting the overall aircraft configuration shape primarily on the basis of aerodynamic considerations, and handing the resulting shape to structures as an envelope to be filled by minimum weight members, is slow to give way to an integrated alternative in which all major disciplines participate equally in setting the configuration shape.

One reason for the slow transition to integrated methodology is that the resulting problem is computationally overwhelming in its dimensionality and cost of analysis. It is, therefore, important to note that a few papers, presented at the workshop, offered a very specific mathematics for a generic integrated methodology (Table 1, line "Methodology..."). These reported several encouraging applications in which the mathematics was successfully tested as a means for overcoming the above dimensionality barrier. Even though the above new mathematical solutions are prototypes unlikely to be implemented in engineering practice in their present forms without changes, they at least provide a springboard from which to launch a development to bridge the gap between the methodology presented at the workshop and the integrated, multidisciplinary methodology needed for optimisation of the whole aircraft treated as a system.

While aeroelastic optimisation presented at the Workshop has become a routine capability, mastery of the mutidisciplinary synergy in aircraft design emerges as a new challenging frontier for research and development. The potential for the multidisciplinary approach was demonstrated in the workshop by the contribution from MBB ref. 11 which augmented the traditional sizing problem by including non-structural design parameters. Even though this paper only made a first pass at the problem by including the augmented approach in the form of a sensitivity analysis the improvement was immediate and significant. In essence the MBB approach imported the ideas expounded in references 2 and 4 but only as a single post-optimal step. Nevertheless, the paper represents a clear pointer to what may be achieved by a full practical application of the methodology.

The final assessment point represents the plea made by several of the panel members for the creation of more user friendly programmes in this area. It is clear that the underlying mathematics of the structural optimisation programmes is complex, particularly when such factors as duality, active set strategies, algorithm applicability need to be considered. It would be convenient if these factors could be ignored by the regular user but this is not possible at the present time. Thus, the main users of the technology presented in the workshop are experts in the field and only those companies with such experts are in a position to fully exploit the capabilities offered by the existing systems. In order to create a wider audience for optimisation which would lead to a greater user of the technology this aspect must be given some consideration.

INFERENCES FROM ASSESSMENT

On the basis of the above assessment it is possible to draw conclusions which point to the future direction for research action and for AGARD action.

1. **Algorithm Development.**
   Although it is to be expected that further work will be undertaken by research workers to strengthen and improve the performance of the basic optimisation algorithms this is not seen as an area of special significance for conventional sizing problems involving strength/aeroelastic constraints on serial computers. In this restricted domain the extension to distributed computing and eventually to massively parallel machines will be developed by commercial companies who currently market optimisation software.

   In the case of multidisciplinary optimisation the picture is more complex and the development of effective solution methods which can accommodate the high level of interaction demanded by this domain of application will require special consideration. The results from references 2, 3 and 11 indicate that solution methods here cannot be separated from the application despite work done in other areas on multi-level optimisation. The eventual transportation of solution techniques to massively parallel computers will require special consideration and the involvement of funding agencies. The benefits from this migration are likely to be very significant for the application of multidisciplinary optimisation in the solution of real world problems. AGARD has a role to play in this area in focusing attention on the need to develop specific sclution methods for the aeronautical industry. A concrete proposal for this involvement is discussed in the next section which links to the main point raised in the current paragraph.

2. **Multi-Disciplinary Optimisation**

In addition to the algorithm considerations discussed above the subject of multidisciplinary optimisation needs to be thought of as a separate research area. Extending the structural optimisation methodology so that it includes all major aeronautical disciplines for applications involving the entire aircraft treated as a system requires a concerted long term effort. Yet the results from the MBB study reviewed in the previous section emphasize the importance of such an effort and indicated the magnitude of the benefits available. The workshop has, therefore, reinforced the opportunity of initiating a new work programme within the aeronautics industry targeted a speeding up progress in this area. The solid core of aeroelastic optimisation technology demonstrated at the workshop forms a foundation on which to build.

Taking this fact into consideration, and the views expressed in the previous section, points to the need for a new AGARD initiative focused on the subject of multidisciplinary optimisation in the field of aeronautical design. This should take into account the changes in computing power and architecture envisaged in the next few years. AGARD is most effective when it initiates an activity and provides a forum to develop ideas in a new research activity. It is, therefore, proposed that a recommendation be made that AGARD sets up a new working group to examine the possibility for a new workshop devoted specifically to "Multidisciplinary, Integrated, System-Based Methodologies for Aircraft Design". This to be held in 1996.

3. **User-Friendly Programmes**

The need to provide optimisation software which is accessible to the design engineer was identified as an important issue which requires addressing. The integration of A.I. Methodologies with optimisation software to create user friendly programmes is a corollary of this consideration. Once more it is appropriate for AGARD to consider this aspect as it represents cross-disciplinary research. Because there are many conferences and workshops on the application of A.I. Methodologies in engineering it is not recommended that AGARD initiate a similar venture. However, the assemblage of a group of highly focused papers pointing the way forward would be useful to both the research community and the practitioner in deciding on appropriate avenues for future action. On this basis it is recommended that the SMP select a group of experts able to address the problem of employing A.I. and Expert System methods to generate very user friendly software and prepared an AGARDOGRAPH on the subject. This could be considered for publication in the 1994/95 time frame.

4. **Education**

A continuing activity is needed to inform practitioners about the tools available and to impart more robustness to their use. It is recommended that the papers from the Bath workshop and the forthcoming AGARD Lecture Series (number 186) are combined in a comprehensive AGARDOGRAPH.

5. **Complex constraints**

The results of the workshop indicate a need to focus special attention on the development of methods to generate derivatives for aerodynamic forces. The continuing lack of an efficient and accurate alternative to finite differencing places a serious barrier to the development of multidisciplinary methods.

Another area which needs an initial push is the integration of active control into the structural sizing problem with aeroelastic constraints The noticeable absence of this topic at the workshop is an accurate reflection of the current state of development in this area.

Whilst not taking specific action in this area it is suggested that the SMP recommend this as an area for study and endeavour to address synergism of these two disciplines in the near future as results start to appear.

SUMMARY OF RECOMMENDED ACTIONS

1. An AGARDOGRAPH be published combining the workshop results with the papers from the forthcoming AGARD Lecture Series on structural optimisation.

2. A group of experts be drawn together to prepare an AGARD publication of the potentialities for the use of A.I. and Expert System methodologies to provide very user friendly front ends to main-stream structural optimisation programmes.

3. A new AGARD activity leading to a workshop to be held in 1996 entitled "Multidisciplinary, Integrated, System-Based Methodology for Aircraft Design", to demonstrate ways and means for, and benefits from, optimisation of entire aircraft as a system governed by a diverse set of design variables with simultaneous participation of all the major engineering disciplines involved.

REFERENCES

1. Integrated Design Analysis and Optimization of Aircraft Structures.
A.J.Morris, Cranfield Inst. of Technology, Bedford, UK. J.Sobieszczanski-Sobieski, NASA Langley Research Center, Hampton, VA, USA.

2. A System Approach to Aircraft Optimization.
J.Sobieszczanski-Sobieski, NASA Langley Research Center, Hampton, VA, USA.

3. Shape Sensitivity Analysis of Dynamic Aeroelastic Response.
R.K.Kapania, Virginia Polytechnic Inst., Blacksburg, VA. USA. J-F. M. Barthelemy, NASA Langley Research Center, Hampton, VA, USA.

4. Multidisciplinary Optimization of a Large Flexible Supersonic Aircraft.
J-F. M.Barthelemy and P.G.Coen, NASA Langley Research Center, Hampton, VA, USA. G.A.Wrenn and A.R.Dovi, Lockheed Eng. & Science Corporation, Hampton, VA, USA.

5. Integrated Design, Analysis and Optimization Exercises for Aircraft Structures.
J.Bohlmann, General Dynamics, Fort Worth, TX, USA.

6. The Structural Optimization System OPTSYS - Current Status and Applications.
T.Brama, SAAB Aircraft Division, Kinköping, Sweden.

7. Application of an Automated Multidisciplinary Analysis and Optimization System to the Design of Aircraft Structures.
D.Thompson and J.C.Ayres, B.Ae., (Military A/C) Ltd., Preston, UK.

8. Multidisciplinary Optimisation Studies Using ASTROS.
V.B.Venkayya and A.G.Striz, WRDC/FIBR, WPAFB, Dayton, OH, USA.

9. Multidisciplinary Redesign of a Fighter Aircraft Vertical Tail for Enhanced Buffet Environment Survivability.
D.M.Pitt and R.W.Scanlon, McDonnell Aircraft Co., St. Louis, MO, USA.

10. Application of ASTROS to the Strength, Aeroelastic Optimization of the MBB Vertical Fin.
D.J.Neill, Northrop Co., Aircraft Div., Hawthorne, CA, USA. E.H.Johnson, MacNeal Schwendler Corp., Los Angeles, CA, USA.

11. First Approach to an Integrated Fin Design.
G.Schneider, H.Krammer and H.Hornlein, MBB (Military A/C) Div., Munich Germany.

12. A Fin Optimization Study.
G.Pollano, Aeritalia GAD, Turin, Italy.

13. Simultaneous Stress and Flutter Optimization for the Wing of a Transport Aircraft Equipped with Four Engines.
H.Zimmermann, D.Schierenbeck and P.Heinze, Deutsche Airbus, Bremen, Germany.

14. L'Optimization des Structures d'Aéronefs - Pratique Courante et Tendances (Structural Optimization of Aircraft - Practice and Trends).
C.Cornuault, Dassault Aviation, Saint-Cloud, France.

TABLE I. INVENTORY OF THE WORKSHOP CONTENT

Topics/Paper No.
Aircraft as a system of interacting physical phenomena and parts 2 4 11
Multidisciplinary - considering two or more disciplines (*) 2 3 4 5 6 7 8 9 10 11 12 13 14
Analysis 2 3 4 5 6 7 8 9 10 11 12 13 14
Analysis includes whole aircraft 2 4 7 9 13 14
Aerodynamics 2 3 4 5 8 10 11 12 13 14
Aircraft Performance 2 4
Structures 2 4 5 6 7 8 9 10 11 12 13 14
Metallic 2 3 6 7 8 9 13 14
Composites 3 4 5 6 7 8 10 11 12 14
Aeroelasticity (static) 2 3 4 5 6 7 8 10 11 12 13 14
Aeroelasticity (dynamic, including flutter) 2 3 5 6 7 8 9 10 11 12 13 14
Thermodynamics of Airflow 2
Propulsion 2
Sensitivity (quasi-analytical) 2 3 4 6 7 8 10 11 12 13 14
Sensitivity (Finite differencing) 2 3 4 5 7 8 10 11 12 13 14
Optimization 2 4 5 6 7 8 9 10 11 12 13 14
Optimization by Nonlinear Mathematical Programming 2 4 5 6 7 8 10 11 12 13 14
Optimization by Optimality Criteria 5 7 8 10 13
Optimization by Branching/Combinatorial Technique 9
Optimization includes variables that govern aerodynamic shape 2 4 11
Hierarchic Decomposition in Analysis and/or Optimization 2
Non-Hierarchic Decomposition in Analysis and/or Optimization 2 4 11
Organization of Numerical Process in Design 2 14
Uncertainties of data in analysis and optimization 14
Methodology as primary subject 2 3 4 9 11
Applications to illustrate a method use 2 3 4 5 6 7 8 9 10 11 12 13 14
Wing 2 3 4 5 6 8 13 14
Empennage 7 9 10 11 12 14
Fuselage 2 4 6 14
MBB fin 7 10 11 12 14
Test cases created for research purposes 3 4 5 8
Test cases derived from a real aircraft being designed 2 6 7 8 9 13 14
Applications to aircraft that have been built 2 6 7 9 13 14
Transport Aircraft 2 4 6 8 13
Fighter Aircraft 5 6 7 8 9 10 11 12 14
Subsonic 2 3 5 6 7 8 9 10 11 12 13 14
Transonic 4 5 6 7 8 9 10 11 12 14
Supersonic 4 6 7 8 9 14
Hypersonic 2
Transatmospheric 2
Non-Aerospace Applications 2 6
Comparison of methods and/or analytical and experimental data 3 4 5
Experimental data 5
Research Software 11
Production Software 5 6 7 8 9 10 11 12 13 14
Research Software with Production Modules 2 3 4 9

(*) If one did not categorize the papers devoted to aeroelasticity as multidisciplinary, then only the following papers would have been shown in this category:

Multidisciplinary - considering two or more disciplines
2 4 11

A SYSTEM APPROACH TO AIRCRAFT OPTIMIZATION

by
Jaroslaw Sobieszczanski-Sobieski
NASA Langley Research Center, MS 246
Hampton Virginia 23665 U.S.A.

SUMMARY

Mutual couplings among the mathematical models of physical phenomena and parts of a system such as an aircraft complicate the design process because each contemplated design change may have a far reaching consequences throughout the system. This paper outlines techniques for computing these influences as system design derivatives useful for both judgmental and formal optimization purposes. The techniques facilitate decomposition of the design process into smaller, more manageable tasks and they form a methodology that can easily fit into existing engineering organizations and incorporate their design tools.

1. INTRODUCTION

The engineering design process is a two-sided activity as illustrated in Fig. 1. It has a qualitative side dominated by human inventiveness, creativity, and intuition. The other side is quantitative, concerned with generating numerical answers to the questions that arise on the qualitative side. The process goes forward by a continual question-answer iteration between the two sides. To support that process one needs a computational infrastructure capable of answering the above questions expeditiously and accurately. For development of such an infrastructure, the idea of "push button design" ought to be discarded in favor of a realistic recognition of the role of human mind as the leading force in the design process and of the role of mathematics and computers as the indispensable tools. It is clear that while conceiving different design concepts is a function of human mind, the evaluation and choice among competing, discretely different concepts, e.g., classical configuration vs. a forward swept wing and a canard configuration, requires that each concept be optimized to reveal its full potential. This approach is consistent with the creative characteristics of the human mind and the efficiency, precision, and infallible memory of the computer.

The computational infrastructure for support of the design process entails data management, graphics, and numerics. The first two embodied in CAD/CAM systems are well-known and are taken for granted as a framework for the numerics. The purpose of this paper is to introduce some new techniques which may be regarded as a subset of the latter. Included in the discussion are the system behavior derivatives with respect to design variables, their use for both judgmental and mathematical optimization purposes, formal decomposition of a system into its components, and ramifications of that decomposition for system sensitivity analysis and optimization, all illustrated by aircraft application examples. The impact on the design process of a methodology formed by these techniques is also examined.

2. EFFECT OF DESIGN VARIABLE CHANGE IN A COMPLEX SYSTEM

An aircraft is a complex system of interacting parts and physical phenomena whose behavior may be influenced by assigning values to the design variables. Since the design process is, generally, concerned with an aircraft that does not yet exist, one works with its surrogate—a system of mathematical models that correspond, roughly, to the engineering disciplines, and to physical parts of the vehicle. These mathematical models send data to each other as depicted in the center of Fig. 2, and they also accept design variable values as inputs from the designers. To know how to change these design variables, designers must know the answers to "what if" questions, such as "what will be the effect on the system behavior if the design variables X, Y, Z will be changed to $X+\Delta X$, $Y+\Delta Y$, $Z+\Delta Z$?", implied by the loop in Fig. 2.

An example of a hypersonic aircraft in Fig. 3 illustrates how difficult it may be to answer an "what if" question for even a single variable change in a complex system in which everything influences everything else. Consider a structural cross-sectional thickness t in the forebody of a hypersonic aircraft shown in the upper half of Fig. 3 as a design variable that is to be changed. The lower half of the figure depicts a complex chain of influences triggered by the change of t and, ultimately, affecting the vehicle performance. The change of t influences the position of the bow shock wave relative to the inlet in two ways: through the nose deflection, and through the weight and the center of gravity position both of which affect the trimmed angle of attack. The shock wave position relative to the inlet is a strong factor in the propulsive efficiency of the engine that, in turn, combines with the weight to influence the aircraft performance. Additional influence on performance is through the angle of attack whose change alters the vehicle aerodynamic lift and drag. The resultant modifications of the performance may require resizing of the vehicle which, of course, may be a sufficient reason to change t again, and so on, until the iteration represented by the feedback loop in Fig. 3 converges.

The above iteration engages a number of mathematical models such as structures, aerodynamics, propulsion, and vehicle performance. For the purposes of this discussion, each such model may be regarded as a black box converting input to output and, consistent with the black box concept, the inner workings of the model will be left outside of the scope of the discussion. While it may not be too difficult to evaluate the input-on-output effect for each single black box taken separately, evaluation of the resultant change for the entire system of such black boxes may be exceedingly difficult, especially

when iterations are involved. In general, the resultant may be a small difference of large numbers, so even its sign may be impossible to predict without a precise reanalysis of the entire system.

To generalize from the above example, let X and Y denote the system input and output, respectively, e.g., the structural cover thickness t and a measure of performance such as the aircraft range. Then, the derivative dY/dX is a measure of the influence of X on Y and its value answers quantitatively the associated "what if" question. More precisely, the derivative value informs only about the rate of change of Y at the value of X for which the derivative was obtained. Determination of the increment of Y for a given finite increment of X, if $Y(X)$ is nonlinear, can be done approximately by a linear extrapolation

$$Y_{\text{new}} = Y_{\text{old}} + \frac{dY}{dX}\Delta X \tag{1}$$

Capability to extrapolate as above for many different X and Y variables, enables one to decide, either judgmentally or by means of an optimization program, which variables X to change and by how much, in order to improve the design in some way. However, that capability is predicated on availability of the derivatives dY/dX termed the system design derivatives (SDD). For large system analysis, especially if the analysis is iterative, its is advantageous to avoid the brute force method of finite differencing on the entire system analysis in computation of these derivatives.

2.1 System Design Derivatives

Remembering that the mathematical model of an engineering system may be an assemblage of a large number of mathematical models representing its components and the governing physical phenomena, it is convenient to limit the discussion to three such black box models since that number is small enough to foster comprehension and, yet, large enough to develop a general solution pattern. Ascribing a vector function representation to each black box, the set of equations representing the system of the black boxes α, β, γ exchanging data as illustrated in Fig. 4 is

$$\begin{aligned} Y_\alpha &= Y_\alpha(X, Y_\beta, Y_\gamma) \\ Y_\beta &= Y_\beta(X, Y_\alpha, Y_\gamma) \\ Y_\gamma &= Y_\gamma(X, Y_\alpha, Y_\beta) \end{aligned} \tag{2}$$

The Y and X variables in the above are vectors entered in the black boxes selectively, e.g., some, but not necessarily all, elements of the vectors X and Y_α enter the black box β as inputs. Regarding $Y_\beta(X, Y_\alpha, Y_\gamma)$ as an example of a black box, the arguments, X, Y_α, Y_γ, are the inputs and Y_β is an output. The functions in eq. 2 are coupled by their outputs appearing as inputs, hence they form a set of simultaneous equations that can be solved for Y for given X. The act of obtaining such a solution is referred to as the system analysis (SA). In the presence of nonlinearities, SA is usually iterative.

For each function in eq. 2, one can calculate derivatives of output with respect to any particular input variable, assuming that other variables are fixed. From the entire system perspective, these derivatives are partial derivatives since they measure only the local input-on-output effect, as opposed to SDD which are total derivatives because they include the effect of the couplings. To prepare for further discussion, the partial derivatives corresponding to the Y-inputs are collected in the Jacobian matrices designated by a pair of subscripts identifying the origins of the output and input, respectively. For example,

$$J_{\gamma\alpha} = [\partial Y_\gamma / \partial Y_\alpha] \tag{3}$$

is a matrix whose j-th column is made of the partial derivatives $\partial Y_{\gamma i}/\partial Y_{\alpha j}$. Assuming the length of Y_γ as N_γ and the length of Y_α as N_α, the dimensions of matrix $J_{\gamma\alpha}$ are $N_\gamma \times N_\alpha$. It will be mnemonic to refer to the partial derivatives in the Jacobian matrices as the cross-derivatives.

The remaining partial derivatives corresponding to the X-inputs are collected in vectors, one vector per each of the NX elements of the vector of design variables X, e.g,

$$\{\partial Y_\alpha/\partial X_k\}' = [\partial Y_\alpha/\partial X_k], \quad k = 1, \ldots, NX; \tag{4}$$

is a vector of the length N_α ($'$ denotes transposition).

Calculation of the above partial derivatives may be accomplished by any means available for a particular black box at hand, and may range from finite differencing to quasi-analytical methods (ref. 1, and 2).

It was shown in ref. 3 that differentiation of the functions in eq. 2 as composite functions and application of the implicit function theorem leads to a set of simultaneous, linear, algebraic equations, referred to as the Global Sensitivity Equations (GSE), in which the above partial derivatives appear as coefficients and the SDD are the unknowns. For the system of eq. 2, the GSE are

$$\begin{bmatrix} I & -J_{\alpha\beta} & -J_{\alpha\gamma} \\ -J_{\beta\alpha} & I & -J_{\beta\gamma} \\ -J_{\gamma\alpha} & -J_{\gamma\beta} & I \end{bmatrix} \begin{Bmatrix} dY_\alpha/dX_k \\ dY_\beta/dX_k \\ dY_\gamma/dX_k \end{Bmatrix} = \begin{Bmatrix} \partial Y_\alpha/\partial X_k \\ \partial Y_\beta/\partial X_k \\ \partial Y_\gamma/\partial X_k \end{Bmatrix} \tag{5}$$

These equations may be formed only after the SA was performed for a particular X, a particular point in the design space because the computation of the partial derivatives requires that all the X and Y values be known. For a given X, the matrix of coefficients depends only on the system couplings and is not affected by the choice of X for the right hand side. Hence that matrix may be factored once and reused in a backsubstitution operation to compute as many sets of SDD's as many different X_k variables are represented in the set of multiple right-hand-side vectors.

As recommended in ref. 3, numerical solution of eq. 5 and interpretation of the SDD values will be facilitated by normalization of the coefficients in the matrix and in the right hand sides by the values of Y_o and X_o of the Y and X variables for which the partial derivatives were calculated. The normalized coefficients take on the following form, illustrated by a few examples from i-th row in the β partition in eq. 5

$$-\frac{\partial Y_{\beta i}}{\partial Y_{\alpha j}} q_{\beta\alpha ij}; \quad -\frac{\partial Y_{\beta i}}{\partial Y_{\gamma j}} q_{\beta\gamma ij}; \quad \frac{dY_{\beta i}}{dX_k} q_{\beta X ik}, \tag{6}$$

where the normalization coefficients q are

$$q_{\beta\alpha ij} = \frac{Y_{\alpha jo}}{Y_{\beta io}}; \quad q_{\beta\gamma ij} = \frac{Y_{\gamma jo}}{Y_{\beta io}}; \quad \bar{q}_{\beta X ik} = \frac{X_{ko}}{Y_{\beta io}}$$

Solution of the normalized eq. 5 yields normalized values of the SDD's from which the unnormalized values may always be recovered given the above definitions.

Formation of the GSE and their solution for a set of SDD's will be referred to as the System Sensitivity Analysis (SSA).

2.2 Utility of the System Design Derivatives

The SDD carry the trend information that under a conventional approach would be sought by resorting to statistical data or to the parametric studies. The former have the merit of capturing a vast precedent knowledge but may turn out to be ineffective if the vehicle at hand is advanced far beyond the existing experience. The latter provide an insight into the entire interval of interest but only for a few variables at a time, and that insight tends to be quickly lost if there are many design variables, in which case the computational cost of the parametric studies also may become an impediment.

In contrast, the SDD information is strictly local but it reflects the influences of all the design variables on all aspects of the system behavior. Therefore, the SSA should not be regarded as a replacement of the above two approaches but as their logical complement whose results are useful in at least two ways.

2.2.1 Ranking design variables for effectiveness

A full set of SDD for a system with NY variables in Y and NX variables in X is a matrix $NY \times NX$. The j-th column of the matrix describes the degree of influence of variable X_j on the behavior variables Y. Conversely, the i-th row shows the strength of influence of all the design variables X on the i-th behavior variable Y_i. For normalized SDD's, comparison of these strengths of influence becomes meaningful and may be used to rank the design variables by the degree of their influence on the particular behavior variable. This ranking may be used as a basis for judgmentally changing the design variable values and for deciding which design variables to use in a formal optimization.

An example of such ranking is illustrated for the wing of a general aviation aircraft shown in Fig. 5. The design variables are thicknesses t of the panels in the upper cover of the wing box and the behavior variable is the aircraft range R. The chain of influences leading from a panel thickness to the range calculated by means of the Breguet formula is depicted on the left side in Fig. 6. In the Breguet formula, W_e denotes the zero-fuel weight and W_p stands for the fuel weight. Increasing t in one of the panels increases the weight W_e and, in general, reduces the drag of a flexible wing by stiffening its structure. Consequently, the range is influenced in conflicting ways that would make prediction by judgment difficult. However, the corresponding SSA yields the SDD's for the upper row of the wing cover panels illustrated by the heights of the vertical bars over the upper wing cover panels in Fig. 6. The bars show that among all the wing cover panels, increasing t in the extreme outboard panel would increase range the most.

2.2.2 Gradient-guided formal optimization

Most of the formal optimization methods applicable in large engineering problems use the first derivative information to guide the search for a better design. Since the SDD values provide such information for all the Y and X variables of interest, the SSA may be incorporated, together with SA, in a system optimization procedure (SOP) based on the well-known piecewise approximate analysis approach (e.g., ref. 4). The SOP flowchart is depicted in Fig. 7. An important benefit of the SOP organization is the opportunity for parallel processing seen in the flowchart operation immediately following the SA. In that operation, one computes concurrently the partial derivatives of input with respect to output for all the system black boxes, in order to form the Jacobian matrices (eq. 3) and the right-hand-side vectors (eq. 4) needed to form the GSE (eq. 5) whose solution yields the SDD's. In a conventional approach, these SDD's would be computed by finite differencing on SA. The SDD values are subsequently used in Approximate Analysis (extrapolation formulas) that supplies the optimizer (a design space search algorithm) with information on the system behavior for every change of the design variables generated by that optimizer, and does it at a cost negligible in comparison with the cost of SA.

A generic hypersonic aircraft similar to the one that was discussed in Fig. 3 was used as a test for the above optimization. The geometrical design variables for the case are shown in Fig. 8. Additional design variables were the deflections of the control surfaces, and the cross-sectional structural dimensions of the forebody. The propulsive efficiency measured by the I_{sp} index, defined as the thrust minus drag divided by the fuel mass flow rate, was chosen as the objective function to be maximized. The aircraft take-off gross weight (TOGW) for a given mission is very sensitive to that index, thus maximization of the index effectively minimizes TOGW. For the reasons discussed in conjunction with Fig. 3, the problem requires consideration of a system composed of aerodynamics, propulsion, performance analysis, and structures. The optimization included constraints on the aircraft as a whole and on behavior in the above disciplines. Results are shown in Table 1 in terms of the initial and final values of the design variables (cross-sectional dimensions omitted) and of the objective function, all normalized by the initial values. Considering that the initial values resulted from an extensive design effort using a conventional approach, the nearly 13% improvement in the propulsive efficiency was regarded as very significant indeed.

Another example of the SOP application is the case of a hypersonic interceptor (Fig. 9a) reported in ref. 5. The optimization objective was the minimum of TOGW for the mission profile illustrated in Fig. 9b. The system comprised the modules of the configuration geometry, configuration mass properties, mission performance analysis, aerodynamics, and propulsion as depicted in Fig. 10, and the design variables were the wing area, scale factor for the turbojet engine, scale factor for the ramjet engine, and the fuselage length. The constraint list included a limit on the time needed to reach the combat zone, the take-off velocity, and the fuel available mass being at least equal to the one required (the fuel balance constraint). It should be noted that in a conventional approach to aircraft design, satisfaction of the latter constraint is one of the principal goals in

development of a baseline configuration whose improvement is subsequently sought by parametric studies in which the design variables are varied while always striving to hold the fuel balance constraint satisfied. In contrast to that practice, the optimization reported in ref. 5 allowed the fuel balance constraint to be violated in the baseline configuration and achieved satisfaction of that constraint in the course of the optimization process. This demonstrated that an optimization procedure may do more than just improve on an initial, feasible configuration; it can actually synthesize an optimal configuration starting with one that is not even capable of performing a required mission.

The optimization results are illustrated by a vertical bar chart in Fig. 11 that shows the changes of the design variables and of a significant (13%) improvement of the objective function. The figure shows also that the initially violated constraints of time to intercept and take-off velocity were brought to satisfaction in the optimal configuration. The SOP converged in only 4 to 5 repetitions of SA and SSA.

3. MERITS AND DEMERITS

Before discussion of the ramifications of the above sensitivity-based optimization in a system design process, it may be useful to examine briefly the merits and demerits of the proposed approach relative to the conventional technique of generating SSD by finite differencing on the entire SA.

3.1 Accuracy and Concurrent Computing

The SSA based on eq. 5 has two unique advantages. First, the accuracy of SDD is intrinsically superior to that obtainable from finite differencing whose precision depends on the step length in a manner that is difficult to predict. As pointed out in ref. 6 it is particularly true in the case of an iterative SA whose result often depends on an arbitrary, "practical" convergence criterion. Second, there is an opportunity for concurrent computing in the generation of the partial derivatives which exploits the technology of parallel processing offered by multiprocessor computers and computer networks. Concurrent computing also enables the engineering workload to be distributed among the specialty groups in an engineering organization to compress the project execution time.

3.2 Computational Cost

Experience indicates that in large engineering applications, most of the optimization computational cost is generated by the finite difference operations. Therefore, relative reduction of the cost of these operations translates into nearly the same relative reduction of the cost of the entire optimization procedure.

The computational cost of the SSA based on eq. 5, designated C_1, may be reduced, in most cases very decisively, below that of finite differencing on the entire SA, denoted by C_2, but to achieve that reduction the analyst should be aware of the principal factors involved. To define these factors, let the computational cost of one SA be denoted by CSA while CBA_i will stand for the computational cost of one analysis of the i-th black box in the system composed of NB black boxes. The i-th black box receives an input of NX_i design variables X, and NY_i variables Y from the other black boxes in the system. Assuming for both alternatives the simplest one step finite difference algorithm that requires one reference analysis and one perturbed analysis for each input variable, the costs C_1 and C_2 may be estimated as

$$C_1 = \sum_i (1 + NX_i + NY_i) CBA_i; \qquad C_2 = (1 + NX) CSA \tag{7}$$

Even though one may expect $CBA_i < CSA$, a sufficiently large NY_i may generate $C_1 > C_2$ and render SSA based on eq. 5 unattractive compared to finite differencing on the entire SA. This points to NY_i, termed the interaction bandwidth, as the critical factor whose magnitude should be reduced as much as possible. Reducing the interaction bandwidth requires judgment as illustrated by an example of an elastic, high aspect ratio wing treated as a system whose aeroelastic behavior is modeled by interaction of aerodynamics and structures, represented by an CFD analysis and Finite Element analysis codes, respectively. If one let the full output from each of these black boxes be transmitted to the other, there might be hundreds of pressure coefficients entering the structural analysis and thousands of deformations sent to the aerodynamic analysis. With the NY_i values in the hundreds and thousands, respectively, it would be quite likely that $C_1 > C_2$. However, one may condense the information flowing between the two black boxes by taking advantage of the high aspect ratio wing slenderness. For a slender wing it is reasonable to represent the entire aerodynamic load by, say, a set of 5 concentrated forces at each of 10 separate chords, and to reduce the elastic deformation data to, say, elastic twist angles at 7 separate chords. This condensation reduces the NY_i values to 50 for structures and 7 for aerodynamics. In the finite element code, that implies 50 additional loading cases all of which can be computed very efficiently by the multiple loading case option—a standard feature in finite element codes. The CFD code would have to be executed only 7 additional times. Thus, the advantage of the interaction bandwidth condensation is evident. In general, a condensation such as the one described above for a particular example may be accomplished by the reduced basis methods, among which the Ritz functions approach is, perhaps, the best known one.

3.3 Potential Singularity

One should be aware when using SSA based on eq. 5 that, in some cases, the matrix of coefficients in these equations may be singular. In geometrical terms, a solution in SA may be interpreted geometrically as a vertex of hyperplanes on which the residuals of the governing equations for the black boxes involved are zero. As pointed in ref. 3, eq. 5 are well-conditioned if these hyperplanes intersect at large angles, ideally when they are mutually orthogonal. For two functions of two variables the zero-residual hyperplanes reduce to the zero-residual contours, and an example of a nearly-orthogonal solution intersection is shown in Fig. 12a. In some cases, the intersection angles may tend to be very acute, in the limit they may be zero in which case a solution exist by virtue of tangency of two curved contours as illustrated in Fig. 12b. It is shown in ref. 3 that eq. 5 imply local linearization of these contours in the vicinity of the intersection point so that the solution point is interpreted as an intersection of the tangents. Consequently, in the situation depicted in Fig. 12b the tangents

coincide and the matrix of eq. 5 becomes singular. In such a case, eq. 5 should be replaced by an altemative formulation of the system sensitivity equations in ref. 3 based on residuals.

There were no cases of singularity reported so far in any applications probably because the system solutions of the type illustrated in Fig. 12b characterize an ill-posed system analysis usually avoided in practice.

3.4 Discrete Variables

Neither the reference technique nor the SSA based on eq. 5 can accommodate truly discrete design variables. Truly discrete design variables are defined for the purposes of this discussion as those with respect to which SA is not differentiable. These are distinct from quasi-discrete variables with respect to which SA is differentiable but which may only be physically realizable in a set of discrete values. An example of the former is an engine location on the aircraft: either under the wing or at the aft end of the fuselage. An example of the latter is sheet metal thickness available in a set of commercial gages.

In the case of truly discrete design variables, different combinations of such variables define different design concepts (alternatives) and each concept may be optimized in its own design space of the remaining continuous variables, in order to bring it up to its true potential. Then, one may choose from among the optimal alternatives. Occasionally, a continuous transformation might be possible between two concepts that seem to be discretely different. For example, a baseline aircraft with a canard, a wing, and a conventional tail may be reshaped into any configuation featuring all, or only some of these three lifting surfaces. This is so because a sensitivity-guided SOP may eliminate a particular feature, if a design variable is reserved for that feature and if the feature is present in the initial design (however, a feature initially absent cannot, in general, be created).

3.5 Non-utilization of Disciplinary Optimization

Organization of the SOP discussed above may be described as "decomposition for sensitivity analysis followed by optimization of the entire, undecomposed system". It may be regarded as a shortcoming that the procedure leaves no clear place for the use of the vast expertize of optimization available in the individual black boxes representing engineering disciplines. Examples of such local, disciplinary optimization techniques are the optimality criteria for minimum weight in structures, and shaping for minimum drag for a constant lift in aerodynamics. It appears that combining these local, disciplinary optimization techniques with the overall system optimization should benefit the latter. Indeed, one way in which these techniques may be used without changing anything in the SOP organization described above is in the SOP initialization. Obviously, starting SOP from a baseline system composed of the black boxes already preoptimized for minimum weight, minimum drag, maximum propulsive efficiency, etc. should accelerate the SOP convergence and improve the end result. Such local optimizations could be accomplished separately for each black box, assuming X and guessing at the Y inputs.

Beyond that, the issue of incorporating the local, disciplinary optimization in SOP remains to be a challenge for further development. Some solutions were proposed in ref. 7 and 8 but their effectiveness is yet to be proven in practice. This issue will be taken up again in the later discussion in conjunction with the special case of a hierarchic system decomposition which does accommodate the local optimizations.

4. FORMAL DECOMPOSITION

When the system at hand contains a large number of black boxes and, especially, if there is little or no experience with its solution, it is useful to apply a formal technique to determine the data flow among the black boxes. The data flow information is useful because it characterizes the system as non-hierarchic, hierarchic, or hybrid, and this, in turn, helps to choose an optimization approach and to establish an efficient organization of computing. Such formal techniques are available in Operations Research and some of them were adapted for the system analysis and optimization purposes, e.g., ref. 9.

4.1 *N*-square Matrix

A brief introduction to one such technique begins with a formalization of a black box (a module) in the system as one that receives inputs through the top and bottom horizontal sides and sends the output through the left and right vertical sides as as shown in Fig. 13. Using that formalism, one can represent a four-module system example depicted by the diagram (known as the graph-theoretic format) in Fig. 14a in a different format shown in Fig. 14b. That format is known as the N-square Matrix format because N modules placed along the diagonal form an N^2 table. The N-square Matrix format assumes that the modules are executed in order from upper left to lower right (although, if possible, concurrent executions are allowed). If the execution order is not yet known, the order along the diagonal may be arbitrary. Referring to Fig. 13, each module may, potentially, send data horizontally, left and right, and receive vertically from above and from below. The actual data transmissions from and to i-th module are determined by comparing the module input list to the predecessor module output lists while moving upward in column i. Wherever a needed input item is found on the output list from module j, a dot is placed at the intersection of the i-th column and j-th row as a data junction indicating transmission of output from module j to input of module i. After the predecessor module search gets to the first module, it switches to module $i+1$ and continues downward through all the successor modules to module N. If more than one source is found for a particular input item, a unique, single source must be judgmentally selected. However, an output item may be used by several receiver modules and may also be sent to the outside. The input items that could not be found in the vertical search are designated primary inputs to be obtained from the outside of the system. The above search is readily implementable on a computer.

When the above search procedure is completed for all the modules, the result is an N-square Matrix as in Fig. 14b that conveys the same information as the diagrem in Fig. 14a but is amenable to computerized manipulation. To see what such manipulation may achieve, observe that each dot in the upper triangle of the N-square Matrix denotes an instance of the data feedforward, and each dot in the lower triangle notes an

instance of the data feedback. Of course, every instance of a feedback implies an iteration loop required by the assumed diagonal order of the modules. However, that order may be changed at will by a code that may be instructed to switch the modules around, with the associated permutations of the rows and columns to preserve the data junction information, in order to eliminate as many instances of feedback as possible. If all of them are eliminated the system admits a sequential module execution, and may offer opportunities for concurrent executions of some modules. If a complete elimination of the feedbacks is not possible, they are reduced in number and clustered. An example of a fairly large N-square Matrix in the initial, arbitrary order is shown in Fig. 15a while its clustered state is shown in Fig. 15b. In the clustered state the system is hybrid—partially hierarchic and partially non-hierarchic. A software tool that is available to make the above transformation is described in ref. 9. All the modules in one of the clusters in Fig. 15b may be regarded as a new supermodule, and the system diagram may be drawn in terms of these supermodules as shown in Fig. 16. This diagram defines a hierarchic decomposition of a system because the data flow from the top of the pyramidal hierarchy to the bottom, without reversing the flow and without lateral flow, while inside of each cluster there is a system whose modules define a non-hierarchic decomposition.

The N-square Matrix structure has a reflection in the structure of the matrix of coefficients in eq. 5: each feedforward instance in the former gives rise to a Jacobian matrix located below the diagonal in the latter and each feedback is reflected in a Jacobian above the diagonal. Hence, a sequential system without feedbacks has a matrix of coefficients populated only below the diagonal so that eq. 5 may be solved by backsubstitution of the right hand sides without factoring of the matrix of coefficients.

4.2 SOP Adapted to Hierarchic System

When a decomposed system has a hierarchic structure, its SOP may be reorganized to include separate optimizations in each black box. This SOP version was introduced in ref. 10 and called an optimization by linear decomposition. It has found a number of applications, for example, it was the basis for an algorithm for multilevel structural optimization by substructuring in ref. 11, and its use in multidisciplinary applications was reported in ref. 12 for control-structure interaction and in ref. 13 for optimization of a transport aircraft.

Multilevel optimization of a hierarchic system by a linear decomposition exploits the top-down flow of the analysis information. At the bottom level, the inputs obtained from analysis at the next higher level and the appropriate design variables are regarded as constants in optimization of each, bottom-level black box. Derivatives of each such optimization are computed with respect to these input constants by means of an algorithm described in ref. 14 and are used in linear extrapolations (hence the name of the technique) to approximate the effect of the input constants on the optimization results. Optimizations in the black boxes at the next higher level approximate their influence on the lower level optimization by means of these extrapolations. Thus, the top black box optimization is performed taking an approximate account of the effect of its variables (the system level variables) on all the black boxes in the hierarchic pyramid. As mentioned in the foregoing, the advantages of the SOP exploiting the hierarchic structure of the system is a separation of the bottom level detailed optimizations from the top level system optimization, and breaking the large system optimization problem into a number of smaller optimization problems, in contrast to the non-hierarchic system SOP (Fig. 7) in which optimization is performed for the system as a whole. However, if any of these black boxes in a hierarchic system contains a cluster (see discussion of Fig. 16) of black boxes forming a non-hierarchic system, the non-hierachic system SOP (Fig. 7) may be used to optimize it locally. Hence, both methods for system optimization described above, the one based on the linear decomposition (ref. 10) as well as the SOP based on Fig. 7 flowchart have their place in optimization of a general case of a hybrid engineering system that exhibits both the hierarchic and non-hierarchic structures depicted in Fig. 16.

As reported in ref. 13, the linear decomposition method was used to optimize the variables of configuration geometry and cross-sectional structural dimensions of a transport aircraft illustrated in Fig. 17a for minimum fuel burned in a prescribed mission, under constraints drawn from the disciplines of aerodynamics, performance and structures. The analysis was relatively deep, e.g., a CFD code in aerodynamics, and a finite element model of the built-up structure of the airframe structures. The number of design variables was over 1300, and the number of constraints was also in thousands. Optimization was conducted decomposing the problem into a three-level hierarchic system shown in Fig. 17b. A sample of results is depicted in Fig. 18 showing a smooth convergence of the fuel mass and the structural weight in only 4 to 6 cycles (one cycle comprised the top-down analysis and the bottom-up optimizations), for both feasible and infeasible initial design.

5. GENERALIZATION TO ENTIRE VEHICLE DESIGN PROCESS

The approach to the system sensitivity and optimization discussed in the foregoing may be generalized to serve the entire design process as shown in ref. 15 using as an example a definition of that process given in ref. 16. The process defined in ref. 16 is a conventional, sequential process illustrated in Fig. 19. As suggested in the upper right corner of the flowchart, any change in a major design variable such as the wing or engine size requires reentry into the sequence and repetition of all the operations in the chain. However, the black boxes forming the sequence are also forming a coupled system whose diagram is depicted in Fig. 20. The arrows in the diagram represent the data flow among the black boxes, examples of the data being defined in Table 2. Application of the SSA based on eq. 5 to the system in Fig. 20 leads to GSE in the format shown in Fig. 21. In the abbreviated notation used in that figure, Y_{ij} stands for a Jacobian matrix J_{ij} defined in eq. 3. Solution of the equations shown in Fig. 21 yields the SDD values that answer the "what if" questions implied in the upper right corner of the flowchart in Fig. 19, and does it for all the variables of interest simultaneously and without repeating the entire chain for every question. The SDD values may then be used to support judgmental design decisions and/or to guide a formal optimization

according to the SOP in Fig. 7.

6. CONCLUDING REMARKS

Design of an engineering system, such as an aircraft, is a formidable task involving a myriad of cross-influences among the engineering disciplines and parts of the system. The time-honored approach to that task is to decompose it into smaller, more manageable tasks. The paper outlines some recently developed techniques that support such an approach by building an engineering system optimization on a modular basis, that comprises engineering specialty groups and their black box tools and allows engineers to retain responsibility for their domains while working concurrently on manageable tasks and communicating with each other by means of sensitivity data. The modularity and concurrence of operations map onto the familiar structure of the engineering organizations and are compatible with the emerging computer technology of multiprocessor computers and distributed computing. The only major new requirement is the generation of derivatives of output with respect to input in each specialty domain.

The use of sensitivity data as the communication medium is the distinguishing feature of the proposed approach and represent a major improvement over the present practice because it adds the trend information to the function value information. Both types of information enhance the human judgment and intuition while being readily usable in guiding the formal optimization procedures.

Acknowledgment: Contribution of the NASP configuration optimization example (Fig. 8 and Table 1) by Dr. F. Abdi and Mr. J. Tulinius of Rockwell International—North American is gratefully acknowledged.

7. REFERENCES

1. Proceedings of the Symposium on Sensitivity Analysis in Engineering, NASA Langley Research Center, Hampton Va, Sept. 1986; Adelman, H. M.; and Haftka, R. T.—editors. NASA CP-2457, 1987.

2. Adelman, H. A.; and Haftka, R. T.: Sensitivity Analysis of Discrete Structural Systems, AIAA J., Vol. 24, No. 5, May 1986, pp. 823–832.

3. Sobieszczanski-Sobieski, J.; On the Sensitivity of Complex, Internally Coupled Systems; AIAA/ASME/ASCE/AHS 29th Structures, Structural Dynamics and Materials Conference, Williamsburg, Va, April 1988; AIAA Paper No. CP-88-2378, and AIAA J., Vol. 28, No. 1, Jan. 1990, also published as NASA TM 100537, January 1988.

4. Sobieszczanski-Sobieski, J.: From a Black-Box to a Programing System, Ch.11 in Foundations for Structural Optimization—A Unified Approach; Morris, A. J., ed.J.; Wiley & Sons, 1982.

5. Consoli, R. D.; and Sobieszczanski-Sobieski, J.: Application of Advanced Multidisciplinary Analysis and Optimization Methods to Vehicle Design Synthesis; 17th Congress of the International Council of the Aeronautical Sciences (ICAS), Stockholm, September 1990, Proceedings of.

6. Thareja, R.; and Haftka, R. T.: Numerical Difficulties Associated with Using Equality Constraints to Achieve Multi-level Decomposition in Structural Optimization, AIAA Paper No. 86-0854, AIAA/ASME/ASCE/AHS 27th Structures, Structural Dynamics, and Materials Conference, San Antonio, Texas, May 1986.

7. Sobieszczanski-Sobieski, J.: Optimization by Decomposition: A Step from Hierarchic to Non-Hierarchic Systems; Second NASA/Air Force Symposium on Recent Advances in Multidisciplinary Analysis and Optimization; Hampton, Virginia, September 28–30 1988; Proceedings published as NASA CP - No. 3031; editor: Barthelemy, J. F.

8. Bloebaum, C. L.: Non-Hierachic System Decomposition in Structural Optimization Formal and Heuristic System Decomposition Methods in Multidisciplinary Synthesis; Ph.D. Dissertation, School of Engineering, Department of Aerospace Engineering, University of Florida, Gainsville, FL., 1991.

9. Rogers, J. L.: A Knowledge-Based Tool for Multilevel Decomposition of a Complex Design Problem; NASA TP 2903, 1989.

10. Sobieszczanski-Sobieski, J.: A Linear Decomposition Method for Large Optimization Problems—Blueprint for Development; NASA TM 83248, February 1982.

11. Sobieszczanski-Sobieski, J., James, B. B.; and Riley, M. F.: Structural Sizing by Generalized, Multilevel Optimization, AIAA J. Vol. 25, No. 1, January 1987, p. 139.

12. Zeiler, T. A.; and Gilbert, M. G.: Integrated Control/Structure Optimization by Multilevel Decomposition, NASA TM 102619, March 1990.

13. Wrenn, G. A.; and Dovi, A. R.: Multilevel Decomposition Approach to the Preliminary Sizing of a Transport Aircraft Wing; AIAA Jornal of Aircraft, Vol. 25, No. 7, July 1988, pp. 632–638.

14. Sobieszczanski-Sobieski, J.; Barthele. y, J. F.; and Riley, K. M.: Sensitivity of Optimum Solutions to Problem Parameters; AIAA J, Vol. 21, Sept. 1982, pp. 1291–1299.

15. Sobieszczanski-Sobieski, J.: Sensitivity Analysis and Multidisciplinary Optimization for Aircraft Design: Recent Advances and Results; Int'l Council for Aeronautical Sc., 16th Congress, Jerusalem, Aug.–Sept., 1988; Proceedings of, Vol. 2, pp. 953–964.

16. Torenbeek, E.: Synthesis of Subsonic Airplane Design; Delft University Press; 1982.

Table 1
Hypersonic aircraft optimization results

Optimization parameter	Baseline value	Optimization results
Design variable		
1. Forebody length	1.000	1.0209
2. Cone angle	1.000	0.9693
3. Upper surface height	1.000	1.0029
4. Geometric transition length	1.000	1.0760
5. Elevon deflection	1.000	0.8620
6. Bodyflap deflection	1.000	1.0320
Objective		
Effective trimmed lsp	1.000	1.1259

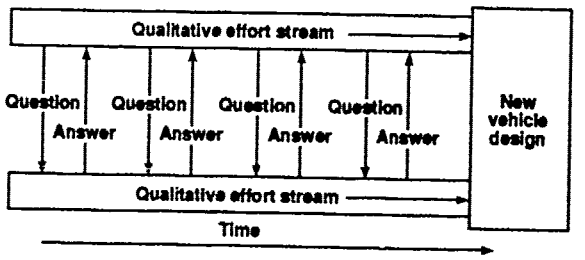

1. Qualitative and quantitative sides of a design process.

Table 2
Coupling data in aircraft system

Vector Y	Content examples
1	See the box labeled INPUT.
2	Wing area, aspect ratio, taper, sweep angle, airfoil geometry data. Engine thrust.
3	Fuel tank locations and assumed volumes.
4	Wing structural weight and internal volume.
5	Take-off Gross Weight.
6	See box 6.
7	Landing gear weight and location, in stowed and extended position. Take-off field length.

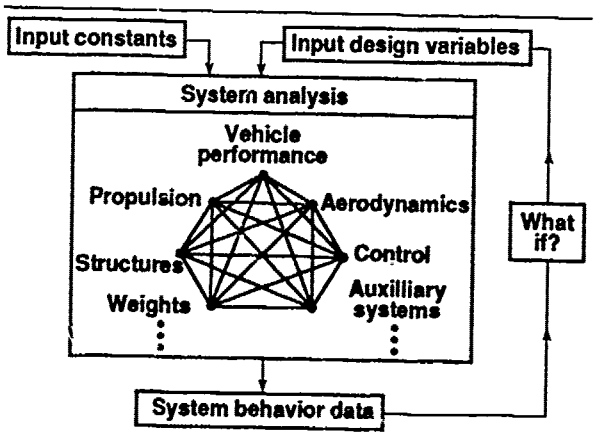

2. Interactions in a system analysis and "What if" questions.

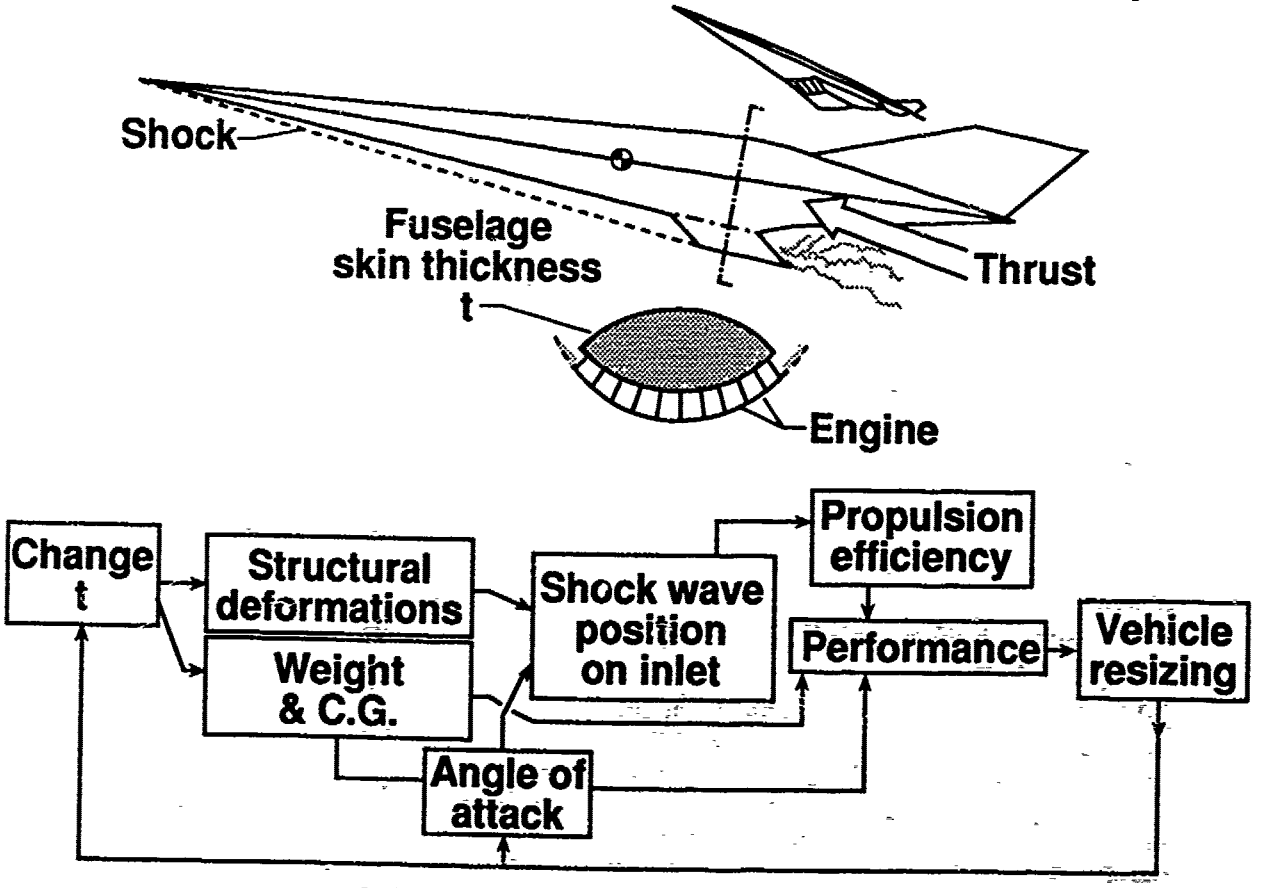

3. A design change triggering a complex chain of effects.

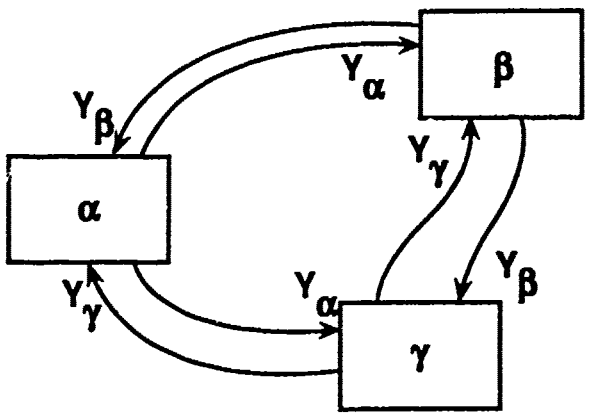

4. Example of a three component system.

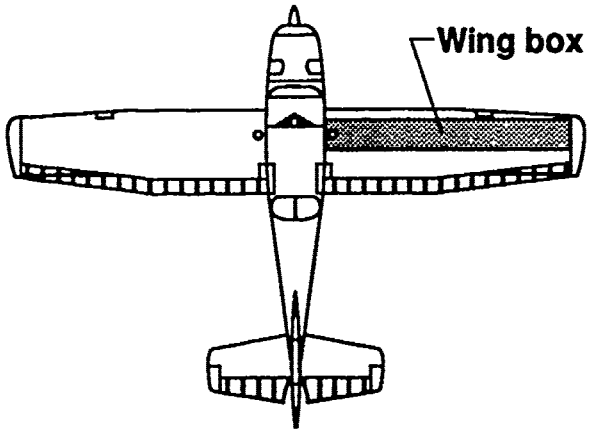

5. Wingbox in aircraft wing.

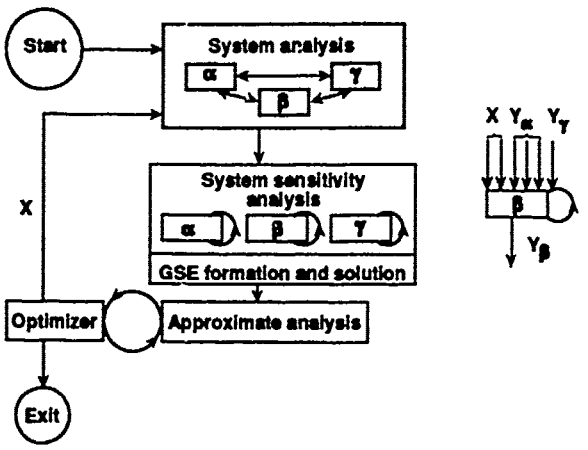

7. Flowchart of the System Optimization procedure (SOP).

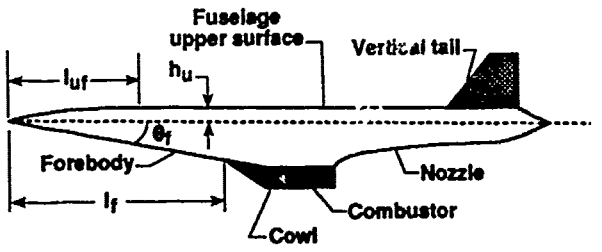

8. Hypersonic aircraft; some of the configuration design variables.

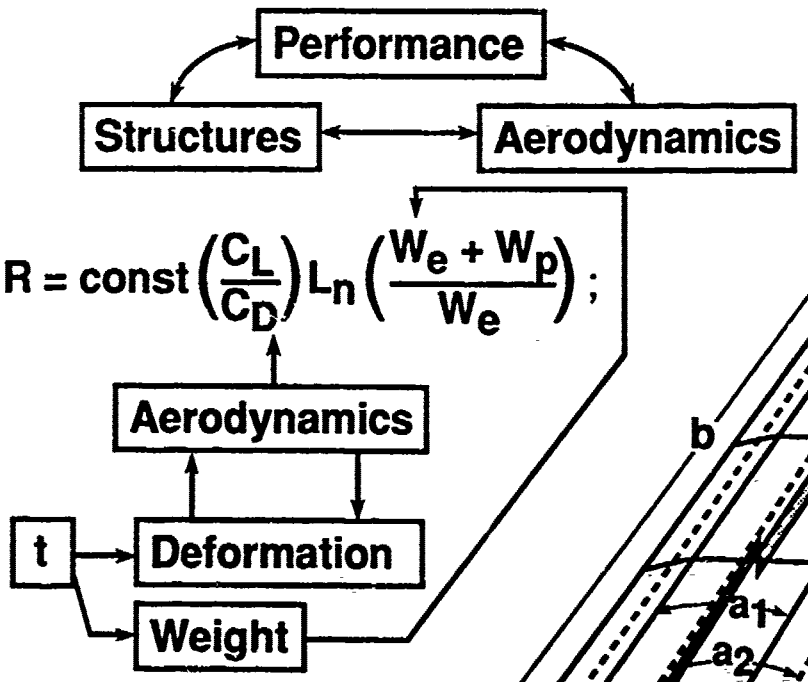

6. a) System of mathematical models, the Breguet formula, and the channels of influence for the wing cover thickness;

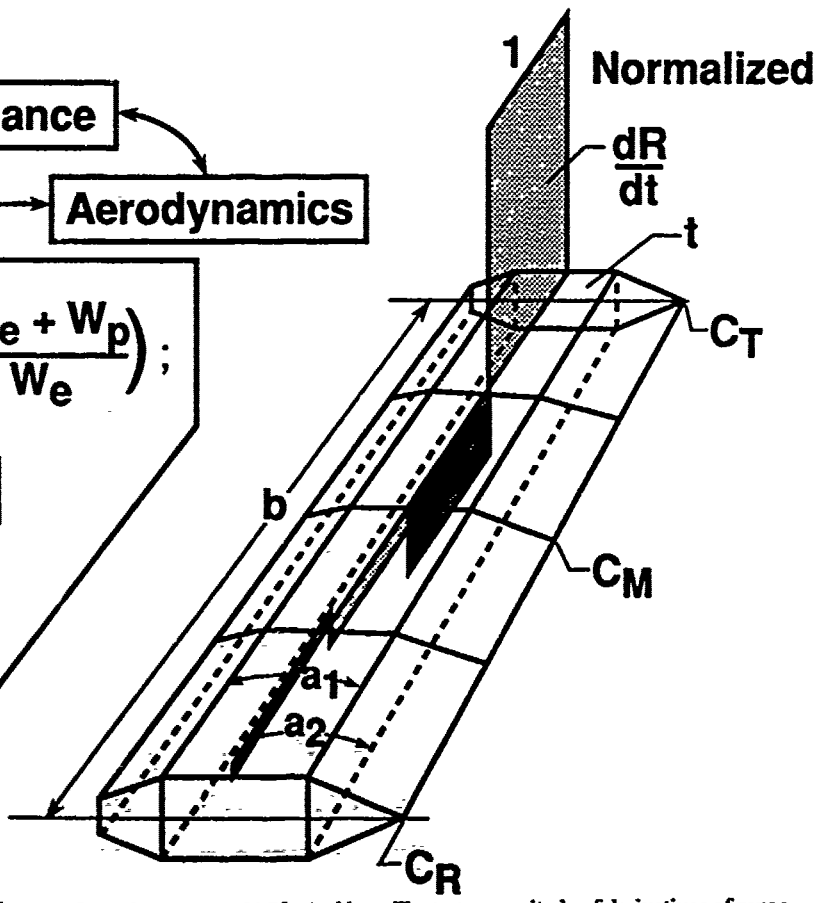

b) Vertical bars illustrate magnitude of derivatives of range with respect to thickness.

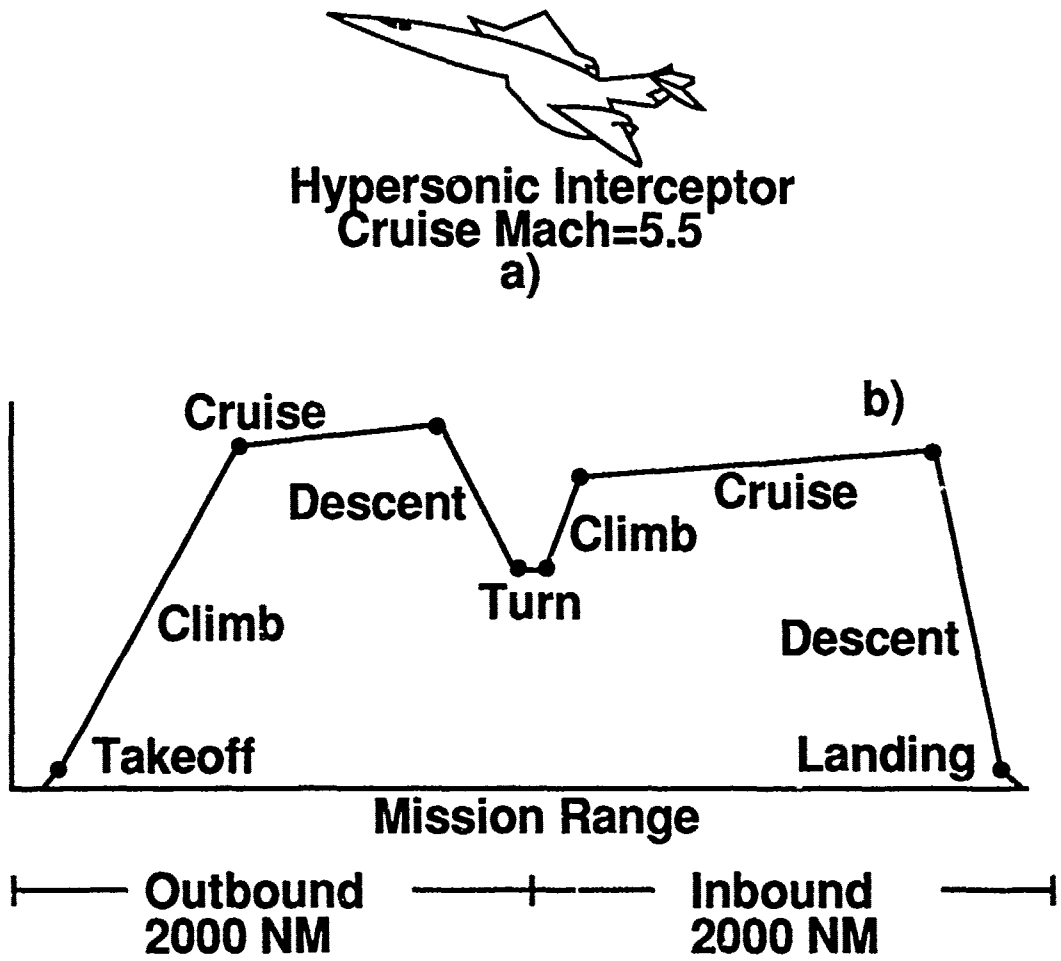

9. a) Hypersonic interceptor; b) Mission profile.

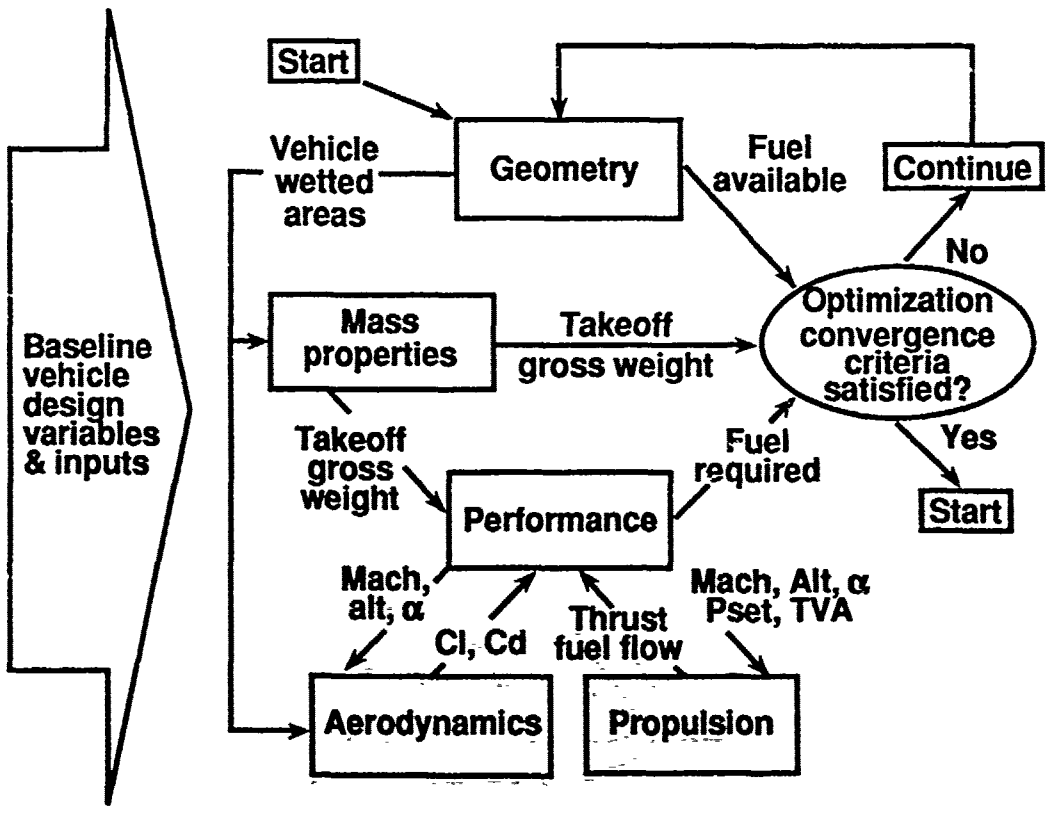

10. System of mathematical models for hypersonic interceptor optimization.

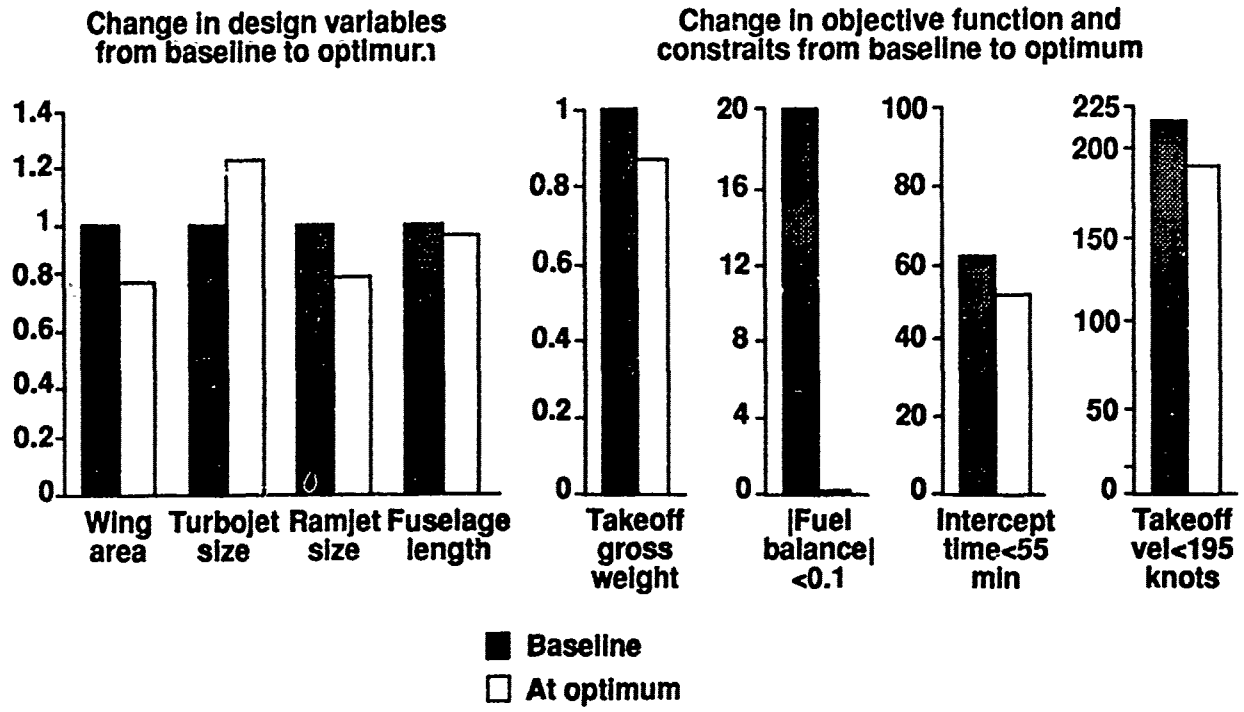

11. Sample results from hypersonic interceptor optimization.

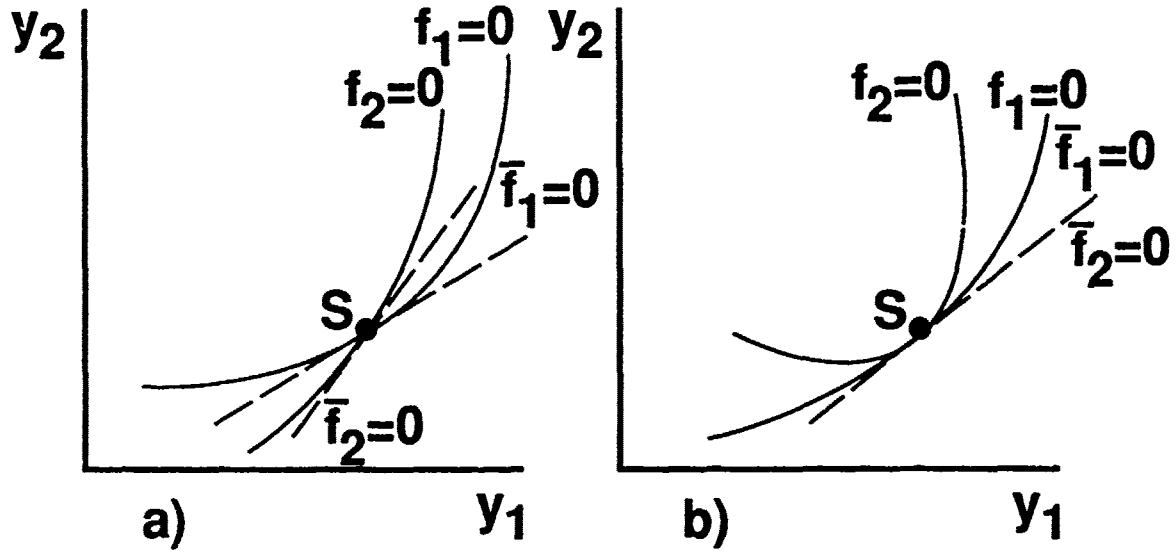

12. System solution: a) Intersection point; b) Tangency point.

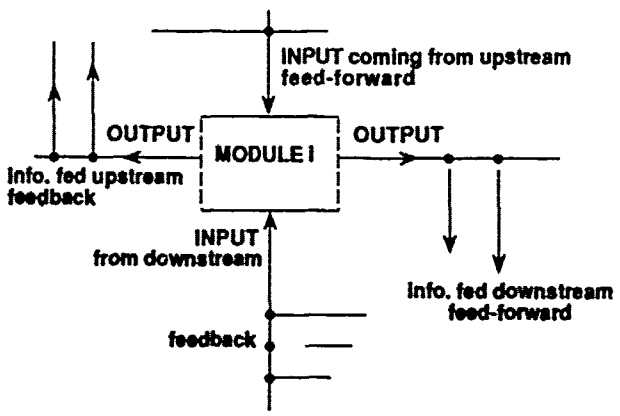

13. Schematic definition of a module.

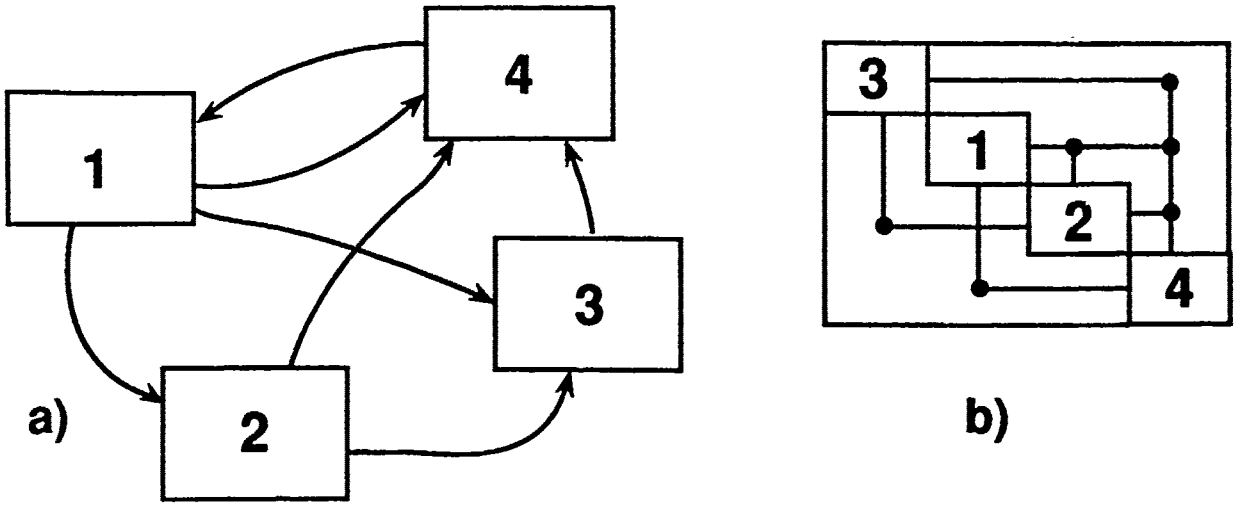

14. Example of a system: a) Graph format; b) N-square Matrix format.

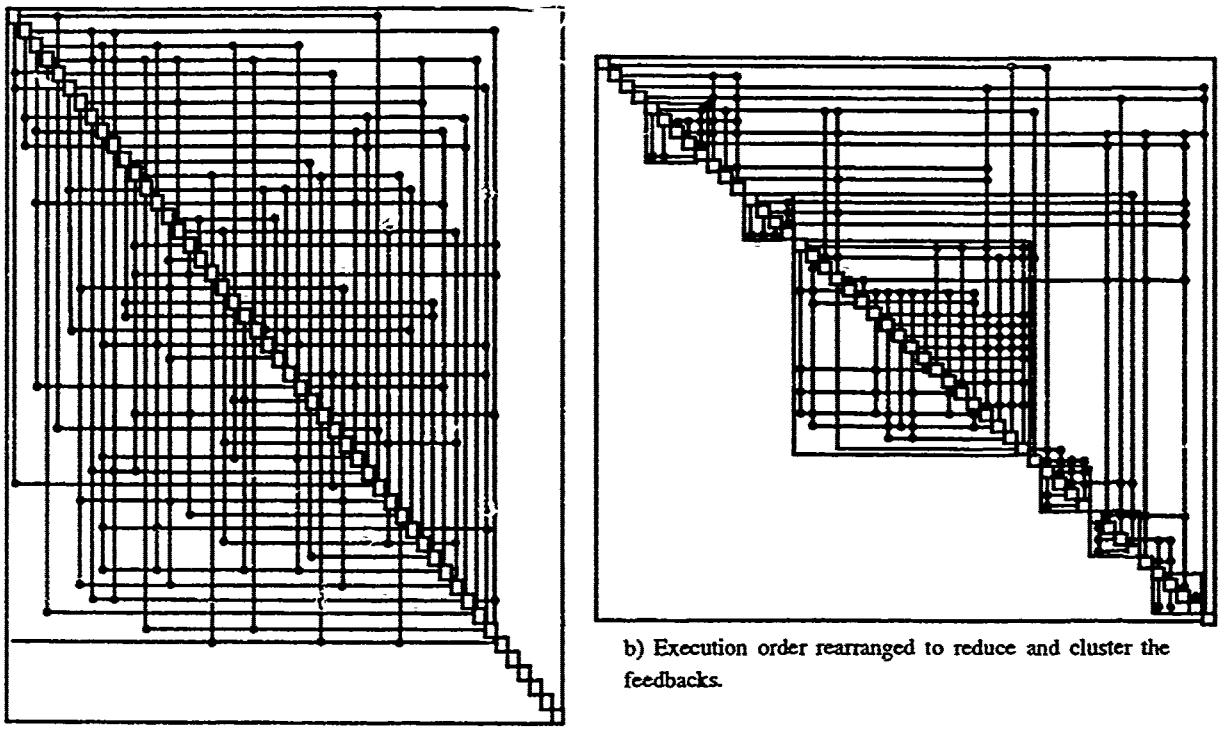

b) Execution order rearranged to reduce and cluster the feedbacks.

15. System *N*-square Matrix: a) Random execution order;

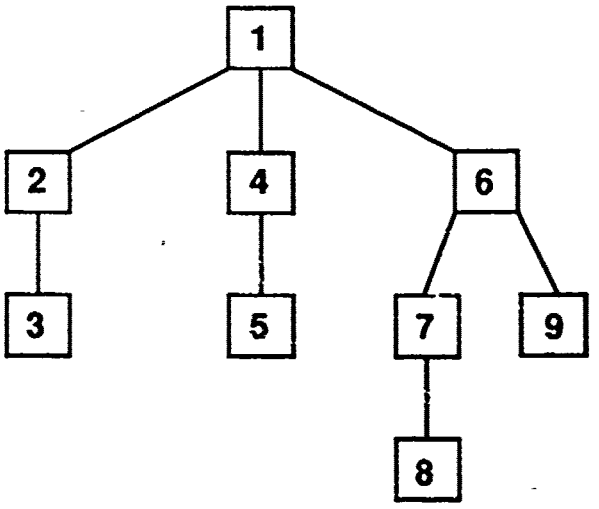

16. Hierarchic structure of clusters in a system.

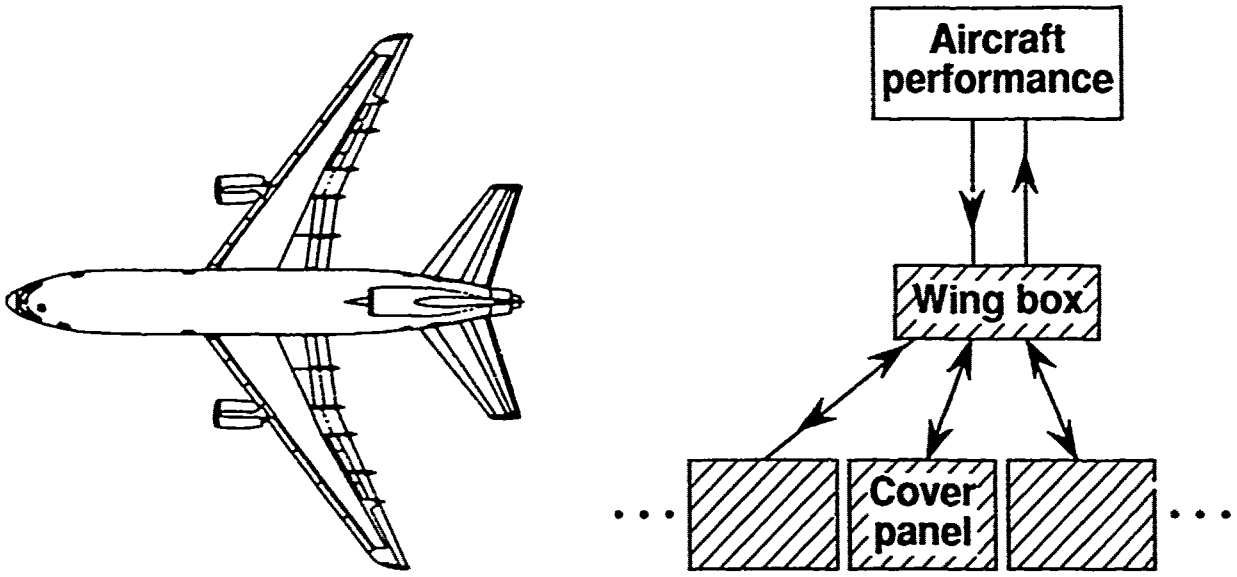

17. Optimization of a transport aircraft: a) Configuration; b) Hierarchic system of modules.

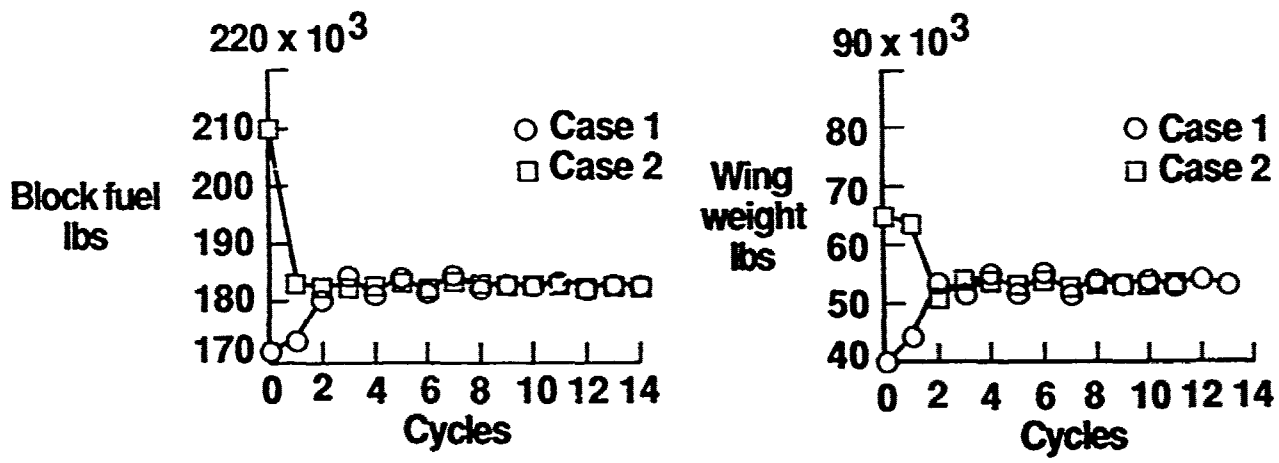

18. Sample of results from transport aircraft optimization.

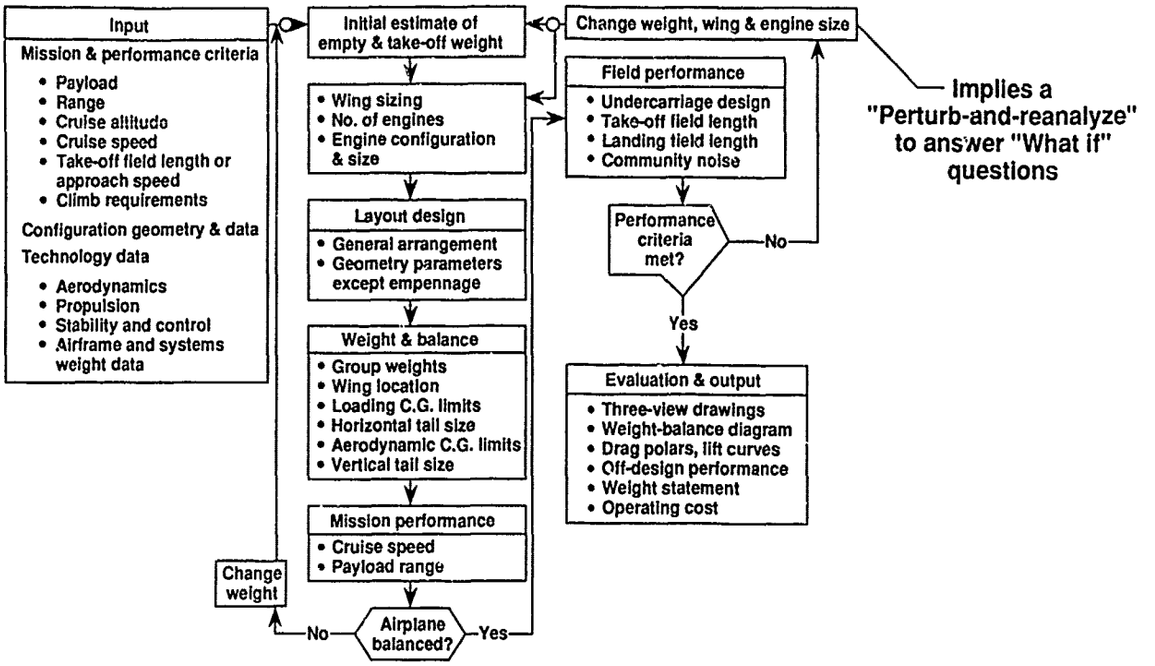

19. A conventional, sequential design process for aircraft.

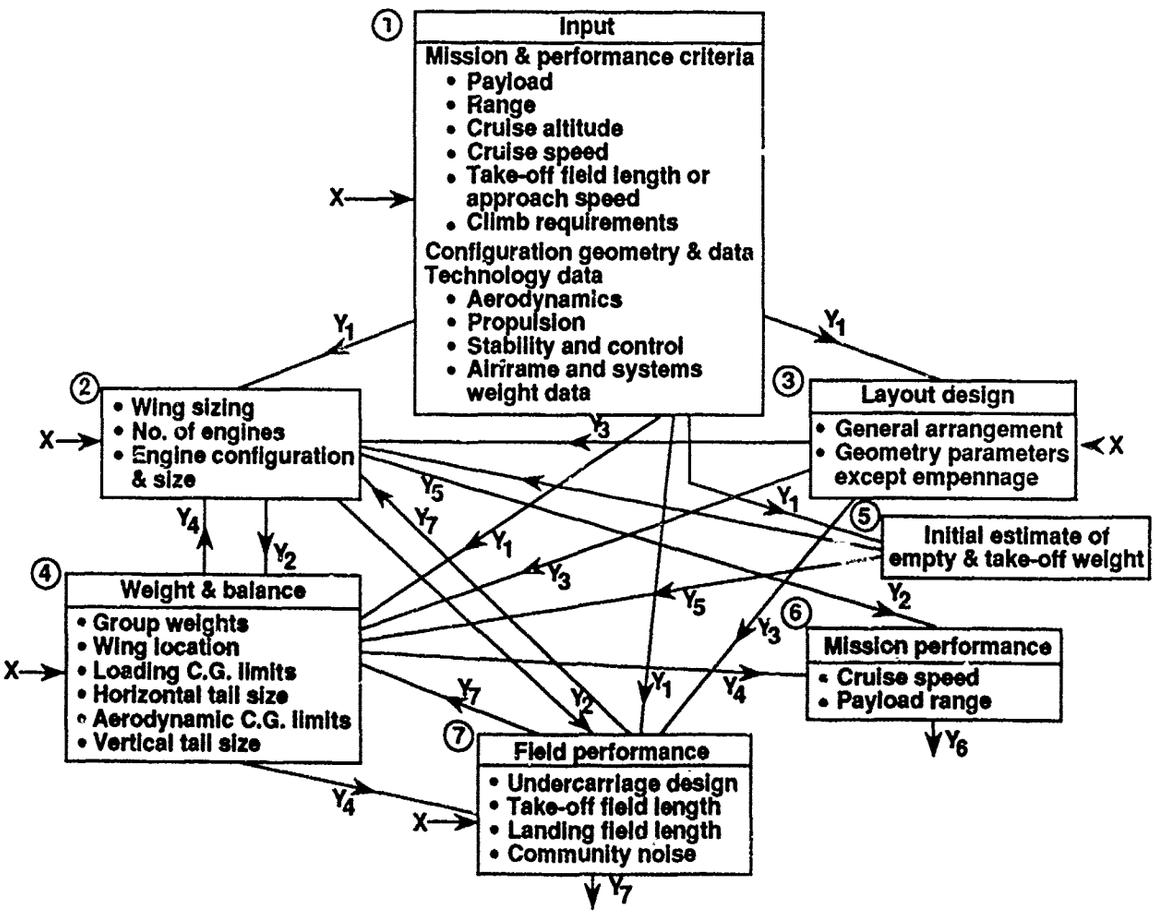

20. Black boxes from Fig. 19 forming a system.

- System sensitivity equations of design represented as coupled system

$$\begin{bmatrix} I & 0 & 0 & 0 & 0 & 0 & 0 \\ -Y_{21} & I & -Y_{23} & -Y_{24} & -Y_{25} & 0 & -Y_{27} \\ -Y_{31} & 0 & I & 0 & 0 & 0 & 0 \\ -Y_{41} & -Y_{42} & -Y_{43} & I & -Y_{45} & 0 & -Y_{47} \\ -Y_{51} & 0 & 0 & 0 & I & 0 & 0 \\ 0 & -Y_{62} & 0 & 0 & -Y_{65} & I & 0 \\ -Y_{71} & -Y_{72} & -Y_{73} & -Y_{74} & 0 & 0 & I \end{bmatrix} \begin{Bmatrix} \frac{dY_1}{dX_k} \\ \frac{dY_2}{dX_k} \\ \frac{dY_3}{dX_k} \\ \frac{dY_4}{dX_k} \\ \frac{dY_5}{dX_k} \\ \frac{dY_6}{dX_k} \\ \frac{dY_7}{dX_k} \end{Bmatrix} = \begin{Bmatrix} \frac{\partial Y_1}{\partial X_k} \\ \vdots \\ \frac{\partial Y_i}{\partial X_k} \\ \vdots \end{Bmatrix} \begin{Bmatrix} \frac{\partial Y_1}{\partial X_L} \\ \vdots \\ \frac{\partial Y_i}{\partial X_L} \\ \vdots \end{Bmatrix} \cdots$$

- These system derivatives answer "What if" questions regarding these variables without reanalyzing the system

21. GSE matrix for the system of Fig. 20.

SENSITIVITY ANALYSIS OF DYNAMIC AEROELASTIC RESPONSES

Rakesh K. Kapania*
Virginia Polytechnic Institute And State University
Blacksburg, VA 24061,U.S.A.

1. SUMMARY

This paper summarizes ongoing research on the sensitivity analysis of dynamic aeroelastic response of wings. Two approaches are being used to express the unsteady aerodynamic loads, namely: (1) the frequency-domain approach and the (2) the state-space approach. The frequency domain approach is demonstrated on a 3-D box wing and the state-space domain approach is demonstrated on a simple 2-D sectional (i.e. a rigid airfoil supported by torsional and rotational springs, respectively) model. For the 3-D box wing structure, equivalent plate analysis is used to model the structure of the wing and a modified strip theory is used to obtain the unsteady aerodynamic loads. For the 2-D sectional model a recently proposed state-space model of the unsteady aerodynamics loads acting on an airfoil is used. For the 3-D wings, results are obtained for the sensitivity of the dynamic aeroelastic responses (flutter speed, flutter frequency and the reduced frequency) to various shape parameters namely, aspect ratio, taper ratio, surface area, and sweep angle. Three different methods are used to find these sensitivities, namely: (i) a purely finite difference approach; (ii) a semi-analytical approach in which an analytical expression is used for calculating the sensitivity of an eigenvalue of the complex-valued aeroelastic matrix, but the derivatives of various components of this matrix (i.e. the mass, stiffness, and aerodynamic matrices) are obtained using the finite difference; and (iii) a semi-analytical approach that differs from the approach number (ii) in the sense that the sensitivity of the aerodynamic matrix is now obtained analytically. A good agreement is seen between the three sets of results. For the 2-D sectional model, the results for the sensitivities of the flutter speed with respect to various parameters (the two natural frequencies, mass ratio, static unbalance, the radius of gyration and the distance between mid chord and the elastic axis) are obtained.

2. INTRODUCTION

Flutter, an aeroelastic instability, is a self-sustaining oscillation that involves a coupling between inertial, elastic, and aerodynamic forces. The flutter analysis capabilities have been available for well over four decades. Yates[1] developed a modified strip analysis to analyze flutter characteristics for finite-span swept and unswept wings at subsonic and supersonic speeds. The method is still used today to calculate the lift and moment forces. For example, Landsberger and Dugundji[2] used these expressions, with a modification for camber effects given by Spielberg[3], to study the flutter and divergence of a composite plate. The present day computers allow complex aerodynamic programs to be developed and used.[4–6] But these codes can not be used at early design stage where a large number of aeroelastic analyses are needed. Approximate unsteady aerodynamic models are still being used at the design stage.

It would be advantageous for the designer to have a mathematical tool which can be used to predict the changes in flutter with the changes in basic shape parameters. Sensitivity analysis was first recognized as a useful tool for assessing the effects of changing parameters in mathematical models of control systems. The gradient based mathematical programming method used in optimal control and structural optimization furthered the development of sensitivity derivatives, because sensitivity derivatives are used in search directions to find optimum solution.[7] Sensitivity analysis has also become a versatile design tool, rather than just an instrument of optimization programs.[8]

Shape sensitivity analysis of any physical system under aeroelastic loads can be important for different reasons: (i) to understand and predict the system's response and (ii) to optimize the response of the system for a set of physical constraints. The sensitivity derivatives can be found by a finite difference or analytical methods. Analytical sensitivity analysis has found increased interest in engineering design as it eliminates uncertainty in the choice of step size needed in the finite difference method. The step size if too large leads to truncation errors and if too small leads to ill-conditioning.

*Associate Professor, Aerospace and Ocean Engineering, Senior Member AIAA.

Adelman and Haftka[8] have shown that structural sensitivity analysis has been available for over two decades. Structural sensitivity analysis has been sufficient in the past because sizing variables such as plate thickness and cross-sectional areas affect the mass and stiffness properties of the airframe but, not its basic geometry. Therefore, aerodynamic sensitivity analysis capability has been limited in development until recently. For example, Rudisill and Bhatia[9] developed expressions for the analytical derivatives of the eigenvalues, reduced frequency and flutter speed with respect to structural parameters for use in minimizing the total mass.

Pedersen and Seyranian[10], examined the change in flutter load as a function of change in stiffness, mass, boundary conditions or load distribution. They showed how sensitivity analysis can be performed without any new eigenvalue analysis. The solution to the main and an adjoint problem provide all the necessary information for evaluating sensitivities. Their paper mainly focused on column and beam critical load distributions.

Hawk and Bristow[6] developed aerodynamic sensitivity analysis capabilities in subcritical compressible flow. They first analyzed a baseline configuration, and then calculated a matrix containing partial derivatives of the potential at each control point with respect to each known geometric parameter by applying a first-order expansion to the baseline configuration. The matrix of partial derivatives is used in each iteration cycle to analyze the perturbed geometry. However, this analysis only handles chordwise perturbation distributions, such as changes in camber, thickness and twist. A new approach, which is still under development, has been proposed by Yates[11] that considers general geometric variations, including planform, and subsonic, sonic and supersonic unsteady, nonplanar lifting-surface theory.

Barthelemy and Bergen[12] explored the analytical shape sensitivity derivatives of the wing's aeroelastic characteristics, such as section lift, angle of attack, rolling moment, induced drag, and divergence dynamic pressure, for subsonic subcritical flow, with respect to geometric parameters. Results showed the characteristics nonlinearity to be small enough to be well approximated by sensitivity based linear approximations. These approximations are valid within a range that is useful to designers in the initial design phase.

The present work details the theoretical and computational derivation of a method to obtain the sensitivity of a wing flutter response to changes in its geometry. Specifically, the object is to determine the derivatives of flutter speed and frequency with respect to wing area, aspect ratio, taper ratio, and sweep angle. The present study uses a structural formulation which was originally formulated at the NASA Langley Research Center by Giles.[13] The program is based upon a Raleigh-Ritz formulation in which the displacement functions are made up of polynomial expressions. The aerodynamic formulation used in this study was developed by Yates,[1,11] The expression for lift and moment are derived from potential flow theory and have been modified to account for finite span.

The structural and aerodynamic formulation were validated using examples found in other works. Once there was sufficient confidence in the flutter speed prediction capabilities, sensitivity analyses to predict the flutter speed for changes in the geometric shape parameters was performed. Three different approaches were used to obtain the sensitivities of the flutter speed; the frequency; and the reduced frequency to various shape parameters. The three approaches are: (i) a purely numerical approach using the finite difference method; (ii) a semi-analytical method that uses an analytic expression given in Ref. 14 for calculating the sensitivity of the eigenvalues of a generalized eigenvalue problem and a finite difference approximation of the derivatives of the aerodynamic, mass and stiffness matrices with respect to the geometric parameters; and (iii) an analytic approach that uses the analytic expression for calculating the sensitivity of the eigenvalues and an analytically derived expression for the sensitivity of the aerodynamic matrix with respect to geometric parameters. The results obtained using the three approaches were compared and were found to be in good agreement with each other and also with those obtained from complete reanalysis.

Anticipating the future need for obtaining the sensitivity of the flutter characteristics and the stability margins for the aeroservoelastic design, it is desirable to express the unsteady aerodynamic loads in the state-space form.[15–16] In this form, the unsteady aerodynamics is represented by a set of first-order ordinary differential equations. These equations can be easily integrated with the first order differential equations that govern the structural (and control) behavior. The stability of the aeroelastic system can then be obtained either by performing an eigenvalue analysis or by time integration of the combined aeroelastic equations.[17] The state-space aerodynamic model as given in Leishman and Nguyen[14] is used to study the aeroelastic behavior of a 2-D sectional model (a rigid

wing supported elastically and allowed to plunge and pitch about the elastic axis). For this model, the sensitivity derivatives of the flutter speed are obtained for a number of pertinent variables. These are: (i) the two natural frequencies of the system; (ii) the mass ratio, (iii) distance between the elastic axis and the mid chord point; (iv) the static unbalance, and (v) the radius of gyration. Two approaches are used; namely: (1) a purely finite difference approach, and (ii) an analytical approach in which the derivatives of the aeroelastic matrix are obtained analytically. Excellent agreement was observed between the two sets of results.

3. FREQUENCY-DOMAIN ANALYSIS

Structural Modeling: This section briefly describes the structural formulation which was originally developed by Giles.[13] The program is based upon a Ritz solution technique using the energy functionals for a laminated plate which includes the bending and stretching of the reference surface. This program is capable of analyzing unsymmetric wing box sections arising from airfoil camber, laminate sequences, or different thicknesses in upper and lower covers skins.

The aerodynamic formulation restricts the chordwise length to remain straight during oscillations, therefore only high aspect ratio wings will be analyzed in this representation. Only bending and torsional deformations are considered in this analysis procedure. In the theory of plates, the Kirchhoff assumption is made that lines normal to the reference plane remain straight and normal after deformations.

The planform geometry of the wing is represented by a trapezoidal segment. To represent cranked wing boxes, multiple trapezoidal segments can be defined. Each segment has a separate local coordinate system. The local coordinates are nondimensional such that ξ refers to a fraction of the chord and η a fraction of the span as shown in Fig. 1. Figure 2 illustrates a possible geometry of the wing box and coordinate system. The mid-camber surface is measured from a reference plane. The distance, Z_c, is represented as a polynominal in the global coordinates x and y.

$$Z_c(x,y) = Z_{00}+Z_{10}x+Z_{20}x^2+Z_{01}y+\ldots+Z_{mn}x^m y^n \tag{1}$$

The depth of the wing box, $H(x,y)$ is measured from the midchord surface and the thickness $t(x,y)$ of each laminate is also defined by polynomial expressions in x and y. The expressions for the depth and thickness are:

$$H(x,y) = H_{00}+H_{10}x+H_{20}x^2+H_{01}y+\ldots+H_{mn}x^m y^n \tag{2}$$

$$t(x,y) = t_{00}+t_{10}x+t_{20}x^2+t_{01}y+\ldots+t_{mn}x^m y^n \tag{3}$$

In the present formulation, the depth of the wing box and thickness of the skins is assumed to be constant throughout. The wing box used for this presentation is shown in Fig. 3.

Displacement Function: The Rayleigh-Ritz formulation assumes a deflection shape for the wing structure. This deflection shape is a linear combination of n assumed displacement functions. The assumed displacement functions are specified as products of polynomial in the x-direction and y-direction global coordinates.

The deflection equation can also be written as:

$$\begin{aligned} W(x,y) &= \sum_{n=0}^{N}\sum_{m=2}^{M} C_{nm}\left(\frac{x}{x_{\max}}\right)^n\left(\frac{y}{y_{\max}}\right)^m \\ &= \sum_{i=1}^{NP}\gamma_i(x,y)C_i \end{aligned} \tag{4}$$

where $\gamma_i(x,y)$ is the nondimensional displacement function and NP is the number of trial functions used. All the assumed displacement functions satisfy the geometric boundary conditions for a cantilever plate. The displacement functions are nondimensional quantities in order to prevent numerical difficulties in manipulation of the matrices. For the complete description of the structural formulation, the reader is referred to Ref. 13.

Aerodynamic Model: An incompressible, 2-dimensional, unsteady strip theory, first developed by Barmby, et al.[18] and modified by Yates [11] to include the effects of finite span, was used to calculate the aerodynamic coefficients. Lift and moment forces are defined along the midchord and acting upon sections perpendicular to this midchord line (called the reference line hereafter). The flow field is represented by a uniform stream (non-circulatory component) superposed by a disturbance-velocity distribution (circulatory component) which models the effect of the position and motion of the wing such that the condition of tangential flow at the wing surface is met. The lift and moment forces can be reduced to simple expressions assuming the wing is undergoing infinitesimal harmonic oscillations about its steady-state position.[18]

$$L = -\pi\rho b^3\omega^2(B_{ch}h + B_{c\theta}\theta) \tag{5}$$

$$M = -\pi\rho b^4\omega^2(B_{ah}h + B_{a\theta}\theta) \tag{6}$$

The coefficients B_{ch}, $B_{c\theta}$, B_{ah}, and $B_{a\theta}$ are given in Reference 18. The bending deflection, h, and the torsional deflection, θ, are defined along the reference line.

Special attention must be paid when expressing the quantities which relate the aerodynamic and structural models. The aerodynamic forces and moments are derived in terms of sections perpendicular to the reference line. The displacement functions (see Eq. 4) and their derivatives define rotations parallel to the free stream flow. In order to be consistent in the formulation $\gamma_{i,x}$, $\gamma_{i,y}$, and $\gamma_{i,xy}$ must be transformed to define θ, τ, and σ in the plane perpendicular to the reference line. These transformations are as follows:

$$\theta(\tilde{x},\tilde{y}) = \sum_{i=1}^{np} C_i(\gamma_{i,x}(\tilde{x},\tilde{y})\ \cos\Lambda - \gamma_{i,y}(\tilde{x},\tilde{y})\ \sin\Lambda) \tag{7}$$

$$\tau(\tilde{x},\tilde{y}) = \sum_{i=1}^{np} C_i(\gamma_{i,x}(\tilde{x},\tilde{y})\ \sin\Lambda + \gamma_{i,y}(\tilde{x},\tilde{y})\ \cos\Lambda) \tag{8}$$

Similar expression for σ is given in Ref. 19. In Eqs. 8 and 9, Λ is the midchord sweep angle. The superscripts $\tilde{}$ represents the fact that x, y are not any arbitrary values of x and y, but $\tilde{x}$, $\tilde{y}$ are the coordinates along the reference line in x and y. Furthermore, $\tilde{x} = \tilde{y}\ \tan\Lambda$. Therefore, h, θ, τ, and σ are functions of $\tilde{y}$ only, where $\bar{y}(= \frac{y}{\cos\Lambda})$ is the distance of the point $\tilde{x}, \tilde{y}$ from the origin along the reference line. The functions h, θ, τ, and σ, which are functions of $\tilde{y}$ only are given in Ref. 19. The lift and moment forces can then be written in terms of the displacement functions $\bar{\gamma}_i(\bar{y})$ and the unknown coefficients, C_i. The expressions for lift and moment are given in Ref. 19.

Virtual Work: The lift and moment forces are nonconservative forces, therefore, the principle of virtual work was employed. The definition of virtual work gives:

$$\delta W_{NC} = \int_0^\ell L\delta h d\bar{y} + \int_0^\ell M\delta\theta d\bar{y} = \sum_{j=1}^{n} Q_j\delta C_j \tag{9}$$

where δh, and $\delta\theta$ are the virtual displacements and Q_j are the generalized forces and the δC_j are the generalized displacements. The generalized forces Q_j are defined as:

$$Q_j = \omega^2 \sum_{i=1}^{np} A_{ji}C_i \tag{10}$$

The term A_{ji} in aerodynamic matrix [A] are given in Ref. 19. It is noted that the various integrations in the expression for the aerodynamic matrix are performed numerically by a 15 point Gaussian quadrature numerical integration scheme.[20]

Flutter Analysis: The U-g method was used in computing the flutter speeds. This method introduces a structural damping coefficient g into the equations of motion. Neutral stability (flutter) is attained for a given velocity, when the damping of the structure goes to zero. Assuming harmonic motion the equations of motion become:

$$[[K](1+ig) - \omega^2[M]]\ \{C\} = \omega^2[A]\{C\} \tag{11}$$

In the absence of non-aerodynamic external forces, the resulting generalized eigenvalue problem can be written as:

$$[[I]\lambda - [B]]\ \{C\} = \{0\} \tag{12}$$

B is a generalized complex matrix, λ is the eigenvalue and $\{C\}$ is the eigenvector. The eigenvalue λ is defined as $\lambda = (1+ig)/\omega^2$, and the generalized complex matrix $[B]$ is defined as:

$$[B] = [K]^{-1}[M + A] \tag{13}$$

The flutter speed perpendicular to the midchord is given as $V_n = \left(\frac{\omega b}{k_n}\right)\cos\Lambda$.

Evaluative Analysis: The present aeroelastic formulation was first evaluated by studying various examples for which alternative results are available in literature. The evaluative process was broken down into four sections. To validate the stiffness matrix, the static deflections were checked. The mass matrix was verified by comparing the natural frequencies of vibration with isotropic as well as composite materials. Once sufficient verification of the structural model was complete, the static aerodynamic loads were checked for divergence of swept and unswept wings. The dynamic aerodynamic matrix was verified by comparing the flutter frequencies and speeds with results found by Castel and Kapania.[21] These authors developed a simple element for the aeroelastic analysis of laminated wings. Their formulation allows for unsymmetric laminations, arbitrary geometry including chord and thickness taper, and multiple sweep angles.

The comparisons made in this presentation are for a wing consisting of top and bottom flat laminated skins rigidly connected as shown in Figure 3.

For all isotropic comparisons, the material properties of the rectangular box beam were taken to be those of Aluminum: $E = 6.8948 \times 10^{10} N/m^2$, and $\nu = 0.30$. The material properties of the material used in the laminated wing are: $E_{11} = 6.9 \times 10^{10} N/m^2$; $E_{22} = 5.0 \times 10^{10} N/m^2$; $\nu_{12} = 0.28$; $G_{12} = 1.5 \times 10^{10} N/m^2$; $\rho_{mat} = 2.71 \times 10^3 kg/m^3$. It should be noted that these material properties were arbitrarily chosen.

The result for aeroelastic response of swept and unswept wings were compared with the results from two different codes: (i) a code written by Barthelemy and Bergen[12] and (ii) a code written by Castel and Kapania.[18] Barthelemy and Bergen used Weissinger's L-Method to obtain the static aerodynamic loading matrix. The wing dimensions used for comparison with the present method are: $S = 20.0\ m^2$; $AR = 10.0$; $tp = 1.0$ where tp is the taper ratio of the half wing. An excellent agreement was observed between the two sets of results.[19]

Castel and Kapania[21] used Yates' modified strip method[1] to obtain both the static and dynamic aerodynamic loadings for swept and unswept composite wings. For different values of sweep the fiber orientation was varied and the results for the divergence and flutter speed were obtained and compared with those given by Kapania and Castel.[21] A very good agreement between the two sets of results were observed for unswept wings and wings with a forward sweep of 30°. The agreement for the case of 30° sweepback was not as good. The disagreement between the two sets of results increased as the sweep angle was increased. It is felt that this disagreement is due to two different models and in the two studies, namely: (i) a skewed model used in this study and, (ii) a rotated model used by Castel and Kapania.[21]

Sensitivity Analysis Results (Frequency-Domain Analysis)

This section presents the calculation for the sensitivity of the flutter speed, flutter frequency, and reduced frequency to geometric shape parameters namely: (i) aspect ratio, (ii) surface areas, (iii) taper ratio, and (iv) sweep angle. The sensitivity calculations require the sensitivity of the aerodynamic, mass and stiffness matrices with respect to various shape parameters. A key objective of this study is to check the viability of calculating the desired derivatives using an analytical approach. It was decided to analytically obtain the sensitivities of the aerodynamic matrix. The analytical derivatives eliminate the uncertainty in the choice of step size which if too large can lead to truncation errors and if too small can lead to ill-conditioning.

To validate the expressions for the eigenvalue derivatives, these derivatives are calculated using three different methods. The first method is a purely a numerical approach that uses a finite difference approximation to find the eigenvalue derivatives. The second method is a semi-analytic approach, because the derivatives of the aerodynamic matrix are found using finite difference approximations, and then using the expression for the derivative of the eigenvalue as given in Murthy and Haftka.[14] The third (analytic) method uses an analytically derived derivative of the aerodynamic matrix, along with the eigenvalue derivative expression given in Murthy and Haftka.[14]

Eigenvalue Derivatives and Solution Procedures

In the first method of calculating the derivatives, the flutter problem is solved twice and the derivatives of the eigenvalues are approximated using a forward finite difference scheme.

The second and third methods use the expression for the eigenvalue derivative, that is derived using the main and the adjoint problem. For the i^{th} eigenvalue, λ^i, the eigenvalue derivative with respect to the shape parameter p_s is expressed as:

$$\frac{\partial \lambda^i}{\partial p_s} = \frac{\{e_l^i\}^t \frac{\partial [B]}{\partial p_s} \{e_r^i\}}{\{e_l^i\}^t \{e_r^i\}} \tag{14}$$

where $\{e_l^i\}$ and $\{e_r^i\}$ are the i^{th} left and right eigenvectors respectively; and $[B]$ is the complex matrix (see Eq. 13). The eigenvalue derivative in terms of flutter frequency, damping, and their derivatives can be easily written. To obtain the derivative of the generalized complex matrix $[B]$, the derivatives of the aerodynamic matrix $[A]$; of the inverse of the stiffness matrix $[K]^{-1}$, and of the mass matrix $[M]$ are needed. The derivatives of the mass matrix, and the inverse of the stiffness matrix are obtained using the forward finite difference method. A study was first conducted to obtain an appropriate step size for the finite difference calculations. This study indicated that the calculated derivatives are stable.

Sensitivity of Aerodynamic Stiffness Matrix. The derivatives of the aerodynamic matrix $[A]$ with respect to a geometric shape parameter are obtained using two different methods: (i) finite difference method; and (ii) analytic method. The calculation

of the sensitivity of the aerodynamic matrix $[A]$ is made difficult by the fact that this matrix depends upon shape parameters p_s and also on the reduced frequency k_n. The reduced frequency is not really an independent variable, as its value for a new value of $p_s(= p_s^{old} + \Delta p_s)$ should be such that the imaginary part of the eigenvalue corresponding to the perturbed configuration should be zero.

In the finite difference method, the sensitivity of the aerodynamic matrix $[A]$ is obtained as follows:

$$\frac{d[A]}{dp_s} = \frac{[A(p_s + \Delta p_s, k_n + \Delta k_n)] \; - \; [A(p_s, k_n)]}{\Delta p_s} \quad (15)$$

To obtain the value of Δk_n, an iterative procedure was used. As a first step, Δk_n was put equal to zero, and the sensitivity of the eigenvalue is obtained. Obviously, the imaginary part of the new eigenvalue thus obtained will not be zero. This fact is used to obtain the value of Δk_n as explained in the following.

The change in the damping coefficient g, a function of both the shape parameters and reduced frequency, can be written as:

$$dg = \frac{\partial g}{\partial p_s} dp_s + \frac{\partial g}{\partial k_n} dk_n \quad (16)$$

At flutter speed: $g = 0$; $dg = 0$. Therefore,

$$\frac{dk_n}{dp_s} = -(\partial g/\partial p_s) \; / \; (\partial g/\partial k_n) \quad (17)$$

Note that $\frac{\partial g}{\partial k_n}$ was already obtained during the calculations of the flutter speed. The values of reduced frequency are varied in the initial problem to compute the value at the point the damping coefficient goes to zero. Therefore, $\frac{\partial g}{\partial k_n}$ is easily computed by a forward finite difference scheme. The value of $\frac{\partial g}{\partial p_s}$ is obtained from the imaginary part of the sensitivity of the eigenvalue obtained in the first step. This is computed directly from the eigenvalue derivative. The term $\partial g/\partial p_s$ can be obtained as

$$\frac{\partial g}{\partial p_s} = imag\left(\frac{\partial \lambda}{\partial p_s}\right) \omega^2 \; + \; \frac{2\frac{\partial \omega}{\partial p_s}}{\omega} \quad (18)$$

where ω is obtained from the original flutter problem and $\partial\omega/\partial p_s$ can be obtained from ω and $\partial\lambda/\partial p_s$. If $\frac{\partial g}{\partial p_s}$ is not within a tolerance of 10^{-6}, the aerodynamic matrix $[A]$ is recalculated at a new value of the reduced frequency while also keeping the same perturbation in the shape parameter. One $\frac{dk_n}{dp_s}$ is known, an approximation to the value of k_n, corresponding to flutter speed for a new value of p_s, is obtained as: $k_n^{new} = k_n^{old} + (dk_n/dp_s)\Delta p_s$. This process is repeated until the tolerance is met.

In the "analytical" method, the sensitivity of the generalized complex matrix $[B]$ is obtained in a similar fashion except that the sensitivity of the aerodynamic matrix $[A]$ is computed analytically. This is expressed as follows:

$$\frac{d[A]}{dp_s} = \frac{\partial[A]}{\partial p_s} + \frac{\partial[A]}{\partial k_n} \frac{dk_n}{dp_s} \quad (19)$$

Both $\frac{\partial[a]}{\partial p_s}$ and $\frac{\partial[A]}{\partial k_n}$ were derived in this study. The value of $\frac{dk_n}{dp_s}$ is computed from the eigenvalue derivative, as explained above. In the first iteration, $\frac{dk_n}{dp_s}$ is assumed to be zero. The aerodynamic matrix derivative is computed and combined with the derivatives of the mass $[M]$, inverse stiffness matrices $[K]^{-1}$ to form $\frac{\partial[B]}{\partial p_s}$. The eigenvalue derivative is then computed.

The derivatives of the displacement function with respect to a general shape parameter p_s are given as follows:

$$\frac{\partial}{\partial p_s} = \frac{\partial}{\partial x} \frac{\partial x}{\partial p_s} + \frac{\partial}{\partial y} \frac{\partial y}{\partial p_s} \quad (20)$$

The global coordinates x and y are given in terms of the local coordinates and the geometric shape parameters.[19] The derivatives of x and y with respect to various geometric shape parameters are given in Ref. 19 along with the derivatives of the halfchord with respect to the same parameters.

The aerodynamic coefficients are functions of the reduced frequency. The reduced frequency changes as the shape parameters change therefore these terms are functions of the shape parameters and must be included in the formulation. The derivatives of aerodynamic coefficients with respect to the reduced frequency are given in Ref. 19.

The "analytic" derivative of the eigenvalue with respect to various parameters, namely the surface area S, the aspect ratio AR, the taper ratio tp and sweep were compared with those obtained using the two previously described methods, namely: (i) the purely finite differency method and (ii) a

semi-analytic approach in which the desired derivatives were obtained using a forward finite difference scheme. The results are shown in Table 1. An excellent agreement exists between the various sets of results. The "analytically obtained" derivative (case (iii)) is about 6.95 percent more than that obtained using a purely finite difference approach (case (i)). Similarly, the value of the same derivative obtained using a semi-analytic approach (case (ii)), is about 9.36 percent less than that obtained using the analytic approach.

4. STATE SPACE APPROACH

In recent years, considerable efforts are being made to integrate the aerodynamic, structural and control aspects of the design of an aircraft. Since the control and the structural dynamic behaviors can easily be expressed in terms of the state-space form (i.e. in terms of a set of first-order ordinary differential equations in time), it is desireable that the unsteady aerodynamic loads be also expressed in the same form. In recent years, considerable efforts have been made in that direction.

In the state-space form, any linear continuous dynamical system is expressed as[22]:

$$\{\dot{x}\} = [A]\{x\} + [B]\{u\} \tag{21}$$

$$\{y\} = [C]\{x\} + [D]\{u\} \tag{22}$$

where $\{x\}$ is an ordered set of n variables required to completely describe the state of the system at a given time; $\{u\}$ is a real-valued vector of m input or control variables; and $\{y\}$ is a real-valued vector of r system outputs; and $[A]$, $[B]$, $[C]$, and $[D]$ are matrices of dimension $n \times n$, $n \times m$, $r \times n$, and $r \times m$ respectively.

State-Space Representation of Aerodynamic Loads:

In the previous section on Frequency-Domain Approach, the aerodynamic loads on an oscillating airfoil were represented in terms of the Theodorsen's function. An alternative approach is the Wagner's function approach; in that the aerodynamic loads on an airfoil given an impulsive motion at speed U are obtained as a function of time. This approach is also called the Indicial Function Approach. The Indicial or the Wagner's function ϕ is given as[23]

$$\phi(\tau) = 1 - \int_0^\infty \left[(K_0 - K_1)^2 + \pi^2(I_0 + I_1)^2\right]^{-1} e^{-\tau x} x^{-2} dx \tag{23}$$

where $\tau = Ut/b$ is a nondimensional quantity proportional to time t, b is the semichord of the airfoil, I_0, I_1; and K_0, K_1 are modified Bessel functions of the first and second kind, respectively. The circulatory lift L_C, on an airfoil strip of unit span, having a vertical translation h called plunging, (positive downwards) and rotation α, called pitching, (positive nose up) about an axis located at a distance $a_h\, b$ from the mid-chord point (a_h being positive towards the trailing edge) can be written as

$$L_C(\tau) = 2\pi b U^2 \int_{-\infty}^{\tau} \phi(\tau - \tau_0) \left[\alpha'(\tau_0 + \frac{1}{b}h''(\tau_0) + \left(\frac{1}{2} - a_h\right)\alpha''(\tau_0)\right] d\tau_0 \tag{24}$$

Since the expression for $\phi(\tau)$ as given in Eq. 23 is quite complicated, a two-pole simplified form of ϕ given by Jones:

$$\phi(\tau) = 1.0 - 0.165 exp(-0.0455\tau) - 0.335 exp(-0.300\tau) \quad \tau > 0 \tag{25}$$

is often used.

Note that the Wagner's function and the Theodorsen's function are related to each other; the latter being the Fourier Transform of the former.

The unsteady aerodynamic loads can be represented still in another form, the state-space approach. Using this approach Jones' 2-pole approximation give rise to a single dynamical system that can be expressed as[15]

$$\begin{Bmatrix} \dot{x}_1 \\ \dot{x}_2 \end{Bmatrix} = \begin{bmatrix} 0 & 1 \\ \tilde{a} & \tilde{b} \end{bmatrix} \begin{Bmatrix} x_1 \\ x_2 \end{Bmatrix} + \begin{Bmatrix} 0 \\ 1 \end{Bmatrix} \alpha_{3/4}(t) \tag{26}$$

with the normal force coefficient of the circulatory lift $C_{N_C}(t)$ given as:

$$C_{N_C}(t) = 2\pi \left[\begin{bmatrix} \tilde{c} & \tilde{d} \end{bmatrix} \begin{Bmatrix} x_1 \\ x_2 \end{Bmatrix} + 0.5\, \alpha_{3/4}(t) \right] \tag{27}$$

where $\tilde{a} = -0.01375[U/b]^2$; $\tilde{b} = -0.3455(U/b)$; $\tilde{c} = .006825\ (U/b)^2$; and $\tilde{d} = 0.10805(U/b)$. Note that 2π is the lift curve slope for incompressible flow. This can be replaced by the actual slope of the lift curve.

It is noted that the Jones' approximation represents the exact frequency response (Theodorsen's function) within a very few percents. Accuracy of such approximations of the indicial function can be improved by increasing the number of poles in the representation. Venkatesan and Friedmann[16] have given a three-pole indicial response function that can

express the Theodorsen's function over the entire reduced frequency range.

Aeroelastic Equations: The governing equations of a 2-D rigid model, elastically supported and allowed to plunge and pitch can be written as:[23]

$$m\ddot{h} + s\ddot{\alpha} + k_h\, h \;=\; Q_h(t) \tag{28}$$

$$s\ddot{h} + I_\alpha\ddot{\alpha} + k_\alpha\, \alpha \;=\; Q_\alpha(t) \tag{29}$$

Let ω_h and ω_α are the natural frequencies (in Rad/sec) of the system in bending and torsion respectively; $\omega_h = \left(\frac{k_h}{m}\right)^{\frac{1}{2}}$, $\omega_\alpha = (k_\alpha/I_\alpha)^{\frac{1}{2}}$, s = wing static moment about the elastic axis, and a dot represents derivative with respect to time.

In Eqs. (28) and (29), Q_h (t) and $Q_\alpha(t)$ are the externally applied force and moment. In general, Q_h and Q_α will include the both aerodynamic and mechanical forces and moments. If we restrict our attention to aerodynamic forces only, and use the nondimensional time $\tau = Ut/b$, we obtain

$$m\frac{U^2}{b^2}h'' + \frac{sU^2}{b^2}\alpha'' + m\omega_h^2\, h = -L(\tau) \tag{30}$$

$$s\frac{U^2}{b^2}h'' + I_\alpha\frac{U^2}{b^2}\alpha'' + I_\alpha\omega_\alpha^2\alpha = M(\tau) \tag{31}$$

where a prime represents derivative with respect to the nondimensional time τ. Let $\xi = h/b$, the nondimensional displacement; Eq. 30 can be written as:

$$\xi'' + x_\alpha\, \alpha'' + K_h^2\xi + \frac{C_{N_C}}{\pi\mu} + \frac{\alpha'}{\mu} = 0 \tag{32}$$

where $\mu = m/\pi\rho b^2$ is the mass ratio, $x_\alpha = s/mb$ is the non-dimensional distance representing the dynamic coupling between the plunging and pitching motions, $K_h^2 = \omega_h^2 b^2/U^2$, and C_{N_C} is the lift coefficient of the circulatory lift.

Similarly, the governing equation for the equilibrium in pitching can be written as:

$$x_\alpha\xi'' + r_\alpha^2\, \alpha'' + r_\alpha^2\, K_\alpha^2\, \alpha - \frac{2}{\mu}\,\frac{C_m(\tau)}{\pi} = 0 \tag{33}$$

where $r_\alpha = (I_\alpha/mb^2)^{1/2}$ is the radius of gyration in semichords; and $C_m(\tau)$ is the moment coefficient, and $K_\alpha^2 = \omega_\alpha^2 b^2/U^2$. It is noted that the contribution of the terms related to the apparent mass of the air to the lift and moment is neglected in this study.

Let $\tilde{x}$, and $\tilde{x}_2$ be the two states describing the dynamics of the unsteady loads, such that

$$\tilde{x}_1 = \left(\frac{U}{b}\right)^2 x_1 \tag{34}$$

$$\tilde{x}_2 = \left(\frac{U}{b}\right) x_2 \tag{35}$$

where x_1 and x_2 are defined in Eqs. 26, and 27. The dynamics of unsteady loads can now be written as

$$\begin{Bmatrix}\tilde{x}_1' \\ \tilde{x}_2'\end{Bmatrix} = \begin{bmatrix}0 & 1 \\ A & B\end{bmatrix}\begin{Bmatrix}\tilde{x}_1 \\ \tilde{x}_2\end{Bmatrix} + \begin{Bmatrix}0 \\ 1\end{Bmatrix}\alpha_{3/4}(\tau) \tag{36}$$

and

$$C_{N_C}(\tau) = 2\pi\left[\begin{bmatrix}C & D\end{bmatrix}\begin{Bmatrix}\tilde{x}_1 \\ \tilde{x}_2\end{Bmatrix} + 0.5\alpha_{3/4}(\tau)\right] \tag{37}$$

where $A = -0.01375$, $B = -0.3455$, $C = .006825$ and $D = .10805$.

Combining the structural (Eqs. 32 and 33) and the aerodynamic (Eqs. 36 and 37) equations, we obtain the governing equations, which can be written as

$$[M]\{X''\} + [C]\{X'\} \;+\; [K]\{X\} = \{0\} \tag{38}$$

where

$$[M] \;=\; \begin{bmatrix}\mu & \mu x_\alpha & 0 \\ \mu x_\alpha & \mu r_\alpha^2 & 0 \\ 0 & 0 & 1\end{bmatrix}$$

$$[C] \;=\; \begin{bmatrix}1 & (\frac{3}{2} - a_h) & 2D \\ -(1+2a_h) & -(1-2a_h)a_h & -2D(1+2a_h) \\ -1 & -(\frac{1}{2} - a_h) & B\end{bmatrix}$$

$$[K] \;=\; \begin{bmatrix}\mu K_h^2 & 1 & 2C \\ 0 & -(1+2a_h) + \mu r_\alpha^2 K_\alpha^2 & -2C(1+2a_h) \\ 0 & -1 & A\end{bmatrix}$$

and $$\{X\} \;=\; \begin{Bmatrix}\xi \\ \alpha \\ \tilde{x}_1\end{Bmatrix}$$

The prime indicates the derivative with respect to nondimensional time τ. Note that Eq. 36 is included in Eq. 38 as a second order ordinary differential equation.

These equations can be easily written in the state-space form as

$$\{\dot{q}\} \;=\; [\bar{A}]\,\{q\} \tag{39}$$

where $\{q\}$ consists of ξ, α, $\tilde{x}_1$ and their derivatives with respect to non-dimensional time τ, and

$$[\bar{A}] \;=\; \begin{bmatrix}0 & I \\ -[M]^{-1}[K] & -[M]^{-1}[C]\end{bmatrix} \tag{40}$$

The flutter characteristics of Eq. 39 are found by calculating the complex eigenvalues of $[\bar{A}]$ at various values of dynamic pressure. The flutter occurs at the lowest value of the dynamic pressure for which the real part $Re(\lambda_f)$ of any eigenvalue becomes positive. The sensitivity of the flutter speed with respect to any parameter can then be found using the method described earlier.

In this study the flutter calculations were performed for the example given in Ref. 23. The base data is $\mu = 76$, $a_h = -0.15$, $x_\alpha = 0.25$, $r_\alpha^2 = 0.388$, $b = 5in.$, $\omega_\alpha = 64.1$ rad/sec., and $\omega_h = 55.9$ radians per sec. Good agreement was achieved between the present results and those given in Ref. 23. For example, the present analyses yielded a flutter speed of 89.63 ft/sec. as opposed to a flutter speed of 90.8 ft/sec given in Ref. 23. The derivatives of the flutter speed with respect to various governing parameters, namely: ω_h, ω_α, x_α, r_α, μ, and a_h were obtained. The results for the sensitivity of the flutter speed with respect to these parameters are given in Table 2. Two different techniques are used; namely: (1) using Eq. 14 and analytical derivatives of the matrices $[M]$, $[C]$, and $[K]$; and (2) using a purely finite difference approach. In the latter approach, the flutter derivatives are obtained by slightly perturbing the system and recalulating the flutter speed. Forward finite difference approach was used to calculate the sensitivity of the flutter speed. For each variable, the sensitivity of the flutter speed was obtained using three different step sizes; 1%, .1% and 0.01%. It is seen that the derivative due to radius of gyration is very sensitive to the step size. But in all cases, results obtained using a step size of 0.01% are in very good agreement with those obtained by the analytical approach.

5. CONCLUDING REMARKS

A method for analyzing the dynamic aeroelastic behavior of a laminated wing has been developed. The aerodynamic formulation was taken from Yates' modified finite strip method. This was combined with Giles' equivalent plate model which is capable of analyzing cranked wing box structures. Three different approaches were used to obtain the sensitivity of the flutter speed, frequency, and reduced frequency. The first was a purely numerical approach using finite difference method. The second used the analytic expressions for the derivative of the eigenvalue and a finite difference method to calculate the derivatives of the aerodynamic, mass and stiffness matrices. The third method also used analytical expressions for the eigenvalue derivative but the derivative of the aerodynamic matrix is computed analytically.

It was shown that the eigenvalue derivatives for all three cases are in good agreement with each other. Also the results for flutter speed and reduced frequency obtained using sensitivity based analysis, for a significant range of parameter, are found to be in good agreement with those obtained using a complete reanalysis.

Results for the sensitivity of the flutter speed are also obtained using the state space approach. This is done for a two-D rigid sectional model elastically supported and restricted to plunging and pitching. The unsteady aerodynamics is represented in state-space form i.e. by representing the aerodynamics as a set of first order ordinary differential equations. An advantage of this approach is that the aerodynamic equations can be easily appended to structural equation of motion. Also the matrix whose eigenvalues yield the flutter speed is a real-valued matrix. The results obtained using the state space approach for an example are found to be in good agreement with those available in the literature. The sensitivities of the flutter speed are obtained with respect to various parameters. Two different approaches are used; (i) a purely finite difference approach, and (ii) an analytic approach. The sensitivities obtained using the two approaches are in excellent agreement with each other. It is felt that the state space approach is very well suited for obtaining the sensitivity of the flutter speed with respect to a given parameter.

6. ACKNOWLEDGEMENTS

This research was conducted under a NASA contract, No. NAS-1-18471-Tasks 5 and 27. The results for the frequency domain analysis were obtained in collabration with Fred Bergen. The author likes to sincerely thank Dr. Jean-Francois M. Barthelemy of NASA Langley for his constant advise and encouragement throughout this project.

7. REFERENCES

1. Yates, E.C., "Calculation of Flutter Characteristics for Finite-Span Swept or Unswept Wings at Subsonic and Supersonic Speeds by a Modified Strip Analysis," NACA RM L57110, March 18, 1958 (Declassified Feb. 6, 1962).

2. Landsberger, B.J. and Dugundji, J., "Experi-

mental Aeroelastic Behavior of Unswept and Forward-Swept Cantilever Graphite/Epoxy Wings," *Journal of Aircraft*, Vol. 22, No. 8, August 1985.

3. Spielberg, I.N., "The Two-Dimensional Incompressible Aerodynamic Coefficients for Oscillatory Changes in Airfoil Camber," *Journal of the Aeronautical Sciences*, Vol. 20, June 1953, pp. 389-396.

4. Strganac, T.W. and Mook, D.T., "A New Method to Predict Unsteady Aeroelastic Behavior," *AIAA 28th Structures, Structural Dynamics and Materials Conference*, April 6-8, 1987.

5. Guruswami, G.P., "ENSAERO - A Multidisciplinary Program for Fluids/Structural Interaction Studies of Aerospace Vehicles," *Computing Systems in Engineering*, Vol. 1, nos2-4, 1990, pp. 237-256.

6. Hawk, D.J. and Bristow, D.R., "Development of MCAERO Wing Design Panel Method with Interactive Graphics Module," NASA CR-3775, 1984.

7. Brayton, R.K. and Spence, R. *Sensitivity andd Optimization*, Elsevier, New York, 1980.

8. Adelman, H.M. and Haftka, R.T., "Sensitivity Analysis of Discrete Structural Systems," *AIAA Journal*, Vol. 24, No. 5, May 1986, pp. 823-831.

9. Rudisill, C.S. and Bhatia, K.G., "Optimization of Complex Structures to Satisfy Flutter Requirements," *AIAA Journal*, Vol. 9, No. 8, August 1971, pp. 1496-1491.

10. Pedersen, P. and Seyranian, A.P., "Sensitivity Analysis for Problems of Dynamic Stability," *International Journal of Solids and Structures*, Vol. 19, No. 4, 1983, pp. 315-335.

11. Yates, E.C., "Aerodynamic Sensitivity from Subsonic, Sonic, and Supersonic Unsteady, Nonplanar Lifting Surface Theory," NASA TM-100502, 1987.

12. Barthelemy, J-F.M. and Bergen, F.D., "Shape Sensitivity Analysis of Wing Static Aeroelastic Characteristics," NASA TP-2808, May 1988.

13. Giles, G.L., "Equivalent Plate Analysis of Aircraft Wing Box Structures with General Planform Geometry," NASA TM 87697, March 1986.

14. Murthy, D.V. and Haftka, R.T., "Derivatives of Eigenvalues and Eigenvectors of a General Complex Matrix," Department of Aerospace and Ocean Engineering, VPI&SU, June 1986.

15. Leishman, J.G., and Nguyen, K.Q., "State-Space Representation of Unsteady Airfoil Behavior", *AIAA Journal*, Vol. 28, No. 5, May, 1990, pp. 836-844.

16. Venkatesan, C., and Friedmann, P.P., "New Approach to Finite State Modeling of Unsteady Aerodynamics", *AIAA Journal*, Vol. 24, Dec., 1986, pp. 1889-1897.

17. Strganac, T.W., and Mook, D.T., "Numerical Model of Unsteady Subsonic Aeroelastic Behavior," *AIAA Journal*, Vol. 28, No. 5, May 1990, pp. 903-909.

18. Barmby, J.G., Cunningham, H.J. and Garrick, I.E., "Study of Effects of Sweep on the Flutter of Cantilever Wings," NACA TN 2121, June 1950.

19. Bergen, F.D. and Kapania, R.K., "Shape Sensitivity Analysis of a Flutter Response of a Laminated Wing," NASA CR 181725.

20. Carnahan, B., Luter, H.A. and Wilkes, J.O., *Applied Numerical Methods*, 1st ed., Vol. 1, Wiley, New York, 1969, p. 103.

21. Castel, F. and Kapania, R., "A Beam Element for the Aeroelastic Analysis of Undamaged and Damaged Laminated Structures," CCMS-88-13, Center for Composite Materials and Structures, Virginia Polytechnic Institute and State University, Blacksburg, Virginia, July 1988, see also, *AIAA Journal*, Vol. 28, No. 2, Feb., 1990, pp. 329-337.

22. Brogan, W.L., *Modern Control Theory*, Quantum Publishers, Inc., 1974. Chapter 9.

23. Fung, Y.C., *An Introduction to the Theory of Aeroelasticity*, Dover Publications Inc., 1969.

Table 1: Comparison of Eigenvalue Derivatives w.r.t Four Parameters
(Frequency Domain Approach)

	Case (i) Finite Difference	case (ii) Semi-analytic	case (iii) Analytic
SWEEP	2.8831 E-5	2.4199 E-5	2.6761 E-5
S	2.4151 E-5	2.4593 E-5	2.4571 E-5
AR	7.8769 E-6	8.1694 E-6	8.1562 E-6
TP	2.6719 E-4	2.6571 E-4	2.6330 E-4

Table 2. Sensitivity of the Flutter Velocity of a 2D Section Model with respect to various Parameters using State-Space Approaches. (Base Configuration: $x_\alpha = 0.25$, $r_\alpha = 0.388$, $\mu = 76$, $a_h = -0.15$ Semi chord $= 5in.$, $\omega_\alpha = 64.1$ rad/sec., and $\omega_\alpha = 55.9$ rad./sec.)

	Parameter	Analytic Derivative	Finite Difference 1[a]%	0.1%	0.01%
Static Unbalance	x_α	162.5674	161.9858	162.5076	162.5600
Radius of Gyration	r_α	-0.05458942	.253188	-.02343	-.051373
Mass Ratio	μ	.518695	.516909	.518512	.518671
Dis. between elastic axis and mid chord.	a_h	6.24302	6.04073	6.22267	6.2400
Bending frequency	ω_h	1.60620	1.679999	1.613431	1.606905
Torsional frequency	ω_α	A small number	-	-	0

[a] Indicates step size used in finite difference.

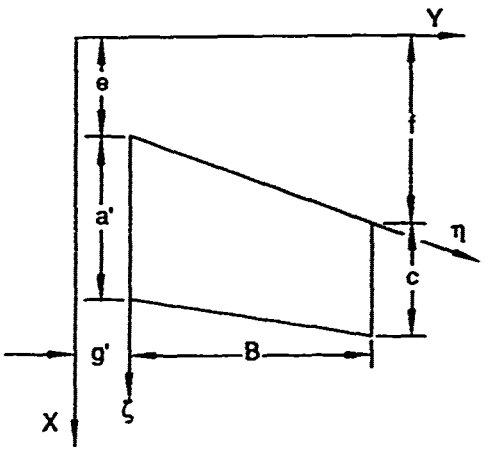

Fig. 1 The Planform of the wing

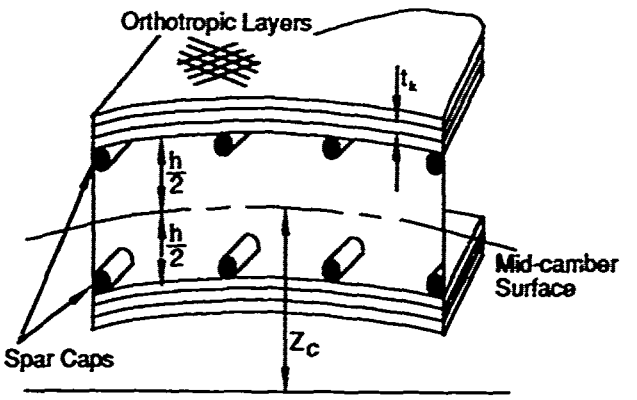

Fig. 2. The cross-section of the wing box.

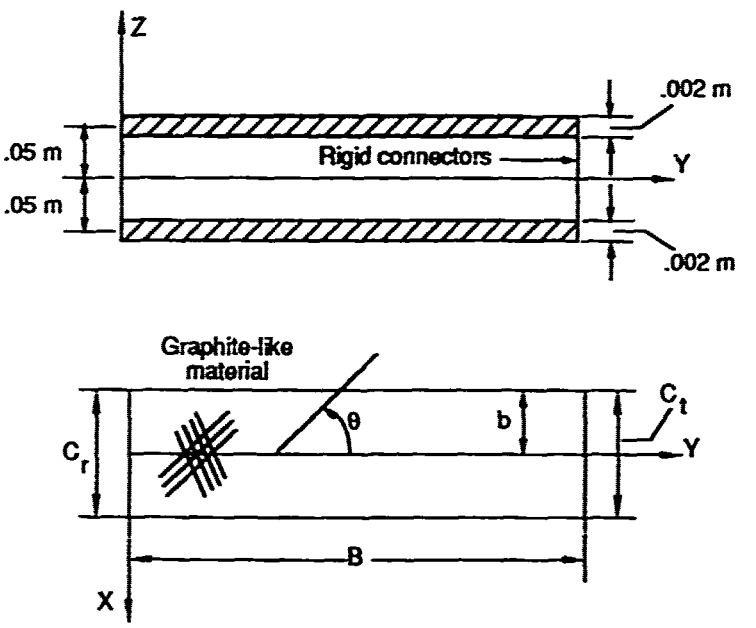

Fig. 3 The Wing-box used in this study

APPLICATION OF MULTIDISCIPLINARY OPTIMIZATION METHODS TO THE DESIGN OF A SUPERSONIC TRANSPORT

J.-F.M. Barthelemy and P.G. Coen, NASA Langley Research Center
Hampton, Va. 23665–5225, U.S.A.
G.A. Wrenn, M.F. Riley and A.R. Dovi, Lockheed E.&S. Co.
L.E. Hall, Unisys Corp. Inc.

ABSTRACT

A new optimization-based design method is discussed. This method is based on integrating existing disciplinary analysis and sensitivity analysis techniques by means of generalized sensitivity equations. A generic design system implementing this method is described. The system is being used to design the configuration and internal structure of a supersonic transport wing for optimum performance. This problem combines the disciplines of linear aerodynamics, structures and performance. Initial results which include the disciplines of aerodynamics and structures in a conventional minimum weight design under static aeroelastic constraints are presented.

INTRODUCTION

An effort is underway at the NASA Langley Research Center (LaRC) to improve multidisciplinary interactions in the processes of analysis and optimization of complex engineering systems. As presented by Dollyhigh and Sobieski [1], this effort named HiSAIR (High-Speed Airframe Integration Research) is focused on the HSCT (High-Speed Civil Transport) design activity. This paper describes the component of the HiSAIR effort which researches methodology for optimization and design of complex multidisciplinary engineering systems.

The objective of the research is to develop and demonstrate new mathematical methods for the integrated design of aircraft. The application selected is the optimization of a supersonic transport configuration developed at the NASA LaRC. Ultimately, the aircraft wing shape and structural layout are to be optimized for best overall vehicle performance.

To reach that objective, existing structural, aerodynamic and performance analysis and sensitivity analysis capabilities are first combined to predict the behavior of the aircraft. Since this project is one of demonstration, the level of analysis is deliberately kept low initially; the intent is to include progressively higher level capabilities as the methodology matures. Integration of analysis capabilities is discussed at length by Wrenn and Coen [2]. Second, sensitivity information is integrated using Sobieski's [3] recently introduced generalized sensitivity equations. This methodology has been validated with several different disciplinary and multidisciplinary design problems. It has being applied by Bloebaum *et al.* [4] in simultaneous shape optimization and structural sizing, by Woodward *et al.* [5] to the design of a controlled space structure, by Unger *et al.* [6] to the design of a subsonic transport, and by Levine *et al.* [7], to the design of a hypersonic aircraft. Third, the design itself is carried out with an optimization-based computer system which interacts with a relational database.

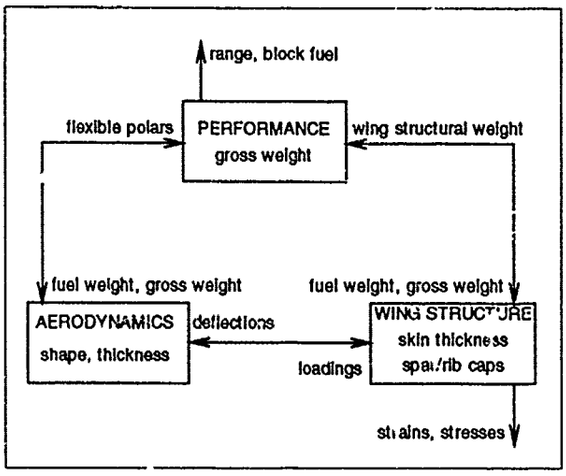

Figure 1 Multidisciplinary problem description

The product of this research will be firstly an improved methodology for design integration. Second, the resulting experimental design system will be used to produce trade studies in support of the HiSAIR effort.

In the following sections, the paper presents the formulation of the complete design problem and a brief description of the design model. The generic optimization system used for design is described. Finally, initial design results are presented for an early implementation of the procedure where design constraints are calculated accounting for aeroelastic effects, but derivatives include only structural effects.

DESIGN PROBLEM FORMULATION

The design problem considered is that of a supersonic transport aircraft. The wing internal structure, planform and thickness are varied for optimum performance. Figure 1 presents a schematic representation of the analysis problem. It combines the three disciplines of structures, aerodynamics and performance. Performance estimates for the airplane require knowledge of the flexible lift curves and drag polars and of the wing structural weight. Likewise, aerodynamic calculations depend on aircraft gross weight

meet the camber constraints. Each de-

and wing flexible deflections. Finally, structural analysis is performed for given gross weight and aerodynamic loads.

The problem's independent design variables are manipulated in each discipline to produce a design; they are denoted X_i with i indicating in which discipline they are manipulated (a= aerodynamics, p= performance and s= structure). They include the structural (sizing) variables X_s, the aerodynamic configuration variables X_a and the performance gross weight X_p. The dependent variables are calculated in each discipline and may be needed in other disciplines; they are denoted Y_{ij}, with i indicating the originating discipline and j, the discipline in which it is used. For example, the aerodynamic discipline obtains the aerodynamic loads (Y_{as}) in the different load cases, and the aircraft polar datapoints (Y_{ap}). Likewise, the performance discipline computes performance measures which include gross weight and fuel weights ($Y_{pa} = Y_{ps}$) as well as range and block fuel (Y_{pp}). Finally, the variables calculated by the discipline of structure include the wing static deformations under loads (Y_{sa}) in the different load cases, the structural weight (Y_{sp}), the structural stresses and strains (Y_{ss}).

In formal notation, the following analysis equations result which express the coupled relationships among the different variables

$$
\begin{aligned}
Y_a^t &= \{Y_{ap}^t(X_a, X_p, Y_{sa}, Y_{pa}), Y_{as}^t(X_a, X_p, Y_{sa}, Y_{pa})\} \\
Y_p^t &= \{Y_{pa}^t(X_a, X_p), Y_{pp}^t(X_a, X_p, Y_{ap}, Y_{sp}), Y_{ps}^t(X_a, X_p)\} \\
Y_s^t &= \{Y_{sa}^t(X_a, X_p, X_s, Y_{as}, Y_{ps}), Y_{sp}^t(X_a, X_s), \\
&\quad Y_{ss}^t(X_a, X_p, X_s, Y_{as}, Y_{ps})\}
\end{aligned} \tag{1}
$$

The equation for Y_p, for example, expresses the fact that the dependent design variables calculated by the performance discipline include i) the gross weight and fuel weights which depend on gross weight and wing shape and ii) the aircraft range and block fuel which depend on wing shape, gross weight, flexible polar curves and wing structural weight.

Sensitivity of the dependent design variables with respect to the independent ones yields a linear system of equations in the form of Sobieski's [3] *generalized sensitivity equations.* If

$$
Y^t = \{Y_a^t, Y_p^t, Y_s^t\} \text{ and } X^t = \{X_a^t, X_p^t, X_s^t\} \tag{2}
$$

then:

$$
S\left[\frac{dY}{dX}\right] = \left[\frac{\partial Y}{\partial X}\right] \tag{3}
$$

where

$$
S = \begin{bmatrix}
I & 0 & -\frac{\partial Y_{ap}}{\partial Y_{pa}} & 0 & 0 & -\frac{\partial Y_{ap}}{\partial Y_{sa}} & 0 & 0 \\
0 & I & -\frac{\partial Y_{as}}{\partial Y_{pa}} & 0 & 0 & -\frac{\partial Y_{as}}{\partial Y_{sa}} & 0 & 0 \\
0 & 0 & I & 0 & 0 & 0 & 0 & 0 \\
-\frac{\partial Y_{pp}}{\partial Y_{ap}} & 0 & 0 & I & 0 & 0 & -\frac{\partial Y_{pp}}{\partial Y_{sp}} & 0 \\
0 & 0 & 0 & 0 & I & 0 & 0 & 0 \\
0 & -\frac{\partial Y_{sa}}{\partial Y_{as}} & 0 & 0 & -\frac{\partial Y_{sa}}{\partial Y_{ps}} & I & 0 & 0 \\
0 & 0 & 0 & 0 & 0 & 0 & I & 0 \\
0 & -\frac{\partial Y_{ss}}{\partial Y_{as}} & 0 & 0 & -\frac{\partial Y_{ss}}{\partial Y_{ps}} & 0 & 0 & I
\end{bmatrix} \tag{4}
$$

Equation (4) gives the sensitivity derivatives of the coupled disciplines ($d(.)/d(.)$) as a function of the sensitivity derivatives of the uncoupled disciplines ($\partial(.)/\partial(.)$).

It is critical to maintain the size of the individual Y_{ij} vectors small. Indeed, they not only affect the size of the S matrix but, more importantly, drive the number of derivatives required from each discipline. Since those derivatives are found by finite difference, they make up a substantial part of the total optimization cost. Wrenn and Coen [2] discuss that point in detail and show that size control is achieved by the use of a reduced basis approach to model elastic displacements and pressure distributions and a polynomial approach to model the elastic polar curves.

OPTIMIZATION SYSTEM DESCRIPTION

Figure 2 presents a graphic description of the generic optimization capability developed for this study. It is a VAXstation II-based system currently implemented to handle 5 disciplines with up to 100 independent variables and 500 dependent variables. The system is designed to provide for user intervention at any point in the design process. It proceeds in *design cycles*, each requiring full analysis and sensitivity analysis of the problem. Within each cycle, different *design alternatives* can be produced by changing such things as the type of problem approximation, the type of algorithm used, the combination of dependent and independent variables optimized, the move limits for approximations.

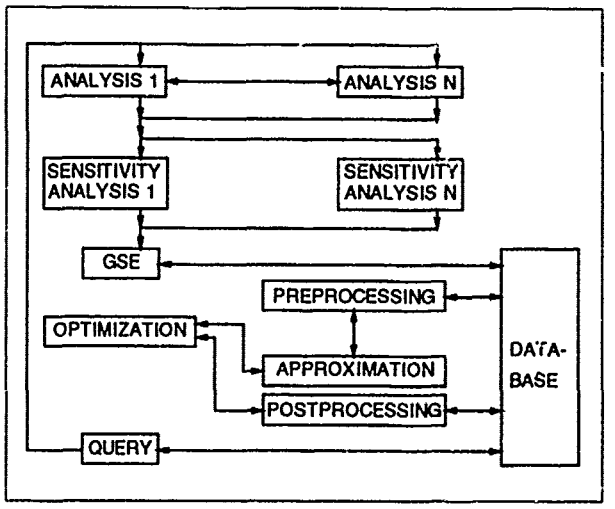

Figure 2 Integrated design system

The heart of the system is the commercial package OPTDES [8] which offers several optimization algorithms. Those used in this study are linear programming, sequential linear programming, method of centers, generalized reduced gradients and sequential quadratic programming. Since analyses and sensitivity analyses are quite expensive, OPTDES optimizes a sequence of approximations to the actual design problem. These approximations are all based on zeroth and first order information on the dependent variables

and include linear, reciprocal and the two-points approximation of Fadel *et al.* [9].

To provide an audit trail for the design process and allow for restart from any design cycle, critical optimization information is stored primarily in RIM [10], a commercial relational database management system. Cycle information retained includes initial values and upper and lower bounds on the independent and dependent variables. Because of its potential size, cycle gradient information is kept in conventional file format. Design alternative information retained includes final independent and dependent variables for each alternative design within each cycle.

Each design cycle begins with system analysis and sensitivity analysis. This step can be conducted with any existing analysis package and on any computer or distributed system of computers. Each discipline produces one file containing its own analysis and sensitivity analysis information. This information is then input to program GSE which sets-up and solves Eq. 3 and stores the relevant data in the RIM database and the gradient files. Once optimization is completed, the user may interactively query the database and track graphically or in tabular output any combination of independent or dependent variables. The user may also gauge the accuracy of the approximations selected by comparing analysis results predicted with those obtained after reanalysis. The user may then decide to produce more design alternatives within the current cycle or to initiate a new cycle using as starting design any of the design alternatives generated previously.

MODEL DESCRIPTION

For the sake of completeness, this section gives a very brief description of the aircraft design model; Wrenn and Coen give an extensive description in [2]. The initial configuration for the aircraft was proposed by Robins *et al.* [11].

The wing structure is analyzed with Giles' [12] equivalent plate analysis capability. As shown on Fig. 3, the wing structure is modelled by 10 independent plates. The two plates making up the wing box have skin thickness distributions varying linearly both chordwise and spanwise. The remaining plates on the wing glove, leading and trailing edges and tip have constant thickness. In addition, wing spar and rib caps are modelled with the four main spars having linearly varying cap areas. The upper and lower wing surfaces are identical. The wing structure is of metal-matrix composite made of silicon-carbide fibers embedded in a titanium matrix. Its layout is quasi-isotropic. There are 16 design variables for the skins and 16 for the caps.

Aerodynamic loads are obtained with the linear code WINGDES developed by Carlson [13]. The static aeroelastic problem is solved by iterating between structural and aerodynamic disciplines until convergence of the wing deformations and the resulting loads. The aircraft is trimmed by adjusting the angle-of-attack and redistributing the fuel in the fuel tanks.

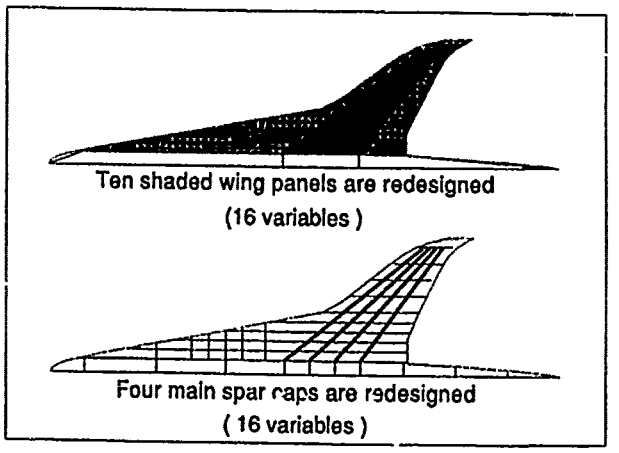

Figure 3 Layout of plates and caps

Five load cases are considered as shown in Table 1. The first three cases are chosen to calculate the aircraft's elastic polars, the last two are true structural loading cases and correspond approximately to the two corners of the upper horizontal limit on the V-n diagram.

For each load case, there are constraints limiting the strains and stresses (Tsai- Hill failure criterion) in the skins, panel buckling of the skins, and the normal strains and stresses in the caps. Each constraint is formulated as an envelope function (see Barthelemy and Riley [14]). In addition, there are minimum gauge constraints on wing skin thicknesses and cap areas.

All the partial derivatives of disciplinary response with respect to independent variables or to dependent variables from other disciplines are obtained by forward differences.

Load case	Load factor (g)	Mach Number	Altitude (ft)
Mid-cruise	1.0	3.0	72700
Transonic climb	1.0	1.2	21300
Reserve cruise	1.0	0.9	43000
Max load, low speed	2.5	0.6	10000
Max load, high speed	2.5	3.0	59000

Table 1 Load cases description

INITIAL NUMERICAL RESULTS

The results discussed in this paper were generated while integrating the disciplines of aerodynamics and structures (Fig. 1). The analysis is the traditional iterative static aeroelastic analysis while the coupling between the two disciplines is temporarily ignored for sensitivity analysis and the gradients generated for optimization assume no redistribution of loads. Later implementations of this procedure will fully account for all the couplings.

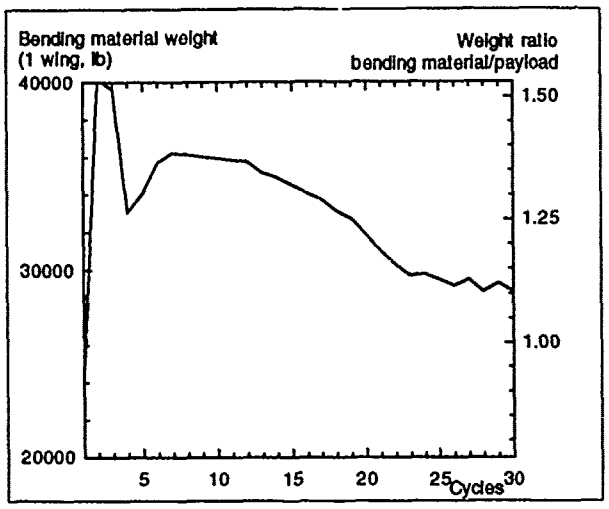

Figure 4 Wing weight convergence history

Figure 4 shows convergence of the wing structural weight from a constant skin thickness, constant spar cap area design scaled to match the weight estimates from Robins *et al.* [11]. These weight estimates were based on statistical expressions and, since there is very little data on supersonic transport design, they are likely to be used in an extrapolation mode, rather than in the more reliable interpolation mode. During the design process, the wing bending material weight increases by approximately 20%.

Each design cycle takes a full 4 hours on VAXstation II computers. About 3.5 hours are required for the analysis and sensitivity analysis processes. The remaining .5 hour is spent in optimizing the problem in an interactive mode. In view of this high computing time, the design follows a somewhat pragmatic approach so that if changes must be made in the design problem formulation or, even, if minor programming errors must be fixed, the process is restarted from the latest design generated. This particular design took 30 cycles. During the first few cycles, the optimizer worked at overcoming the initial constraint violation. In general, progress was somewhat limited at each iteration since tight move limits (mostly 10%, sometimes 5%) must be set to preserve approximation accuracy. After cycle 18,

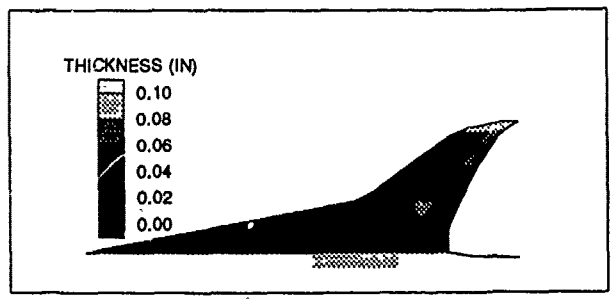

Figure 5 Wing skin thickness distribution

the structural weight dipped as the buckling constraints were reformulated to be more realistic.

Figure 5 shows the wing skin thickness distribution. In general, the spanwise caps loaded up during the redesign while the skin thickness was reduced to minimum gauge or close to it. This is attributed to using the same material for the spar caps and the skins. In the caps, the material is unidirectional and laid-up spanwise, while in the skins, the material is quasi-isotropic, resulting in lower stiffness and lower allowables achievable in the skins and, therefore, lower loads and lower load levels. The active design constraints were either geometrical (minimum gauge on the skins) or corresponded to the two 2.5g load cases. The Tsai-Hill failure criterion, panel buckling constraint, skin shear strain constraint, and cap normal stress constraints were active for the low-speed pull-up. Both panel buckling and skin shear strains were active for the high-speed pull-up. Figure 6 shows the evolution of the Tsai-Hill constraint in the upper wing panel in the low-speed pull-up. The constraint is violated, if its value is positive. While it is initially violated in the center of the outboard panel and at the wing tip, optimization reduces violation so that the constraint becomes critical at the end of the design exercise.

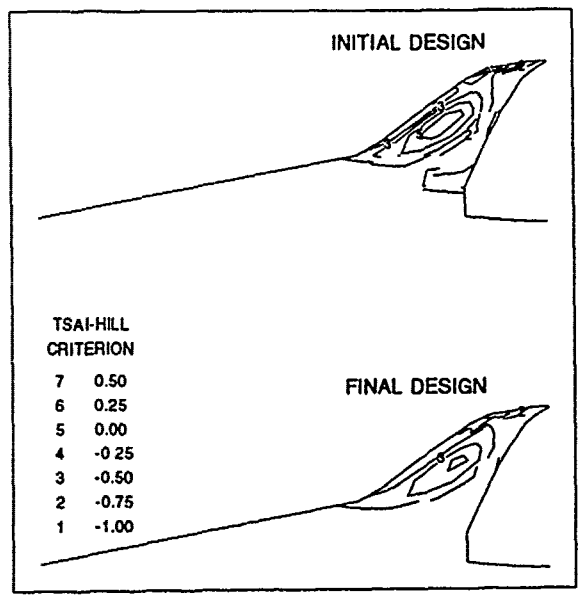

Figure 6 Tsai-Hill criterion, upper wing skin, M=0.6, n=2.5g

EXTENSIONS

This multidisciplinary design exercise serves as a pathfinder for method development in the activities described by Dollyhigh and Sobieski [1]. In its present formulation, it is to include three basic disciplines in the design process: linear aerodynamics, structural analysis and performance. When completed, it will permit optimum performance design of a wing configuration and internal structure under static aeroelastic constraints.

Eventually, the design exercise should be expanded to increase the realism of the model. Of particular interest would be the inclusion of dynamic (flutter) constraints. The level of details available within the individual disciplines should be increased as well. Finite element stress analyses and non-linear aerodynamics-based performance and load predictions must be included in a computationally efficient manner.

REFERENCES

1. Dollyhigh, S.M., and Sobieszczanski-Sobieski, J., "Recent Experiences with Multidisciplinary Analysis and Optimization in Advanced Aircraft Design," in proc. of III Air Force/NASA Symposium on Recent Advances in Multidisciplinary Analysis and Optimization, Sep. 24-26, 1990, San Francisco, CA.
2. Wrenn,G.A., and Coen, P.G., "Development of an Efficient Aeroelastic Analysis and Sensitivity Analysis Capability for a Supersonic Transport Aircraft" in proc. of III Air Force/NASA Symposium on Recent Advances in Multidisciplinary Analysis and Optimization, Sep. 24-26, 1990, San Francisco, CA.
3. Sobieszczanski-Sobieski, J.. "On the Sensitivity of Complex Internally coupled Systems," AIAA J., Vol. 28, No. 1, 1990, pp. 153-160.
4. Bloebaum, C., Hajela, P., and Sobieszczanski-Sobieski, J., "Non-Hierarchic System Decomposition in Structural Optimization," in proc. of III Air Force/NASA Symposium on Recent Advances in Multidisciplinary Analysis and Optimization, Sep. 24-26, 1990, San Francisco, CA.
5. Woodward, S.R., Padula, S.L, Graves, P.C., and James, B.B., " A Multidisciplinary Approach to Optimization of Controlled Space Structures," in proc. of III Air Force/NASA Symposium on Recent Advances in Multidisciplinary Analysis and Optimization Sep. 24-26, 1990, San Francisco, CA.
6. Unger, E.R., Rais-Rohani, M., Hutchison, M.G., Haftka, R.T., and Grossman, B., "Multidisciplinary Design of a Subsonic Transport Wing," in proc. of III Air Force/NASA Symposium on Recent Advances in Multidisciplinary Analysis and Optimization, Sep. 24-26, 1990, San Francisco, CA.
7. Levine, M., Ide, H., and Holowell, S., "Multidisciplinary Hypersonic Configuration Optimization," in proc. of III Air Force/NASA Symposium on Recent Advances in Multidisciplinary Analysis and Optimization, Sep. 24-26, 1990, San Francisco, CA.
8. Parkinson, A., Balling, R., and Free, J., "OPTDES.BYU A Software System for Optimal Engineering Design, User's Manual," Bringham Young University, 1988.
9. Fadel, G.M., Riley, M.F., and Barthelemy, J.-F.M., "Two Point Exponential Approximation Method for Structural Optimization," Structural Optimization, Vol. 2, 1990, pp. 117-124.
10. Erikson, W.J., "User Guide: Relational Information Management (RIM)" Report Number D6-IPAD-70023-M, Boeing Commercial Airplane Company, Seattle, WA, 1981.
11. Robins, A.W., Dollyhigh, S.M., Beissner, F.L.Jr., Geiselhart, K., Martin, G.L., Shields, E.W., Swanson, E.E., Coen, P.G., and Morris, S.J.Jr., "Concept Development of a Mach 3.0 High-Speed Civil Transport," NASA TM-4058, Sep. 1988.
12. Giles, G.L., "Equivalent Plate Analysis of Aircraft Wing Box Structures with General Planform Geometry," J. Aircraft, Vol, 23, No. 11, Nov. 1986, pp. 859-864.
13. Carlson, H.W., and Walkey, K.B., "Numerical Methods and a Computer Program for Subsonic and Supersonic Aerodynamic Design and Analysis of Wings with Attainable Thrust Considerations," NASA CR-3808, 1984.
14. Barthelemy, J.-F.M., and Riley, M.F., "Improved Multilevel Optimization Approach for the Design of Complex Engineering Systems," AIAA J., Vol. 23, No. 3, Mar. 1988, pp. 353-360.

Application of Analytical and Design Tools for Fighter Wing Aeroelastic Tailoring

Jonathan D Bohlmann
Michael H. Love
Daniel K. Barker
William A. Rogers
Beth E. Paul

General Dynamics, Fort Worth Division
P.O. Box 748, MZ 2824
Fort Worth, Texas 76101 USA
Advanced Methods Group

Summary

General Dynamics, Fort Worth Division, has been participating in the AGARD "Integrated Design, Analysis, and Optimization for Aircraft Structures" study to test and evaluate modern analysis and optimization tools. Specifically, wing analysis and design studies have been performed for the Validation of Aeroelastic Tailoring (VAT) configuration. The VAT represents a series of static and dynamic wind tunnel tests, performed under United States Air Force contract in the 1970's, to verify the beneficial use of aeroelastic tailoring for fighter aircraft wing design. The VAT provides a useful database for evaluation of various aeroelastic methodologies. Static analysis predictions for ELAPS, a Ritz structural analysis code, are compared to the VAT results, with excellent agreement. ASTROS, a new multidisciplinary, finite element optimization code, is also used for static and dynamic analyses of the VAT. The results demonstrate several analysis capabilities of ASTROS. The composite wing skin of the VAT is also optimized by ASTROS for strength and displacement constraints simulating aeroelastic loads. ASTROS was able to design the composite skin to achieve desired twist and camber deformation behavior. ASTROS is thus a viable tool for aeroelastic tailoring design.

Introduction

The role of aeroelastic tailoring in preliminary and conceptual design has grown in importance since its conception in the 1970's (see, for example, References 1-4). A key impetus for this growth was a series of three contractual efforts sponsored by the United States Air Force and performed by General Dynamics Corporation in the 1970's and early 1980's. These research programs were the Dynamic Characteristics of Advanced Filamentary Composite Structures (Reference 5, early 1970's), Aeroelastic Tailoring of Advanced Composite Structures for Military Aircraft (Reference 6, mid-1970's), and the Validation of Aeroelastic Tailoring by Static Aeroelastic and Flutter Tests (Reference 7, late 1970's and early 1980's). Together these efforts developed an efficient tailoring optimization code known as TSO, applied TSO to a realistic preliminary design of a tailored fighter wing skin, and demonstrated the aeroelastic tailoring concept with static aeroelastic and flutter wind tunnel testing. The experimental study was conducted under the Validation of Aeroelastic Tailoring (VAT) contract, and generated useful aeroelastic data for analytical prediction comparisons. The study reported in this paper uses the VAT data to evaluate several modern analytical and design optimization capabilities.

The VAT program generated wind tunnel test data with static aeroelastic and flutter models to demonstrate aeroelastic tailoring performance benefits, evaluate aeroelastic analytical procedures, and develop aeroelastic and flutter model scaling and fabrication techniques. The VAT full-scale wing planform is shown in Figure 1. The full-scale configuration was used for analysis and composite skin design, while

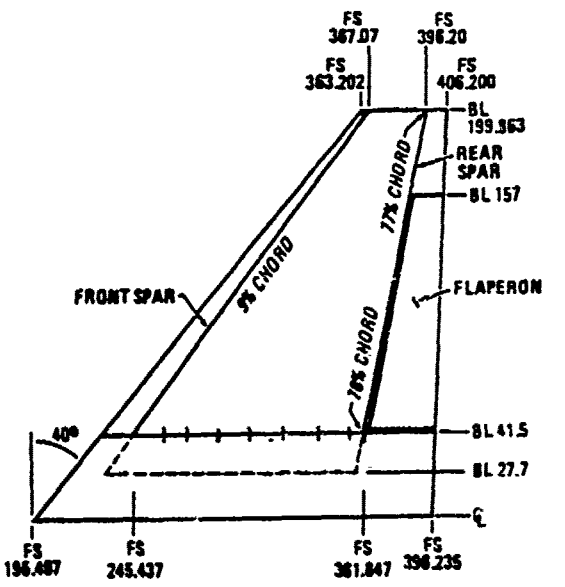

Figure 1: VAT Full-Scale Wing Planform

several composite aeroelastically scaled models were built for wind tunnel testing. Washin and washout 1/4-scale models were built, but experimental flutter results exist only for the washin model because of a test failure of the washout model. Three 1/9-scale static aeroelastic wind tunnel models were also built - washin tailored, washout tailored, and non-tailored. The five volume final report fully documents the analytical and experimental results.[7] The VAT program was very successful in validating the benefits of aeroelastic tailoring for fighter wing design, and showed TS0 to be a valid tailoring design tool.

General Dynamics' approach to this AGARD study utilizes the VAT configuration and consists of three tasks:

I. 1/4-Scale Modal and Flutter Analyses
II. 1/9-Scale Static Aeroelastic Analyses
III. Full-Scale Aeroelastic Tailoring Design

The first task is to demonstrate the usefulness of the Automated Structural Optimization System (ASTROS) for dynamic analysis. ASTROS is a new multidisciplinary structural optimization code, developed under United States Air Force contract, with finite element structural and aerodynamic modeling.[8] The washin 1/4-scale model is emphasized in this task since wind tunnel flutter results exist for this wing. The ASTROS results are also compared to analytical predictions generated during the VAT contract, as disclosed in the final report.[7]

The second task uses the 1/9-scale VAT model data to conduct static loads analyses and static aeroelastic analyses. Several sets of static loads were applied to MSC/NASTRAN, ASTROS, and ELAPS structural models. MSC/NASTRAN is a commercial finite element code developed by the MacNeal-Schwendler Corporation, based on the original NASTRAN™* created by NASA, the National Aeronautics and Space Administration.[9] ELAPS, the Equivalent Laminated Plate Solution, is a Rayleigh Ritz structural code developed at NASA's Langley Research Center.[10] The static analyses give a comparison of the structural modeling of the different codes. This task also includes static aeroelastic analyses using ASTROS, which uses USSAERO for aerodynamic predictions. The washout 1/9-scale model is used for these analyses. The data generated is compared to the wind tunnel data and analytical predictions documented in the VAT report.[7] ASTROS and ELAPS are the codes of main interest, with MSC/NASTRAN giving further analytical data for comparison.

The first two tasks give a clear indication of some of the analysis capabilities of ASTROS and ELAPS. The third task concentrates on the optimization of a full-scale VAT wing subject to various strength and flexibility constraints. ASTROS is used for this task to study its capabilities as a preliminary design tool for composite lifting surfaces. ASTROS' finite-element based structural optimization can add a new dimension to the aeroelastic tailoring design process, which is typically restricted to using Ritz-based codes such as TS0. The sections that follow describe in detail the three separate tasks and present results for each. Concluding remarks and further issues are outlined in the last section.

* NASTRAN is a registered trademark of the National Aeronautics and Space Administration

1/4-Scale VAT Analytical Results

The VAT study used 1/4-scale models for flutter wind tunnel testing. Washout and washin tailored models were fabricated and tested. Analytical and ground vibration test (GVT) data exist for both 1/4-scale models. Unfortunately, the washout model failed prematurely during wind tunnel testing, so experimental flutter data exists only for the washin model. Volume III of Reference 7 gives full details of the flutter model and tests.

Figure 2 shows the finite element model (FEM) of the 1/4-scale VAT wing. The model wings were constructed of graphite/epoxy tape and glass fabric cloth with a honeycomb core. The built-up sandwich structure was modeled with plate bending elements. Quadrilateral, triangular, and bar elements are used to represent the composite structure. The washout and washin wing finite element models used during the VAT contract were retrieved and converted to modern MSC/NASTRAN and ASTROS formats. To verify the integrity of the models, a simple static analysis documented in the VAT contract report was conducted. The input loads were:

1) 100 pound point shear at the wing tip
2) Tip pitching moment via 100 pound shear at the rear spar tip and -100 pound shear at the front spar tip

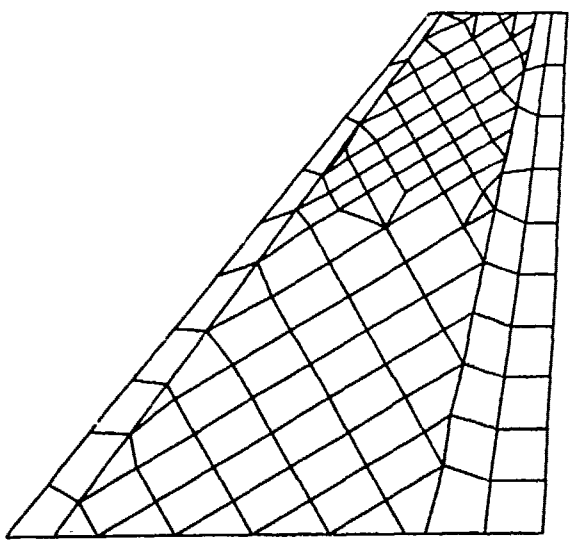

Figure 2: 1/4-Scale VAT Finite Element Model

For both the washout and washin models, the MSC/NASTRAN and ASTROS analytical results compared quite favorably to the finite element results documented in the VAT report.[7]

Modal analyses for the washout and washin models were then run in both MSC/NASTRAN and ASTROS. Table 1 compares those results to the documented analytical and experimental GVT results. The table shows excellent agreement between the MSC/NASTRAN and ASTROS results. The mode shapes also compared well. Differences between analytical and GVT results are due to inaccuracies in modelling the actual wind tunnel model mass distribution. No explanation has been found as to why the documented analysis results differ from the ASTROS and MSC/NASTRAN results.

Table 1: Frequency Comparison for 1/4-Scale VAT Model

WASHIN

Mode	GVT (Hz)	Documented Analysis (Hz)	MSC NASTRAN (Hz)	ASTROS (Hz)
1	11.3	11.69	13.55	13.50
2	37.1	31.92	33.62	33.61
3	47.3	44.33	47.17	46.82
4	75.4	63.27	67.58	67.39
5	96.1	84.54	85.35	84.77

WASHOUT

Mode	GVT (Hz)	Documented Analysis (Hz)	MSC NASTRAN (Hz)	ASTROS (Hz)
1	8.5	7.61	7.43	7.43
2	32.5	27.33	25.88	25.84
3	49.1	46.50	44.65	44.68
4	72.1	57.87	54.33	54.33
5	93.2	87.14	85.04	84.87

An ASTROS flutter analysis of the 1/4-scale washin model was then conducted for a Mach 0.9 condition. ASTROS uses a doublet lattice method for unsteady aerodynamic calculations at subsonic Mach numbers,[11] and the p-k method for flutter analysis. The doublet lattice model used for the ASTROS analysis is a wing-only model, shown in Figure 3. At Mach 0.9, for the 1/4-scale model, ASTROS predicted a flutter dynamic pressure of 120 pounds per square foot and a flutter frequency of 21.6 Hertz. The documented analytical results from the VAT contract report was a flutter dynamic pressure of 118 psf. These are matched point results. The wind tunnel results at Mach 0.9 measured flutter at 160 psf. The discrepancy between the analytical and experimental results is due mainly to structural modeling inaccuracies, as indicated by the analytical-to-experimental comparison in Table 1. The VAT contract report

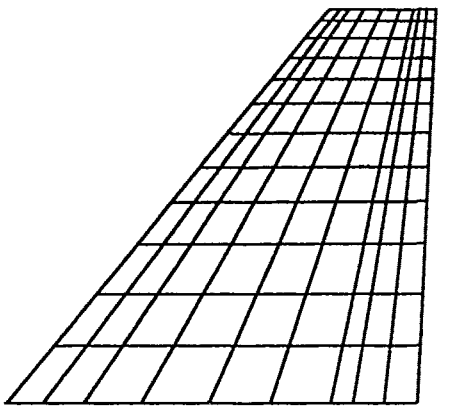

Figure 3: 1/4-Scale VAT Doublet Lattice Model

presents an analytical flutter prediction of 174 psf when measured mode shapes are used instead of analytical mode shapes. The good correlation of ASTROS results to the documented VAT analysis results with calculated mode shapes verifies ASTROS' flutter analysis capability, at least subsonically. This 1/4-scale VAT model study has demonstrated the modal and flutter analysis capabilities of ASTROS, complementing previous such work.[12]

1/9-Scale VAT Analytical Results

The VAT study utilized 1/9-scale models for static aeroelastic demonstration of aeroelastic tailoring design. A synopsis of the static aeroelastic results is given in Reference 13, while the VAT contract report gives more detailed information.[7] Wind tunnel models with washin and washout composite tailoring were constructed, as well as a nontailored flexible wing. Graphite/epoxy and glass tape were used for the models' skin structure. A "rigid" 1/9-scale wing made of steel was also tested to provide a baseline performance of the wing.

As for the 1/4-scale wing, finite element models of the 1/9-scale wings used during the VAT contract were retrieved and converted to MSC/NASTRAN and ASTROS input formats. MSC/NASTRAN nonlinear structural analyses were performed to answer a question lingering since the VAT contract in the late 1970's about how severe were the structural nonlinearities in the 1/9-scale wind tunnel models. Suspicions arose due to the high percentage of ±45's in the composite skins, and some discrepancies between analytical and experimental deflection results. A Ritz structural model was also made for ELAPS static analyses. In addition to static loads analyses with MSC/NASTRAN, ASTROS, and ELAPS, an ASTROS static aeroelastic analysis was conducted. Only the washout tailored wing was used for the 1/9-scale model analyses.

The finite element model for the 1/9-scale wing is shown in Figure 4. The built-up structure was

modeled with membrane elements for the upper and lower composite skins, and with shear elements and rods through the box thickness for the honeycomb core. The ELAPS Ritz model consisted of the graphite/epoxy, glass, and bond layers as the only structural material. The bond layer represents the adhesive between the skins and the honeycomb core of the wing, and is a non-negligible contributor to the stiffness of the wind tunnel model. Volume V of the VAT contract report contains details of the 1/9-scale wing model structure.

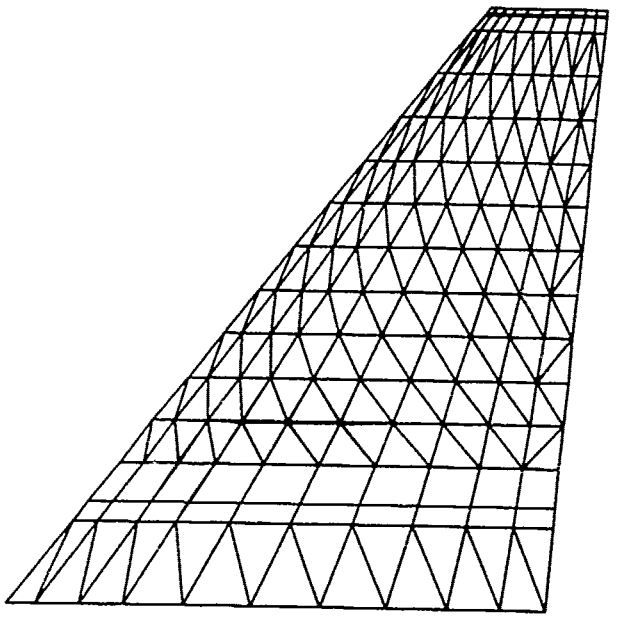

Figure 4: 1/9-Scale VAT Finite Element Model

For the static analyses, three load conditions, corresponding to VAT contract load conditions, were used:

1) Load Case 117/4
Mach = 0.9 altitude = 10000 feet $C_L = 0.70$

2) Load Case 126/12
Mach = 1.2 altitude = 10000 feet $C_L = 0.39$

3) Load Case 107/6
Mach = 0.6 altitude = 10000 feet $C_L = 0.70$

The load conditions are fully documented in Volumes II, IV, and V of the VAT report.[7] For each load condition, three different sets of loads were available:

1) Analytical loads predicted by Carmichael, a linear aerodynamic panel method.[14] The Carmichael loads include aeroelastic effects as predicted by TSO, the Ritz optimization code used for aeroelastic tailoring designs for the VAT contract.

2) Analytical loads predicted by Bailey Ballhaus, a nonlinear aerodynamic analysis code.[15] These loads were calculated for the aeroelastically deformed wing shape input to Bailey Ballhaus as a rigid wing jig shape.

3) Experimental loads as measured in the wind tunnel with pressure taps in the 1/9-scale aeroelastic models.

Hence, a total of nine load cases were applied to the washout, 1/9-scale VAT model for MSC/NASTRAN, ASTROS, and ELAPS analyses. For each load case, the resulting analytical displacements were compared to experimentally measured wind tunnel displacements and documented finite element analysis results found in the VAT contract report.

The ELAPS static analysis results are shown in Figures 5 through 10. The rear spar deflections and spanwise twist distributions are shown for Carmichael, Bailey Ballhaus, and experimental load sets for Load Case 117/4. Front spar deflections were also compared, but are not shown for brevity. Each figure compares the ELAPS deflection predictions with wind tunnel model deflections and finite element analytical results documented in the VAT contract report. The figures show a good agreement of ELAPS results to documented results. Similar comparisons were seen for Load Cases 126/12 and 107/6 analytical results. When the ELAPS results were compared to deflection predictions based on experimentally measured influence coefficient data, the agreement was also very good.

The close agreement between the ELAPS and finite element analysis results indicates that ELAPS possesses good structural accuracy in a computationally efficient Ritz algorithm. As such, ELAPS could provide a sound basis for a preliminary structural sizing code that considers global criteria such as strength, clean-wing flutter, and aeroelastic response, much as TSO accomplishes.[7] Thus, the effective use of finite element analyses is indicated where more detailed concerns of the wing such as stress concentrations, wing-store flutter, wing-to-fuselage attach structure, and rib and spar arrangements are being considered. The relative complexity and computational power of finite element procedures leave a large space for Ritz procedures to fill for conceptual and early preliminary structural design.

Static analysis results of MSC/NASTRAN and ASTROS match extremely well. Figures 11 and 12 show results of rear spar displacement and spanwise twist distribution for experimental loads for Load Case 117/4. MSC/NASTRAN, ASTROS, and documented finite element analysis results are shown. This superb agreement was exhibited for all the load sets. The strains in the composite skin predicted by MSC/NASTRAN and ASTROS also compared well. The agreement confirms the static analysis capability of ASTROS.

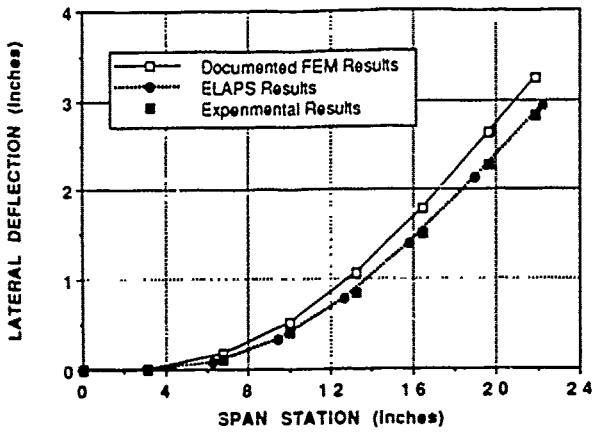

Figure 5: ELAPS/FEM Comparison, 1/9-Scale Washout Model, Rear Spar Deflection, Load Case 117/4, Carmichael Loads

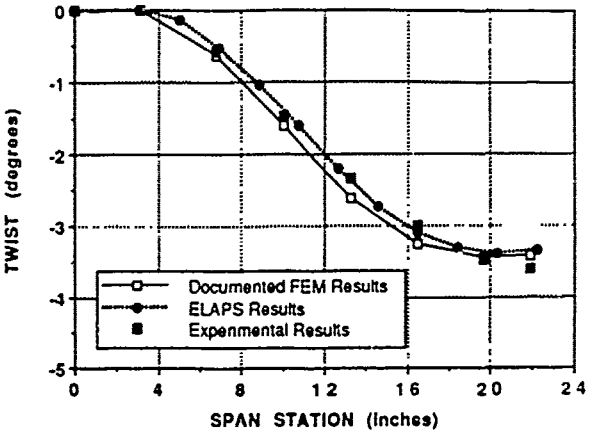

Figure 8: ELAPS/FEM Comparison, 1/9-Scale Washout Model, Spanwise Twist Distribution, Load Case 117/4, Carmichael Loads

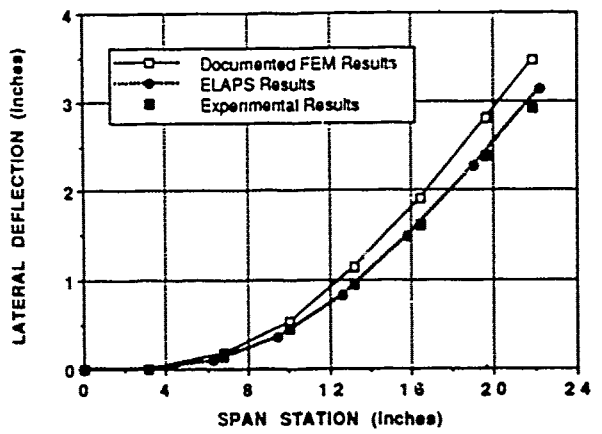

Figure 6: ELAPS/FEM Comparison, 1/9-Scale Washout Model, Rear Spar Deflection, Load Case 117/4, Bailey Ballhaus Loads

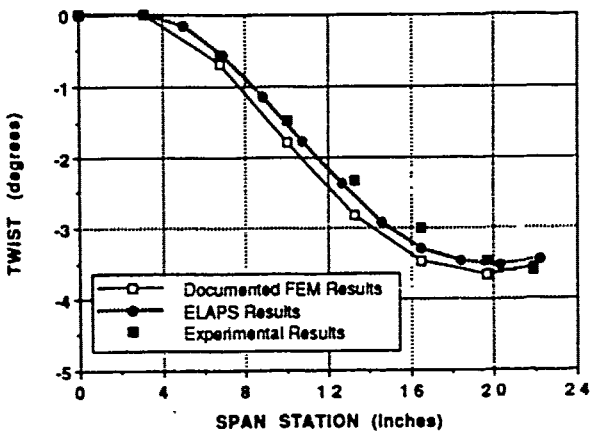

Figure 9: ELAPS/FEM Comparison, 1/9-Scale Washout Model, Spanwise Twist Distribution, Load Case 117/4, Bailey Ballhaus Loads

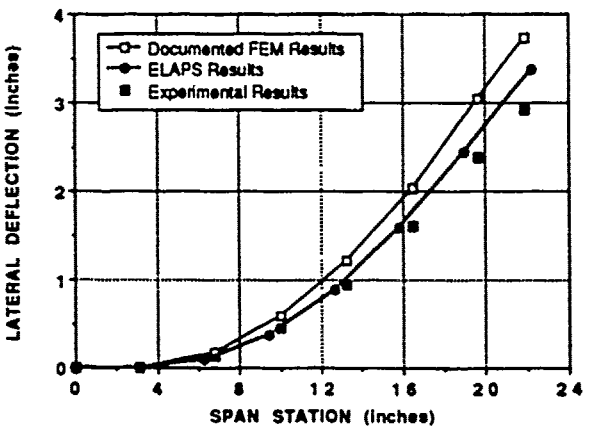

Figure 7: ELAPS/FEM Comparison, 1/9-Scale Washout Model, Rear Spar Deflection, Load Case 117/4, Experimental Loads

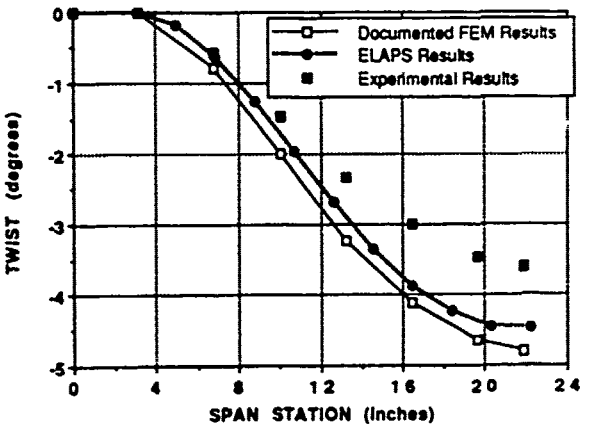

Figure 10: ELAPS/FEM Comparison, 1/9-Scale Washout Model, Spanwise Twist Distribution, Load Case 117/4, Experimental Loads

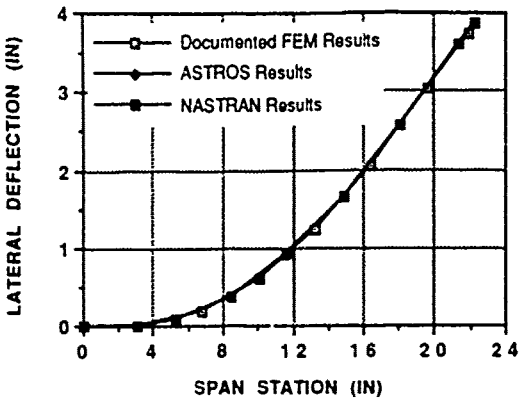

Figure 11: Finite Element Analysis Comparison for 1/9-Scale Washout Model, Rear Spar Deflection, Load Case 117/4, Experimental Loads

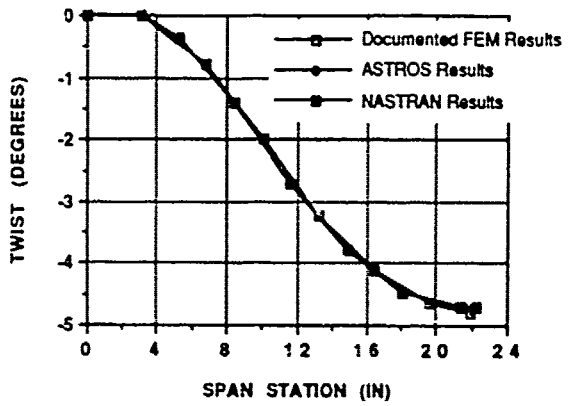

Figure 12: Finite Element Analysis Comparison for 1/9-Scale Washout Model, Spanwise Twist Distribution, Load Case 117/4, Experimental Loads

Unexplained from the VAT contract were the differences between predicted displacements from static analysis with experimental loads and measured displacements in the wind tunnel tests for the washout 1/9-scale model. The design of the washout skin resulted from negative twist and minimum weight objectives and a roll moment effectiveness constraint. This led to a design that exhibited significant twist and camber due to the opposing criteria of washout twist and increased roll moment effectiveness.

A geometric nonlinear analysis was performed with MSC/NASTRAN to see if nonlinearities would account for the overpredicted analytical displacements of the washout model. In the analysis the applied experimental forces were required to remain vertical instead of perpendicular to the model surface. Figures 13 through 15 show that nonlinearities account for a minor difference in displacements. Front and rear spar vertical displacements and spanwise twist distribution results are shown for the nonlinear analysis and ASTROS linear static analysis with experimental applied loads, and the experimentally measured displacements.

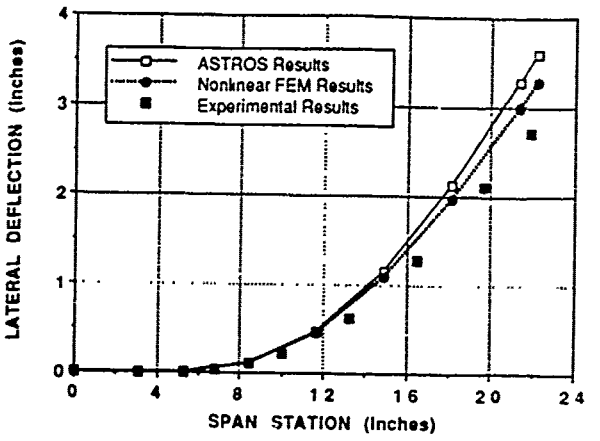

Figure 13: Nonlinear Finite Element Analysis Results for 1/9-Scale Washout Model, Front Spar Deflection, Load Case 117/4, Experimental Loads

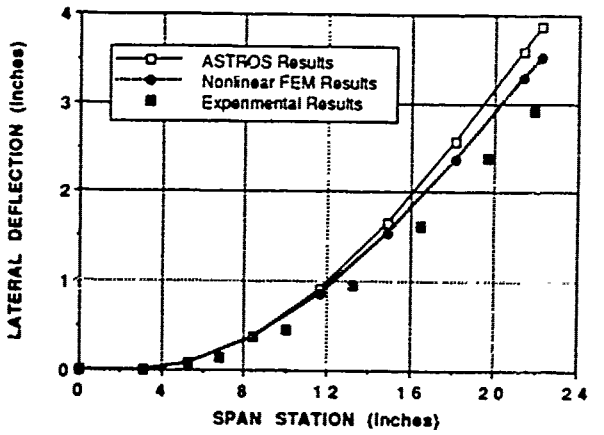

Figure 14: Nonlinear Finite Element Analysis Results for 1/9-Scale Washout Model, Rear Spar Deflection, Load Case 117/4, Experimental Loads

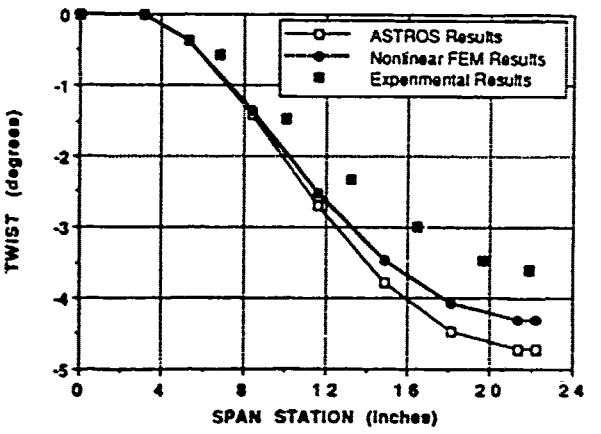

Figure 15: Nonlinear Finite Element Analysis Results for 1/9-Scale Washout Model, Spanwise Twist Distribution, Load Case 117/4, Experimental Loads

The question remains as to why static analysis deflection results using experimentally measured loads do not compare better to the experimentally measured deflections of the washout wind tunnel model. One possible contributor to this discrepancy is that upper surface and lower surface pressure taps were located on different wings (left-hand and right-hand) of the full-span wind tunnel model. Asymmetries would cause errors in the loads. Also, the nonlinear analysis should perhaps have used follower loads that remained perpendicular to the model surface, instead of vertical loads.

It is interesting that in the VAT contract analyses for the washin and nontailored wing designs, correlation with test data was good. The larger twist and camber deformation of the washout wing seems to be the significant difference between the tests of the three models.

The last analysis conducted for the 1/9-scale VAT model was a static aeroelastic analysis using ASTROS. This aeroelastic analysis simulated Load Case 117/4. Note that this condition has a specified lift coefficient, achieved in wind tunnel testing with an angle of attack of 8.9° for the washout wing model. Hence, this aeroelastic simulation in ASTROS is not a lift-pitch trim solution, but an aeroelastic prediction for a specified angle of attack.

ASTROS uses USSAERO for linear steady aerodynamic computations.[8] The USSAERO model used for this analysis is shown from two perspectives in Figure 16. The model is symmetric about the fuselage centerline. The fuselage is a body of revolution that matches the geometry of the wind tunnel model. The USSAERO model includes no thickness effects for the wing.

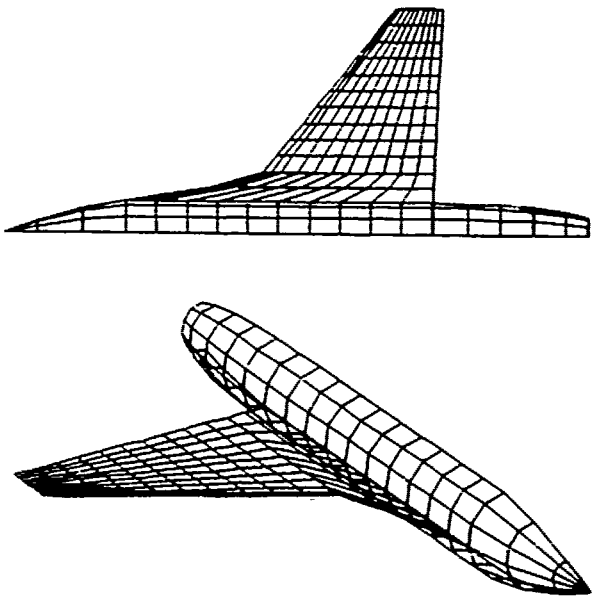

Figure 16: USSAERO Model of 1/9-Scale VAT, Planform View and 3-D Perspective

The ASTROS static aeroelastic analysis results are shown in Figures 17 through 22. Rear spar deflections and spanwise twist distributions are shown, comparing ASTROS aeroelastic results, ASTROS static analysis results with Carmichael, Bailey Ballhaus, and experimental applied loads, and experimental deflection results. The agreement is very good. It is not surprising that the ASTROS aeroelastic results compare best to the static analysis with Carmichael predicted loads, since USSAERO and Carmichael are both similar aerodynamic panel methods, and the Carmichael loads included flexibility effects.

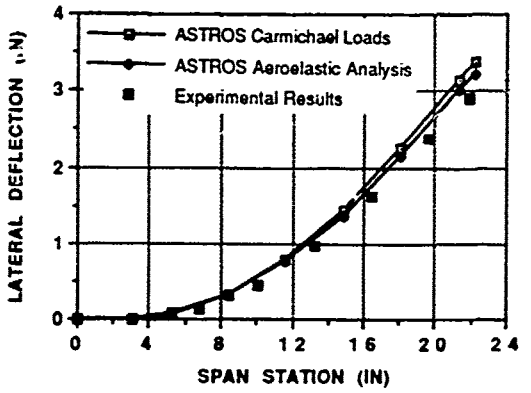

Figure 17: ASTROS Results, 1/9-Scale Washout Model, Rear Spar Deflection, Load Case 117/4, Carmichael Loads

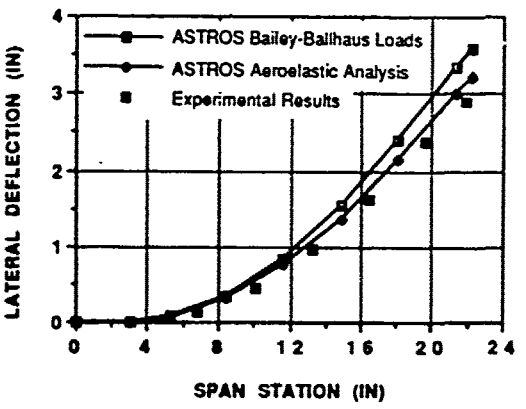

Figure 18: ASTROS Results, 1/9-Scale Washout Model, Rear Spar Deflection, Load Case 117/4, Bailey Ballhaus Loads

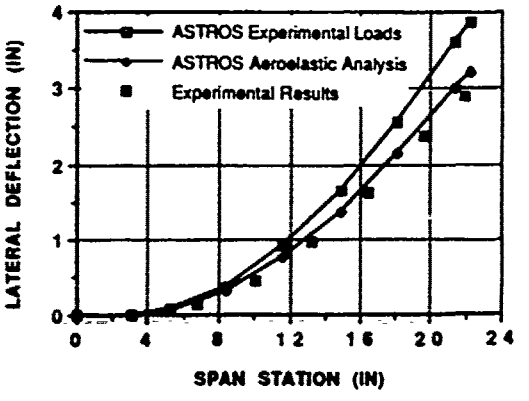

Figure 19: ASTROS Results, 1/9-Scale Washout Model, Rear Spar Deflection, Load Case 117/4, Experimental Loads

The 1/9-scale washout model analyses have demonstrated the static analysis capabilities of ELAPS and ASTROS. The static aeroelastic analysis capability of ASTROS was also presented, verifying its use for composite wing analysis.

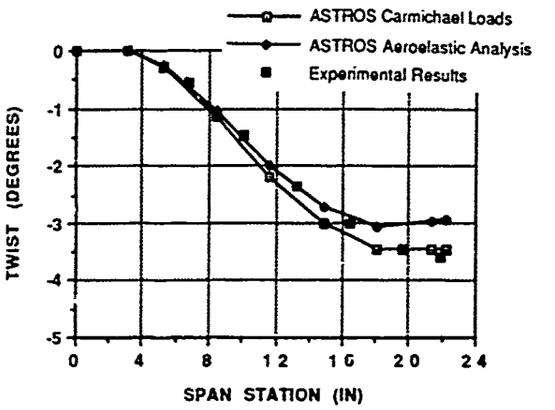

Figure 20: ASTROS Results, 1/9-Scale Washout Model, Spanwise Twist Distribution, Load Case 117/4, Carmichael Loads

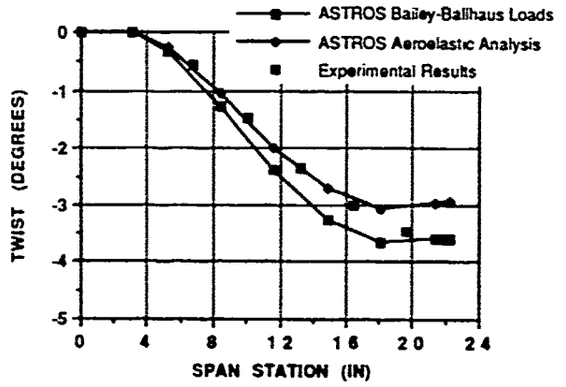

Figure 21: ASTROS Results, 1/9-Scale Washout Model, Spanwise Twist Distribution, Load Case 117/4, Bailey Ballhaus Loads

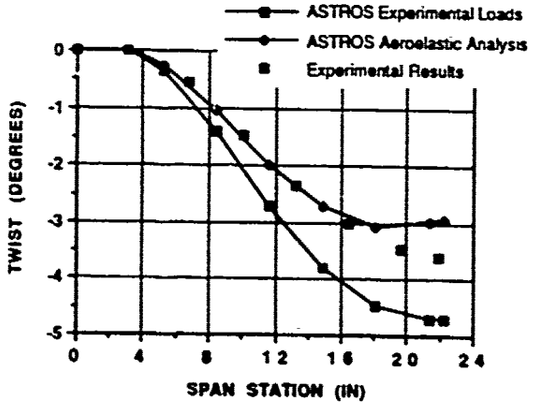

Figure 22: ASTROS Results, 1/9-Scale Washout Model, Spanwise Twist Distribution, Load Case 117/4, Experimental Loads

Full-Scale VAT Aeroelastic Design Results

The 1/4-scale and 1/9-scale VAT analyses have shown the fundamental aeroelastic analysis capabilities of ASTROS. The next issue of interest is the use of ASTROS for aeroelastic tailoring optimization. The full-scale VAT wing planform is used for this purpose.

Volume I of the VAT contract report details the full-scale aeroelastic tailoring designs found with TSO optimization.[7] As with the 1/9-scale VAT model, washout and washin tailored wing skin designs, plus a nontailored composite skin, were optimized subject to strength, flutter, and roll moment effectiveness constraints. The full-scale designs were scaled for the 1/9-scale model skins of the VAT contract.

Because of the computational intensity of ASTROS multidisciplinary optimization, the goal of this full-scale VAT design study is not to optimize a wing skin subject to the full range of disciplines available in ASTROS. Rather, the purpose is to obtain a fundamental look at how ASTROS would optimize a composite wing skin from an aeroelastic tailoring perspective. Since aeroelastic loads and deformations are already available from the VAT contract, this ASTROS exercise applies those loads to a full-scale VAT model, and optimizes the skin for minimum weight subject to strength and deformation (twist and camber) constraints. The constraints are consistent with the documented VAT aeroelastic deformations for the full-scale washout design. The loads and constraints simulate the aeroelastic design behavior of the washout composite skin. This gives a fundamental understanding of how ASTROS attempts to achieve twist and camber of a composite wing skin. Since achieving aeroelastic twist and camber is the means through which benefits are achieved in static aeroelastic tailoring, these ASTROS optimizations with deflection constraints will provide basic insights to ASTROS' use in composite wing aeroelastic design. The washout design of the VAT contract provides the design loads and constraints for this study.

Figure 23 shows the finite element model of the full-scale VAT. Membrane elements model the upper and lower composite skins, with shear elements and rods representing understructure. Stiffnesses for flap actuators and wing-to-fuselage attach structure are represented as springs. The upper and lower composite skins are modeled with three layers of elements, one layer each for the 0°, ±45°, and 90° orientations of a [0°/±45°/90°] composite laminate. The 0° layer is oriented at a 75° angle counterclockwise from the x-axis, which points aft along the aircraft centerline. Hence, the 0° layer points out the wing span approximately along the center of the wing box. This orientation was derived from the VAT contract washout wing skin design.

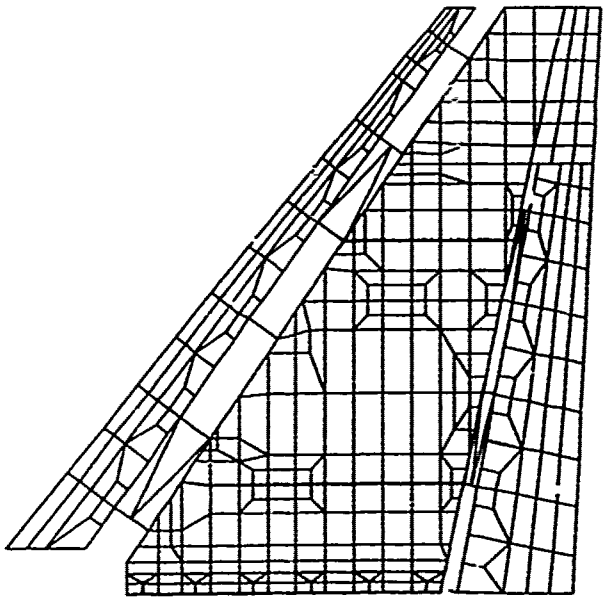

Figure 23: Full-Scale VAT Wing Finite Element Model

For the ASTROS optimization, the upper and lower wing box skins, and each of their three composite layers, were designed individually. Also, the portion of the box inboard of Buttline 50 (BL 50) represented one design region, and the box skin outboard of BL 50 represented another design region. This was done so that stress concentrations near the wing-to-fuselage attach structure could be better treated in the design. The ASTROS design variables were the thickness of each layer for each design region. Shape function linking was used, forcing the layer thicknesses to be smooth according to the function

$$\text{thickness} = a_0 + a_1\xi + a_2\xi^2 + a_3\eta + a_4\xi\eta + a_5\eta^2$$

where ξ and η are non-dimensional chordwise and spanwise box coordinates, respectively, and a_i are constant coefficients. The coefficients a_i are the actual design variables for shape function linking. Only the box skins are optimized. The flap skins, including the fixed trailing edge of the outboard portion of the wing, were held at a fixed thickness consistent with the VAT contract design.

Three ASTROS optimizations were performed, each with the objective to minimize wing box skin weight. The three runs represent three sets of constraints:

1) Strength constraint, 3800 microstrain compression and 4200 microstrain tension, in terms of principal strains.

2) Strength constraints and specified washout twist constraints

3) Strength and twist constraints as above, with specified wing camber constraints.

The twist and camber constraints were based on increasing the twist and camber deformations of the strength optimized skin (see Figures 25 and 26 below). Table 2 gives the values used for the twist and camber constraints, noting which buttline the constraints are applied. In ASTROS, twist and camber constraints are imposed as displacement constraints - twist being the difference between front and rear spar deflections, and camber being the displacements of the mid-box relative to front and rear spar deflections, for a given span station.

Table 2: Twist and Camber Constraints for ASTROS Optimization

Buttline	Twist Constraint	Camber Constraint (% chord)
78	-1.0°	0.4
98	-1.8°	0.5
128	-3.3°	0.5
151	-4.6°	- -
174	-5.4°	0.5
199	-5.6°	- -

Figure 24 shows the iteration history for the three ASTROS optimization runs. The figure shows box skin weight for a single wing versus ASTROS iteration number. Iteration 0 is the starting design point. Strength optimization refers to the design subject to only strength constraints, twist optimization refers to the design with strength and twist constraints, and camber optimization refers to the ASTROS design resulting from strength, twist, and camber constraints. From the figure, the strength optimization and twist optimization designs arrive at nearly the same skin weight, while considerable weight is added in an attempt to

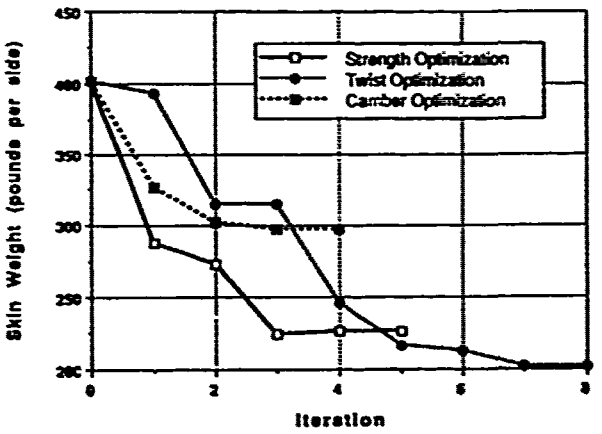

Figure 24: ASTROS Iteration History for Full-Scale VAT Wing Skin Design

meet the camber constraints. Each design was effective in that it had strains that were near the maximum strains allowed, primarily around the inboard portion of the wing box. Also, the region of the skin inboard of BL 50 varied relatively little among the three designs because no twist or camber constraints were placed on the wing in this area.

Figure 25 shows the resulting twist of each ASTROS design, while Figure 26 shows the camber results. Each figure shows the constraint values used during the ASTROS optimization. The twist constraints were formulated so that the twist had to be as negative or more negative than the constraint value, while the camber constraint was a minimum camber allowed for the design. It is interesting to note that the twist optimized skin shows more negative twist than is required by the twist constraint towards the wing tip. This is likely due to a combination of using a shape function for the skin thicknesses and the way in which the twist constraints are formulated. As noted, the twist is represented as the difference between the front and rear spar displacements. The box chord decreases as progressing outboard, so that although the desired negative twist increases outboard, the twist constraint displacement value actually decreases outboard of Buttline 151. For example, the twist constraint displacement value at BL 151 is -3.2" (corresponding to -4.6° twist), while the constraint value is -1.6" at BL 199 (for -5.6° twist). Coupling this with strength being critical towards the box root and forcing the skin to follow a polynomial thickness function could mean the design is not very sensitive to twist constraints in the outboard box regions.

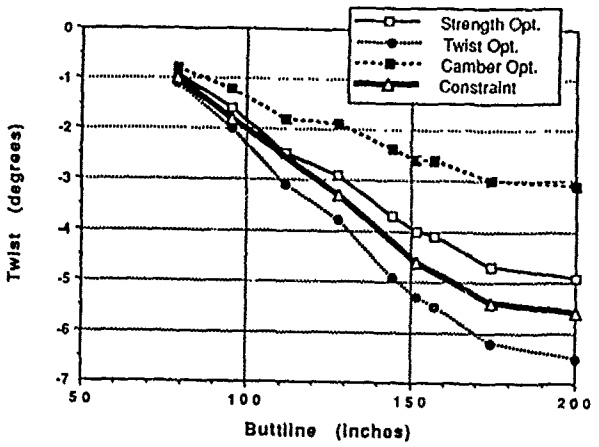

Figure 25: Full-Scale VAT Wing Box Twist Results for ASTROS Optimization

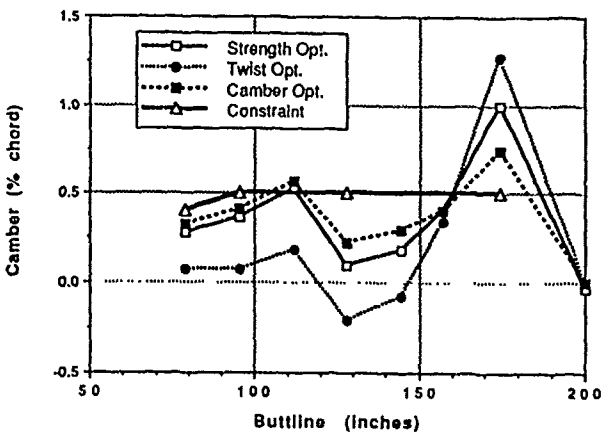

Figure 26: Full-Scale VAT Wing Box Camber Results for ASTROS Optimization

The camber optimization design sacrificed washout twist to increase camber, but note that the twist constraints were violated, as was the minimum camber value at BL 128. Hence, the camber optimization skin is not a converged design. The "hill and valley" pattern that appears in the camber plot is likely due to the use of a polynomial for the skin thickness design variables. The shape function does not allow ASTROS to design local areas of the wing skin to meet local constraints (such as increasing camber near a rib). Hence, in attempting to meet the camber constraint at BL 128, other areas of the wing are "overdesigned" because of the shape function smoothing. The camber optimization does indicate, however, the difficulty of tailoring in general to achieve washout (negative) aeroelastic twist and positive camber at the same time. Aeroelastic washout twist is beneficial to reduce roll damping and alleviate drag due to lift-induced flow separation. Positive camber can benefit roll moment effectiveness for roll power, and in conjunction with washout twist, provide lift-induced drag performance benefits as observed in the VAT program. The inherent conflict in achieving multiple aeroelastic objectives is one that often makes quick achievement of an optimum design difficult.

Further investigation of the camber optimization revealed that some of the camber constraints occur close to where the three ribs of the wing structure appear. Box ribs are located at BL 71, BL 120, and BL 157, and the camber constraints are at Buttlines 78, 95, 128, and 174. A rib will hinder the ability of the box to camber under load. Imposing camber constraints near rib placements may mean that the camber constraints are unrealistic.

To test this hypothesis, another camber optimization was performed. This second camber optimization was identical to the first except that no camber constraint was imposed at BL 128. This spar station is where the design had the most difficulty achieving the desired camber, due possibly to the nearby rib. The other three camber constraints and the twist

constraints were still applied. Figure 27 shows the iteration history of the two camber designs - camber optimization #1 is the original camber design, and camber optimization #2 is the design without the BL 128 camber constraint. Note that when the BL 128 camber constraint is removed, the skin weight decreases by 17%.

Figures 28 and 29 show the resulting twist and camber deformations for the two camber designs. The new camber design is much better able to meet the desired twist and camber than the original camber design. The second camber design still has not met all the deformation constraints, but the exercise has shown that unrealistic camber constraints were being imposed due to the proximity of the camber constraints to the wing ribs. The design is only as valid as the design criteria applied.

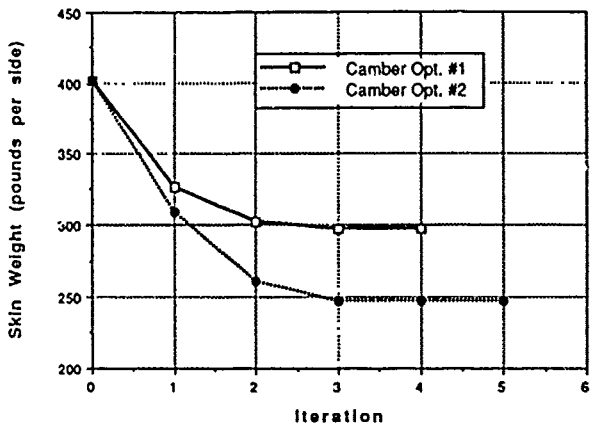

Figure 27: ASTROS Iteration History for Full-Scale VAT Wing Skin Camber Designs

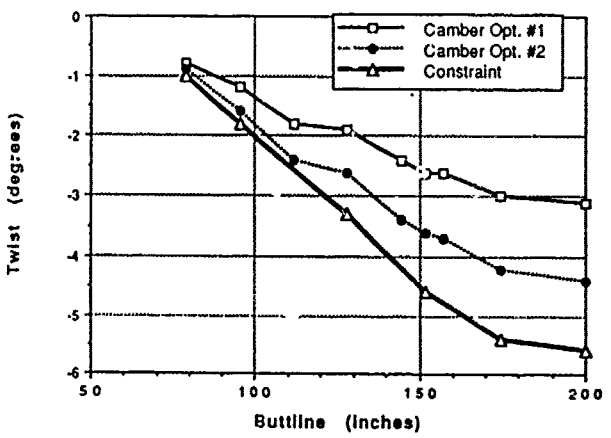

Figure 28: Full-Scale VAT Wing Box Twist Results for ASTROS Camber Optimizations

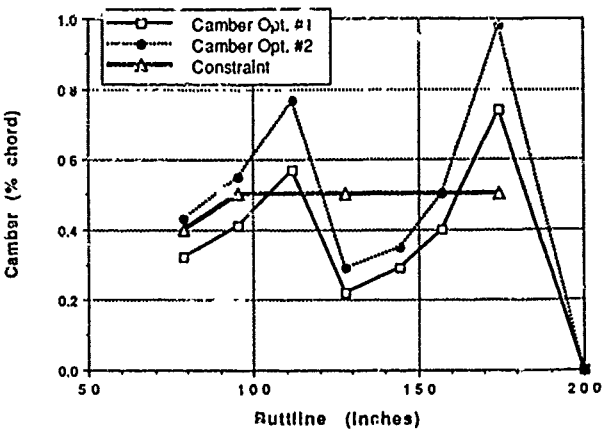

Figure 29: Full-Scale VAT Wing Box Camber Results for ASTROS Camber Optimizations

The evaluation of ASTROS' performance for these designs is accomplished by noting how ASTROS attempted to achieve the twist and/or camber constraints. Figures 30 through 32 show the skin thickness differences (in inches) between the twist optimization skin and the strength optimization skin. Only the wing box outboard of BL 50 is shown. A positive thickness difference means that the twist optimization skin is thicker than the strength skin. Since the lower skin thickness was close to (but not identical to) the upper skin thickness, the figures show only the upper surface skin thicknesses. Figure 30 shows the 0° layer thickness, Figure 31 shows the ±45° layer thickness, and Figure 32 shows the 90° layer thickness. In general, one would expect from previous tailoring experience that greater aeroelastic washout twist would be accomplished by stiffening the front spar area of the wing box. This is what ASTROS indeed did for the twist optimization skin, putting more thickness for the 0° layer near the front spar, and slightly less thickness at the rear spar. Hence, the ASTROS twist optimization is making expected design decisions in attempting to achieve washout twist.

Figures 33 through 35 show the skin thickness differences between the second camber optimization skin (no BL 128 camber constraint) and the twist optimization skin. As before, upper wing surface thicknesses are shown. A positive difference means that the camber optimization skin is thicker. To achieve aeroelastic camber, we expect a tailoring algorithm to increase the thickness of the ±45° layer relative to the 0° and 90° layers. Noting Figure 34 specifically, we see that ASTROS significantly increased the ±45° thickness to achieve more camber than the twist skin. Again, ASTROS is tailoring the composite skin to effectively meet the desired aeroelastic deformation.

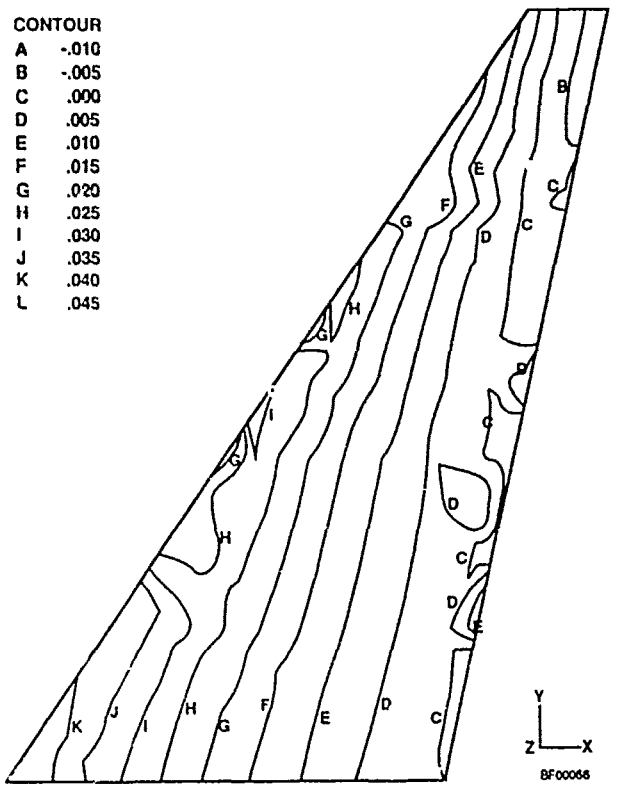

Figure 30: Skin Thickness Difference (inches) Between Strength Optimization and Twist Optimization Skins, Upper Surface, 0° Layer

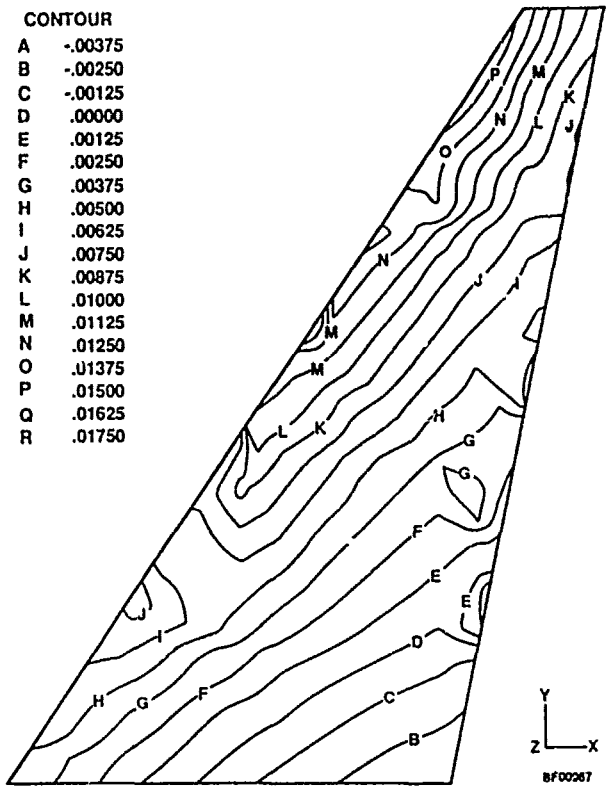

Figure 32: Skin Thickness Difference (inci. .) Between Strength Optimization and Twist Optimization Skins, Upper Surface, 90° Layer

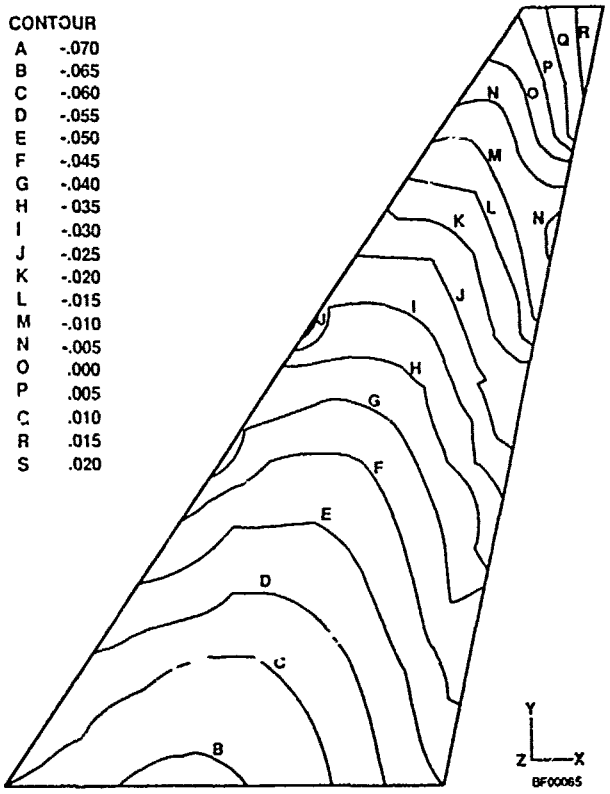

Figure 31: Skin Thickness Difference (inches) Between Strength Optimization and Twist Optimization Skins, Upper Surface, ±45° Layer

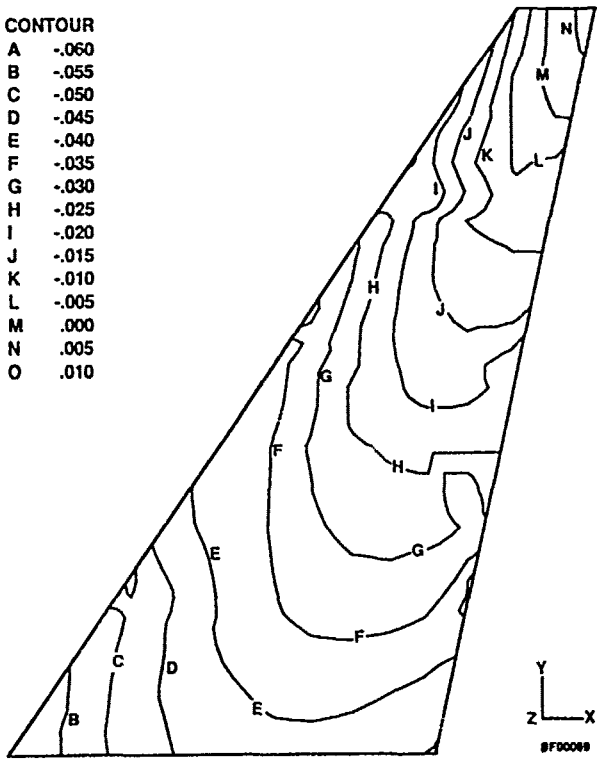

Figure 33: Skin Thickness Difference (inches) Between Twist Optimization and Camber Optimization Skins, Upper Surface, 0° Layer

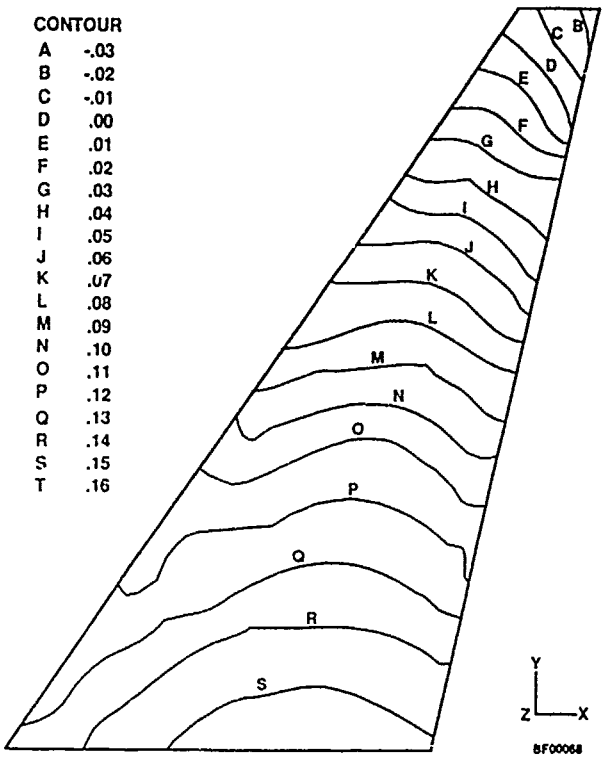

Figure 34: Skin Thickness Difference (inches) Between Twist Optimization and Camber Optimization Skins, Upper Surface, ±45° Layer

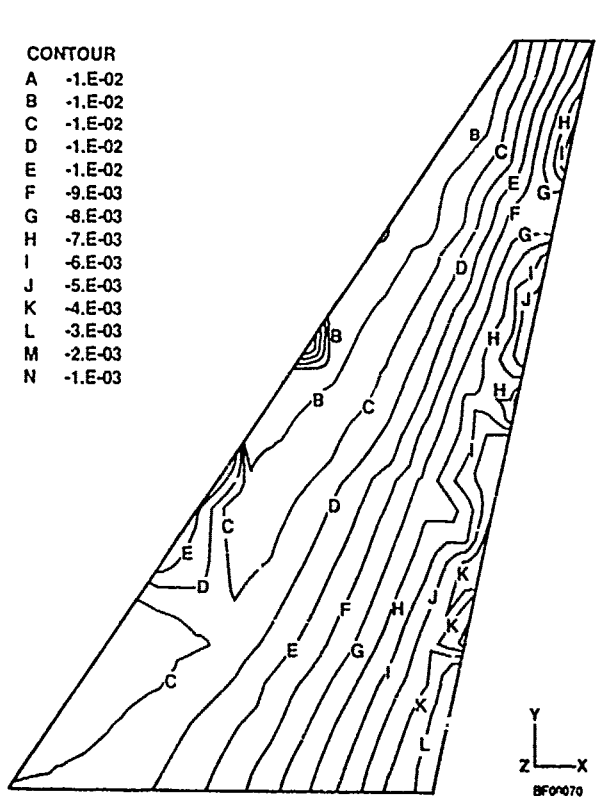

Figure 35: Skin Thickness Difference (inches) Between Twist Optimization and Camber Optimization Skins, Upper Surface, 90° Layer

These three ASTROS optimization runs, although not strictly multidisciplinary, have shown that ASTROS can achieve aeroelastically tailored designs that are minimum weight and achieve desired washout twist and aeroelastic camber. These runs showed that ASTROS also recognized the conflict in designing both camber and washout twist, and demonstrated its ability to reach an optimum design despite opposing constraints.

Conclusions and Future Directions

The static analysis results for the 1/9-scale VAT model have shown ELAPS to be an efficient and accurate tool for structural analysis. Its ease of use and flexibility in modeling various types of configurations make ELAPS a tool that could readily be integrated into a modern aeroelastic analysis and optimization tool that would be beneficial for conceptual and early preliminary aeroelastic design. The use of such Ritz tools, including TSO, is valuable to achieve initial lifting surface skin designs that may be placed on finite element models for more detailed analysis and optimization.

The ASTROS analysis of the 1/9-scale and 1/4-scale VAT models also demonstrated the static, modal, flutter, and static aeroelastic analysis capabilities that ASTROS possesses. The ASTROS results matched extremely well with documented VAT finite element and experimental results from the VAT contract. ASTROS is therefore a multidisciplinary analysis tool that can conduct many analyses in a single run.

The ASTROS optimization with strength and displacement (twist and camber) constraints showed that ASTROS can be effective at designing composite wing skins for desired aeroelastic behavior. The design conflict between washout twist and positive camber, as is frequently encountered in aeroelastic tailoring, is recognized by ASTROS as it strives for a minimum weight design. Also, while the imposition of smooth camber constraints may be desired, it may also be unrealistic given structural arrangements such as rib placement The optimization will only perform as well as the design information given. The design results point to the ability of ASTROS to optimize composite skins for desired aeroelastic performance. Certainly, further characterization of ASTROS' multidisciplinary capabilities is warranted, and is even presented in other discussions at this AGARD workshop.

Much work remains, particularly in integrating controls and performance into the aeroelastic configuration design process. Full modeling of

the aircraft control aspects is needed to establish critical load cases, evaluate control authority, simulate maneuvers, determine hinge moment requirements, among others. Also, aeroelastic benefits that typically require more skin weight, such as washout twist, must be fully evaluated from an aircraft performance viewpoint before tailoring benefits can truly be justified for actual configurations. Further design integration is necessary to accomplish this. The design of the configuration itself, together with control surface size and location, is another issue. Several studies have already begun to address these topics (see, for example, References 2 through 4 and 16 through 20), but continued efforts are needed to implement such design techniques into the aerospace community.

References

1. Shirk, M.H., T.J. Hertz, and T.A. Weisshaar, "Aeroelastic Tailoring - Theory, Practice, and Promise," *Journal of Aircraft*, Volume 23, January 1986, pages 6-18.

2. Love, M.H., R.T. Milburn, and W.A. Rogers, "Some Considerations for Integrating Aeroelasticity in CAE," Presented at the ASME Winter Annual Meeting, Boston, Massachusetts, 13-18 December 1987.

3. Sensburg, O., K. Fullhas, and G. Schmidinger, "Interdisciplinary Design of Aircraft Structures for Minimum Weight," *Proceedings of the 29th Structures, Structural Dynamics and Materials Conference*, Williamsburg, Virginia, 18-20 April 1988, pages 710-738.

4. Love, M.H., and J.D Bohlmann, "Aeroelastic Tailoring in Vehicle Design Synthesis," Presented at the 32nd Structures, Structural Dynamics, and Materials Conference, Baltimore, Maryland, 8-10 April, 1991.

5. McCullers, L.A., and R.W. Lynch, "Dynamic Characteristics of Advanced Filamentary Composite Structures," AFFDL-TR-73-111, September 1974.

6. Lynch, R.W., W.A. Rogers, and W.W. Braymen, "Aeroelastic Tailoring of Advanced Composite Structures for Military Aircraft," AFFDL-TR-76-100, April 1977.

7. Rogers, W.A., W.W. Braymen, A.C. Murphy, D.H. Graham, and M.H. Love, "Validation of Aeroelastic Tailoring by Static Aeroelastic and Flutter Tests," AFWAL-TR-81-3160, Sept. 1982.

8. Johnson, E.H., and V.B. Venkayya, "Automated Structural Optimization System (ASTROS): Volume I - Theoretical Manual," AFWAL-TR-88-3028, December 1988.

9. The MacNeal-Schwendler Corporation, *MSC/NASTRAN User's Manual*, November 1989.

10. Giles, G.L., "Further Generalization of an Equivalent Plate Representation for Aircraft Structural Analysis," *Journal of Aircraft*, Volume 26, Number 1, January 1989, pages 67-74.

11. Albano, E., and W.P. Rodden, "A Doublet-Lattice Method for Calculating Lift Distributions on Oscillating Surfaces in Subsonic Flows," *AIAA Journal*, Vol. 7, No. 2, February 1969, pages 279-285; also Errata *AIAA Journal*, Vol. 7, No. 11, November 1969, page 2192.

12. Johnson, E.H., and D.J. Neill, "Automated Structural Optimization System (ASTROS): Volume III - Applications Manual," AFWAL-TR-88-3028, December 1988.

13. Rogers, W.A., W.W. Braymen, and M.H. Shirk, "Design, Analyses, and Model Tests of an Aeroelastically Tailored Lifting Surface," *Journal of Aircraft*, Volume 20, Number 3, March 1983, pages 208-215.

14 Carmichael, R.L., C.R. Castellano, and F.C. Chen, "The Use of Finite Element Methods for Predicting the Aerodynamics of Wing-Body Combinations," NASA-SP-228, October 1969.

15. Ballhaus, W.F., F.R. Bailey, and J. Frick, "Improved Computational Treatment of Transonic Flow About Swept Wings," *Advances in Engineering Science*, Volume 4, NASA CP-2001, 1976, pages 1311-1320.

16. Zeiler, T.A., and T.A. Weisshaar, "Integrated Aeroservoelastic Tailoring of Lifting Surfaces," *Journal of Aircraft*, Volume 25, Number 1, January 1988, pages 76-83.

17. Barthelemey, J.-F. M., and F.D. Bergen, "Shape Sensitivity Analysis of Wing Static Aeroelastic Characteristics," NASA TP-2808, May 1988.

18. Sobieski, J., "Optimization by Decomposition: A Step from Hierarchic to Non-Hierarchic Systems," *Recent Advances in Multidisciplinary Analysis and Optimization*, NASA CP-3031, September 1988, pages 51-78.

19. Gilbert, M.G., "An Analytical Sensitivity Method for Use in Integrated Aeroservoelastic Aircraft Design," NASA TM-101583, May 1989.

20. Weisshaar, T., and C. Nam, "Aeroservoelastic Tailoring for Lateral Control Enhancement," *Journal of Guidance, Control, and Dynamics*, Vol. 13, No. 3, May-June 1990, pages 458-465.

THE STRUCTURAL OPTIMIZATION SYSTEM OPTSYS – CURRENT STATUS AND APPLICATIONS

Torsten Bråmå
SAAB–SCANIA AB, Saab Aircraft Division
S – 581 88 LINKÖPING, SWEDEN

SUMMARY

OPTSYS is a modular structural optimization system with well defined interfaces to FE–programs and codes for aeroelasticity. A mathematical programming approach is adopted were a sequence of convex approximations of the initial problem is solved, using the MMA method. This approach makes it possible to take all design criteria into account simultaneously. Gradients are calculated semi–analytically. OPTSYS can treat design variables associated to the shape of the structure, the element cross section properties or the material direction in the case of composite materials. Constraints can be defined on displacement, stress, eigenfrequency, local buckling, flutter and aileron efficiency. Recent developments has concerned constraints on dynamic response and acoustics.Other important ingredients are; the integration of a preprocessor to define shape variables, the treatment of discrete variables and the possibility to deal with substructured FE models. The current status of the system capabilities and methods will be discussed and illustrated with applications on aircraft and automotive structures.

LIST OF SYMBOLS

$\mathbf{K}$	stiffness matrix,
$\mathbf{D}$	damping matrix,
$\mathbf{M}$	mass matrix,
ω	eigenfrequency
Φ	eigenmode
ω_f	excitation frequency
$\mathbf{u}$	response vector
$\mathbf{F}$	load vector
$\mathbf{k_e}$	element stiffness matrix,
$\mathbf{d_e}$	element damping matrix,
$\mathbf{m_e}$	element mass matrix,
$\mathbf{v_e}$ $\mathbf{u_e}$	element parts of the response vectors
$\mathbf{X}$	design variable vector
x	design variable
ξ	element variable
$w(X)$	objective function
$g(X)$	constraint function

1 INTRODUCTION

OPTSYS originates from an early version of the OASIS system developed by Esping (Ref 1) and has since 1984 been developed further at Saab Aircraft Division together with the Aeronautical Research Institute in Stockholm. A major contribution has also been made by Svanberg (Ref 2) at the Royal institute of Technology.

Recent OPTSYS developments has concerned constraints on dynamic response and in particular acoustic response. The ASKA FE–system has been developed, in a joint project by Saab Aircraft Division and the Aeronautical Research Institute of Sweden, to include also acoustic analysis (Ref 3). New finite elements have been developed to model the free fluid, porous damping materials and the interaction between the fluid and structural degrees of freedom. The FE approach to the acoustic analysis is best suited for lower frequencies up to a few hundred Hz. For accurate analysis of interior cabin noise, large 3–D FE–models are built but also 2–D models are considered to be useful for parametric studies and optimization.

The OPTSYS system will first be briefly described. Next the possibilities in problem formulation and the methods for the solution of the optimization problem are presented. The methods used in sensitivity analysis regarding dynamic response and flutter are presented in more detail, since this has not been published previously.

OPTSYS has been applied to both aerospace and automotive structures, e.g. an investigation of the potential weight savings in a composite wing of a fighter aircraft involving more than 700 design variables, simultaneous shape and thickness optimization of a Saab 9000 car suspension arm. These applications have been presented elsewhere (Ref 4) but included here for the sake of completeness, followed by an application concerning reduction of cabin noise in a civil aircraft.

2 THE OPTSYS SYSTEM

Figure 1 shows a simplified picture of the system in terms of included software and files. The Pre–processor can be used interactively to create both input to FE–programs and at least parts of the OPTSYS–input (primarily the linking between the formulation of the optimization problem and quantities in the FE model). In the case of shape optimization the pre–processor is also executed in batch mode in order to collect updated node coordinates corresponding to current shape variable values. The analysis programs involved are two alternative FE–programs (ASKA or ABAQUS) and codes for aeroelastic analysis (AEREL and WINGBODY). The sensitivity analysis is performed inside OPTSYS collecting the required data from the analysis programs.

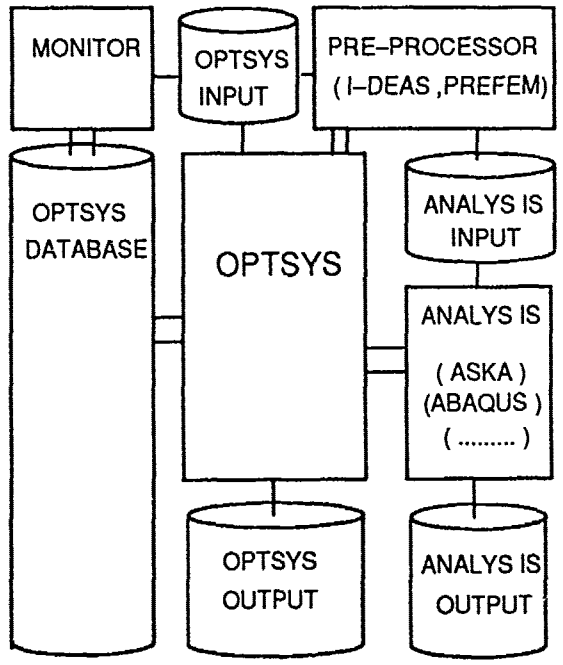

Figure 1

OPTSYS consists of a number of modules communicating only through the OPTSYS database. The sequence of modules to be executed depends of the application. The Monitor is a collection of pre– and post– processing functions for problem formulation, diagnosis of the optimization process and documentation.

The iteration process, illustrated in figure 2, can briefly be described as follows. First the current design is analyzed with respect to all required design criteria. The different analysis are often independent but for instance the aeroelastic programs require structural stiffness data from a preceding FE analysis. Next the status of the optimization process is evaluated and an active set strategy is used to select which gradients to calculate. The gradients are then calculated with the same dependencies as in the analysis step. Finally in the redesign step an explicit subproblem is formulated and solved producing a new set of design variables

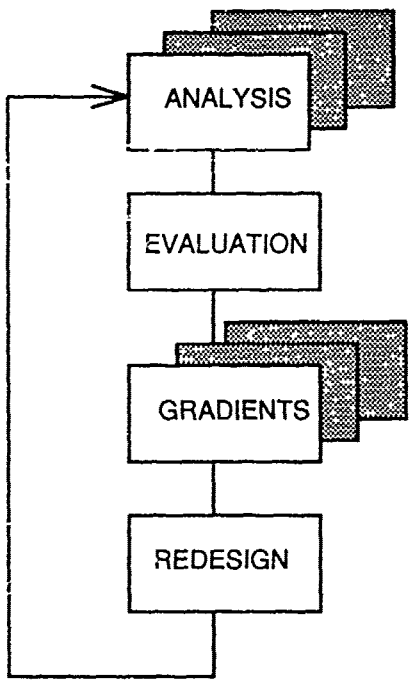

Figure 2

3 METHODS

3.1 Formulation and solution of the optimization problem

A mathematical programming approach is adopted with the following general problem formulation.

$$\text{Min } w(\mathbf{X})$$
$$g_i(\mathbf{X}) < 1$$
$$\mathbf{X}_{min} < \mathbf{X} < \mathbf{X}_{max}$$

The design variables X are linked to element properties ξ in the FE model ; cross section area in rod elements, thickness in shell or membrane elements, material direction in shell/membrane elements in the case of anisotropic material, individual node coordinates or general shape of the structure defined through a geometry model in a preprocessor. For instance can the thickness of several elements be linked to the same design variable by the linear relation

$$\xi(x) = \text{konstant} + \text{coefficient} \cdot x$$

The objective function $w(\mathbf{X})$ can be associated to the structural weight or moment of inertia.

A constraint function $g(\mathbf{X})$ can represent displacement, stress or local buckling in the case of static response, structural or acoustic response in the dynamic case, structural eigenfrequency, flutter or aileron efficiency criteria.

In each global iteration an explicit convex subproblem is formulated using the MMA method (Ref 2), where first order gradients of the included functions are needed. If discrete variables are included in the problem, MMA makes a search for the best discrete point in the neighbourhood of the continuous solution.

An active set strategy is applied to select a subset of the constraints to be included in the subproblem. The active set can be modified from iteration to iteration.

3.2 Sensitivity analysis

A semi–analytical approach is adopted where the derivatives of element properties are derived numerically.

$$\frac{\partial \mathbf{k}_e}{\partial \xi} = \frac{\mathbf{k}_e(\xi + \Delta\xi) - \mathbf{k}_e(\xi)}{\Delta\xi}$$

Element properties considered so far are weight, moment of inertia, stiffness matrix, mass matrix, strain–displacement matrix, load vector and transformation matrix to material directions.

The increments are derived differently depending on the type of design variable. For example, if it is thickness variable the increment is simply a constant factor times the current thickness. If it is a shape variable, disturbed node coordinates are first produced by the preprocessor corresponding to increments in the shape variable values. The disturbed node coordinates are then used when calculating the element properties.

The element properties and their derivatives are stored on the database and used later in different types of sensitivity calculations.

Static response constraints

The static response problem in matrix form ;

$$\mathbf{K}\,\mathbf{u} = \mathbf{F}$$

The displacement constraint is generally formulated as a linear combination of the components in the response vector.

$$f = \mathbf{q}^t \mathbf{u}$$

The derivative of f with respect to a design variable x is derived as follows, assuming that q not is dependent of x ;

$$\frac{\partial f}{\partial x} = \mathbf{q}^t \frac{\partial \mathbf{u}}{\partial x} = \mathbf{v}^t \frac{\partial \mathbf{F}}{\partial x} - \mathbf{v}^t \frac{\partial \mathbf{K}}{\partial x} \mathbf{u}$$

where v is the solution to the following problem ;

$$\mathbf{K}\,\mathbf{v} = \mathbf{q}$$

An element strain component is also a linear combination of the components in the response vector and can be calculated similarly.

$$\varepsilon_i = \mathbf{q}^t \mathbf{u}$$

The vector q corresponds in this case to the element strain–displacement relation which depends on the element formulation. In this case q can be dependent of x ;

$$\frac{\partial \varepsilon}{\partial x} = v^t \frac{\partial F}{\partial x} - v^t \frac{\partial K}{\partial x} u + u^t \frac{\partial q}{\partial x}$$

In the case of anisotropic material, it is desired to calculate strains in the material direction. If the material direction is connected to a design variable we get the derivative as ;

$$\frac{\partial \varepsilon_m}{\partial x} = \frac{\partial T_m}{\partial x} \varepsilon + T_m \frac{\partial \varepsilon}{\partial x}$$

T_m is here the transformation matrix to material directions.

Derivatives of corresponding stresses can now be calculated as ;

$$\frac{\partial \sigma}{\partial x} = E \frac{\partial \varepsilon}{\partial x}$$

assuming here that Hooks matrix E is constant.

The local buckling criteria in truss elements is formulated as

$$\frac{\sigma L^2}{E c a} < 1$$

where

σ	the stress in the bar (compression positive)
L	the length of the bar
a	the area of the bar
E	the module of elasticity
c	the buckling constant which depends on the cross section shape (not the size !) and the boundary conditions.

Applying the chain rule again we get

$$\frac{\partial}{\partial x}\left(\frac{\sigma L^2}{E c a}\right) = \frac{L^2}{E c a} \frac{\partial \sigma}{\partial x} - \frac{\sigma L^2}{E c a^2} \frac{\partial a}{\partial x} + \frac{\sigma 2 L}{E c a} \frac{\partial L}{\partial x}$$

The local panel buckling criteria has the following form ;

RG = FUNC(R1, R2, R12) ,

where R1, R2 and R12 are buckling margins for individual stress components. For example $R1 = -\sigma 1 / (C1\ t^2)$ where

σ1	stress in the 1 direction
C1	input parameter
t	total panel thickness

This means that for a compression greater than $\sigma 1 / (C1\ t^2)$ we will have local buckling in the panel. RG takes the total stress state into account by applying the function FUNC to the individual components. FUNC is evaluated from experimental data and explicitly stored into the software.

Eigenfrequency constraints

The structural eigenvalue problem in matrix form ;

$$(K - \omega^2 M) \Phi = 0$$

The derivative of one eigenfrequency with respect to a design variable x is then calculated according to;

$$\frac{\partial \omega^2}{\partial x} = \frac{1}{\Phi^t M \Phi} \Phi^t \left(\frac{\partial K}{\partial x} - \omega^2 \frac{\partial M}{\partial x} \right) \Phi$$

assuming that the eigenmode is normalized with respect to M, the derivative can be calculated with contributions from affected elements as ;

$$\frac{\partial \omega^2}{\partial x} = \sum_e \left[\Phi_e^t \left(\frac{\partial k}{\partial x}_e - \omega^2 \frac{\partial m}{\partial x}_e \right) \Phi_e \right]$$

The constraint is so far simply formulated as a lower limit for the eigenfrequency.

Dynamic Response Constraint

The treatment of dynamic response constraint is similar to the static case but the character of the dynamic response constraint is however not as attractive to deal with.
The dynamic response is not a monotonous function of structural size variables, as a maximum will occur when an eigenfrequency gets close to the excitation frequency. This will lead to unconnected feasible regions in the design space which is a major difficulty for the optimization algorithm.

The dynamic response problem in matrix form ;

$$(K + i \omega_F D - \omega_F^2 M) u = F$$

The vectors **u** and **F** are complex and represent the amplitude and phase in the harmonic vibration. The response vector consists in the structural parts of the usual displacements depending on the type of finite element used and in the acoustic cavity parts of the model we find the acoustic pressure as one degree of freedom.

The dynamic response constraint is now defined as the absolute value of a linear combination of components in the response vector defined as

$$f = q^t u$$

q is a vector containing combination coefficients and

$$|f| = \sqrt{f_{Re}^2 + f_{Im}^2}$$

where Re indicates the real part and Im the imaginary part.

In the acoustic case the constraint can alternatively be applied to the sound pressure level, SPL, defined as;

$$SPL = 20 \log \frac{|f|}{\sqrt{2}\, p_o}$$

where p_o is the acoustic reference pressure.

Using the symbol **Q** for the system matrix

$$Q u = F$$

Differentiating with respect to one variable x and pre–multiplying with q^t gives :

$$q^t \frac{\partial u}{\partial x} = v^t \frac{\partial F}{\partial x} - v^t \frac{\partial Q}{\partial x} u$$

where **v** is the solution of

$$Q v = q$$

Here **v** is complex if **Q** is complex.

Assuming here that the derivative of **F** is zero, we can now write;

$$\frac{\partial f}{\partial x} = \left(\frac{\partial f_{Re}}{\partial x} , \frac{\partial f_{Im}}{\partial x} \right) = \mathbf{q}^t \frac{\partial \mathbf{u}}{\partial x} =$$

$$-\sum_e \left[\mathbf{v}_e^t \left(\frac{\partial \mathbf{k}}{\partial x}_e + i\omega_F \frac{\partial \mathbf{d}}{\partial x}_e - \omega_F^2 \frac{\partial \mathbf{m}}{\partial x}_e \right) \mathbf{u}_e \right]$$

Finally the derivative of the absolute value can be expressed as

$$\frac{\partial |f|}{\partial x} = \frac{f_{Re}}{|f|} \frac{\partial f_{Re}}{\partial x} + \frac{f_{Im}}{|f|} \frac{\partial f_{Im}}{\partial x}$$

and the derivative of the sound pressure level as

$$\frac{\partial (SPL)}{\partial x} = \frac{20 \log e}{f} \cdot \frac{\partial f}{\partial x}$$

Flutter Constraints

Flutter is a serious vibration phenomenon which, if it occurs, might be disastrous. It is therefore vital to be able to avoid flutter in the structural design process. At Saab Aircraft Division the AEREL system is used for flutter analysis (Ref 5). The analysis of this aerodynamic instability yields a nonlinear and complex eigenvalue problem. The location of the eigenvalues in the complex plane indicate if the vibrations are stable or not.

AEREL first calculates generalized aerodynamic forces (transfer functions) using separate AEREL modules for subsonic and transsonic speed. Then the nonlinear (and complex) eigenvalue problem is solved.

$$\left(K_0 + \omega D_0 + \omega^2 M_0 + \frac{v^2}{\pi \mu} A \left(\frac{\omega}{v} \right) \right) \Psi = 0$$

where

$K_o = K / (m_r \omega_r^2)$	dimensionless stiffness matrix
$D_o = D / (m_r \omega_r)$	dimensionless damping matrix
$M_o = M / m_r$	dimensionless mass matrix
$A (p) = A (\omega / v)$	aerodynamic transfer function
ω	flutter eigenvalue
Ψ	flutter eigenmode
m_r	reference mass
ω_r	reference frequency
S , L	reference area and length
U , ρ	free-stream speed and density
$v = U / (\omega_r L)$	dimensionless free stream speed
$\mu = 2 m_r / (\pi \rho S L)$	mass ratio

K, D, M and **A** are expressed in a base of m selected structural eigenmodes, **Φ**.The eigenmodes and the matricies **K** and **M** are obtained from the FE model calculations or from ground vibration tests. $\mathbf{D}_o$ can likewise be obtained from tests but can usually be neglected. **A** , which is calculated by AEREL, depends on the Mach number and the Laplace transform parameter $p = \omega / v$. ρ depends on the air density (altitude).

The complex eigenvalues indicate if the modes are stable or not. If the damping factor defined by

$$g = - \frac{\omega_{Re}}{\omega_{Im}}$$

is negative, the associated mode is unstable. The imaginary part is the circular frequency of the flutter mode.

For desired combinations of Mach numbers and altitudes, m eigenvalues are calculated.

The flutter constraint is formulated to assure a certain amount of damping for all modes and for all flight cases specified.

Derivatives of the damping factor :

Using the symbol **Q** for the system matrix, the eigenvalue problem is written

$$\mathbf{Q} \Psi = 0$$

and we define the associated vector Ψ_a by

$$\mathbf{Q}^t \Psi_a = 0$$

The vectors Ψ and Ψ_a are not identical since Q is not symmetric.

By differentiating with respect to a design variable x and multiplying by Ψ_a^t, we get

$$\Psi_a^t \frac{\partial \mathbf{Q}}{\partial x} \Psi = 0$$

and then

$$\frac{\partial \omega}{\partial x} = - \frac{1}{c} \Psi_a^t \left(\frac{\partial \mathbf{K}}{\partial x}_0 + \omega \frac{\partial \mathbf{D}}{\partial x}_0 + \omega^2 \frac{\partial \mathbf{M}}{\partial x}_0 \right) \Psi$$

where

$$c = \Psi_a^t \left(2 \omega \mathbf{M}_0 + \mathbf{D}_0 + \frac{v}{\pi \mu} \frac{\partial \mathbf{A}}{\partial p} \right) \Psi$$

Differentiating the damping factor with respect to one variable x, we immediately get

$$\frac{\partial g}{\partial x} = \frac{1}{\omega_{Im}^2} \left(\omega_{Re} \frac{\partial \omega_{Im}}{\partial x} - \omega_{Im} \frac{\partial \omega_{Re}}{\partial x} \right)$$

The contribution from $\partial \mathbf{D}_o / \partial x$ is neglected in the program, while $\partial \mathbf{A} / \partial p$ is calculated in AEREL.Accurate calculation of the aerodynamic transfer functions is time consuming and such a calculation is therefore done in AEREL only for a limited number of discrete values of p. A linear combination of simple analytic functions is then fitted to the discrete values and employed in the final routine. The additional statements required in AEREL for calculation of $\partial \mathbf{A} / \partial p$ (via differentiation of the combination) is therefore very simple.

K, M , $\partial \mathbf{K} / \partial x$ and $\partial \mathbf{M} / \partial x$ are calculated by OPTSYS using information obtained from the FE analysis.

For instance , the derivative of the stiffness matrix is calculated as a sum over finite elements affected by **x** ;

$$\frac{\partial \mathbf{K}}{\partial x} = \sum_e \Phi_e^t \frac{\partial \mathbf{k}}{\partial x}_e \Phi_e \quad , \quad (m \times m)$$

4. APPLICATIONS

4.1 Shape optimization of a Saab 9000 suspension arm

In order to investigate the performance of a proposed new wishbone design (figure 3) for the Saab 9000 car, an optimization project was initiated. The new design is of forged aluminium, the one in production is built from pressed steel parts. Optimization is important here since a low unsprung weight of the suspension is crucial for a performance car.

A simple problem formulation for a first re–design attempt was sought.

A FE–model consisting of 230 shell elements was applied with three loading cases; maximum straight line breaking, maximum lateral acceleration (cornering) and maximum combined braking/lateral acceleration.

The cross sectional properties along the wishbone was varied by having the thickness of the elements as variables in the optimization problem. The inner boundary was described by B–splines in the geometry description of the preprocessor PREFEM (Ref 6). The control–points of these splines were connected to design variables. Upper and lower limits on the values of the design variables accounted for various geometrical limitations (figure 4).

Stress constraints were defined to keep the maximum von Mises stress below the yield stress. The basic stiffness requirement was that the stiffness of of the new wishbone should equal the stiffness of the original (steel).

The resulting optimization problem contained a total of 8 thickness variables, 6 shape variables, 1300 stress and 6 deflection constraints.

The problem was solved in 9 iterations. For a weight increase of 40 percent OPTSYS found an optimal solution with sufficient stiffness (63 percent increase). The final design was determined, for this problem statement, completely by the stiffness requirements, two of which were at the critical limit. The stress constraints had no impact on the final design as they all were non–critical (albeit very close). Results are shown in figures 4, 5 and 6.

The thickness distribution of the final design was dominated by the defined lower limit. The exception being the far "left" part which thickness probably was increased to create enough stiffness for the lateral load.

The average CPU time per iteration, on a VAX 8800, was roughly 550 seconds including the FE analysis part taking about 100 seconds.

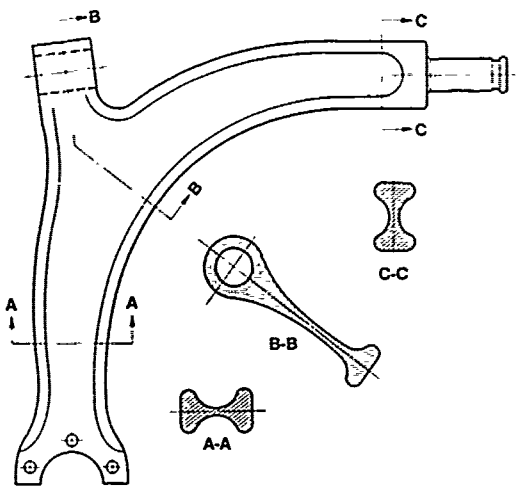

Figure 3 Wishbone layout

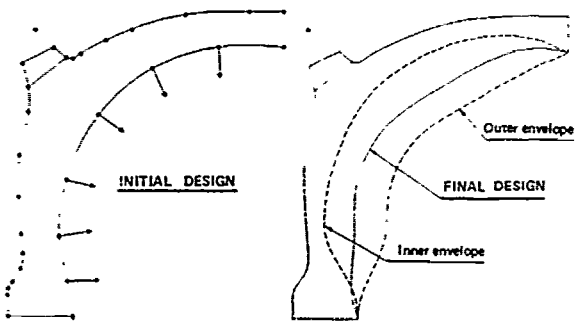

Figure 4. Geometry of initial and final design

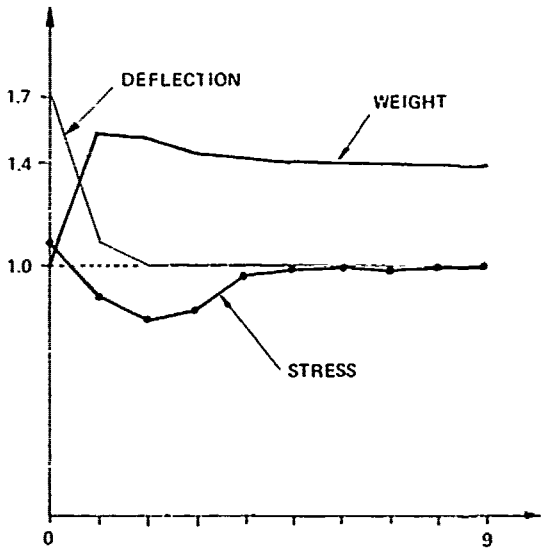

Figure 5. Iteration histories

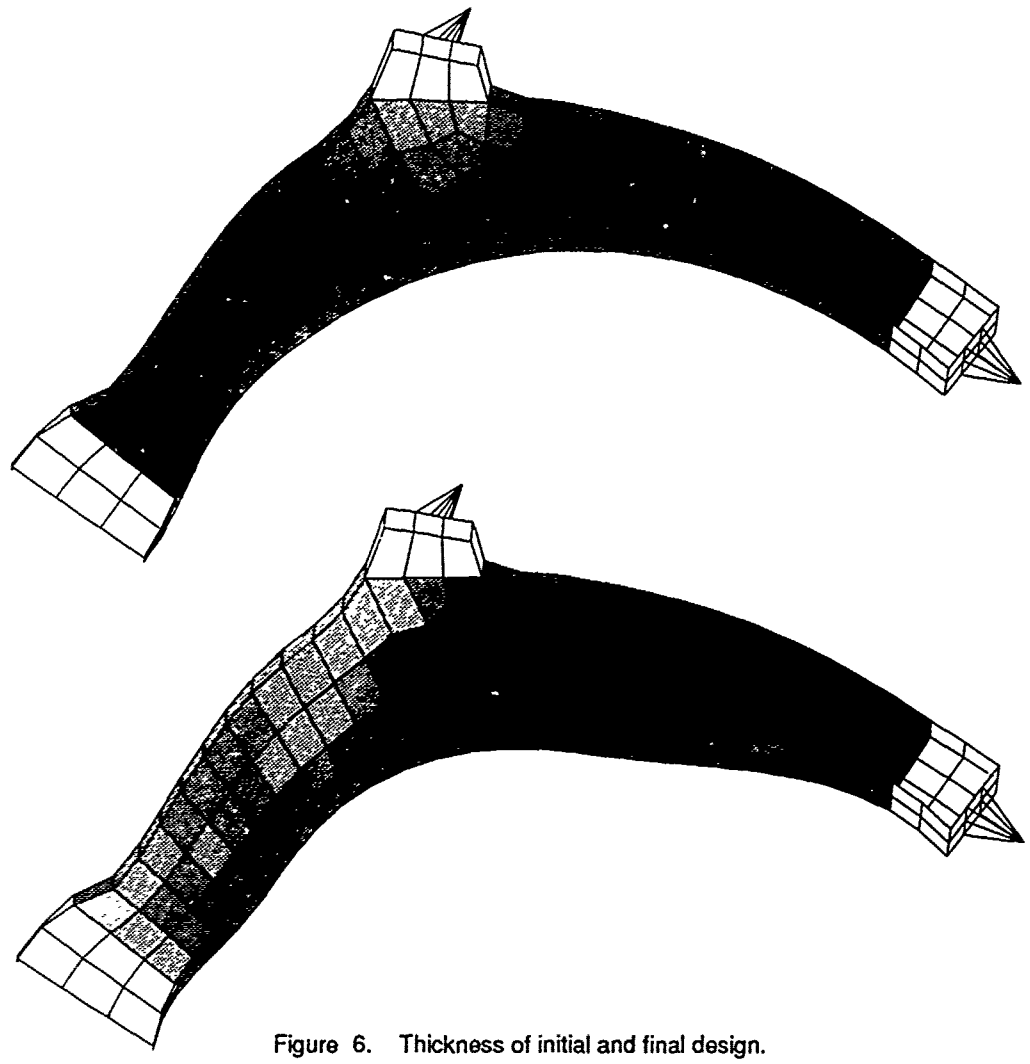

Figure 6. Thickness of initial and final design.
Dark – thin. Light – thick.

4.2 Composite wing of the Gripen aircraft

The main purpose of this very large application was to investigate the possible weight savings for redesign of the wing skins with two choices of new composite materials.

A substructured FE–model of the complete aircraft was used. By including the optimizationwise active parts of the wing structure in a separate substructure, the amount of calculations needed in each iteration was reduced to a reasonable size. The active substructure contained about 5000 degrees of freedom compared to the 125000 in the complete aircraft model. Eight loading cases were selected for this study.

The design variables were associated to layers in 254 different composite stacks. The layup in each stack was defined by three independent variables controlling the number of 0 degree layers, 90 degree layers and +/– 45 degree layers, making a total of 762 design variables. One or several finite elements in the wing panels were then linked to each stack. Explicit linear constraints were defined on the sum of all thickness variables connected to the same stack to limit the total thickness of the wing panel. Constraints were also imposed on fibre strain and local buckling in the composite. Constraints on the aircraft performance such as aeroelastic efficiency should ideally also have been included. However, as the criteria was to maintain current performance, it was here considered sufficient to formulate the aeroelastic requirements as a number of constraints on the wing torsion. A total of about 20000 potential constraints were defined of which a few hundred were active in the final design.

Six global iterations were enough to solve this problem for each of the two alternative materials. Each iteration needed approximately 2000 CPU seconds in the CRAY 1–A ; 130 seconds for the reanalysis, 1000 seconds for the gradient calculation and 800 seconds for the solution of the approximate subproblem. The portion of the iteration time consumed by the subproblem solution was much larger here than in smaller problems. One way to reduce this portion is to lower the accuracy in the solution of the subproblem.

The layups produced by OPTSYS have to be adjusted to production requirements impossible to account for in the original problem formulation. This manual work leads of course to increased weight and can be very tedious. Good post processing aids are absolutely vital when dealing with

4.3 Reducing cabin noise in the Saab 340 aircraft

Passenger comfort is of great importance in most transport vehicles. For instance, in the new generation of regional turboprop aircraft, a low noise level is vital to be competitive on the market. The possibilities to predict noise levels analytically has improved rapidly in recent years. This will make it possible to take acoustic design criteria into account in early project stages.

The 2-D FE-model (figure 9) , representing a cross section of the Saab 340 fuselage close to the plane of the propeller, consists of one substructure for the structural part and another substructure for the cavity. The cavity substructure contains 2-D acoustic elements and interface elements connecting the cavity model to the outer flange. Four tuned dampers are included in the model. The tuned damper is modeled as a point mass connected to the structure with a spring parallel to a dashpot. The introduction of the dashpot makes the system matrix complex.The excitation from the propellers was measured on the outside of the fuselage (amplitude and phase) and translated to complex nodal forces in the FE-model.

The design variables are chosen to be the cross section area of the inner flange to investigate how much stiffening of the frame can reduce the cabin noise. The objective function is the weight of the inner flange, i.e. the weight of the elements associated to design variables. The acoustic design criteria is an upper limit of the sound level in three points in the cabin corresponding to measurement points in flight tests.

The location of the four tuned dampers, the 37 design variables and the three constraint points are indicated in figure 10.

The desired sound level is reach after five iterations by adding material mainly at design variables 24, 25 and 26. The iteration history is given in figure 11. Figure 12 shows the real part of the final structure response including both the structural displacements and the air pressure distribution.

This application was a test problem in connection with the development of acoustic constraints. In a more realistic application of course other design criteria have to be considered as well. Current development includes the possibility to link the properties of the tuned damper to a design variable.

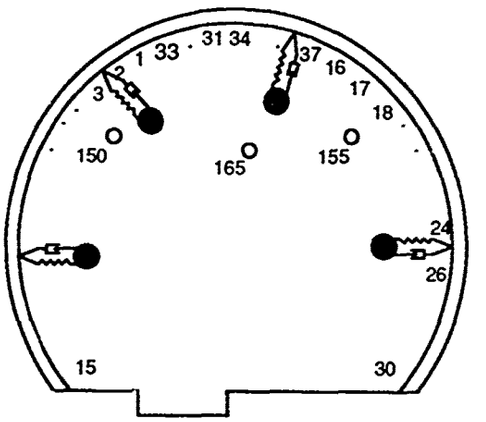

Figure 10

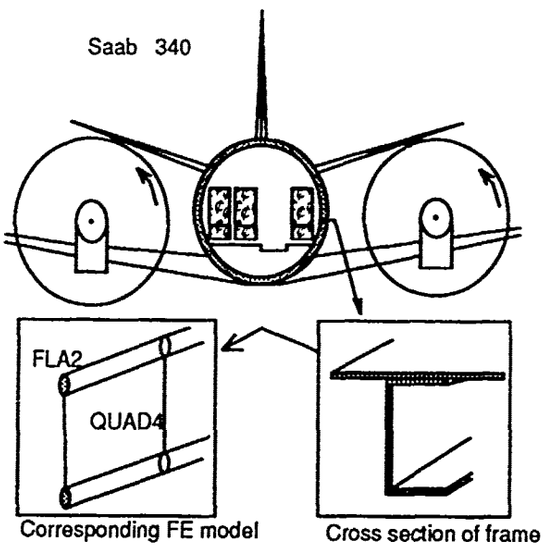

Figure 9

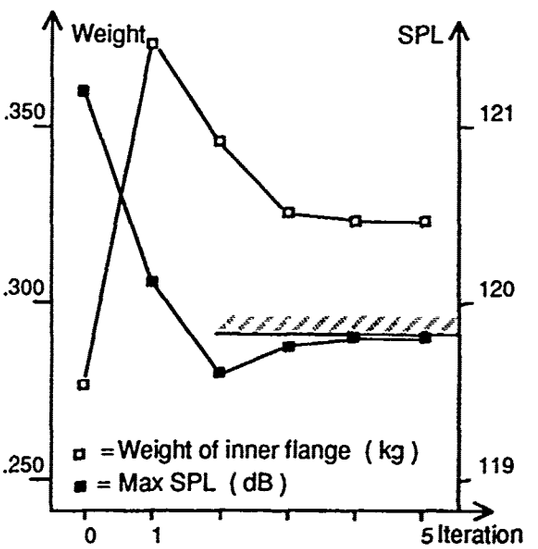

Figure 11

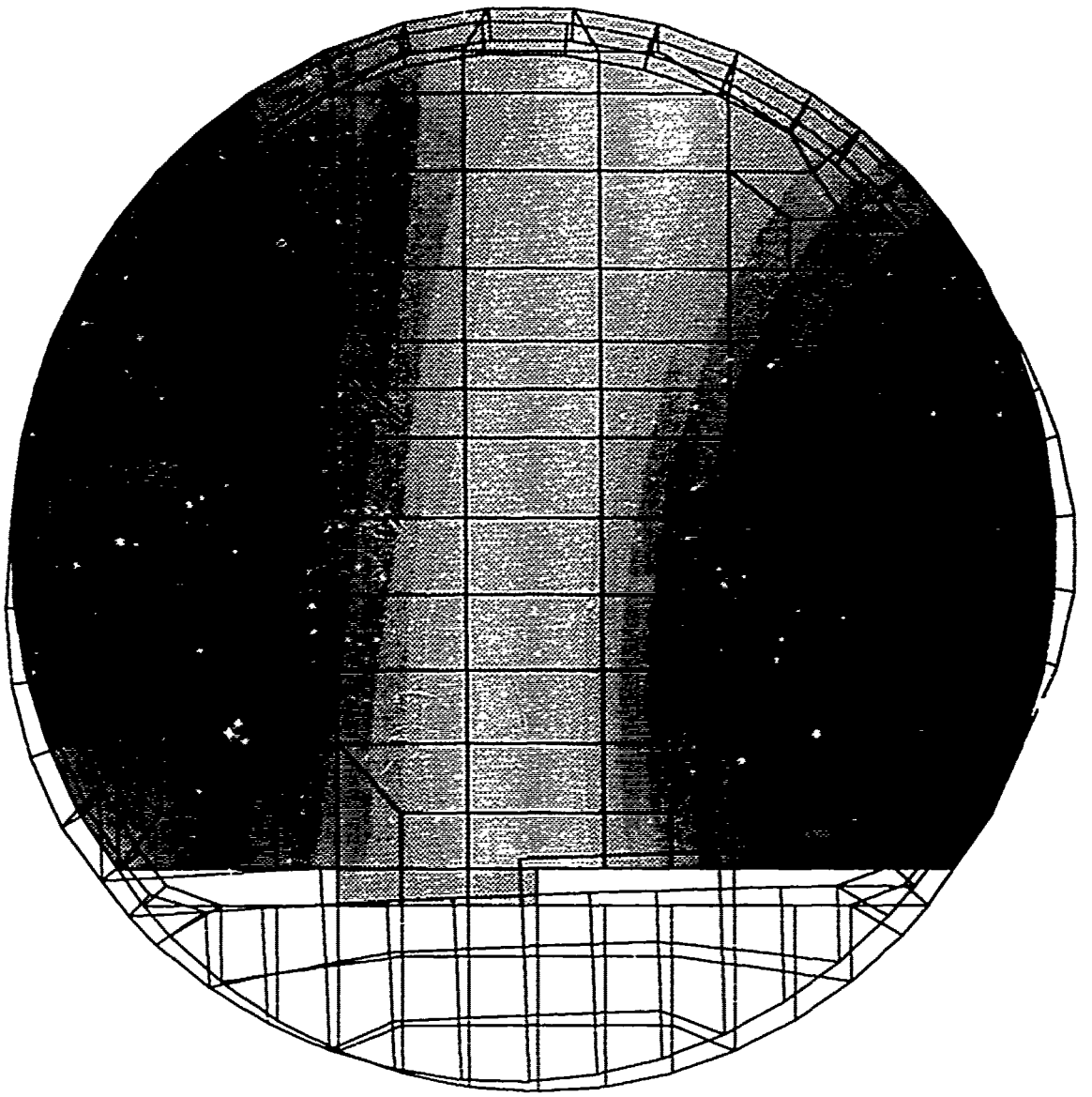

Figure 12. Sound level and real part of structural response

5 REFERENCES

1) Esping, B.J.D. , "The OASIS structural optimization system", Computers and Structures, vol. 23, No 3, pp. 365–377, 1986.

2) Svanberg, K. , "The Method of Moving Asymptotes – a new method for structural optimization", International journal for numerical methods in engineering, Vol. 24, pp. 359–373, 1987.

3) Sandberg, G. and Göransson, P. , "A Symmetric Finite Element Formulation for Acoustic Fluid–Structure Interaction Analysis", JSV, Vol. 123 (2), 1988.

4) Bråmå, T. "Applications of the structural optimization program OPTSYS", ICAS–90–2.1.3 , 1990.

5) Stark, V. J. "The AEREL Flutter Prediction System", ICAS–90–1.2.3 , 1990.

6) PREFEM, User manual, version 5.4, Veritas Sesam Systems A.S.

APPLICATION OF AN AUTOMATED MULTIDISCIPLINARY ANALYSIS AND OPTIMISATION SYSTEM TO THE DESIGN OF AIRCRAFT STRUCTURES.

by

D. Thompson B.Sc., A.R.C.S.
Group Leader - Analysis Development
and
J.C. Ayres B.Sc.
Senior Stress Engineer

British Aerospace,
Military Aircraft Ltd.,
Warton Aerodrome,
Nr. Preston,
Lancashire
PR4 1AX

ABSTRACT

Prior to the development of the ECLIPSE system at Warton, Structural Optimisation was performed by a combination of software and manual methods. These methods proved their worth by the reductions in cost and improvements in quality resulting from their use.

The programme used for Optimisation of structures subject to Stiffness criteria became the focus for development of the Aeroelastic Constraints. This was later extended to incorporate Strength constraints, fabrication constraints and was coupled directly to the NASTRAN Analysis sytem. This process of development continued with the result of the present general Resizing, Optimisation and Post-Processing system.

This paper describes the application of the system to the Optimisation of three structures:- Tailplane, Fin/Rudder and Foreplane. The emphasis is on the use of the system to Optimise for a Flutter Speed Constraint in all three cases. However in the case of the Foreplane the adaption of the system to include a Detail Stressing Constraint is illustrated.

A brief description of some of the developments proposed for the future is also given.

1. INTRODUCTION

Structural Optimisation/Resizing has been performed at BAe MAL ever since the company started designing and building aircraft. In the early days the sizing of structures was performed as an iterative process between the Aerodynamics, Design and Stress departments. Each area would perform their own "Optimisation" exercise then pass the resultant structure to one-another for checking against the departments own constraints. Optimisation methods employed in the Stress Office were based upon the Fully Stressed Design approach in which each each element is loaded to its maximum under at least one loading case.

For a statically determinate structure this is a simple procedure requiring only one step. However for redundant structures an analysis- resize-analysis iteration process is required. Although the analysis had been automated by the use of the Finite Element Method, the resizing was a manual operation on the model input data which in those days was on computer cards. Therefore the first attempts in automated resizing were directed towards removing this manual intervention. Success in this area resulted in the rapid generation by Stress Office of models which satisfied the given Strength constraints. Data in the form of

Flexibility, Stiffness and Mass Matrices generated from these models was then passed to Aerodynamics in order for them to perform their Aeroelastic Analysis.

Mr R. I. Kerr who had earlier investigated the use of classical methods (Calculus of Variations - See Ref 1) to Optimise structures for Stiffness constraints now directed his efforts to adapting Finite Element Analysis methods to the process. This resulted in the development of the so-called "Optimality Criteria" methods which formed the foundation for future work. A system was developed using BAe Warton's "In-House" Finite Element system to Optimise structures for Strength and Stiffness. The Stiffness constraint in this case being simply a limitation on a Grid point deflection which was subsequently extended to a Generalised deflection.

The first attempt at using the system to optimise for Aeroelastic constraints was aimed at Aeroelastic Efficiency. Aerodynamic loading was provided by simple Strip Theory with the constraint transformed into a limitation on the Generalised deflection. As both Stress Office and Aerodynamics became more aware of each others problems and analysis methods it became possible to obtain Aerodynamics in the form of Aerodynamic Influence Coefficients (AICs) at agreed Structural grid points. The Efficiency criteria could then be solved directly using the Rigid and Flexible loading obtained from the AICs and Structure Flexibility. The system then developed rapidly being applied to the following Aeroelastic constraints of Divergence, Hinge Moment and Roll Rate. A frequency constraint was incorporated and then extended to apply to frequency seperation, this was used as an initial attempt to Optimise for Flutter speed.

A major task was the integration of the system with the NASTRAN analysis system and at the same time provide a "User Friendly" interface to the increasing number of people requiring to use

Whilst all the above developments were proceeding, the development of optimisation methods not directly related to F.E. Analysis were being carried out. A program which optimised integrally stiffened panel sizes was produced. This used a Conjugate Gradient technique as the central optimiser. Other methods investigated were Geometric Programming , Linear Programming, Quadratic Programming, Integer Programming and Feasible directions. The Linear Programming methods were later incorporated into the ECLIPSE system.

The optimisation of laminates for strength and local stability constraints was performed by a simple stress ratioing approach which has since been replaced by a method employing a Sequence of Linear Programmes (SLP). Stiffness optimisation of laminates was performed by the "Optimality Criteria" approach, however it was and still is limited to membrane elements that is elements whose in-plane stiffness is independant of stacking sequence.

The ECLIPSE system is under continous change, new constraints are being incorporated, modifications to adapt to data base techniques are being investigated and the coupling of the system to graphical pre and post- processors is on-going. The system has developed from a simple Optimisation tool into a general resizing,optimisation and post processing system coupled to Finite Element Analysis. It has been used in the design and modification of the following aircraft:- Jaguar, Tornado, JAS, EAP and EFA.

2. OVERVIEW OF THE ECLIPSE SYSTEM

As mentioned in the introduction the ECLIPSE system has developed from a simple Optimisation programme into a complex Optimisation, Sizing and Post Processing system. Its development is directly linked to the existing Stress Office requirements. At present the priority is extending the Post-Processing capabilities to include additional detail stressing requirements.

2.1. Scope of the program

It can be seen from Figure 2.1 that ECLIPSE uses NASTRAN as its F.E. Analysis system. A block of ECLIPSE data entries are input describing the constraints,detail stressing and sources of aeroelastic data. This block is followed by the NASTRAN bulk data block. No NASTRAN executive or case control data is required as the ECLIPSE system will generate the required data depending on which types of constraints are being processed. The following types of Analysis are available:

Static Analysis
Normal Modes Analysis
Aeroelastic Analysis
Stability Analysis (VICON)

At present the Super Element analysis is restricted to the Post- Processing facility.

All NASTRAN data entries can be used in the Bulk Data however the system will only re-size the following elements:-

CONROD,CROD - Rod Area
CBAR - Bar Area
CSHEAR - Thickness
CQUAD4,CTRIA3 - Thickness
(CELAS1,CELAS2) - Mass

The sizing of bars is based on the provision of the relationship between the cross-sectional area and the second moments of Area. Similarly the sizing of springs is based on the provision of relationship between the spring mass and stiffness. Shear panels can have associated rods, however these rod areas are related to the element thickness and will therefore not undergo direct resizing. Isotropic CQUAD4 and CTRIA3 elements can have membrane,membrane-bending coupling and bending properties. Elements of this type which correspond to laminated material can only be represented as membrane elements when being optimised for stiffness constraints.

The system is capable of handling the following constraints:-

Strength

Maximum Principal Stress
Maximum Shear Stress
Maximum Fibre Strain
Panel Stability
Local Pressure Effects
Transverse Differential Shear

Stiffness

Generalised Deflection
Frequency
Frequency seperation
Aeroelastic Efficiency
Aeroelastic Hinge Moment

Aeroelastic Deflection
Roll Rate
Flutter and Divergence speed.

Gauge Constraints

Minimum sizes
Maximum sizes
Minimum % sizes
Maximum % sizes
Combined sizes.

2.2. System Operation

The main modules of the system can be seen in Figure 2.1, each of these modules can be broken down further into modules performing a specific task e.g. mode tracking in Flutter analysis. The Pre-Processor is the largest module in the system. From the data contained on the ECLIPSE and NASTRAN data it automatically assigns files, sets up execution flow and performs checks on the input data.

The NASTRAN Flexibilty and/or Normal modes Analysis generates data which is used by the Aero Processor to formulate the derivatives of the Aeroelastic constraints. The Aero Processor checks the AIC matrices, Determines the Flexible Aero loading and generates the Flutter mode shapes.

The NASTRAN Strength,Frequency and Stiffness Analyses generate element forces and energies to be used by the resizing/optimisation module. This module reads the element forces,transforms them according to the detail stressing requirements and adds in any additional forces not present in the analysis. The elements are then resized to meet the required reserve factor assuming the element loading is constant. The sizes resulting from the strength constraints are then used as minimum sizes in the stiffness resizing routines which use the element energies to determine the constraint derivatives. More explanation of this process is described in the theoretical section. The number of iterations of analysis - resizing is specified by the user, in most cases the results converge after four to six loops.

The remaining modules perform the requested NASTRAN analyses and post processing on data produced by these analyses. Detailed output for each element and constraint considered is produced. Processing of elements and criteria not considered in the Optimisation can also be performed. Component mass breakdowns are available with various summary tables which enable the user to get a rapid assessment of re-sizing performed. Finally the sytem produces a comprehensive set of files containing data in PATRAN neutral file format for subsequent Graphical post- processing.

2.3. Machines supported.

The system has been developed on a VAX for execution on an IBM. The majority of the routines are written in VS FORTRAN. The few routines not written in FORTRAN are available in Assembler language on IBM and Macro on the VAX. These routines have been produced by our CAD department, they are used to dynamically allocate core and perform I/O on dynamically allocated files. It is intended to relace the I/O routines by a common set of Fortran routines which will in our case be linked to the NASTRAN data base but in other cases could be linked to any proprietory software's data base. This will leave the dynamic core allocation routine, therefore if this facility can be provided on other computers e.g. CRAY then the conversion to these machines is a relatively simple process.

In the past the system has been run at Warton in a dual environment, data was prepared on the VAX, the Job submitted from the VAX to run on the IBM and return its files for graphical post processing on VAX. We have thus gained considerable expertise in both

environments to such an extent that it can be run entirely in one environment (VAX or IBM) or in the dual environment. We are at present aiming at running all F.E. Analysis Applications on the IBM.

2.4. Documentation and QA

The system is fully documented with User Guide,System Documentation and Theoretical Manual. Also there exists a comprehensive library of test cases compiled during the Beta testing of the system. The QA and Change Control of the system is performed by an automated procedure (APAJAC) which has been developed by our Technical Computing Services.

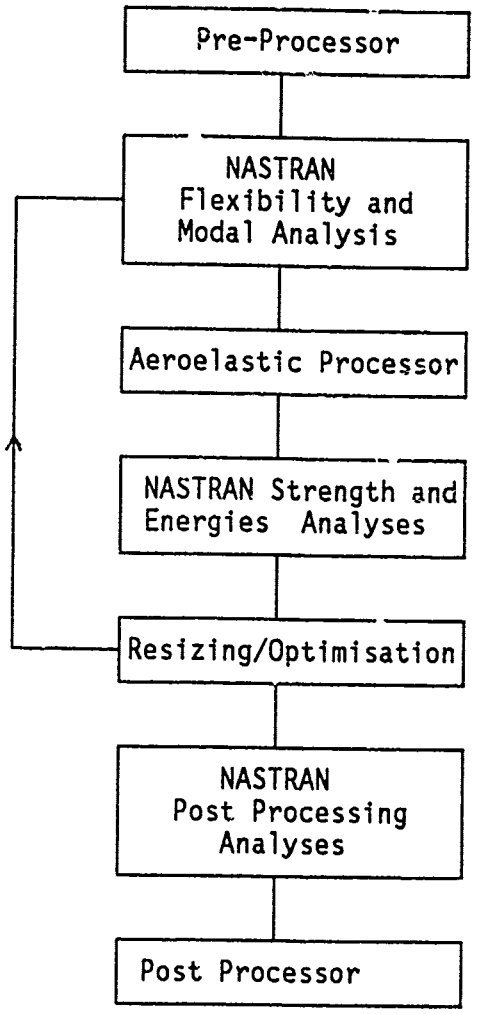

Fig. 2.1 - ECLIPSE MODULAR FLOW

3. THEORY

3.1. Strength Resizing of Isotropic Elements

These constraints are satisfied by the "Constant Stress" solution in which each element has a Reserve factor of unity in at least one loading case. The element stresses are assumed to be independant of the change in the sizes of surrounding elements.

The new element weights are given by the equation:-

$$W_{new} = W_{old} \max(S)$$

The types of criterion considered are :-

(i) Normal membrane and/or bending stresses based on the element local loads derived from F.E. analysis.

(ii) Element Structural Stability(Local Buckling) due to the above loads.

iii) Bending of wing skin panels due to the various local pressure distributions.

The expressions for the Scaling factor S range from a simple ratio in the case of Rod elements:-

$$S = \frac{\sigma}{\sigma_{AL}}$$

a simple cubic for plate stability:-

$$S = \sqrt[3]{\left(\frac{\lambda_{required}}{\lambda_{obtained}}\right)}$$

to a quartic for bending plates:-

$$\sigma_{AL}^2 S^4 - \sigma_{AL}(\sigma_{xm} + \sigma_{ym})S^3$$

$$- [\sigma_{AL}(\sigma_{xb} + \sigma_{yb}) - \sigma_{xm}\sigma_{ym} + \tau_{xym}^2]S^2$$

$$+ [\sigma_{xm}\sigma_{yb} + \sigma_{ym}\sigma_{xb} - 2\tau_{xym}\tau_{xyb}]S + \sigma_{xb}\sigma_{yb} - \tau_{xyb}^2 = 0$$

and a complex polynomial for bar elements:-

$$\sigma_{AL} S^{N1+N2+1} - \frac{P}{A_0} S^{N1+N2} - \frac{M_1}{I_{10}} Y_0 S^{Ny+N2+1} - \frac{M_2}{I_{20}} Z_0 S^{Nz+N1+1} = 0$$

where the bar inertias are related to the area by:-

$$I_1 \alpha A^{N1} \ , \ I_2 \alpha A^{N2} \text{ and } I_{12} = 0$$

and stress recovery coefficients are related by:-

$$Y \alpha A^{Ny} \ , \ Z \alpha A^{Nz}$$

3.2. Strength Resizing - Laminated Plates

Each plate or membrane element is composed of a symmetric lay-up of overlapping plies. It is the total thickness of each orientation which is to be resized to meet the strength and stability constraints.

Isotropic elements are resized using the scaling factor determined as the maximum value computed from the stress and stability constraints. However in the case of Laminated Elements the ply sizes are dependent on one-another in these constraints, therefore although the previous simple scaling method could be used it gives poor results and method based on a Sequence of Linear Programmes (SLP) has been used.

3.2.1. Sequence of Linear Programs (SLP)

The SLP method uses a move limit reduction technique to prevent solution oscillations. These move limits are simply a restriction on the amount of variation that each variable can have during each iteration. This amount is reduced each time a new solution is seen to be diverging from the previous one.

The SLP algorithm is shown schematically in figure 3.1 and is explained as follows:-

0) Let V_0 be the vector of initial thicknesses which in the absence of any known quantities will be the minimum gauge thicknesses.

1) Determine the maximum scaling factor S_0 such that the solution S_0V_0 just satisfies at least one of the strength or buckling constraints. This solution will be called the Primary Feasible Solution V_{PFS} Non- critical strength and stability cases whose reserve factors are greater than specified values will be rejected. These values will be successively reduced in order to accelerate convergence.

2) Perform a first order linearisation of the strength and buckling constraints about the V_{PFS} point. This linearisation will be described in more detail later. Solve the resulting Linear Programmming Problem using the SIMPLEX method (see Ref. 2). If the linear sub problem has no feasible solution then terminate the resizing. However the first time this condition occurs assume it is due to the move limits being too restrictive. Adjust these move limits and the linearisation point and try again.

3) The SIMPLEX method determines the optimum solution to the Linear Sub problem. However the resulting solution may not be feasible, therefore a factor on the sizes is determined such that a just feasible solution is formed.

4) If the solution is diverging, determine a new linearisation point using a step halving process based upon the previous feasible solution and the solution to the linear sub problem. Reduce the move limits on the next linear sub problem.

5) If the solution is converging then repeat the Scaling,Linearisation and SIMPLEX process until the convergence criteria is met. The convergence is met when the difference between successive orientation thicknesses for all orientations is less than the minimum gauge.

3.2.2. Linearisation of non-linear problem

From the previous section assume that we are required to perform a first order linearisation of the non-linear problem about a Just Feasible Solution V.

Vector of thickness variables.

$$V' = [t_1, t_2 \ldots\ldots t_N]$$

Vector of thickness changes.

$$\Delta V' = [\delta t_1, \delta t_2, \ldots\ldots \delta t_N]$$

Vector of strain derivatives.

$$V\varepsilon'_i = \left[\frac{d\varepsilon_i}{dt_1} \; , \; \frac{d\varepsilon_i}{dt_2} \ldots\ldots \frac{d\varepsilon_i}{dt_N} \right]$$

Vector of buckling derivatives.

$$V\lambda' = [\frac{d\lambda}{dt_1} \; , \; \frac{d\lambda}{dt_2} \ldots\ldots \frac{d\lambda}{dt_N}]$$

Then

$$\delta\varepsilon_i = V\varepsilon'_i \, . \, \Delta V \quad and \quad \delta\lambda = V\lambda' \, . \, \Delta V$$

The linearised optimisation problem can then be stated as :-

Find

$$\Delta V' = (\delta t_1 \, , \; \delta t_2 \ldots\ldots \delta t_N)'$$

Which minimises the Total Weight $W_{NEW} = W_{OLD} + \Sigma \rho_i \, \delta t_i$

Subject to:-

$$\varepsilon_{iold} + V\varepsilon'_i \, . \, \Delta V \leq \varepsilon_T$$

$$\varepsilon_{iold} + V\varepsilon'_i \, . \, \Delta V \geq \varepsilon_C$$

$$\lambda_{old} + V\lambda' \, . \, \Delta V \geq \lambda_{req}$$

For each loading case and material orientation.

And

$$V_{old} + \Delta V \leq V^+$$

$$V_{old} + \Delta V \leq V^-$$

The V^+ *and* V^- are the vectors containing the upper and lower bound constraints due to move limits or initial fabrication constraints. Each term is determined from the relationship:-

$$V_i^+ = \min[(1 + \beta)V_{iold} \, , \; V_{imax}]$$

$$V_i^- = \min[(1 - \alpha)V_{iold} \, , \; V_{imin}]$$

Where β and α are the upper and lower move limits.

3.3. Strength-Stiffness Interface.

The interface between the Strength and Stiffness resizing routines is essentialy an adjustment of the minimum size constraints prior to performing the resizing.

For Isotropic elements this ajustment is a relatively simple procedure. Each time the strength resizing is performed the minimum sizes are set at minimum gauge (i.e. sizes set

by manufacturing constraints). If the strength requirement and maximum element sizes conflict the default option is to use the maximum sizes. However the User can select the reverse.

The sizes generated by the strength constraints are used as minimum sizes in the following stiffness constraints. Sizes which become greater or equal to the maximum gauge in the strength constraints will remain fixed in the following stiffness resizing.

For laminated elements the adjustment of minimum sizes is more complex, it is shown schematically in Fig. 3.2 and described as follows.

The first time through the strength and stiffness resizing the adjustment of minumum sizes is the same as in the Isotropic case. However in addition an indication of critical constraint type (Strength or Stiffness) is set.

Subsequent times prior to the strength resizing the minimum size will be set to minimum gauge if that particular size was strength dependent. If the size was stiffness dependent then the minimum size will be set to the size resulting from the stiffness constraints. However if ALL the orientation sizes in a given element are stiffness dependent then the minimum size will be set to minimum gauge. The reasoning behind this is that if strength is determining the size then you can set the minimum size to minimum gauge as the strength will determine the new size with the possibility of reducing it. If the stiffness is sizing a ply then leave the minimum size at the stiffness size to prevent the strength reducing it and hence cause size oscillations. If ALL the sizes have changed because of stiffness then oscillations are not likely to occur therefore you can start from minimum gauge.

Subsequent times prior to the stiffness resizing the minimum sizes will be set to the strength sizes if strength dependent. If they are not strength dependent but were previously stiffness dependent then set the minimum sizes to minimum gauge. However if they are not strength dependent nor previously stiffness dependent then set the minimum sizes to those sizes coming from the strength constraints. This may sound strange, but sizes could have been determined from strength in a previous loop and are converging therefore we do not want the stiffness to change them or they may be minimum gauge in which case there is no problem.

These adjustments are rather "Unfriendly" and would not be needed if all the strength and stiffness constraints were combined into one resizing procedure. However not all the Detail Stressing and Engineering constraints are amenable to Mathematical programming methods therefore some form of interface will be required between them and the Strength/ Stiffness constraints.

3.4. Stiffness Constraints

3.4.1. Optimality Theorem

These constraints are treated by an "Optimality Criteria" method which although originally derived by considering size perturbations of the Optimum structure can be easily obtained from the first Kuhn-Tucker condition for a stationery Lagrangian function.

$$i.e. \sum \lambda_j \frac{dX_j}{dw_i} = 1$$

In the following section it will be shown that whatever type of criterion is denoted by X_j ,

$$\frac{dX_j}{dw_i} = \frac{a\ E_{ji}}{w_i}$$

Where a_j is a constant(independent of i) and E_{ji} an energy term associated with element i and criterion j.

Then defining $C_j = \lambda_j a_j$ *and* $U_{ji} = E_{ji}/w_i$ the Kuhn-Tucker condition becomes:-

$$\sum C_j U_{ji} = 1$$

Which is the condition for the optimum structure. The search for the n unknown values of w_i has been reduce to that for the m values of C_j from which the n values of w_i can be found.

3.4.2. Criterion Derivatives - Generalised Deflection

In order to specify a generalised deflection two loading cases are required,namely

(i) L_A The applied loads

(ii) L_D The loads defining the generalised deflection

The generalised deflection is then defined by the equation:-

$$X = L'_D F L_A = L'_D K^{-1} L_A$$

Differentiating the above equation w.r.t. w_i noting that L_A *and* L_d are constant we obtain:-

$$\frac{dX}{dw_i} = = -L'_D F \left[\frac{dK}{dw_i} \right] F L_A$$

Now

$$K = \sum (K_{1k} + K_{2k} + K_{3k})$$

Therefore

$$\frac{dK}{dw_i} = \frac{1}{w_i} (K_{1i} + 2K_{2i} + 3K_{3i})$$

Hence

$$\frac{dX}{dw_i} = \frac{-2}{w_i} (E_{1i} + 2E_{2i} + 3E_{3i})$$

Expressing the original constraint equation in terms of the element energies we obtain:-

$$X = 2\Sigma (E_{1i} + E_{2i} + E_{3i})$$

Where E_{1i} etc., are the element strain energies due to loads L_D *and* L_A

3.4.3. Criterion Derivatives-Hinge Moment

This constraint is a result of the limitation on the control surface jack load, which is expressed in terms of an Hinge Moment constraint.

If Γ is a vector of moment arms about the hinge line for the control surface nodes.

Then

$$\Gamma' L_F = M_H$$

Were the flexible loading L_F is equal to the rigid loading L_R plus the adjustment due to the structural deflection.

i.e

$$L_F = L_R + A\,\delta$$

The deflections are also related to the flexible loading by the structural flexibility

i.e

$$\delta = F\,L_F$$

Thus δ can be expressed as

$$\delta = (I - FA)^{-1} F\,L_R$$

Then the flexible loading L_F is defined by the equation:-

$$L_F = L_R + A(I - FA)^{-1} F\,L_R$$

And the expression for the Hinge moment becomes:-

$$\Gamma'\,(L_R + A(I - FA)^{-1} F\,L_R) = M_H$$

The above equation can be rearranged into a similar form as the generalised deflection constraint,if we define the Target T as:-

$$T = \Gamma'\,L_R - M_H$$

and the constraint criteria as:-

$$X = -\,\Gamma'\,A(I - FA)^{-1}\,FL_R = L'_1 FL_R$$

Then proceeding as for the Generalised Deflection criteria we obtain:-

$$X = 2\sum (\hat{E}_{1i} + \hat{E}_{2i} + \hat{E}_{3i})$$

Where $\hat{E}_{1i}$ are the element energies due to the loads L_i and L_R

and

$$\frac{dX}{dW_i} = \frac{-2}{W_i}(E_{1i} + 2E_{2i} + 3E_{3i})$$

Where E_{1i} are the element energies due to the loads L_1 and L_F

Note.

The reason for the Jack Load limitation is to limit the Jack Load Mass. It is possible to incorporate this mass dependancy directly into the Optimality criteria formulation, thereby removing it as a constraint.

3.4.4. Constraint Derivative - Flutter speed

If we neglect the Structural Damping Matrix and investigate the Flutter equation at the Flutter point where the Eigen value $\lambda = i\omega_F$ then we obtain the complex Eigen equation.

$$[- A\omega_F^2 + E + iBV_F\omega_F + CV_F^2] X = 0$$

$$i.e.\ \bar{A}X = 0$$

Associated with this equation is the Left Hand Eigen Equation.

$$Y'\bar{A} = 0$$

Then differentiating the first equation w.r.t. the weight of element i, assuming the mode shapes φ constant and premultiplying by Y' we obtain the matrix equation :-

$$\begin{bmatrix} r_{11} & r_{12} \\ r_{21} & r_{22} \end{bmatrix} \begin{bmatrix} \partial\omega_F/\partial w_i \\ \partial v_F/\partial w_i \end{bmatrix} = - \begin{bmatrix} Y'_R\varphi'\partial\Omega\varphi X_R - Y'_I\varphi'\partial\Omega\varphi X_I \\ Y'_R\varphi'\partial\Omega\varphi X_I + Y'_I\varphi'\partial\Omega\varphi X_R \end{bmatrix}$$

Where in terms of real and imaginary parts of X and Y

$$\begin{aligned} r_{11} &= -2\omega_F (Y'_R AX_R - Y'_I AX_I) - V_F (Y'_R BX_I + Y'_I BX_R) \\ r_{21} &= -2\omega_F (Y'_R AX_I + Y'_I AX_R) + V_F (Y'_R BX_R - Y'_I BX_I) \\ r_{12} &= 2V_F (Y'_R CX_R - Y'_I CX_I) - \omega_F (Y'_R BX_I + Y'_I BX_R) \\ r_{22} &= 2V_F (Y'_R CX_I + Y'_I CX_R) + \omega_F (Y'_R BX_R - Y'_I BX_I) \end{aligned}$$

and

$$\frac{\partial K}{\partial w_i} - \omega_F^2 \frac{\partial M}{\partial w_i} = \partial\Omega \ .$$

Defining $r = r_{11}r_{22} - r_{12}r_{21}$ and solving the equation for $\frac{\partial V_F}{\partial w_i}$ yields :-

$$\begin{aligned} \frac{\partial V_F}{\partial w_i} &= \frac{1}{r}\{(r_{21}Y'_R - r_{11}Y'_I)\varphi'\partial\Omega\varphi X_R - (r_{21}Y'_I + r_{11}Y'_R)\varphi'\partial\Omega\varphi X_I\} \\ &= \frac{1}{r}\{\hat{q}_1\partial\Omega\hat{q}_2 - \hat{q}_3\partial\Omega\hat{q}_4\} \end{aligned}$$

Which by expanding $\partial\Omega$ can be expressed in terms of element cross strain and kinetic energies.

$$\frac{\partial V_F}{\partial w_i} = \frac{2}{rw_i}\left\{\begin{array}{l}(E_{a1i} + 2E_{a2i} + 3E_{a3i} - \omega_F^2 E_{aKi}) \\ \qquad - (E_{b1i} + 2E_{b2i} + 3E_{b3i} - \omega_F^2 E_{bKi})\end{array}\right\}$$

Where E_{a1i} etc., are the element cross energies due to mode vectors $\hat{q}_1, \hat{q}_2$ and E_{b1i} etc., are the element cross energies due to mode vectors q_3, q_4

The original equation can also be manipulated to yield the following equation for the Flutter speed V_F

$$V_F = \frac{1}{r}[\hat{q}_1 K \hat{q}_2 - \hat{q}_3 K \hat{q}_4]$$

Which in terms of element energies becomes:-

$$V_F = \frac{4}{r_i}\sum_i \left\{\begin{array}{l}(E_{a1i} + E_{a2i} + E_{a3i}) \\ \qquad - (E_{b1i} + E_{b2i} + E_{b3i})\end{array}\right\}$$

3.5. Resizing Procedure

The iterative process used for resizing is shown schematically in figure 3.3 and explained in the following sections.

3.5.1. Initial estimates of constants C

All that is required at this stage is to estimate the order of the terms in each C, thus gross simplifications are permissible.

Therefore assuming all criteria are equally effective and considering the whole of the variable structure as a single element, then the optimality criteria equation can be written as:-

$$m C_j U_j = 1$$

Consider the case when criterion j is a limitation imposed on the Generalised Deflection.

If the target value T_j to be achieved for a total weight of W_T

Then

$$T_j = 2E_{jv} \div 2E_{jc}$$

and

$$U_j = \frac{E_{jv}}{W_v} = \frac{T_j - 2E_c}{2W_v} = \frac{T_{jv}}{2W_v}$$

Now the starting value of the variable weight is W_{vo}, and this corresponds to a starting variable criterion value of X_{jvo}. The variable criterion value on meeting the target is T_{jv}. If membrane effects are assumed dominant increasing the weight W_{vo} will produce an increase in the criterion value X_{jv}.

Therefore

$$W_v = \frac{X_{jvo}}{T_{jv}} W_{vo}$$

and the equation for C can be written as:-

$$C_j = \frac{2X_{jvo}}{mT_{jv}^2} W_{vo}$$

3.5.2. New Element Sizes

The optimality condition quoted earlier stated:-

$$\Sigma\lambda_j \frac{dX_j}{dw_i} = \Sigma C_j \frac{E_{ji}}{w_i} = \Sigma C_j U_{ji} = 1$$

E_{ji} represents the energy term in the expression for dX_j/dw_i which from previously derived expressions can be written as:-

$$E_{ji} = E_{1ji} + 2E_{2ji} + 3E_{3ji} - E_{kji}$$

Where E_{1ji} etc., are the various element energies determined in the "Outer Analysis loop". If α_i is the ratio of new sizes to analysis sizes, then the energy term corresponding to the new sizes is :-

$$E_{jl} = \frac{E_{1ji}}{\alpha} + 2\frac{E_{2jl}}{\alpha_i^2} + 3\frac{E_{3jl}}{\alpha_i^3} - \alpha_i E_{Kjl}$$

And the new $w_i = \alpha_i w_{0i}$

Substituting these expressions into the optimality condition and rearrange terms we obtain the following quartic equation in α_i

$$(w_{0i} + \Sigma C_j E_{Kji})\alpha_i^4 - (\Sigma C_j E_{1ji})\alpha_i^2 - (2\Sigma C_j E_{2ji})\alpha_i - (3\Sigma C_j E_{3ji}) = 0 \quad 1 \le i \le n$$

Thus knowing the value of C_i the values of α_i can be determined from the above set of quartic equations. In fact if there are no elements present with Membrane-Bending coupling the above equation will be a quadratic in α_i^2.

If the value of α_i results in a new element size being imaginary or less than the minimum value then the minimum value will be used.

3.5.3. Determine constraint values X.

The values of αj computed in the previous section can be used to determine the new values of X_i using the following equations:-

For generalised deflection and aeroelastics the element loads are assumed constant in the "Inner stiffness loop", therefore the equation for X in terms of α_i and the energies E_{1ji} etc.., is:-

$$X_j = 2E_{jc} + 2\Sigma\left[\frac{E_{1ji}}{\alpha_i} + \frac{E_{2ji}}{\alpha_i^2} + \frac{E_{3ji}}{\alpha_i^3}\right]$$

In order that the frequencis increase as the relevant element sizes are increased, it is necessary to make the assumption that the displacements (rather than the element loads) are fixed. Then:-

$$X_j = \frac{2E_{jc} + 2\Sigma(E_{1ji}\alpha_i + E_{2ji}\alpha_i^2 + E_{3ji}\alpha_i^3)}{\delta' M \delta}$$

3.5.4. Determine new values of C.

From a first order expansion of X_i in terms of C_k we obtain:-

$$\Delta X_j = \Sigma \frac{dX_j}{dC_k}\Delta C_k \quad 1 \le j \le m$$

ΔX_i is the change in X_i required to meet the target T_i

i.e

$$\Delta X_j = T_j - X_j$$

Therefore the above equation defines the change in the value of C_k which will produce the required change in X_i.

namely

$$T_j - X_j = \Sigma \frac{dX_j}{dC_k} (C_{kold} - C_{knew}) \quad 1 \leq j \leq m$$

Thus new values of C_j are given by the matrix equation:-

$$C_{new} = C_{old} + D^{-1}(T - X)$$

Where

$$D_{jk} = \frac{dX_j}{dC_k}$$

If the previous values of C are very innaccurate,then the new values derived by the above method tend to fluctuate wildly due to neglecting the second and subsequent derivatives of X_j with respect to C_k In order to overcome this limits are placed on the new values C_k so that:-

$$0.5\, C_{kold} \leq C_{knew} \leq 2.0\, C_{kold}$$

3.5.5. Selection of Critical Criteria

If criteria j is non critical (i.e. it has no effect on the Optimum structure) then the corresponding constant C_j must obviously be zero. Thus after each analysis step, all criteria are assumed to be critical. Then, on subsequent iterations round the inner design loop criterion j whose constant C_j becomes zero may be regarded as non-critical.

However as stated in the previous section C_j is only permitted to change by a factor of 2 on each loop. Thus criterion j may be regarded as non-critical when $C_j < \varepsilon_2 C_{j0}$ were C_{j0} is the original estimate of C_j *and* ε_2 is some small number. For all practical purposes so far considered $\varepsilon_2 = 0.001$ has proved sucessful.

The C_j corresponding to non-critical criterion are dropped from the calculation of the new element sizes and the re-estimation of the new C_j. However, the corresponding X_j continue to be calculated owing to the possibility that in subsequent iterations they may become critical again. If this does occur then new estimates of the corresponding C_j are made using the equations defined previously with X_j replacing X_0

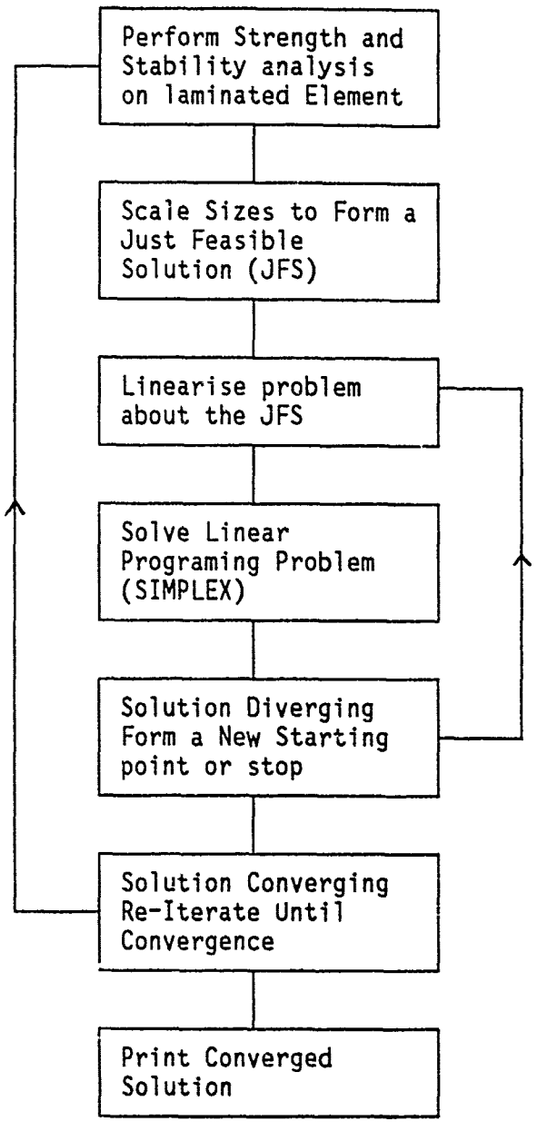

Fig. 3.1 SLP Approach to Laminate Optimisation

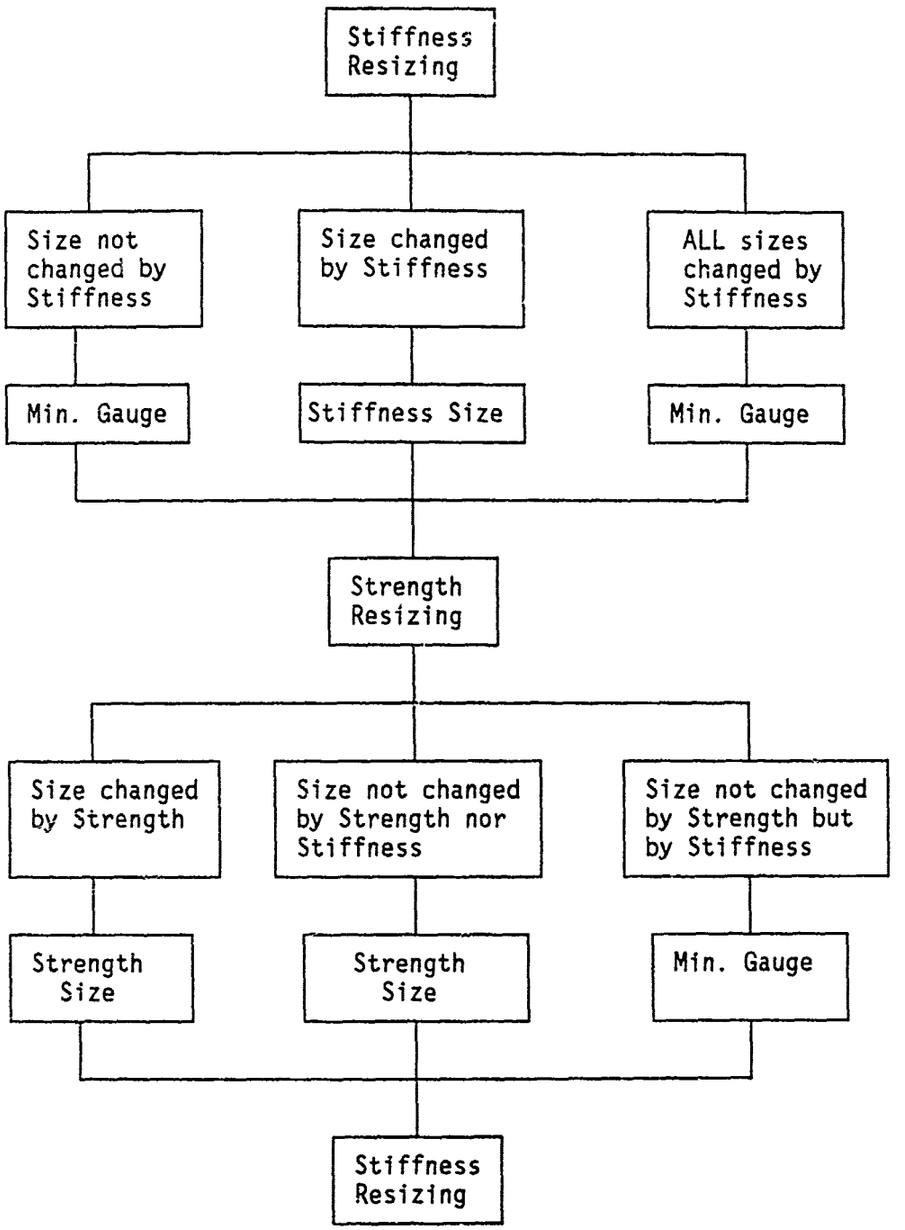

Fig 3.2 Adjustment of Minimum Sizes between Strength and Stiffness Constraints.

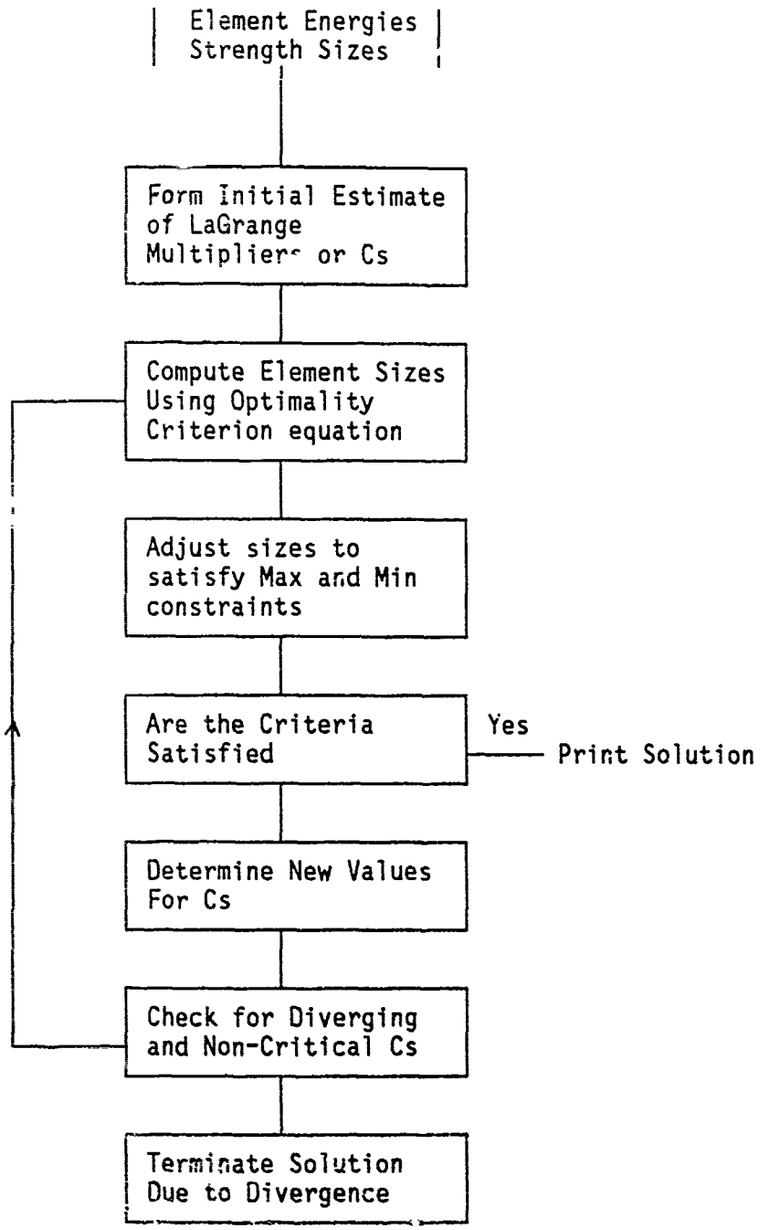

Fig 3.3 Optimality Criteria Approach for Stiffness

4. FIN/RUDDER

There were some slight problems in adapting this model to run on the ECLIPSE system, however I must emphasise that they were slight. They were easily overcome after consulting MBB Munich. Optimisation constraints were easy to define in ECLIPSE to the extent that after qualifying that we had the correct model the problem was set up and run inside a couple of hours. This is a very useful benchmark case it contains a lot of the constraints and element types which we normally deal with, namely :- Laminated plates, Steady and Unsteady Aerodynamics.

One of the problems we came up against was that we could not get the NASTRAN model to give the same deflections and fibre strains as specified in the MBB report Ref. 3. This was due to the fact that although the model was formulated in NASTRAN format the MBB solution had its own F.E. Analysis module within LAGRANGE. The CQUAD4 elements are stiffer in NASTRAN than in LAGRANGE. The effect of this on the Optimisation is that LAGRANGE solution will be heavier!

Figures 4.1 to 4.5 are plots of the complete model and its componant element breakdown.they are produced in the normal course of analysis work in order to check that we have the correct model. They also enabled us to determine the IDs of those elements which are being resized. These plots were produced using PATRAN.

Figures 4.6 to 4.7 are displacement plots due to applying the Rigid Aero loading vector. In this case they correspond to the optimum design but they could also be shown for the initial design. These plots are produced to check that there are no anomolies in the rigid Aero loading and the Interface Grid Flexibility terms. The Interface Grid is the subset of Grid points which is used to transfer AICs and Flexibilities between Aerodynamics and Stress.

The Iteration histories for the Structural Weight and Flutter velocities are shown in Figures 4.8 and 4.9. There are some interesting points to note in these two plots. The ECLIPSE solution could have been terminated after seven iterations as the subsequent iterations are hardly changing the element sizes and constraint values. The LAGRANGE solution could have been terminated after eight iterations based on comparing the results from the seventh and eighth iteration and similarly after the fourteenth iteration. This is no basis to compare the efficiency of either method as I have experienced results from ECLIPSE for other cases which are similar to the LAGRANGE results. The point to be made is that it is extremely difficult to set up convergence criteria based on successive results. In most cases it is best left to the user to define the number of iterations and provide him with a "User Friendly" restart procedure.

The final weights from both Optimisations cannot be compared due to the fact mentioned earlier that the LAGRANGE elements are less stiff than the NASTRAN ones. This fact is also shown in the Frequency results for the initial design (fig 4.16 to 4.18).

The two paths taken to the "Optimum" are very interesting! The mathematical programming method of LAGRANGE is treating all the constraints simultaneously it first of all over achieves the Flutter velocity then starts to take weight off whilst still maintaining the Flutter velocity. This is very similar to the iteration histories from strength optimisation of individual laminated elements using SLP. The ECLIPSE system treats the strength constraints seperate from the Stiffness ones. Also the minimum size adjustment interface between Strength and Stiffness is different the first time through the loop as explained earlier in the theory and shown in fig 3.2. The result of this is that the first iteration is mainly resizing the structure to meet the strenght constraints, this then sets the minimum sizes for the stiffness constraints. The stiffness optimisation is trying to reduce the sizes but it cannot due to the minimum size constraints, however the thicknesses have now become stiffness dependant therefore in subsequent loops the minimum sizes for stiffness will be set to minimum gauge as the strength constraints will not be changing them. The ECLIPSE solution approaches the constraint from an infeasible point which is in fact the DUAL Feasible solution.

Another point to note on these plots is the different Flutter velocities at the start and finish points. All the ECLIPSE points except the final point have been computed using the element strain and kinetic energies at flutter. Thus the energies from structural damping have been

omitted which results in a lower Flutter velocity. The final point has been produced from a Flutter analysis in which we had to specify some structural damping for the mode tracking algorithm to function. The system will be modified to include structural damping in the optimisation. I suspect the LAGRANGE solution has some structural damping in as our initial and final flutter analysis damping plots (see fig 4.23 and 4.24) agree with the LAGRANGE solutions.

Figures 4.11 to 4.15 show the optimised design skin thicknesses in the various layers and their total. These should be compared with Figures 22 to 25 of Ref 3. Although some of the sizes are equal in both designs I suspect this is purely fortuitous. In general the sizes are all different even though the distribution of thicknesses are approximately the same with the ECLIPSE values being less than LAGRANGE. This again is more than likely due to the different element stiffnesses. However there are some conflicting results in the MBB model,the minimum size is stated as 0.25 yet there are some elements with optimised sizes of 0.2. Also although the minimum thickness for a layer is quoted as 0.25 the minimum thickness for the total thickness is 2.0. It is not possible to specify a total thickness constraint in ECLIPSE, if the minimum layer thickness is 0.25 and there are four of them, then the minimum total thickness will be 1.0.

The first three mode shapes for the initial and final design are shown in figures 4.16 to 4.21. Apart from their frequencies they are almost identical to the mode shapes shown in Ref 3. The interesting point to note is the crossing over of modes two and three between the initial and final design. This point is required when comparing the modal damping and stiffness matrices between initial and final design given in figure 4.22. The Flutter for the initial design is mainly due to the interaction between modes one and two (Figure 4.23). The flutter for the final design is between mode 1 and 3 (Figure 4.24). Comparing the corresponding terms in the stiffness and damping matrices we see that there is hardly any change in the damping terms but a large change in the stiffness terms. Also there is a large change in the frequency seperation.

This concludes the reporting of the present work on the MBB Fin/Rudder, however I feel that more work needs to be done on this case after discussion within GARTEUR and AGARD groups.

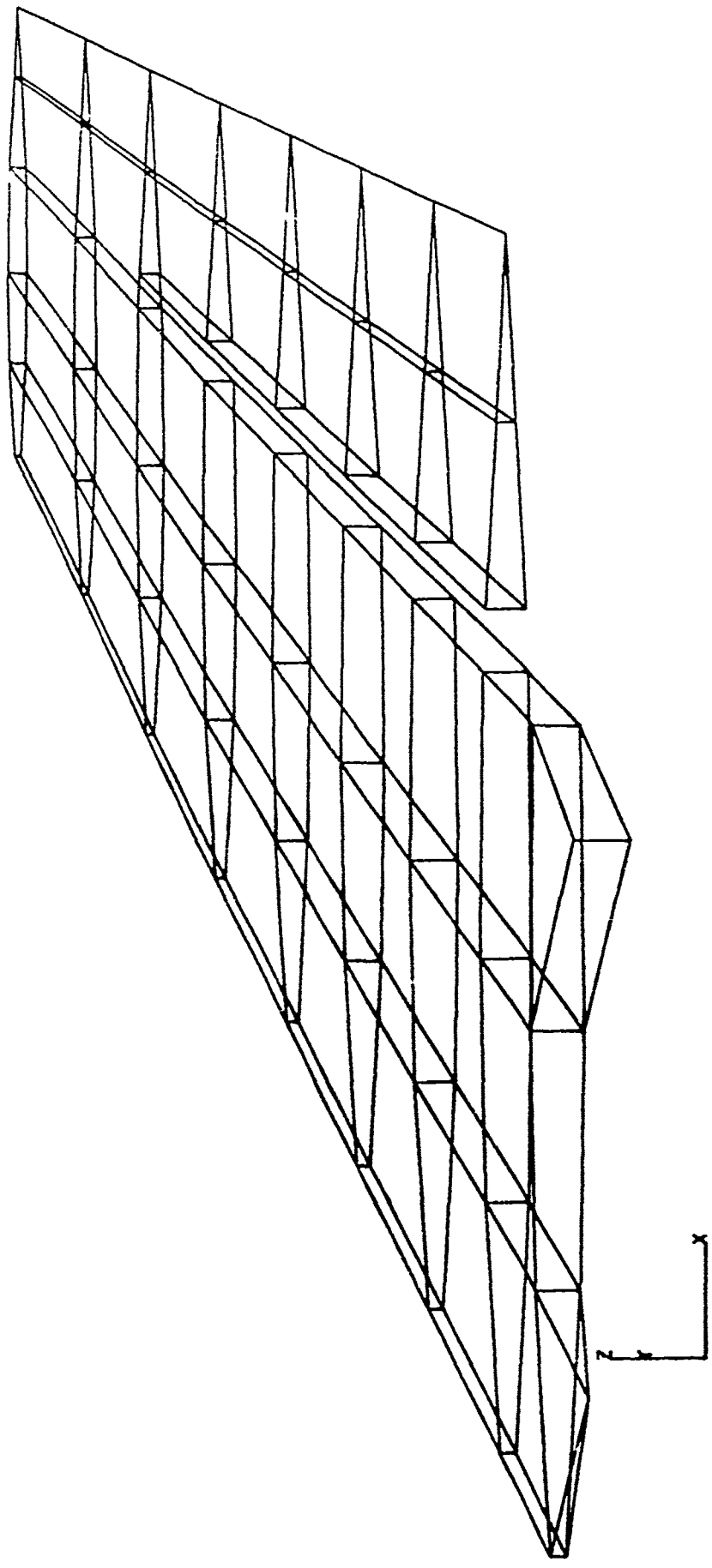

FIG 4.1 : FIN STRUCTURE

FIG 4.2 : TOP SKIN ELEMENT IDS

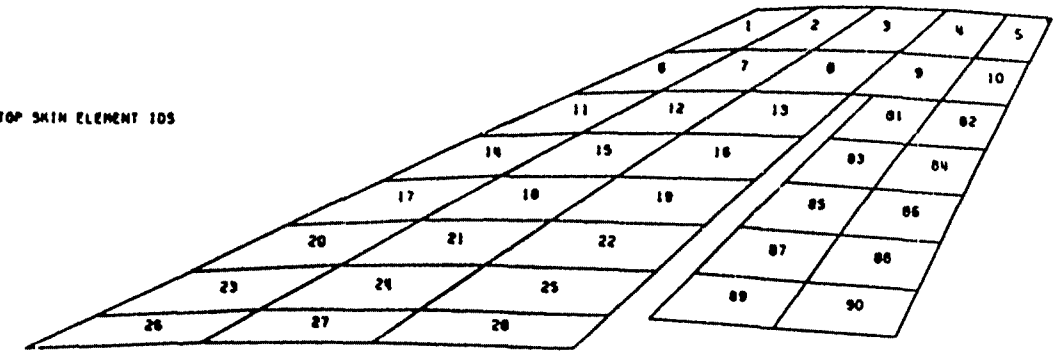

FIG 4.4 : SPAR ELEMENT IDS

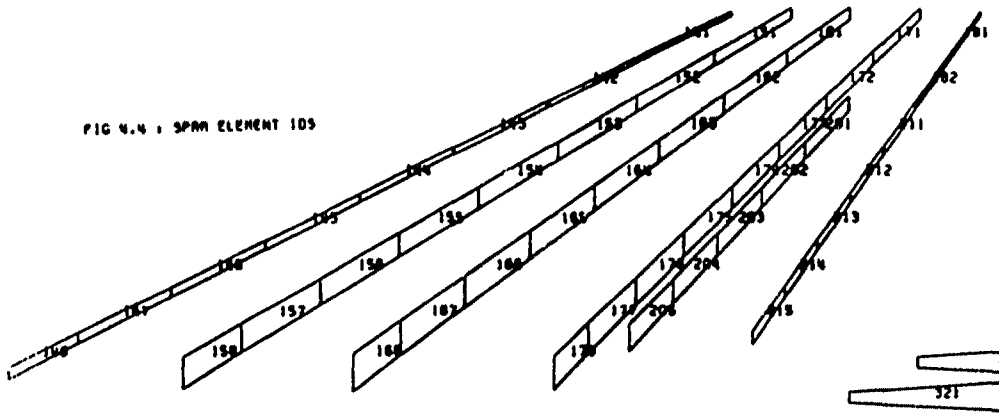

FIG 4.5 : RIB ELEMENT IDS

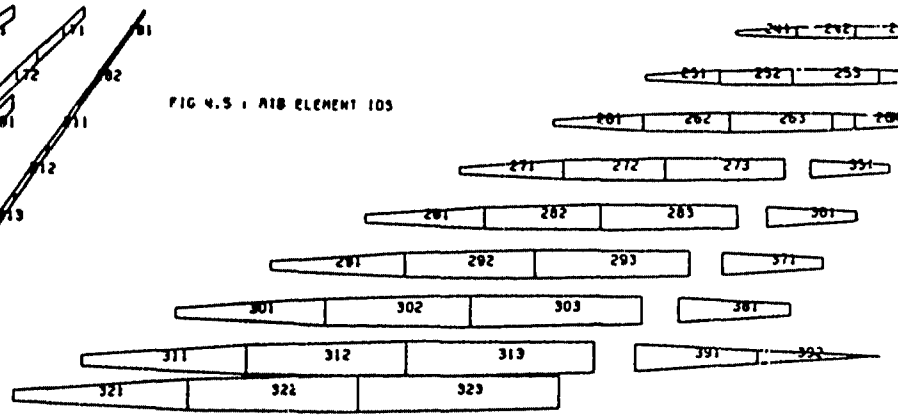

FIG 4.3 : BOTTOM SKIN ELEMENT IDS

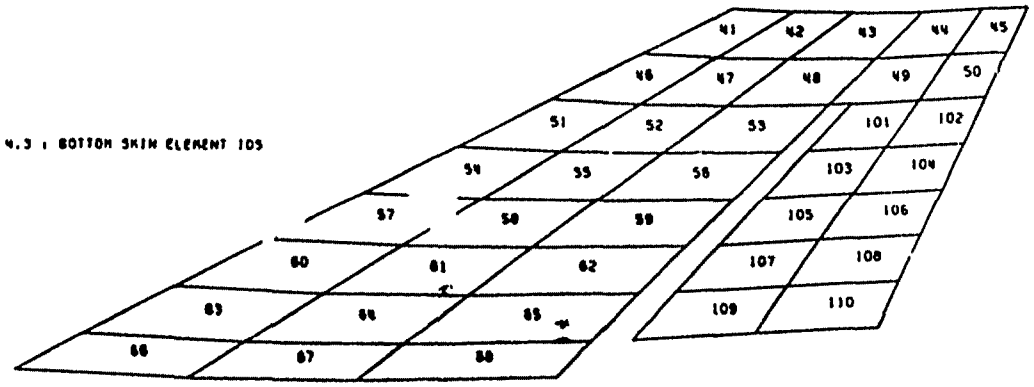

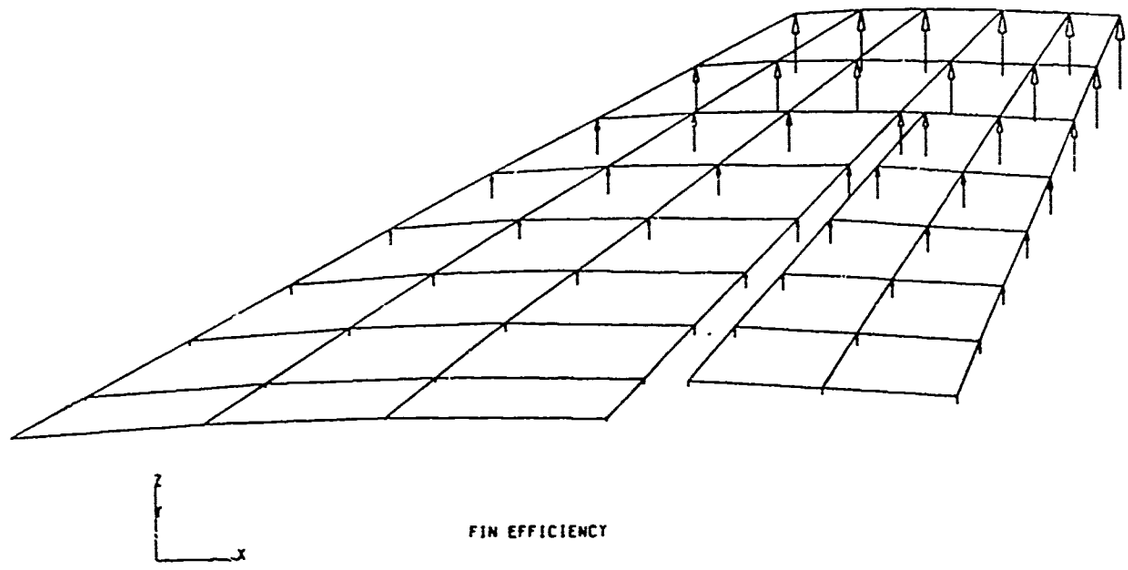

FIG 4.6 : OPTIMISED DESIGN - DEFLECTIONS DUE TO RIGID LOADS

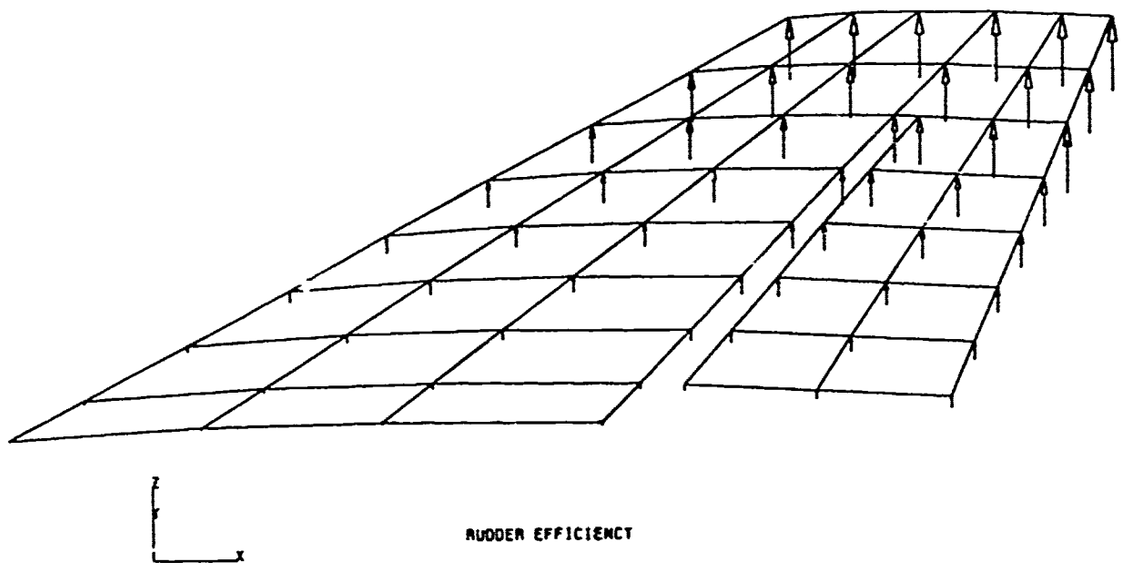

FIG 4.7 : OPTIMISED DESIGN - DEFLECTIONS DUE TO RIGID LOADS

TOTAL STRUCTURE WEIGHT

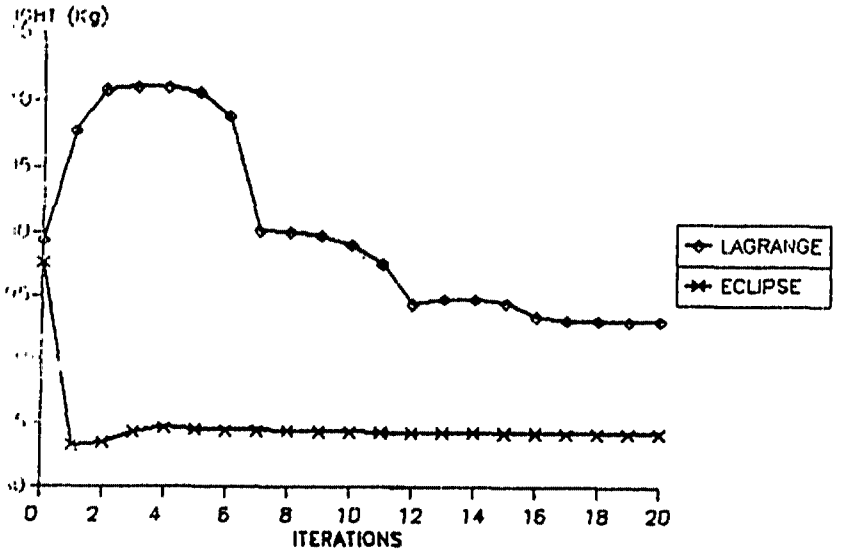

FIG 4.8

ACHIEVED FLUTTER VELOCITY

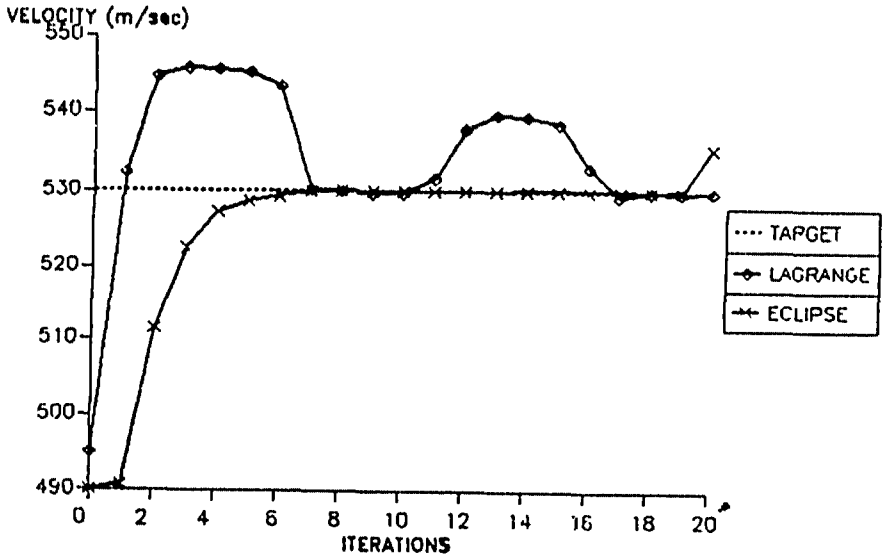

FIG 4.9

TARGETS		530.00	80.000	50.000	1.000
LOOP No	WEIGHT Kg	FLUTTER SPEED m/s	AERO EFFICIENCIES FIN	RUDDER	MINIMUM STRENGTH RF
0	97.672	490.07	76.367	45.841	0.8831
1	83.230	490.72	79.115	49.536	0.8355
2	93.449	511.46	79.868	49.857	0.6875
3	84.284	522.82	79.978	50.083	0.8923
4	84.618	527.25	80.065	50.214	0.9657
5	84.471	528.64	80.033	50.105	0.9819
6	84.396	529.32	80.021	50.054	0.9874
7	84.397	529.96	80.019	50.049	0.9885
8	84.368	530.13	80.014	50.040	0.9927
9	84.306	529.97	80.005	50.018	0.9952
10	84.274	529.96	80.003	50.007	0.9981
11	84.253	529.98	80.000	50.002	0.9981
12	84.236	529.99	80.001	49.999	0.9983
13	84.222	530.00	79.998	49.997	0.9984
14	84.212	530.02	80.000	49.996	0.9985
15	84.202	530.04	80.000	49 996	0.9985
16	84.193	530.03	80.002	49.997	0.9986
17	84.180	530.03	79.997	49.994	0.9986
18	84.169	530.00	79.996	49.992	0.9986
19	84.161	530.03	79.996	49.991	0.9987
20	84.154	535.74	79.997	49.991	0.9991

FIG 4.10

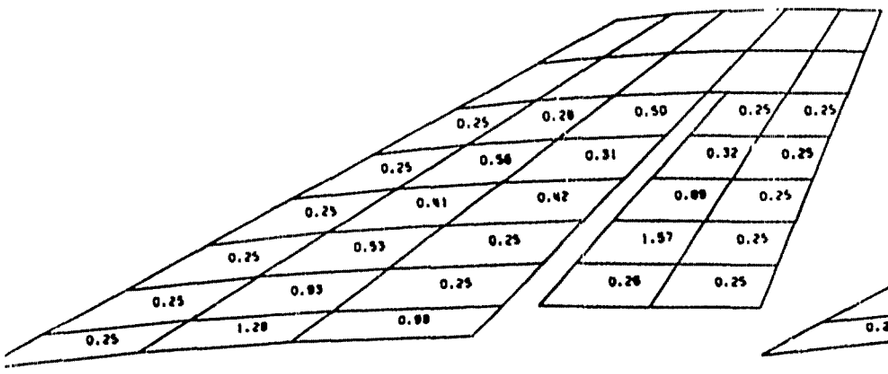

FIG 4.11 : OPTIMISED DESIGN - TOP SKIN THICKNESSES FOR LAYER 1

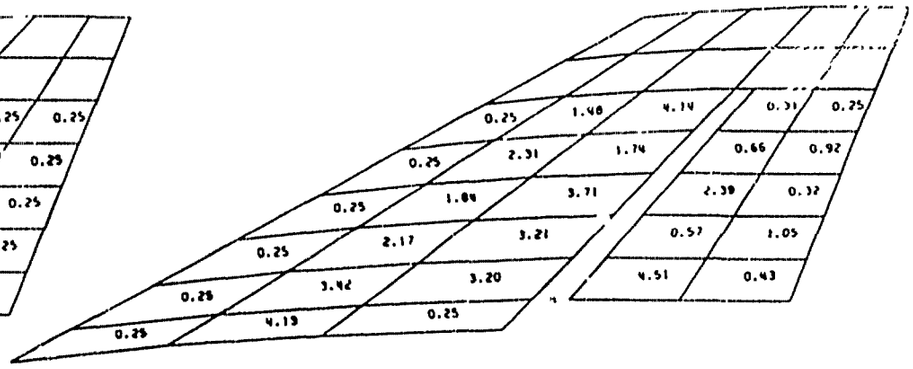

FIG 4.13 : OPTIMISED DESIGN - TOP SKIN THICKNESSES FOR LAYER 3

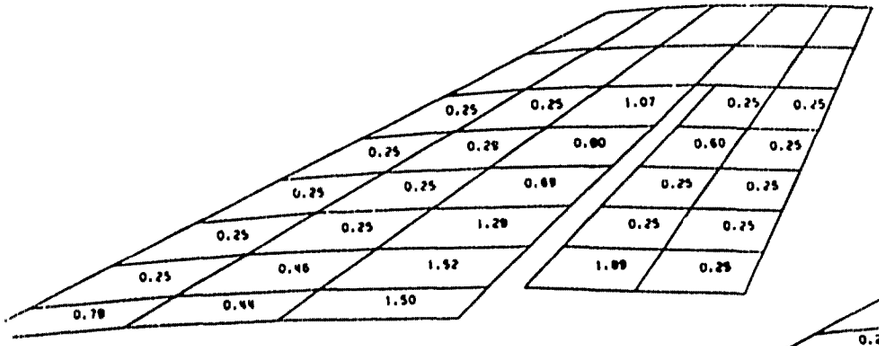

FIG 4.12 : OPTIMISED DESIGN - TOP SKIN THICKNESSES FOR LAYER 2

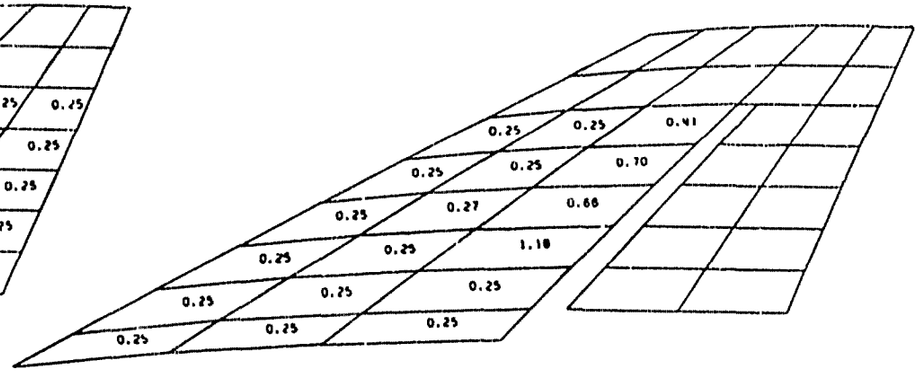

FIG 4.14 : OPTIMISED DESIGN - TOP SKIN THICKNESSES FOR LAYER 4

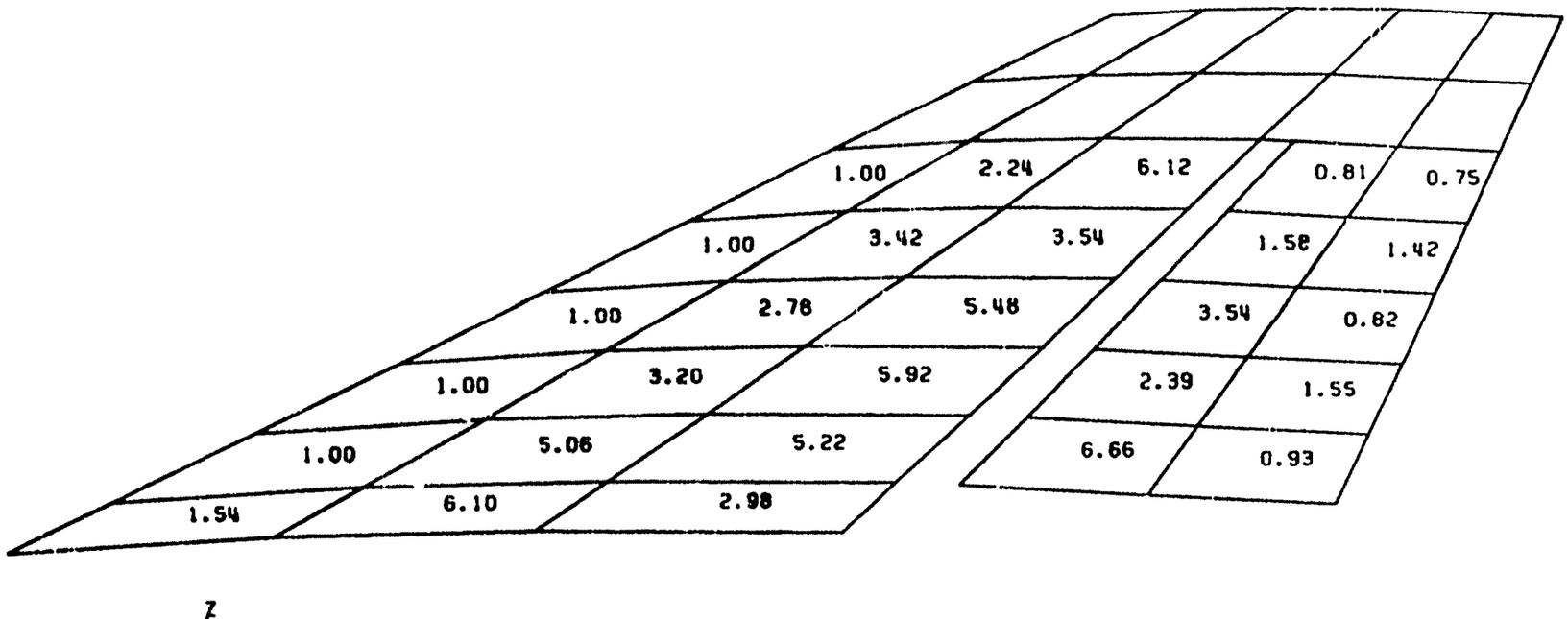

FIG 4.15 : OPTIMISED DESIGN - TOTAL TOP SKIN THICKNESSES

new sizes is :-

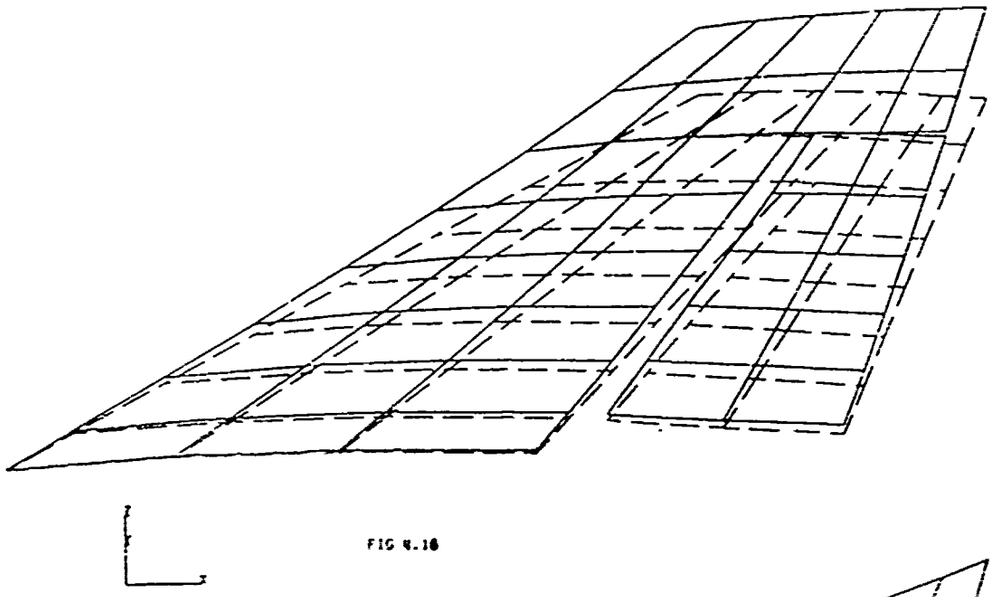

FIG 6.16

ACARD KBB FIN AND RUDDER (DO24MBB1)
INITIAL DESIGN PROCESSING
MODE=1. EIGENVALUE= 3.270049E+03. CYCLES= 9.101171E+00

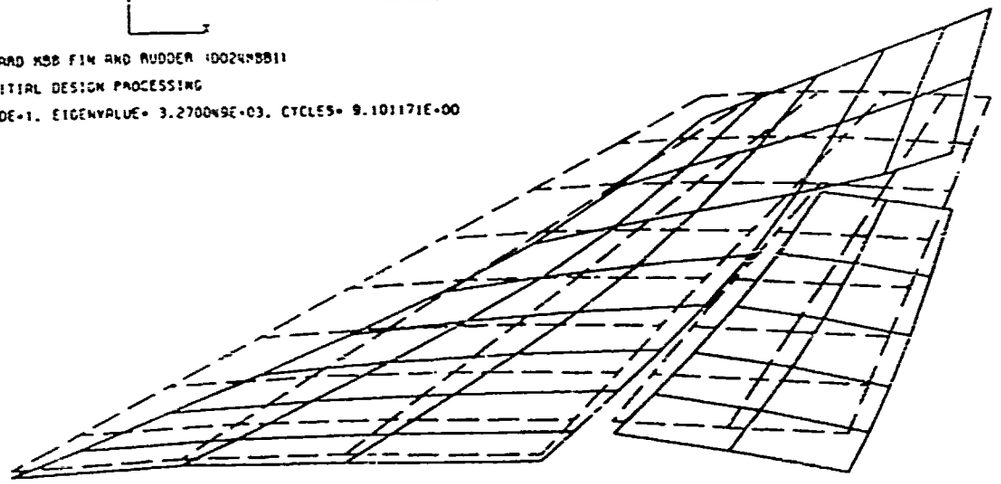

FIG 6.17

ACARD MBB FIN AND RUDDER (DO24MBB1)
INITIAL DESIGN PROCESSING
MODE=2. EIGENVALUE= 3.675070E+04. CYCLES= 3.051074E+01

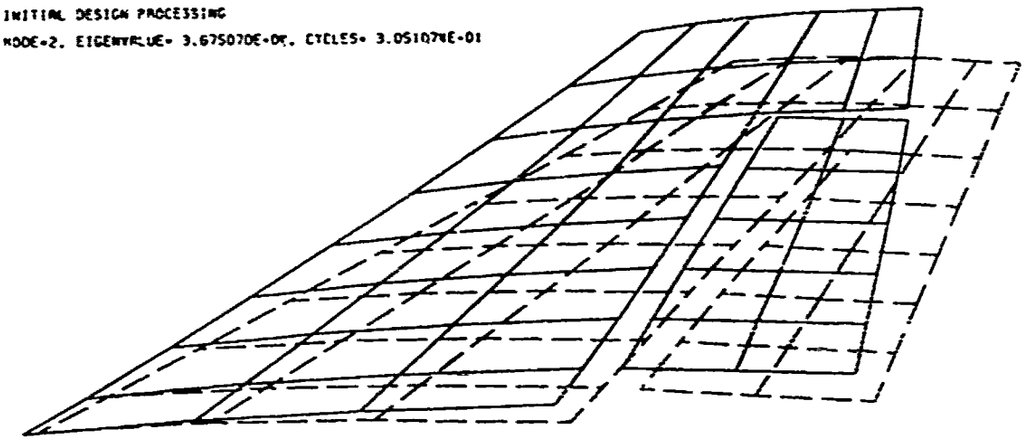

FIG 6.18

ACARD MBB FIN AND RUDDER (DO24MBB1)
INITIAL DESIGN PROCESSING
MODE=3. EIGENVALUE= 9.167552E+04. CYCLES= 3.240981E+01

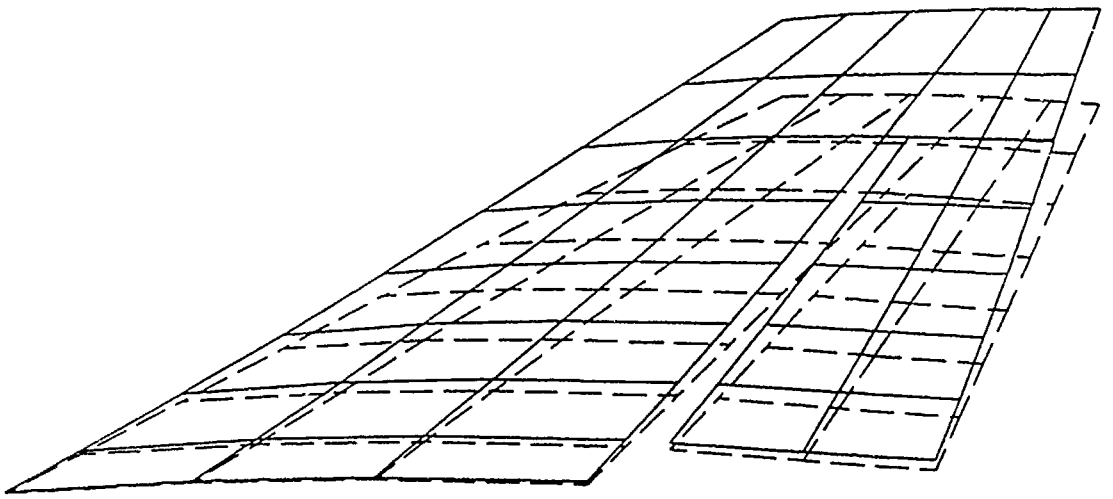

FIG 4.19

AGARD M88 FIN AND RUDDER (DO24M881) K=0.2
STRENGTH + AEROEFFICIENCY + FLUTTER - 20 LOOPS
MODE=1, EIGENVALUE= 3.163139E+03, CYCLES= 8.951159E+00

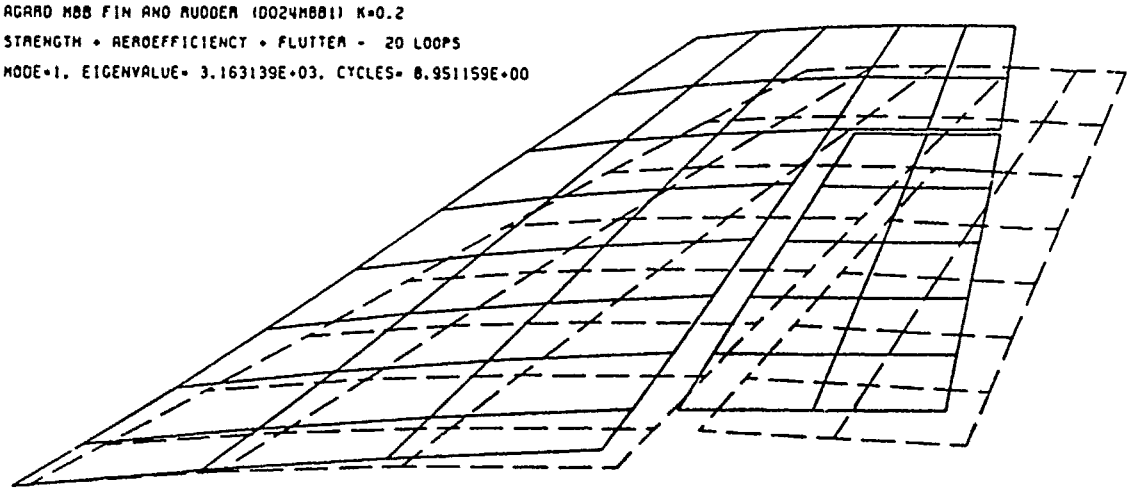

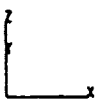

FIG 4.20

AGARD M88 FIN AND RUDDER (DO24M881) K=0.2
STRENGTH + AEROEFFICIENCY + FLUTTER - 20 LOOPS
MODE=2, EIGENVALUE= 3.762871E+04, CYCLES= 3.087306E+01

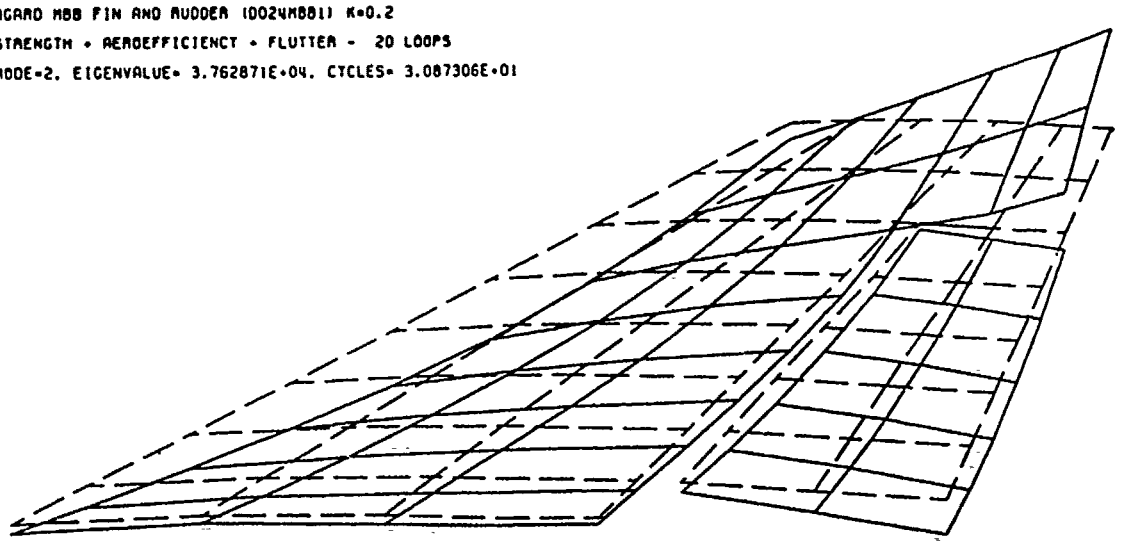

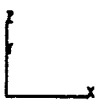

FIG 4.21

AGARD M88 FIN AND RUDDER (DO24M881) K=0.2
STRENGTH + AEROEFFICIENCY + FLUTTER - 20 LOOPS
MODE=3, EIGENVALUE= 4.137676E+04, CYCLES= 3.237415E+01

FREQUENCY COMPARISON

Mode No.	Initial Design	Final Design
1	9.1	8.95
2	30.5	30.87
3	32.5	32.37
4	41.4	43.98
5	55.7	59.28
$f_1^2 - f_2^2$	847.44	967.74

AERO MATRICES COMPARISON

Stiffness - Initial Design ($x10^{-3}$)

5.05	13.57	-1.43	-122.75	6.78
-8.75	-8.94	1.49	116.34	28.67
-0.07	0.34	0.06	4.08	1.22
8.75	43.22	2.38	1.06	52.42
-3.16	-18.54	-0.22	21.58	-30.13

Stiffness - Final Design ($x10^{-3}$)

3.50	-1.64	-17.02	-109.81	-3.11
0.25	-0.04	-0.73	-1.62	-0.53
6.76	-1.39	-13.77	-94.64	-37.19
7.66	-0.26	-44.45	85.81	64.46
-1.19	0.53	13.27	24.42	-22.07

Damping - Initial Design

42.84	30.56	27.51	-25.97	30.11
-36.53	45.81	0.46	-45.32	39.48
-0.87	0.85	0.07	3.24	2.10
-0.61	-6.36	4.48	295.75	86.89
-18.56	-6.56	0.04	3.63	32.98

Damping - Final Design

41.90	-1.27	-32.79	-37.24	24.35
0.09	0.08	1.42	3.55	0.19
35.82	1.52	43.45	33.08	-32.09
1.99	3.53	17.92	257.13	110.35
-17.53	0.56	6.28	22.34	45.44

FIG 4.22 MBB FIN/RUDDER MODAL PROPERTIES

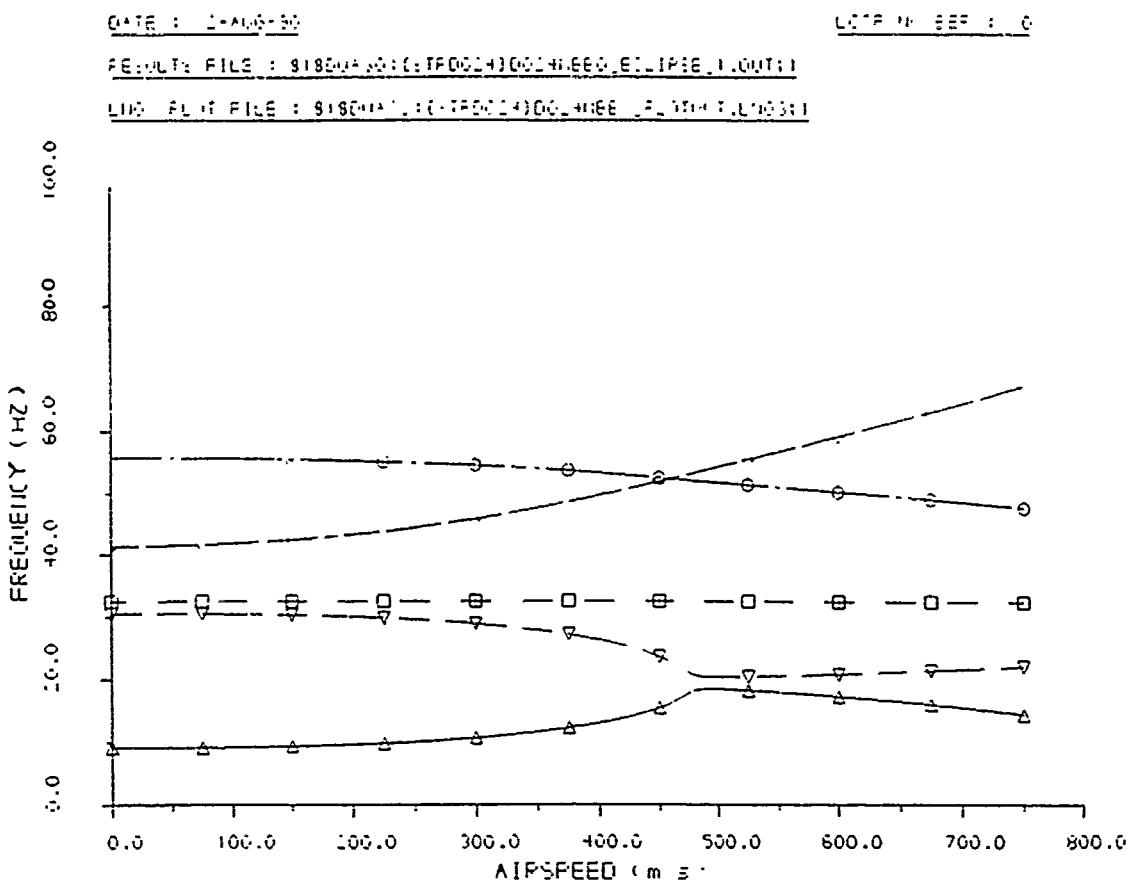

FREQUENCY/DAMPING PLOT
AGARD MBB FIN AND RUDDER (DOC14MBB1)
INITIAL DESIGN PROCESSING

FIGURE 4.23

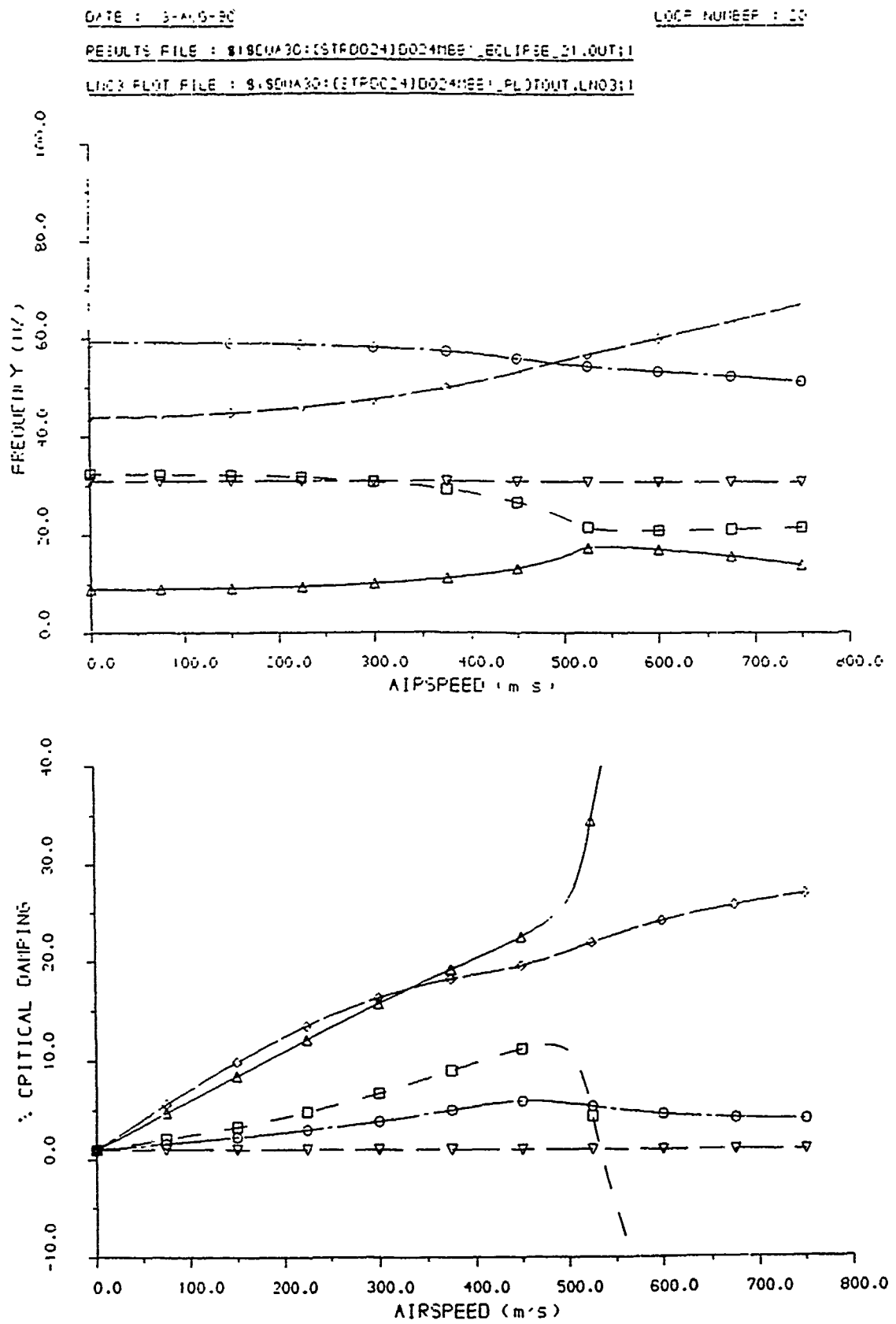

FREQUENCY/DAMPING PLOT
AGARD MBB FIN AND RUDDER (D0241MBB1)
STRENGTH + AEROEFFICIENCY + FLUTTER - 20 LOOPS

FIGURE 4.24

5. TAILPLANE RESULTS

In order to develope the Flutter optimisation capability a small "Unit" test case was required which woud run quickly on the VAX. This would enable us to use the interactive debugger and hence speed up the program development. The case chosen was a small tailplane which was optimised with only a flutter constraint present.

The results presented in Figures 5.1 to 5.23 are in a similar format to the previous section. However this case is much simpler having no control surface and being composed of Isotropic material. The model consists of NASTRAN CQUAD4,CROD AND CSHEAR elements, all of them being allowed to change during the optimisation.

Figure 5.1 to 5.5 are plots of the structure and its component element breakdown. The optimisation was restricted to nine design variable. The elements associated with a particular design variable can be seen from the plots of initial and final sizes given in figures 5.7 to 5.14. One design variable is missing from these plots which combines the shear and rod elements associated with the tailplane to fuselage attachment points.

Figure 5.6 defines the interface grid for the Unsteady Aerodynamic damping and stiffness matrices.

The first five modes were used in the Flutter analysis, however the Flutter can be considered to be due to the interaction of the first bending and torsion modes. These modes for the initial and final design are given in figures 5.15 to 5.18. Although the bending mode shape changes very little during the optimisation the "Zero Deflection Axis" of the torsion mode has moved forward. The frequency seperation of these two modes has also been increased from 3558 to 5571.

A tabulation of the frequencies and aerodynamic matrices for the initial and final designs is given in figure 5.19. Figure 5.20 and 5.21 show the Flutter analyses for the intial and final design.

An iteration history for the flutter constraint and optimised weight is shown in figures 5.22 to 5.23. As mentioned earlier this case was a very simple case used for "Unit testing" however it has proved extremely useful. A copy of the NASTRAN model can be made available for any of the workshop participants.

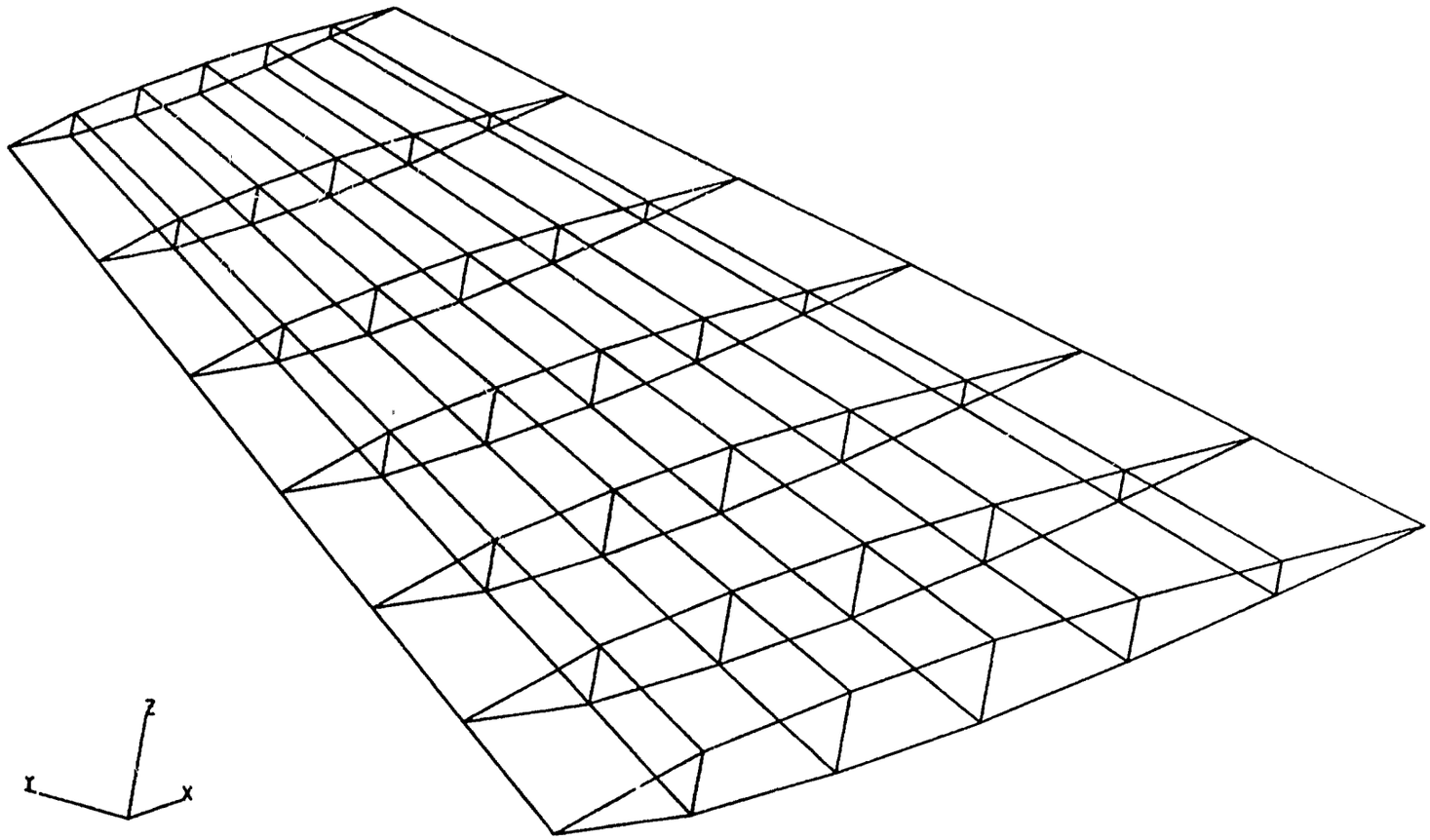

FIG 5.1 : TAILPLANE STRUCTURE

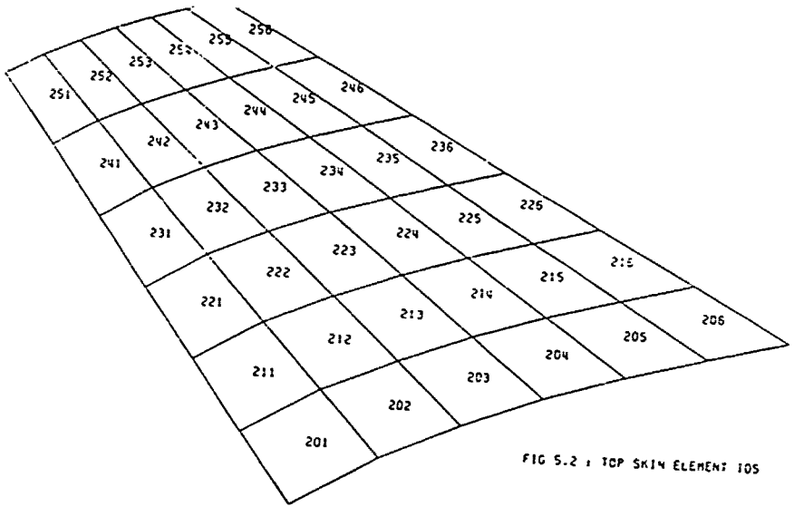

FIG 5.2 : TOP SKIN ELEMENT IDS

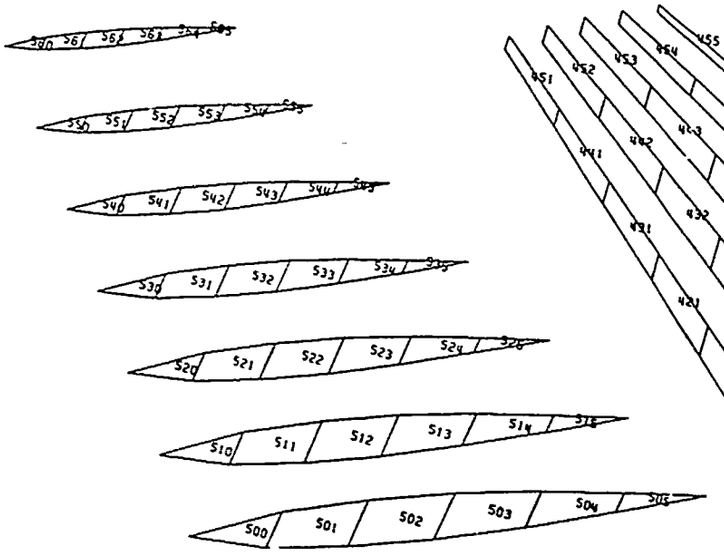

FIG 5.4 : RIB ELEMENT IDS

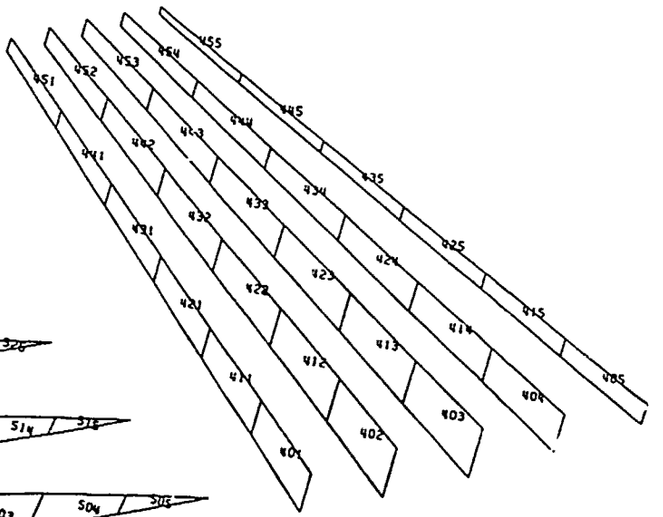

FIG 5.5 : SPAR ELEMENT IDS

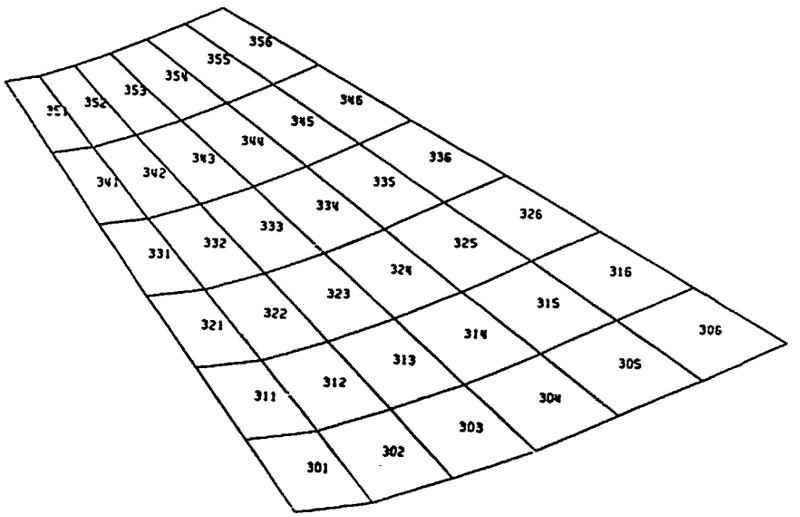

FIG 5.6 : [illegible] ELEMENT IDS

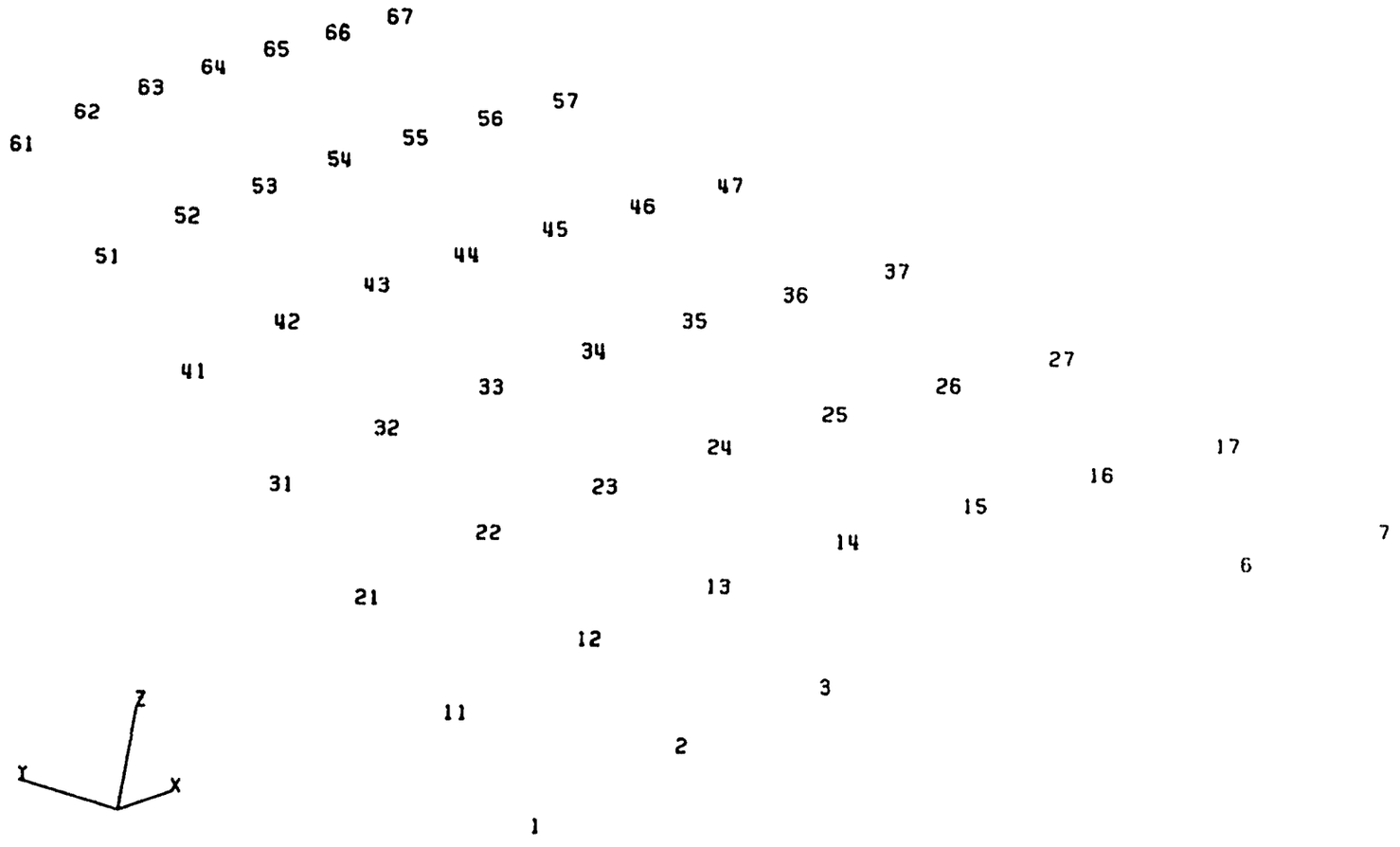

FIG 5.6 : AERODYNAMIC INTERFACE GRIDS

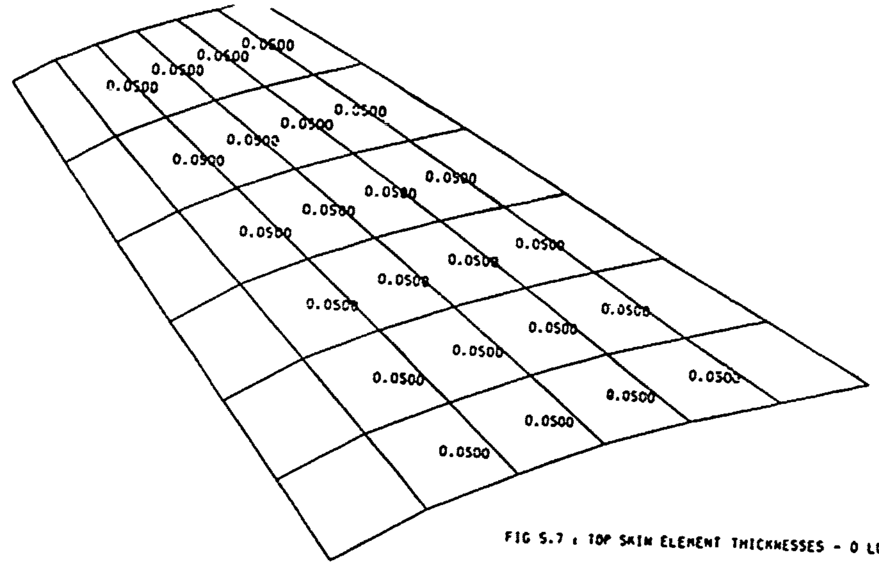

FIG 5.7 : TOP SKIN ELEMENT THICKNESSES - 0 LOOPS

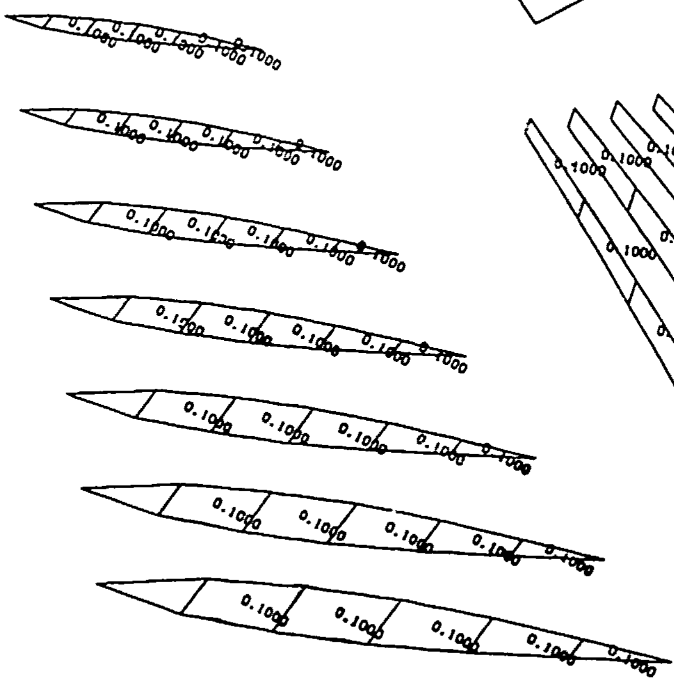

FIG 5.10 : RIB ELEMENT THICKNESSES - 0 LOOPS

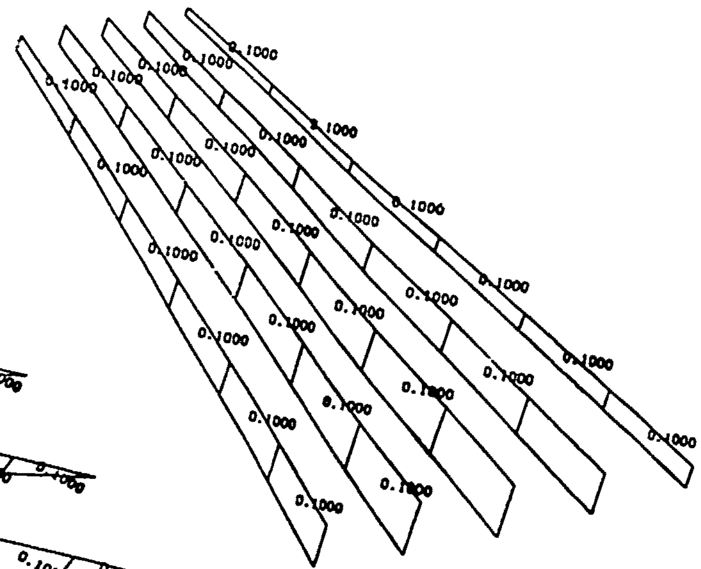

FIG 5.9 : SPAR ELEMENT THICKNESSES - 0 LOOPS

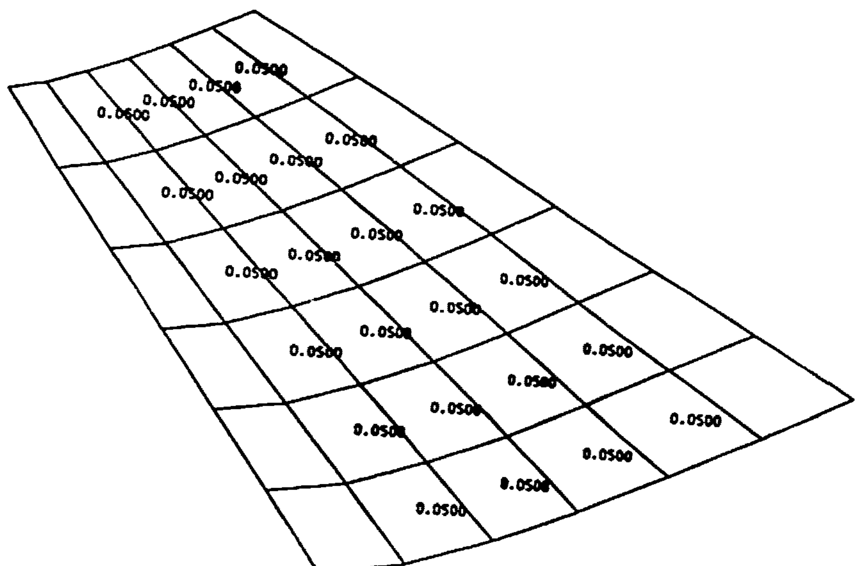

FIG 5.8 : BOTTOM SKIN ELEMENT THICKNESSES - 0 LOOPS

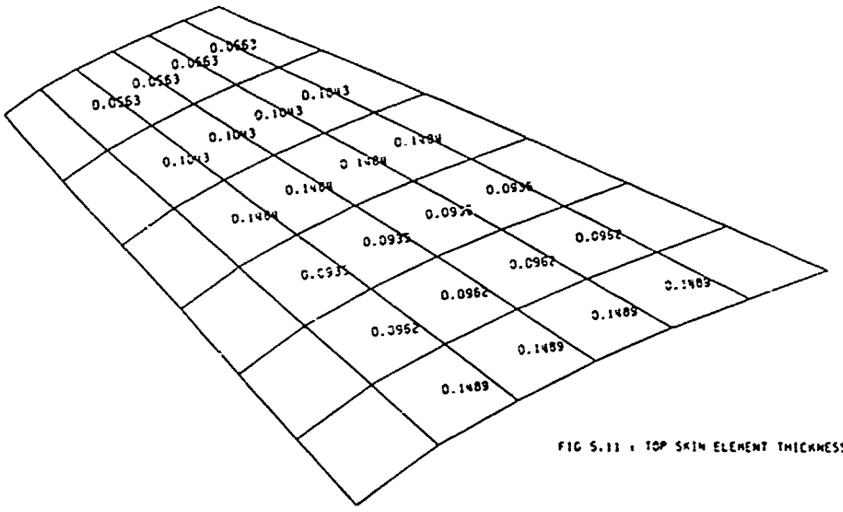

FIG 5.11 : TOP SKIN ELEMENT THICKNESSES - 12 LOOPS

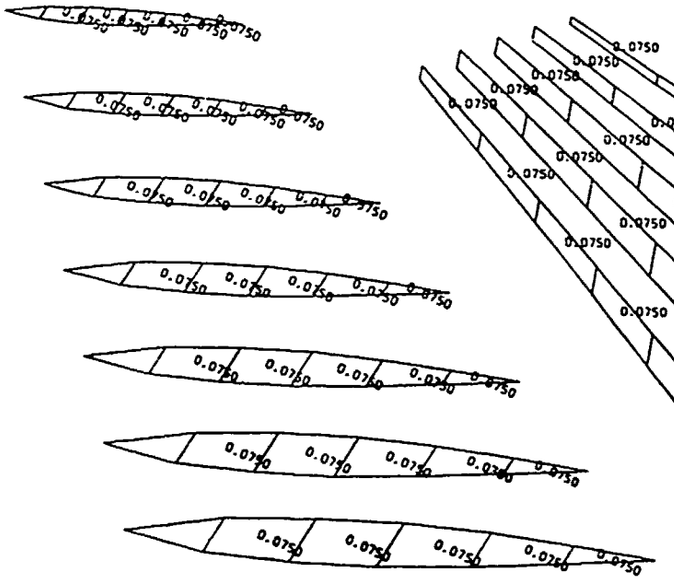

FIG 5.14 : RIB ELEMENT THICKNESSES - 12 LOOPS

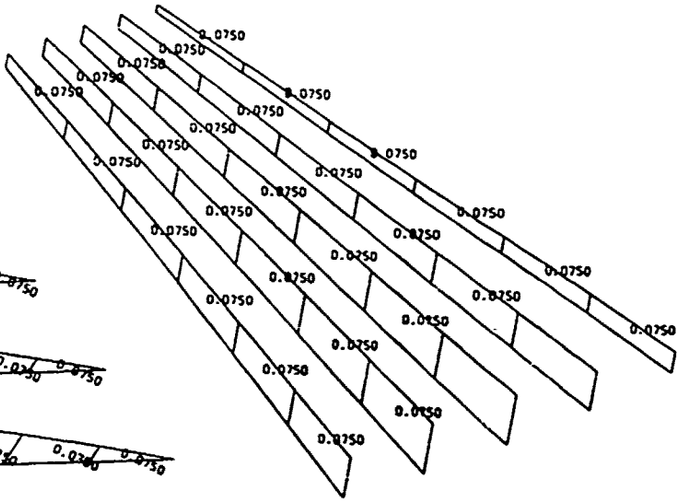

FIG 5.13 : SPAR ELEMENT THICKNESSES - 12 LOOPS

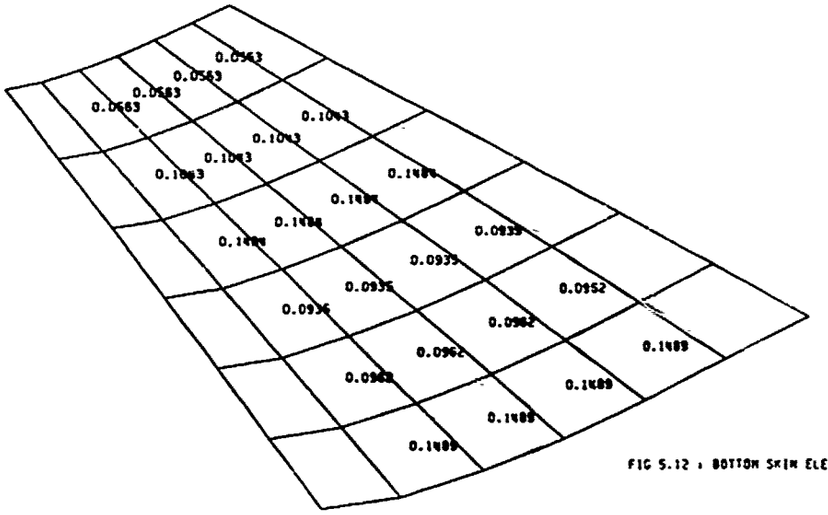

FIG 5.12 : BOTTOM SKIN ELEMENT THICKNESSES - 12 LOOPS

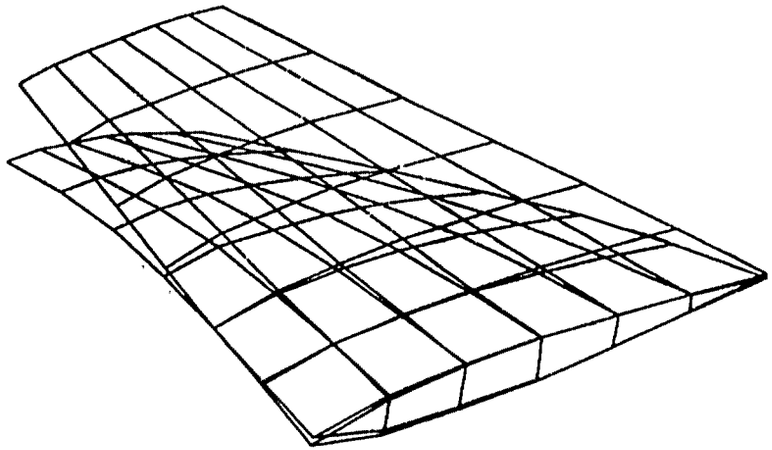

FIG 5.15

STARS TEST TAILPLANE == NOMINAL MODEL ==
FLUTTER OPTIMISATION - 0 LOOPS
MODE=1, EIGENVALUE= 1.320242E+04, CYCLES= 1.828719E+01

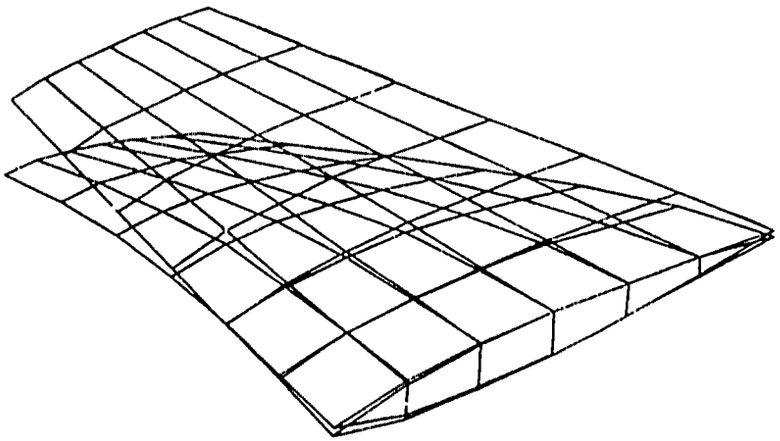

FIG 5.17

STARS TEST TAILPLANE == NOMINAL MODEL ==
FLUTTER OPTIMISATION - 12 LOOPS
MODE=1, EIGENVALUE= 2.055992E+04, CYCLES= 2.282080E+01

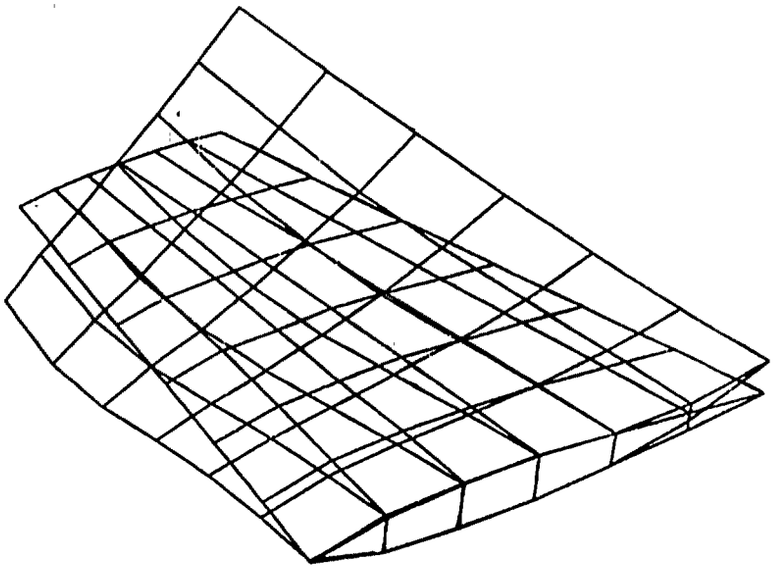

FIG 5.16

STARS TEST TAILPLANE == NOMINAL MODEL ==
FLUTTER OPTIMISATION - 0 LOOPS
MODE= 2, EIGENVALUE= 1.536858E+05, CYCLES= 6.239313E+01

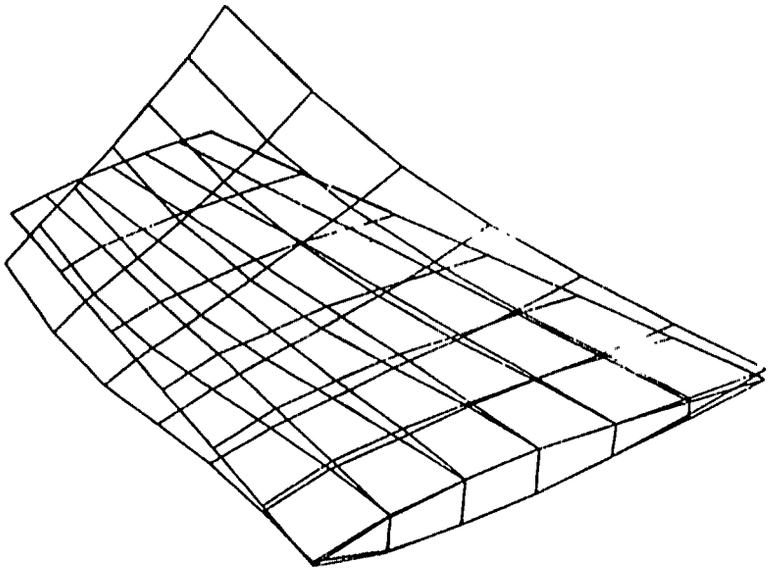

FIG 5.18

STARS TEST TAILPLANE == NOMINAL MODEL ==
FLUTTER OPTIMISATION - 12 LOOPS
MODE=2, EIGENVALUE= 2.405219E+05, CYCLES= 7.805443E+01

FREQUENCY COMPARISON

Mode No.	Initial Design	Final Design
1	18.28	22.82
2	62.39	78.05
3	72.21	89.02
4	78.62	140.55
5	116.22	150.79
$f_1^2 - f_2^2$	3558	5571

AERO MATRICES COMPARISON

Stiffness - Initial Design ($\times 10^{-4}$)

5.11	-26.24	-2.12	≈0.00	12.60
6.84	-23.68	-9.06	≈0.00	-4.54
-2.05	12.57	7.83	≈0.00	-7.46
≈0.00	≈0.00	≈0.00	≈0.00	≈0.00
-1.91	-3.76	7.04	≈0.00	-17.14

Stiffness - Final Design ($\times 10^{-4}$)

4.01	20.00	6.05	-11.87	-14.13
-5.28	-15.65	-13.44	-3.05	-8.12
-0.59	0.06	3.60	-4.36	5.58
-1.47	-1.31	-6.65	-10.91	4.85
-0.57	-0.72	-5.29	1.64	-5.14

Damping - Initial Design

136.95	-182.21	-24.59	≈0.00	8.42
40.93	475.21	57.82	≈0.00	-181.70
-65.37	133.99	189.98	≈0.00	73.49
≈0.00	≈0.00	≈0.00	≈0.00	≈0.00
-28.44	219.64	49.03	≈0.00	-21.25

Damping - Final Design

106.32	142.52	51.91	-9.65	-1.92
-34.11	323.45	96.78	-169.87	-122.59
28.83	153.48	205.17	10.44	60.01
22.77	154.93	65.78	-24.37	41.58
60.49	60.97	-47.98	-61.47	44.92

FIG 5.19 TAILPLANE MODAL PROPERTIES

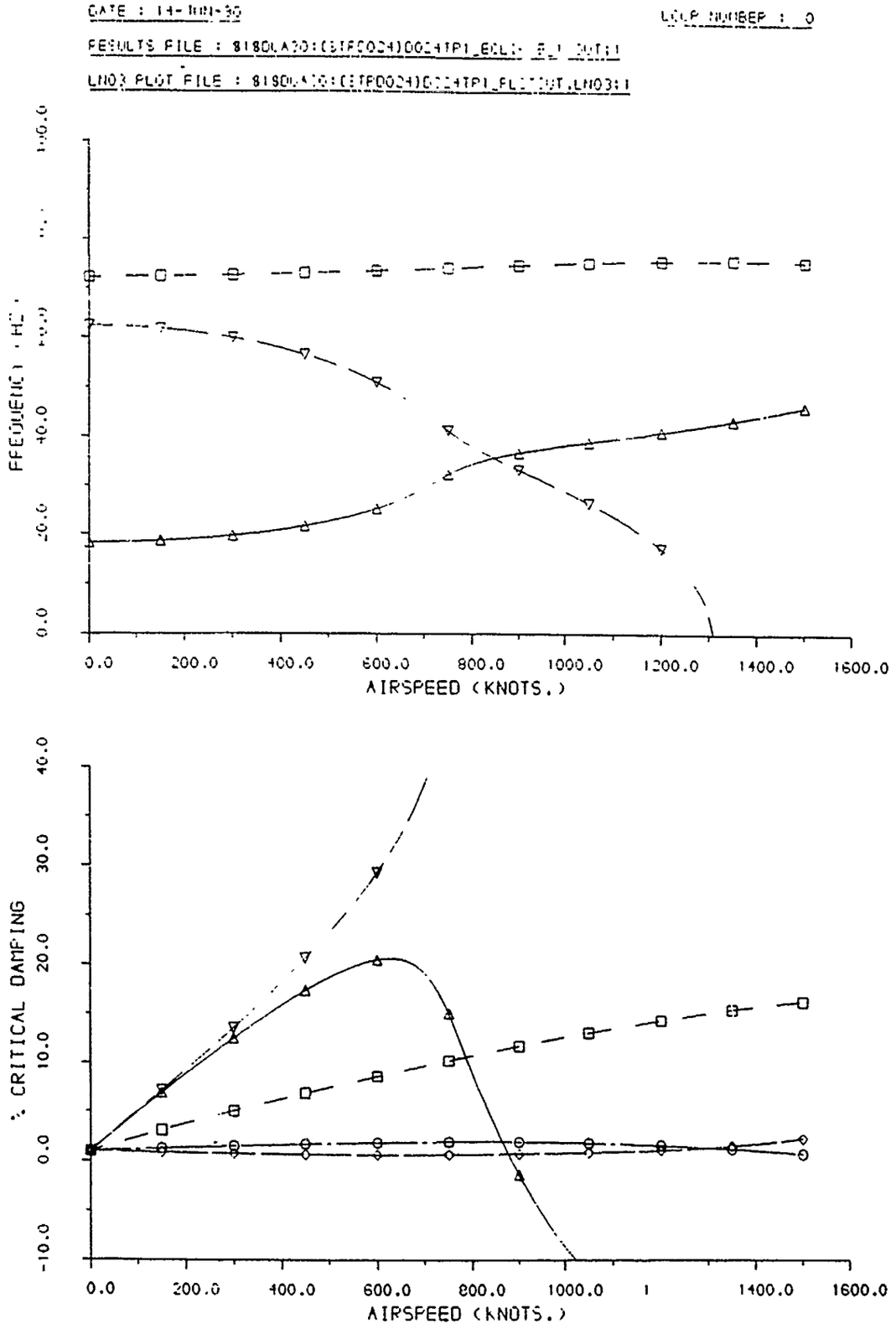

FREQUENCY/DAMPING PLOT
STARS TEST TAILPLANE ** NOMINAL MODEL **
FLUTTER OPTIMISATION - 0 LOOPS

FIGURE 5.20

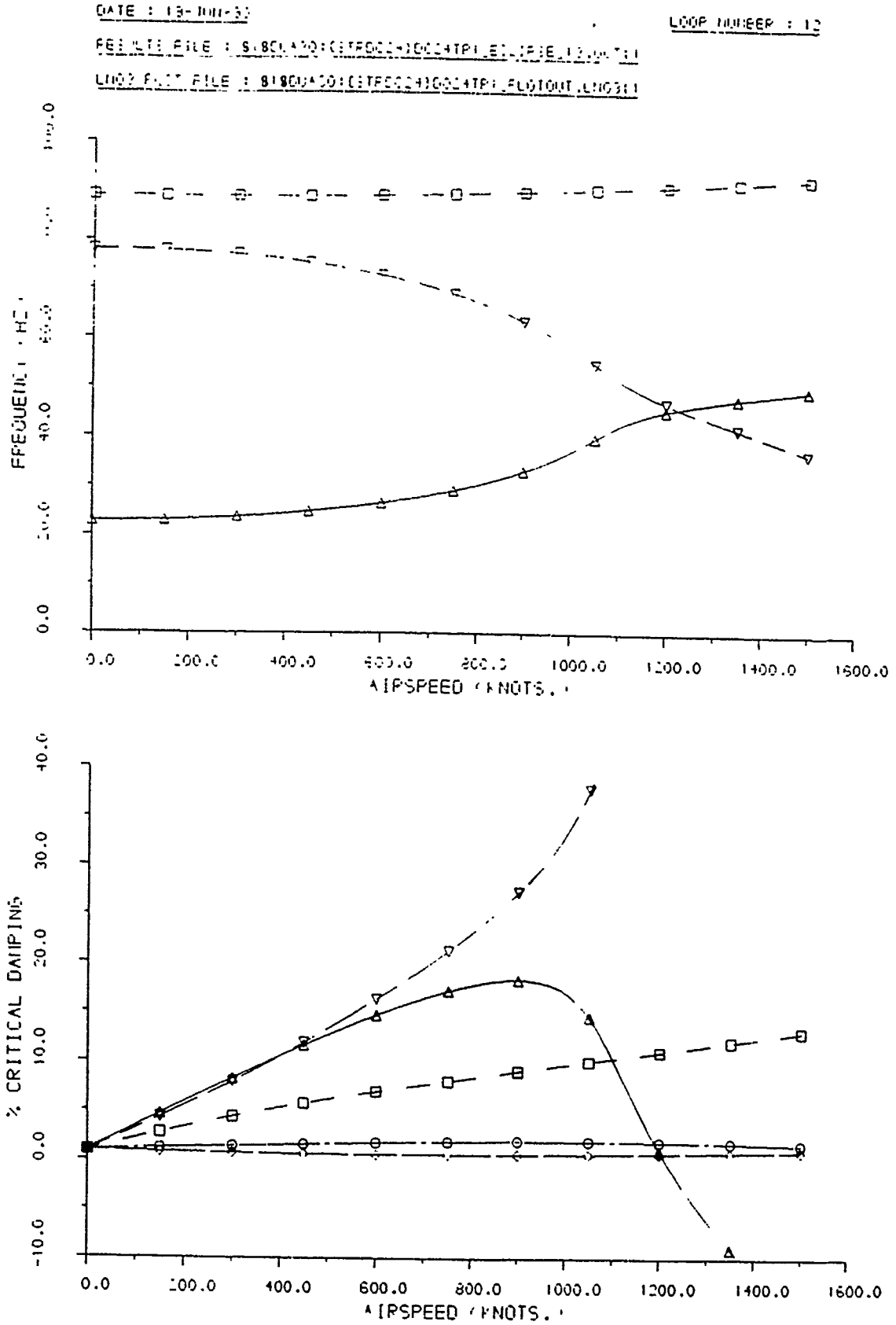

FREQUENCY DAMPING PLOT
STARS TEST TAILPLANE ** NOMINAL MODEL **
FLUTTER OPTIMISATION - 12 LOOPS

FIGURE 5.21

ACHIEVED FLUTTER VELOCITY

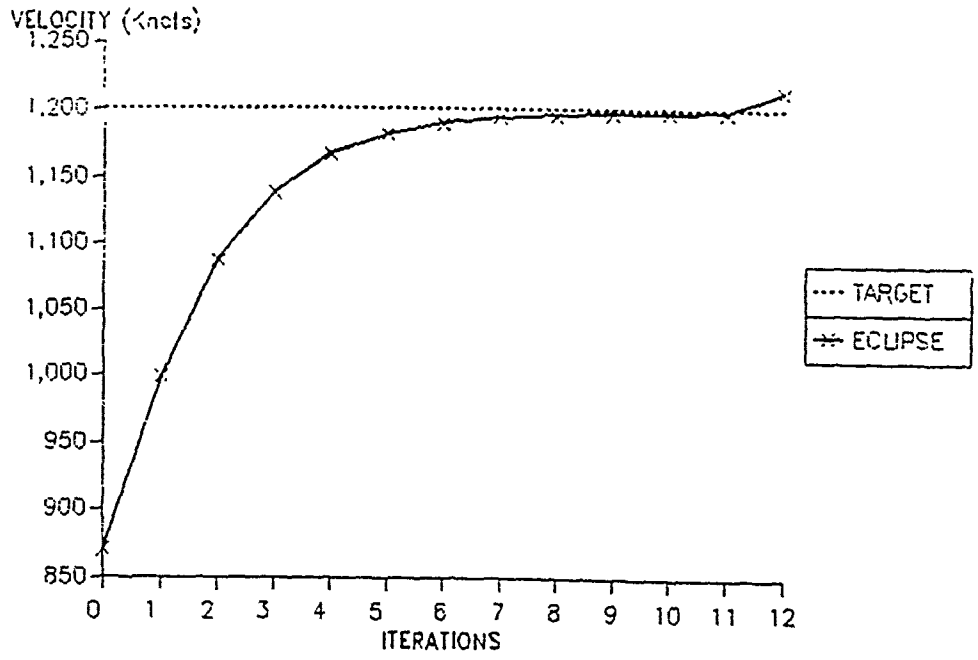

FIG 5.22

TOTAL STRUCTURE WEIGHT

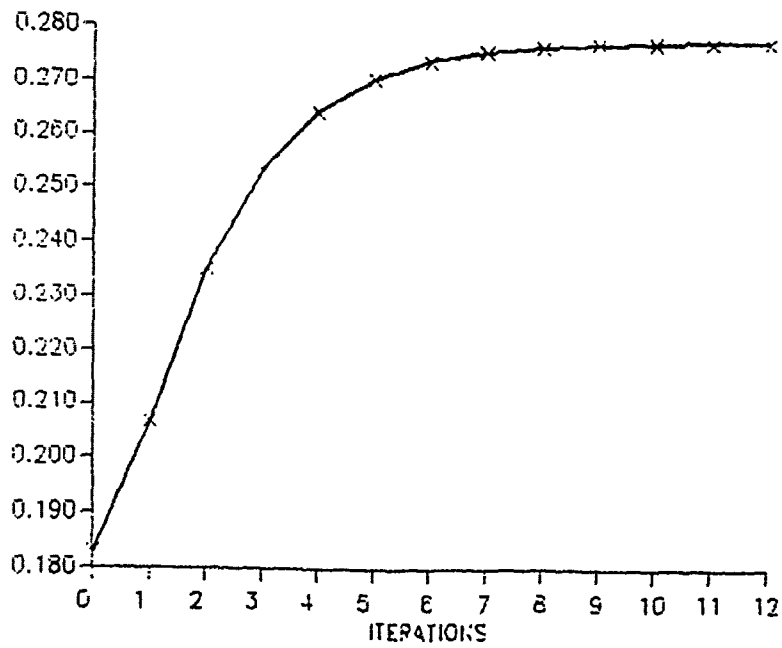

FIG 5.23

6. SPFDB FOREPLANE

This structure was proposed as the BAe MAL workshop example in order to illustrate the inclusion of a Detail Stressing Constraint and a Flutter speed constraint.

The structure used in this example is a Super-Plastic Formed Diffusion Bonded (SPFDB) foreplane of which a finite element model is shown in fig 6.1. The finite element model contained 1083 grids and 1578 elements, the elements were mainly bending plates having various orientations in three dimensions, thus all six degrees of freedom were represented at each grid point. The foreplane has spars in the spanwise direction of the form shown in fig 6.2. However it has no internal chordwise ribs except at the tip and root, hence large chordwise skin bending loads may be generated to transfer loads in the chordwise direction in regions away from the tip and root rib.

Fairings are required to maintain the aerodynamic profile on the leading edge, root and tip. The foreplane is attached to the fuselage by a statically determinate arrangement using a C-lever and a spigot. Fairings, spigot and C-lever sizes have been determined from local detail stress and stiffness calculations and are considered to be independent of the load distribution within the foreplane. Thus these items are already sized and remain unaltered by the optimisation. Individual spars are considered to be symmetric so the appropriate panels are linked. Strength resizing is performed using the internal element loading calculated by NASTRAN and adding the local pressures calculated by ECLIPSE. Local panel resizing for pressure was originally based on using the maximum edge or centre moment due to the applied local pressure. This was used in conjuction with membrane loads from NASTRAN. Since NASTRAN also gives bending moments at element centre due to the overall loading the local pressure effects were added to these.

However, the deflected shape of the foreplane under load indicates that the foreplane construction without internal ribs gives rise to large transverse shears. Thus the centre moment given by NASTRAN is not sufficient as the panel edge moments may be critical. The moments at the edge of the panels can be obtained from the centre moment and the transverse shear (fig 6.3). Since these moments may be critical in the foreplane design a specification to incorporate them was written. The new stress calculation was then incorporated into the system..

The local buckling calculation uses the in-plane loading directly from NASTRAN and the directions and widths specified in the ECLIPSE data. Buckling target Reserve Factors of 0.7 are set to simulate built in edges for narrow skin panels. All other panels have a Reserve Factor target of 1.0.

During the resizing, the thicknesses of elements on the leading and trailing edge in the mid chord region started to increase with no change in reserve factor and very little change in total structure weight. This was found not to occur when the transverse shear effects were omitted. Thus the procedure adopted to obtain a feasible design was to size the structure without the effects of transverse shear, pass the resultant thicknesses to the Design Office were the chemi-etch stages were determined and final drawings produced. Determine new model sizes from these final drawings then re-analyse the structure with the transverse shear included. Plots of the results (sizes and reserve factors) from this final analysis are shown in figs 6.4 to 6.6.

The structure was initialy optimised tc satisfy local strength and aeroelastic effficiency constraints. In the event the aeroelastic efficiency constraints proved to be non-critical. However the structure was later suspected to have a potential Flutter problem and therefore prove a suitable candidate for the recently developed optimisation facility.

The Flutter analysis would normally be performed by providing the Analysts with a set of modal deformations at an agreed subset of structural grid points (interface grid). The deformations at these points would be used to obtain the required deformations at the Aerodynamic points. Given this information the "Unsteady Aerodynamic" programmes will determine the modal damping (B) and stiffness (C) matrices used in the Flutter solution. The calculation of the B and Cs was directly coupled to the modal deformations with no intermediate AICs produced. This is inefficient for size optimisation where the only parameter

changing is the mode shape. Therefore the aerodynamic codes were modified to output the unsteady AICs defined at the interface grid. The calculation of new B and C matrices is then a simple matrix multiplication of the original AICs matrices and the new mode shapes.

In order to check that the new Flutter analysis procedure was working satisfactory, the engineered structure was analysed using ECLIPSE and the results (Fig 6.7) compared with those from the existing method. Identical results were obtained therefore we proceeded with the optimisation. Several problems arose when adapting the model for optimisation, these are explained below, the end result being that the initial Flutter speed increased from 786 to 805 knots. In the normal course of events these differences would have been investigated however in this case we were primarily interested in establishing a working procedure therefore we proceeded to optimise the altered model.

The model used by aerodynamics had all of its structural and non- structural mass represented on NASTRAN CONM2 entries. This was modified such that the structural mass was determined from element volumes and densities. However the resultant structure was 5Kg less than the original!

The set of interface grid freedoms was smaller than the Analysis set (ASET) freedoms used in the normal modes calculation. This wasn't a problem for the Flutter analysis where the displacements corresponding to the interface grid are extracted from the Analysis set vectors. However it is a problem in the derivative calculation were we require vectors of ASET size to be derived from those of IGRID size! The first solution was to reduce the size of the ASET. This had an effect on the frequency and altnough the optimisation "worked" it lead to bizarre results (fig 6.8). The second and successful solution was to modify the vectors in the derivative calculation to be of ASET size by computing them using the original mode shape vectors which were in ASET size (see Theory section 3.4).

6.1. Results

Two Optimisations were performed one starting from Minimum sizes the other from the "Engineered sizes". In oder to obtain realistic derivatives when starting from minimum sizes a one loop strength only case is run prior to the combined strength and Flutter. Post processing of the structures was performed to give the results shown in figures 6.9 to 6.14.

A similar set of results figures 6.15 to 6.20 were produced for the optimisation of the "Engineered structure". On investigating these results the following points can be noted.

The final weights in both cases are almost the same (min sizes 34.116kg engineered sizes 34.113 kg). Similarly the distribution of sizes and reserve factors for the skins is almost identical. The flutter velocity for the minimum sizes case is greater than that for the engineered sizes. This is due to a difference in the distribution of spar element sizes.

On comparing the distribution of skin thicknesses between initial and final structure we see that the optimisation is essentially pulling in material around the spigot area from the rest of the foreplane and in doing so stiffening the spigot attachment region.

Also the stability reserve factors (figs 6.5,6.12 and 6.18) have become more evenly spread for the optimised structure and most of them have reached the critical value. The flutter constraint appears to be helping the convergence of the stability constraint. However in the case of the strength constraints (figs 6.6,6.13 and 6.19), the distribution for the starting values had no areas which were critical, whereas the optimised structure has some critical areas in the leading edge region.

The iteration histories of flutter velocity and total weight for both optimisations are interesting (Fig 6.9,6.10,6.15 and 6.16). The ones starting from minimum sizes are typical of the results obtained from ECLIPSE. That is an initial large increase in weight followed by progressively smaller and smaller variations. The flutter velocity approaches the target value then begins to oscillate about it. The final value is the post processed result which has an increase in velocity due to the inclusion of the structural damping.

The frequency and damping plots Figures 6.7,6.14 and 6.20 indicate that although we have achieved the required Flutter speed, we have introduced more modes with lower damping values at the higher velocities. We therefore need to extend the Flutter constraint to include a prescribed damping target.

The plots obtained from Engineered sizes show an initial increase in weight in order to satisfy the flutter constraint. However on the second iteration the increase in weight resulted in the flutter velocity being above the value at which solutions were regarded as non-critical. Thus no optimisation for flutter was performed at this point which resulted in the strength constraints reducing and stabilising the sizes. The optimisation then followed a similar course to the previous case obtaining large variations in flutter velocity with small changes in total weight.

This structure has been optimised using a Fully Stressed Design method for strength coupled to an "Optimality Criteria" method for Stiffness. It would be very interesting to see the result of applying a Maths Programming Approach to both constraints simultaneously.

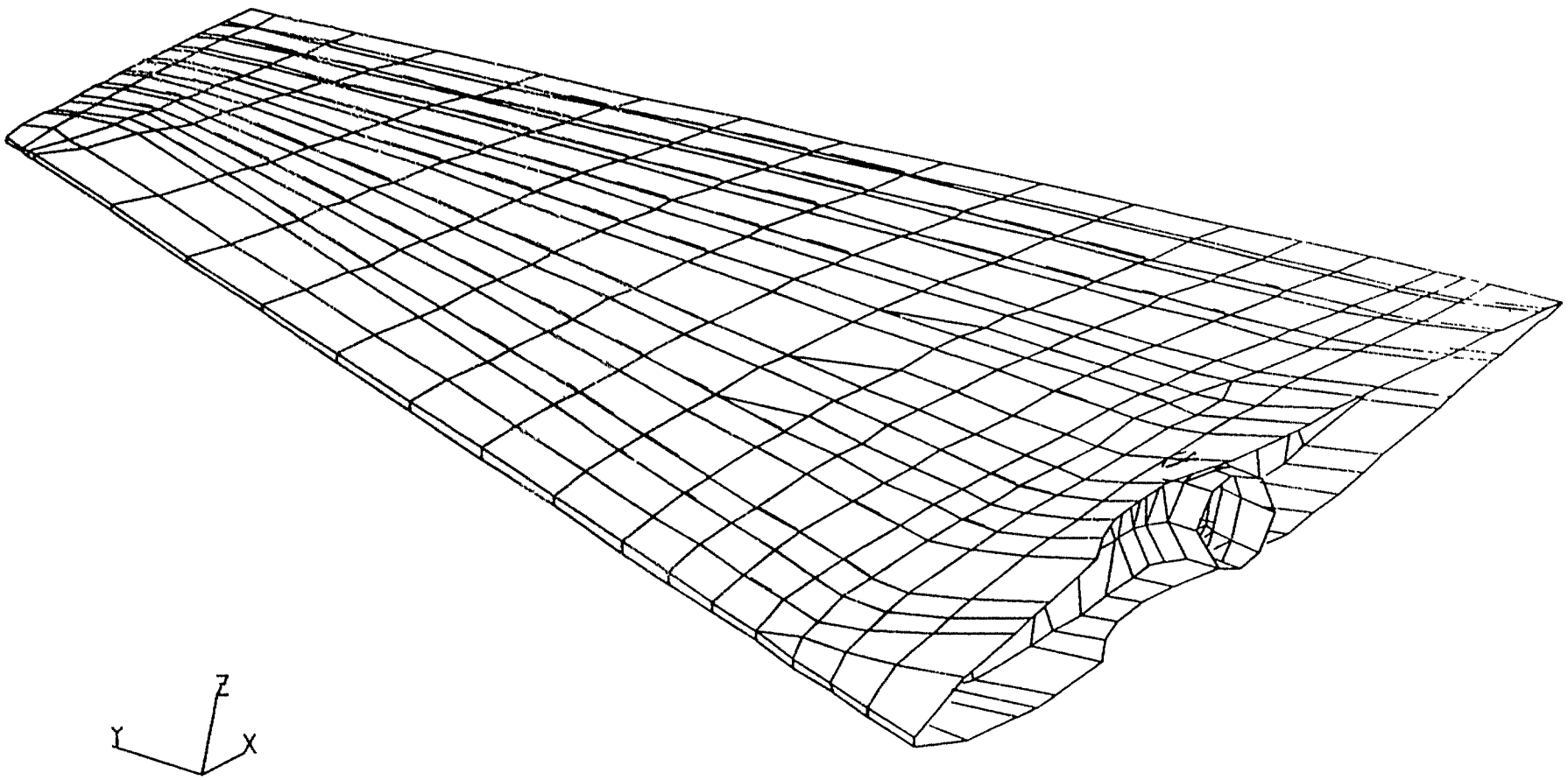

FIG 6.1 FOREPLANE FINITE ELEMENT MODEL

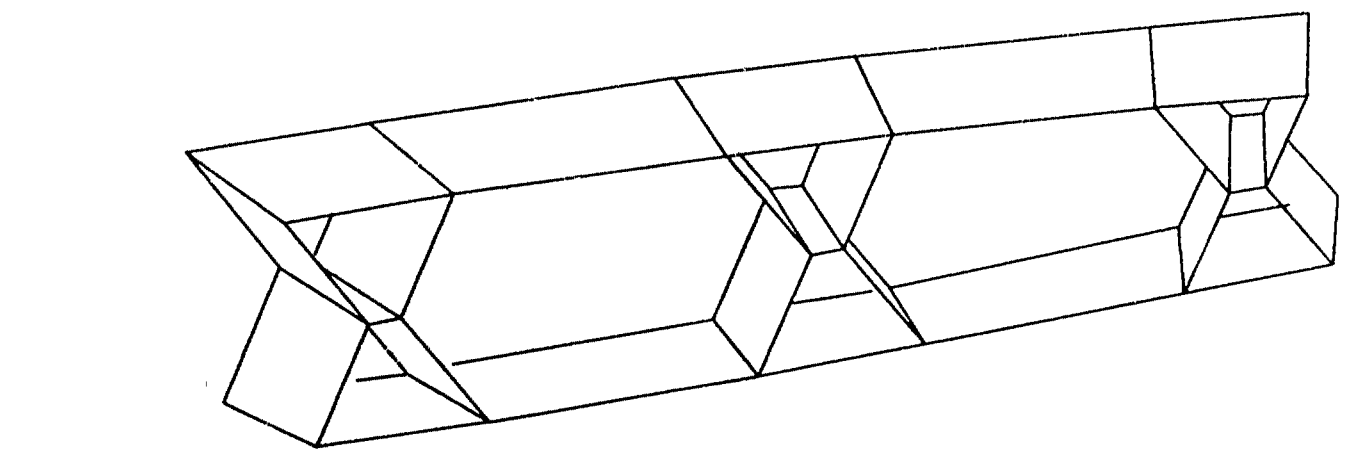

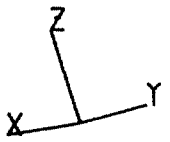

FIG 6.2 SPAR ELEMENTS

PANEL LOCAL BENDING MOMENTS

MOMENT DUE TO LOCAL PRESSURE

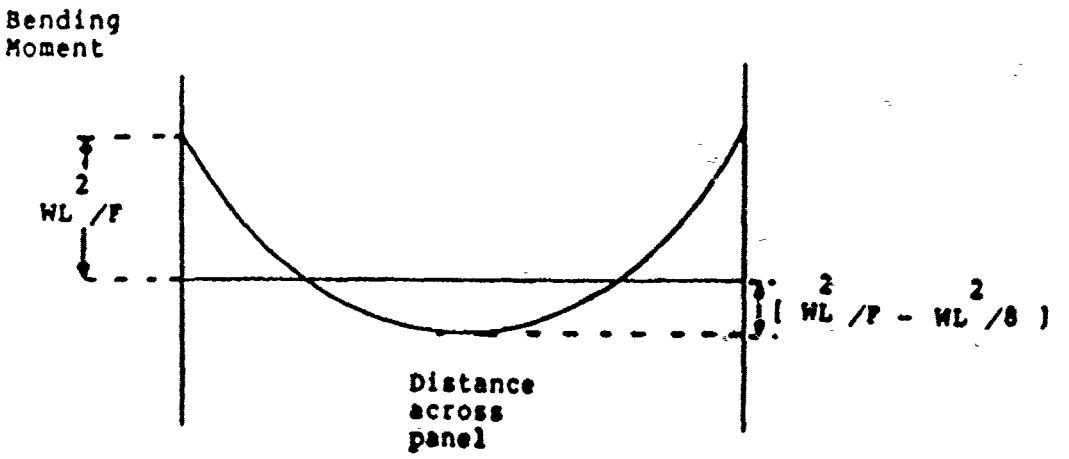

NASTRAN CENTRE MOMENT AND

MOMENT DUE TO TRANSVERSE SHEAR

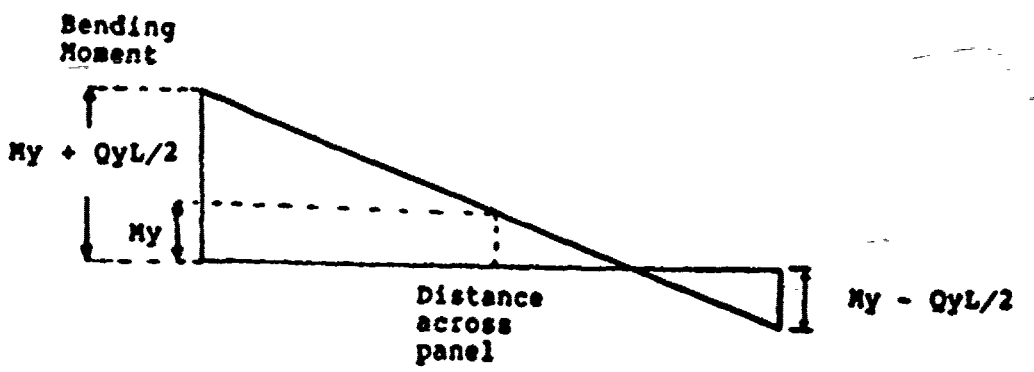

FIG 6.3

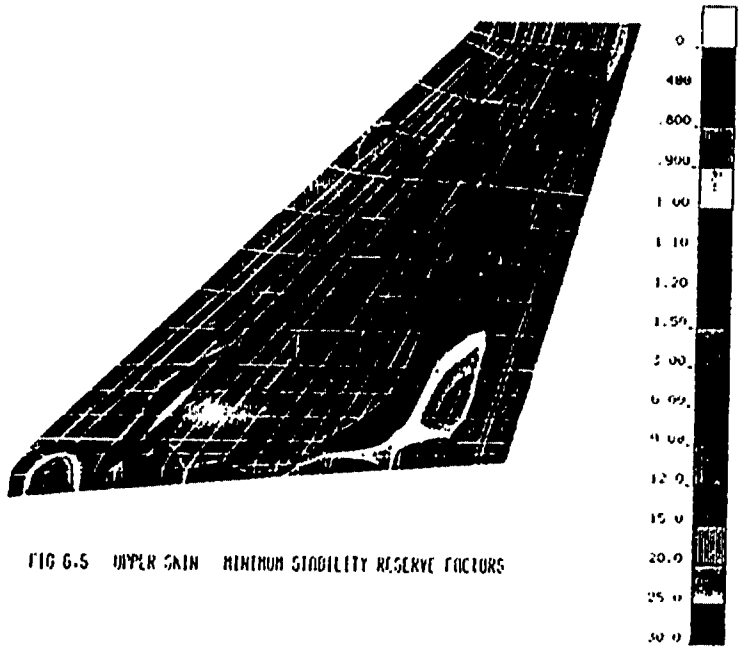

FIG 6.5 UPPER SKIN MINIMUM STABILITY RESERVE FACTORS

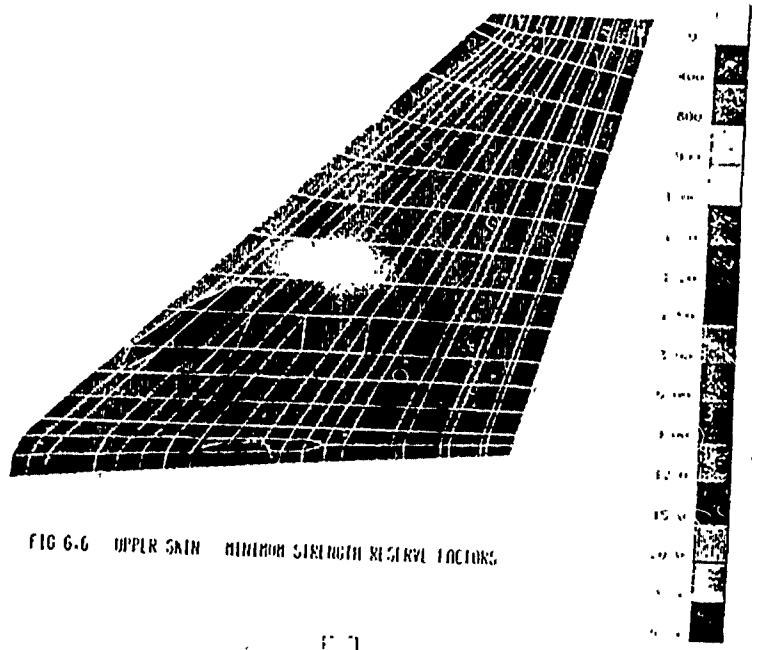

FIG 6.6 UPPER SKIN MINIMUM STRENGTH RESERVE FACTORS

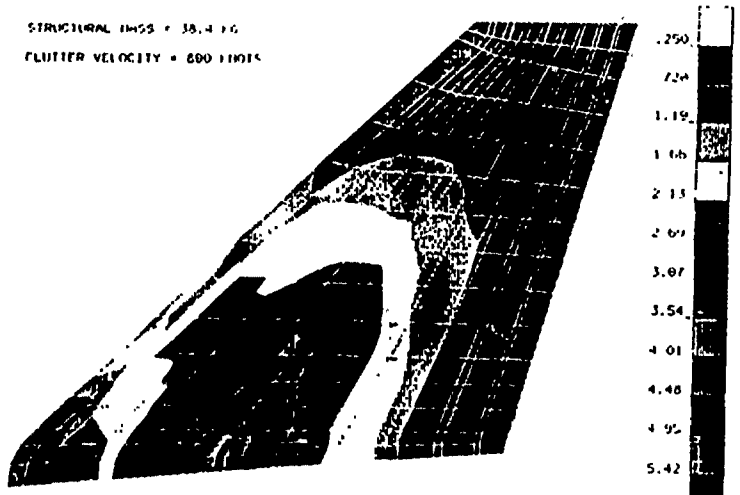

FIG 6.4 UPPER SKIN ELEMENT THICKNESSES

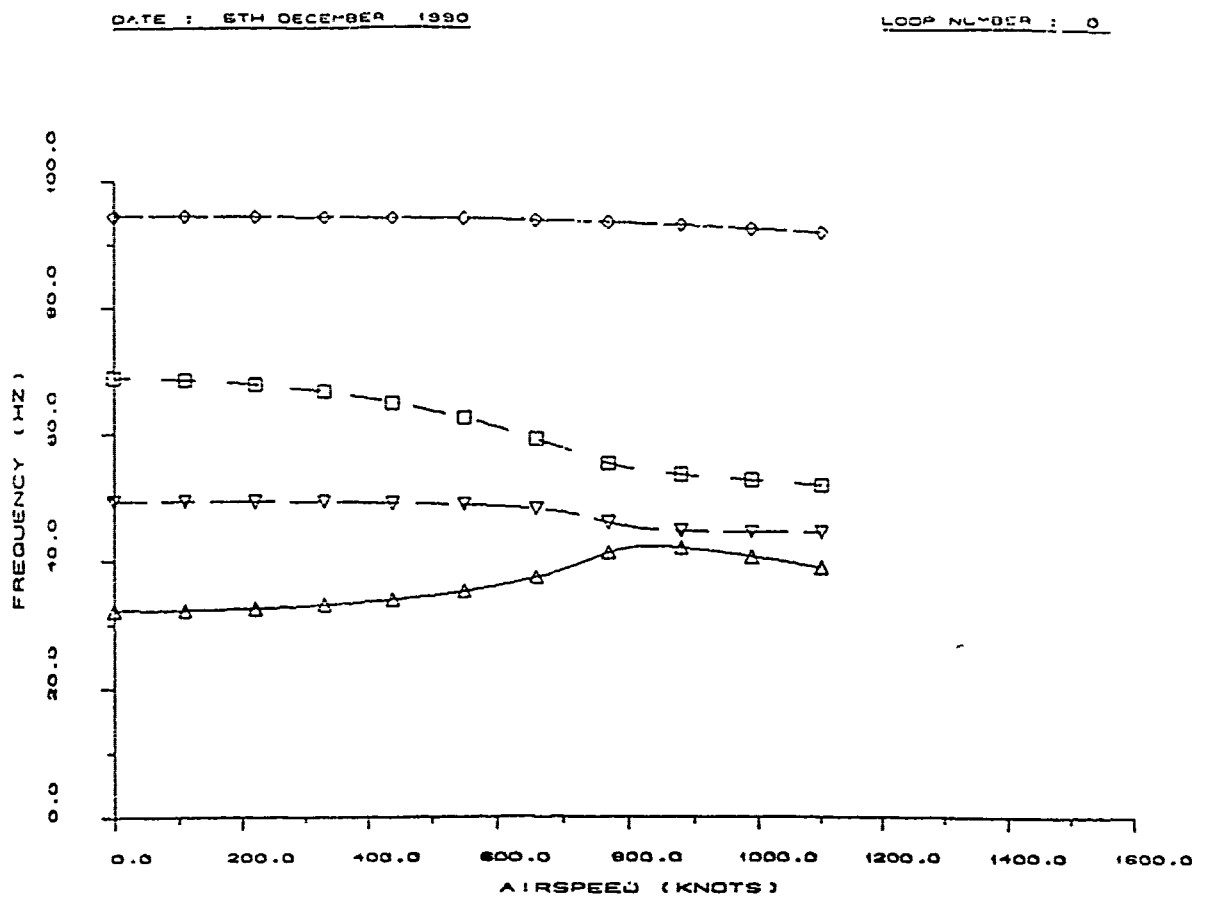

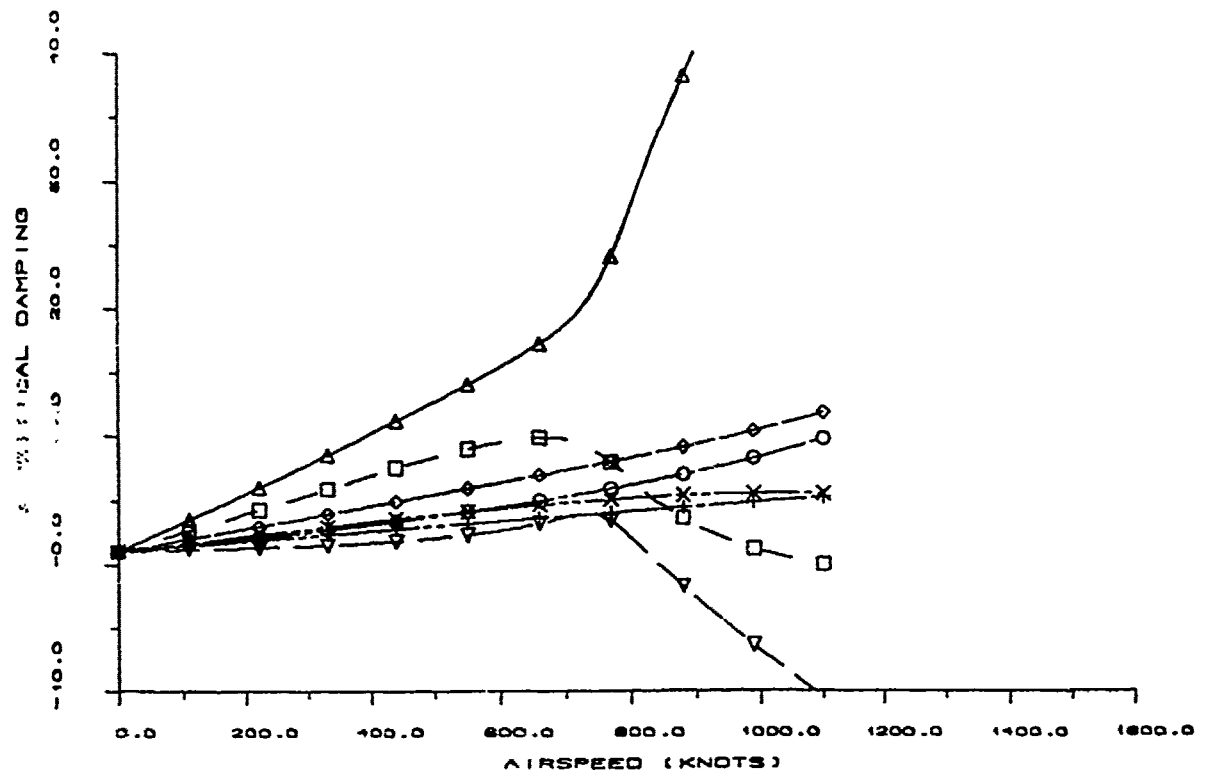

FREQUENCY/DAMPING PLOT

SPFDB FOREPLANE - ENGINEERED SIZES POST PROC. ONLY

STRENGTH + FLUTTER + AEROEFFICIENCY (D024FP6)

FIG 6.7

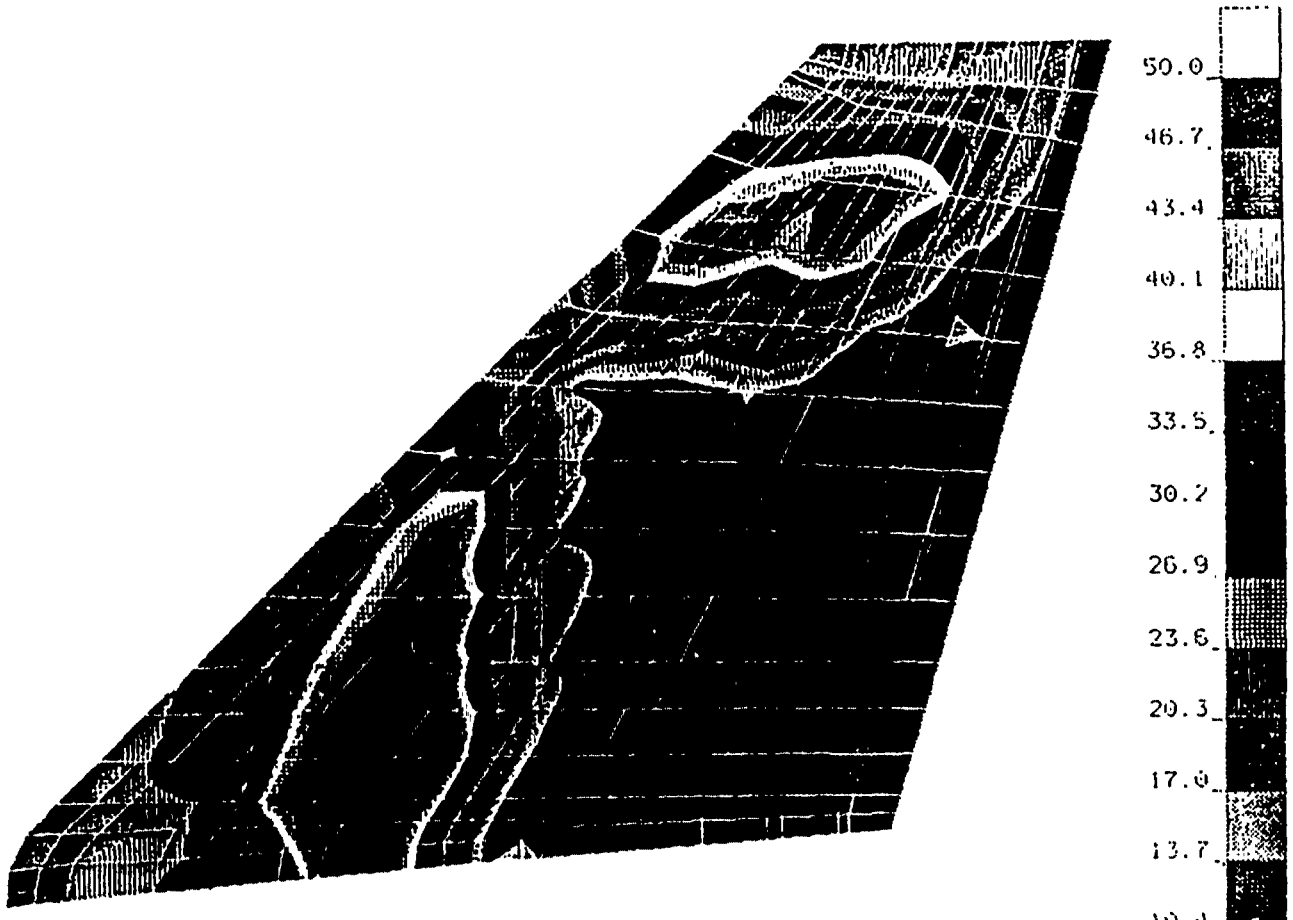

FIG 6.8 UPPER SKIN - ELEMENT THICKNESSES
(REDUCED ASET)

SPFDB FOREPLANE (STRUCTURAL MASS) - MINIMUM SIZES
STRENGTH + FLUTTER (D024FP4) (NO TRANSVERSE SHEAR)
LM95 FORP 1 + DRAG & LATERAL LOADS

ACHIEVED FLUTTER VELOCITY

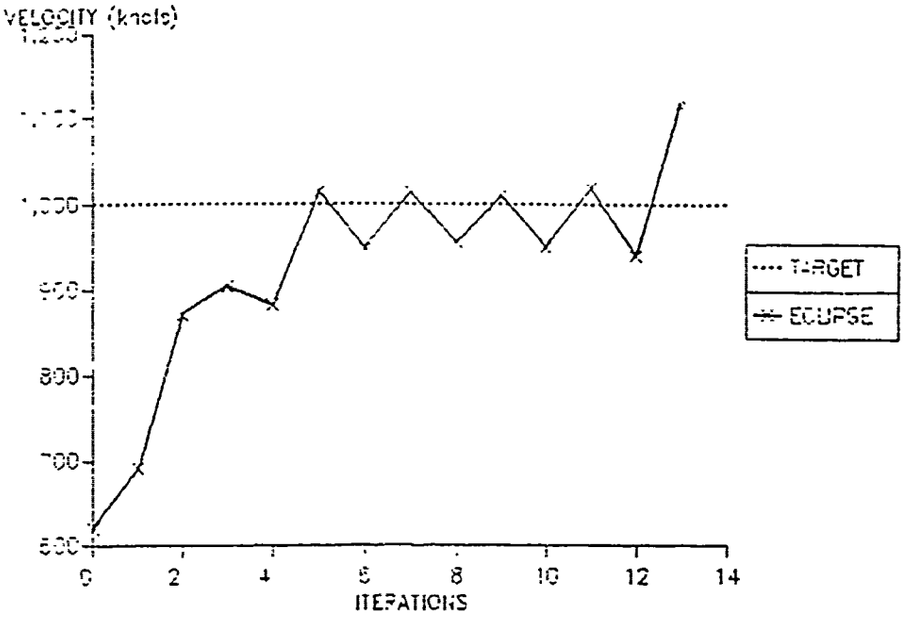

FIG 6.9

TOTAL STRUCTURE WEIGHT

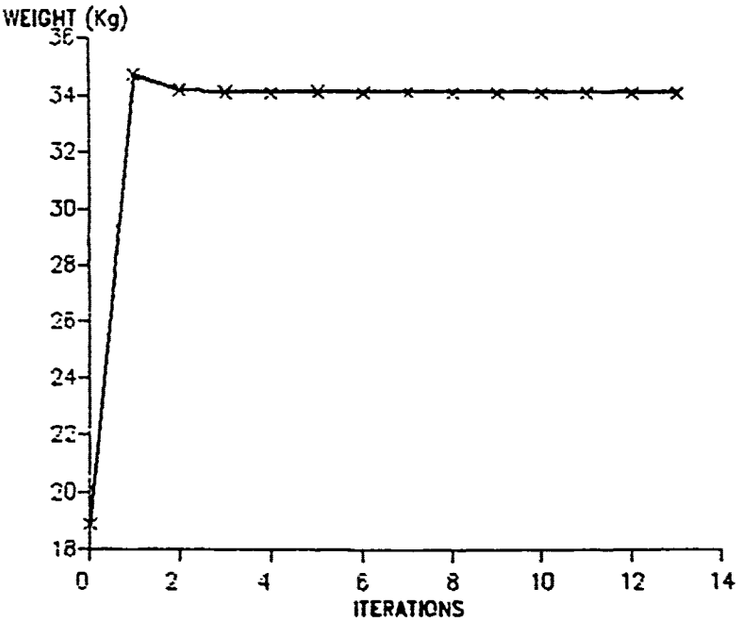

FIG 6.10

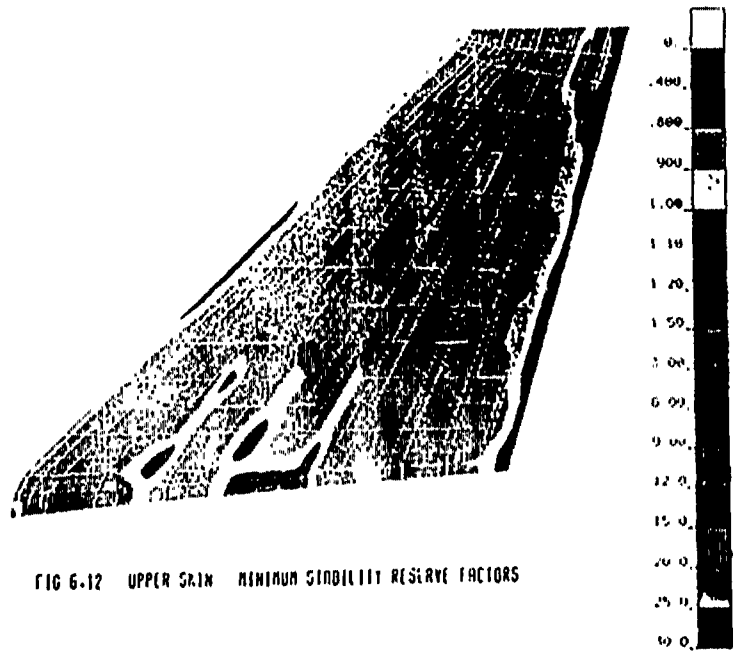

FIG 6.12 UPPER SKIN MINIMUM STABILITY RESERVE FACTORS

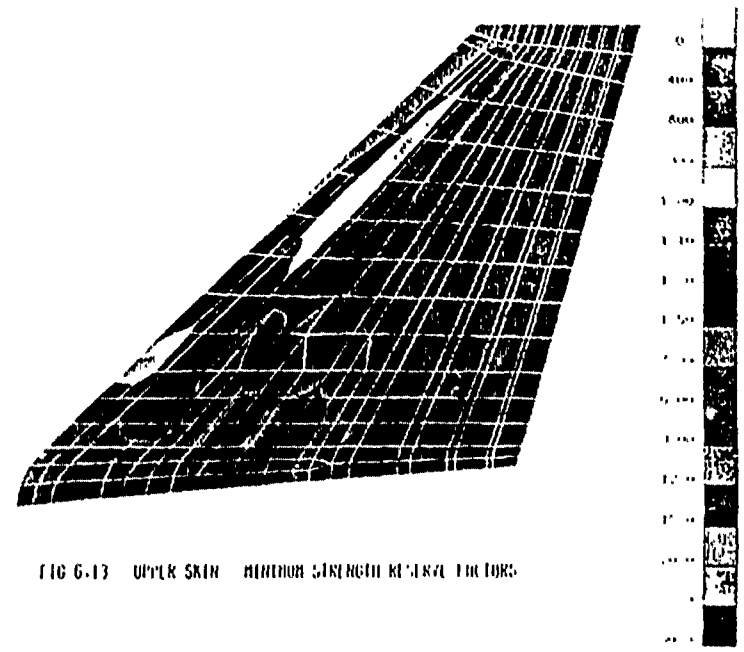

FIG 6.13 UPPER SKIN MINIMUM STRENGTH RESERVE FACTORS

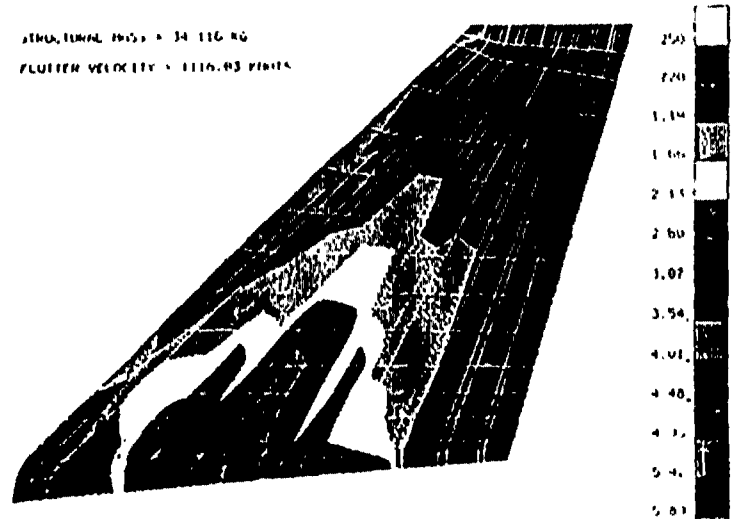

FIG 6.11 UPPER SKIN - ELEMENT THICKNESSES

DATE : 19TH DECEMBER 1990

LOOP NUMBER : 13

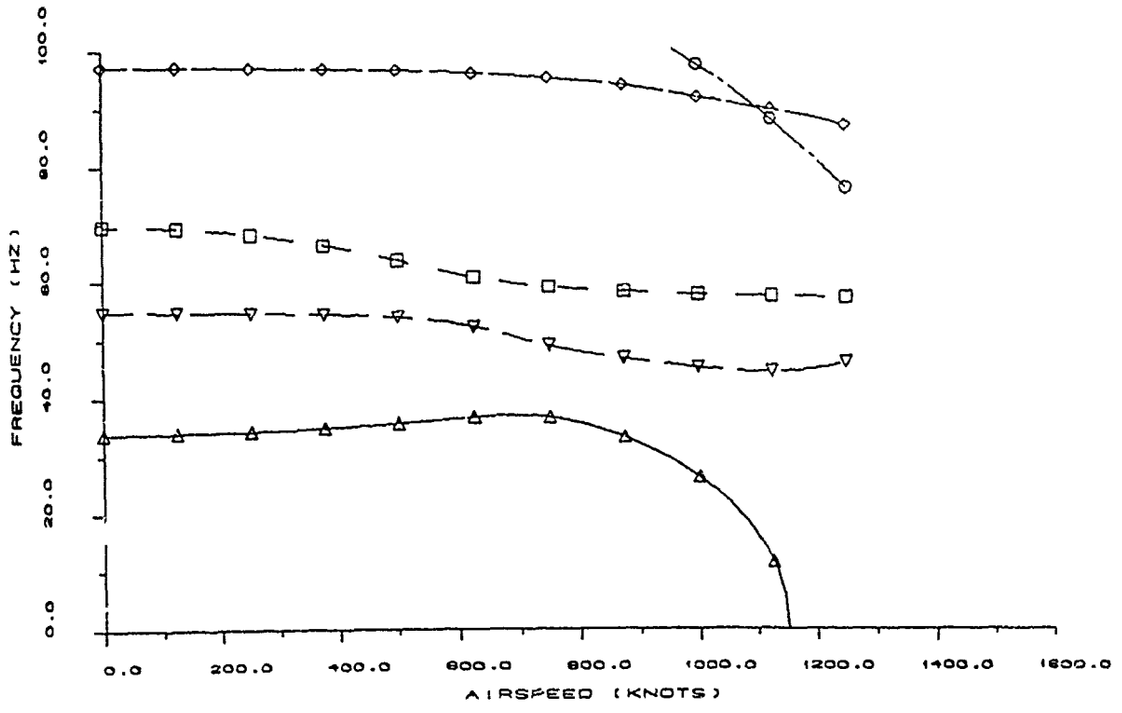

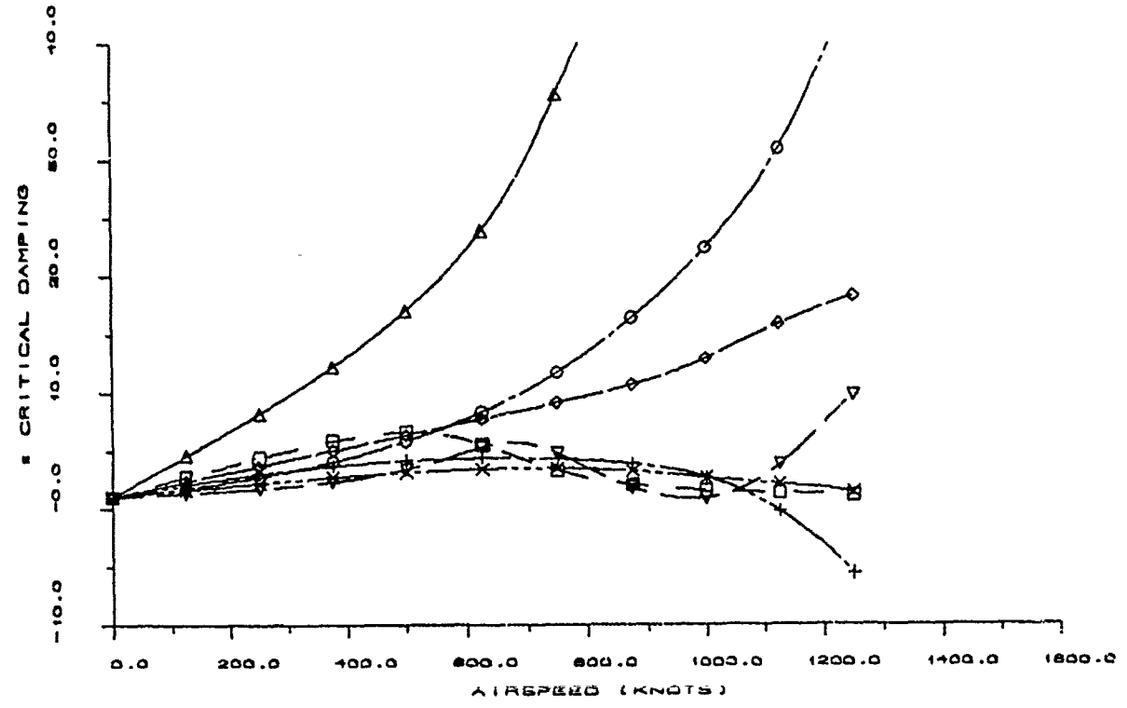

FREQUENCY/DAMPING PLOT

SPFDB FOREPLANE - 12 LOOPS FROM MIN. START SIZES

STRENGTH + FLUTTER + AEROEFFICIENCY (D024FP11)

FIG 6.14

ACHIEVED FLUTTER VELOCITY

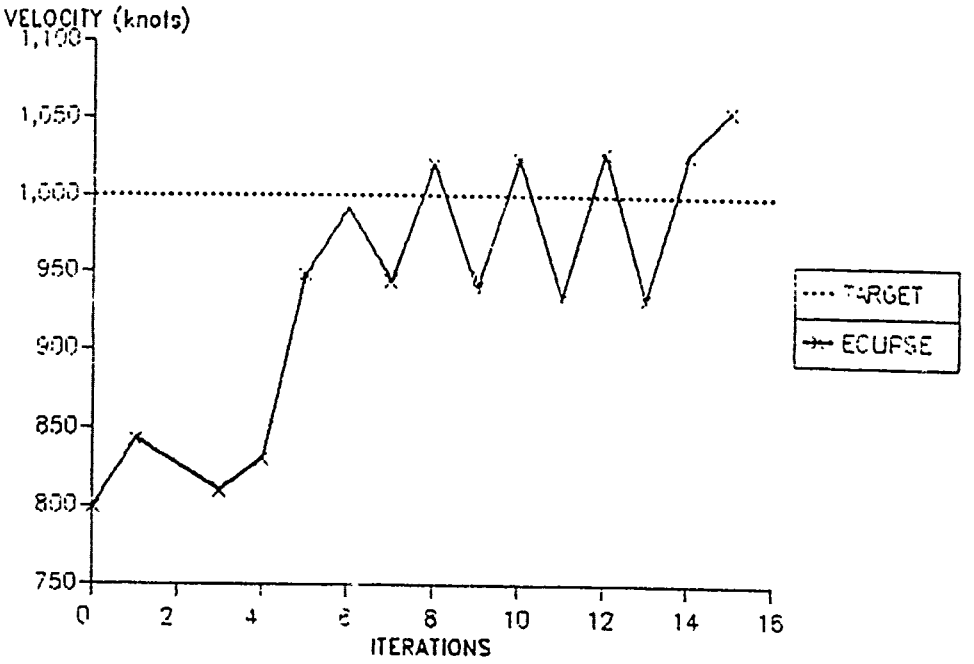

FIG 6.15

TOTAL STRUCTURE WEIGHT

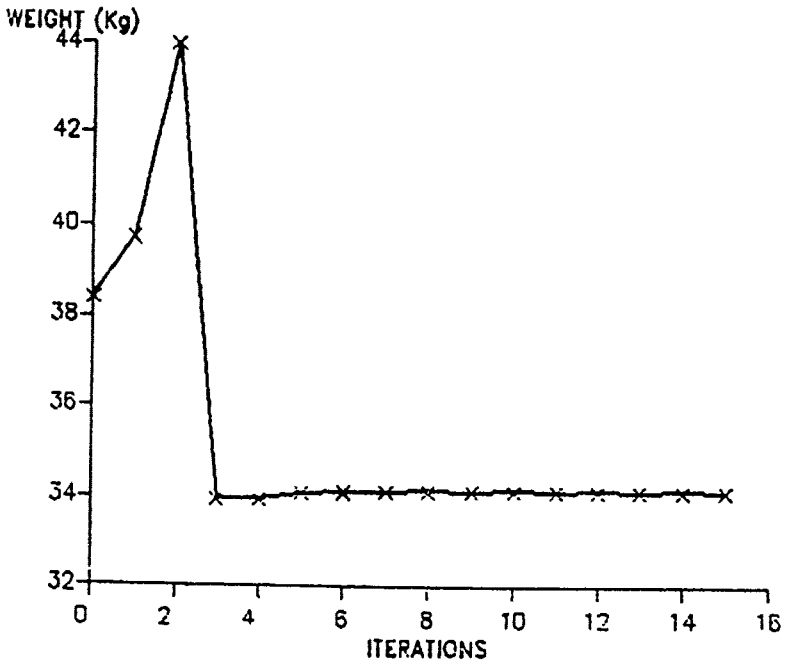

FIG 6.16

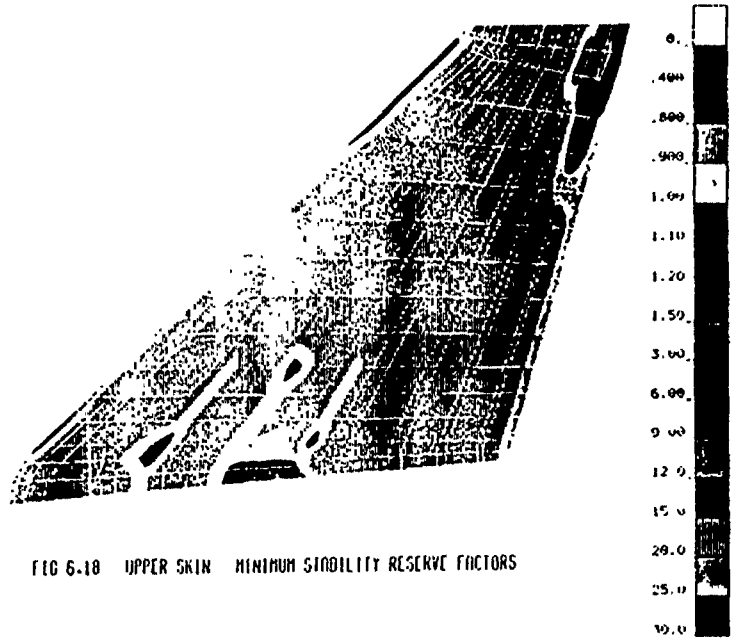

FIG 6.18 UPPER SKIN MINIMUM STABILITY RESERVE FACTORS

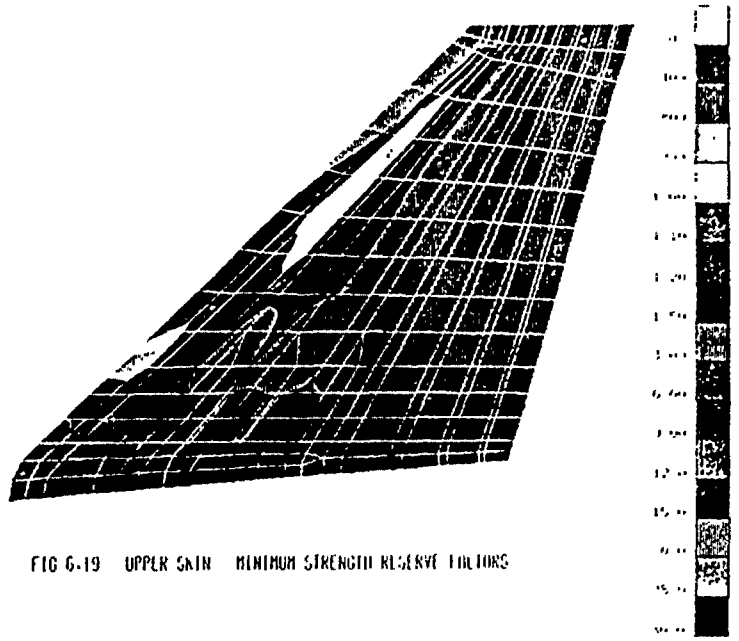

FIG 6.19 UPPER SKIN MINIMUM STRENGTH RESERVE FACTORS

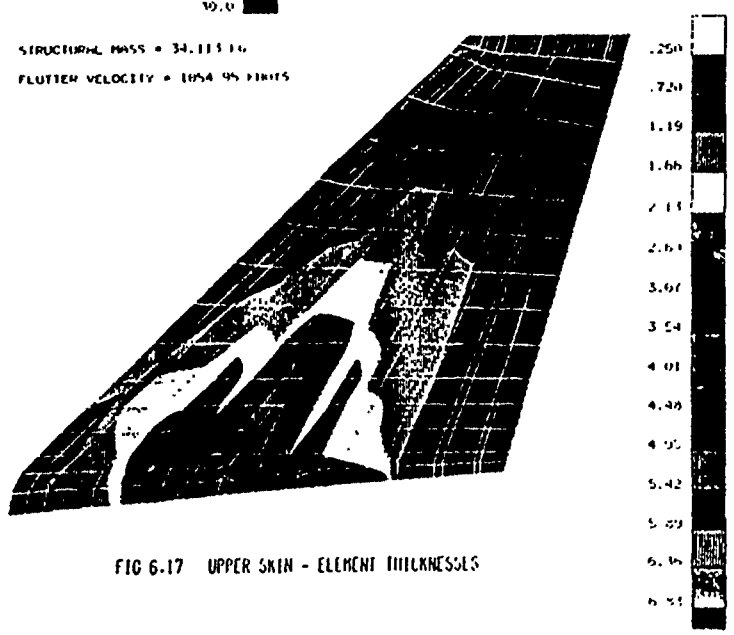

FIG 6.17 UPPER SKIN - ELEMENT THICKNESSES

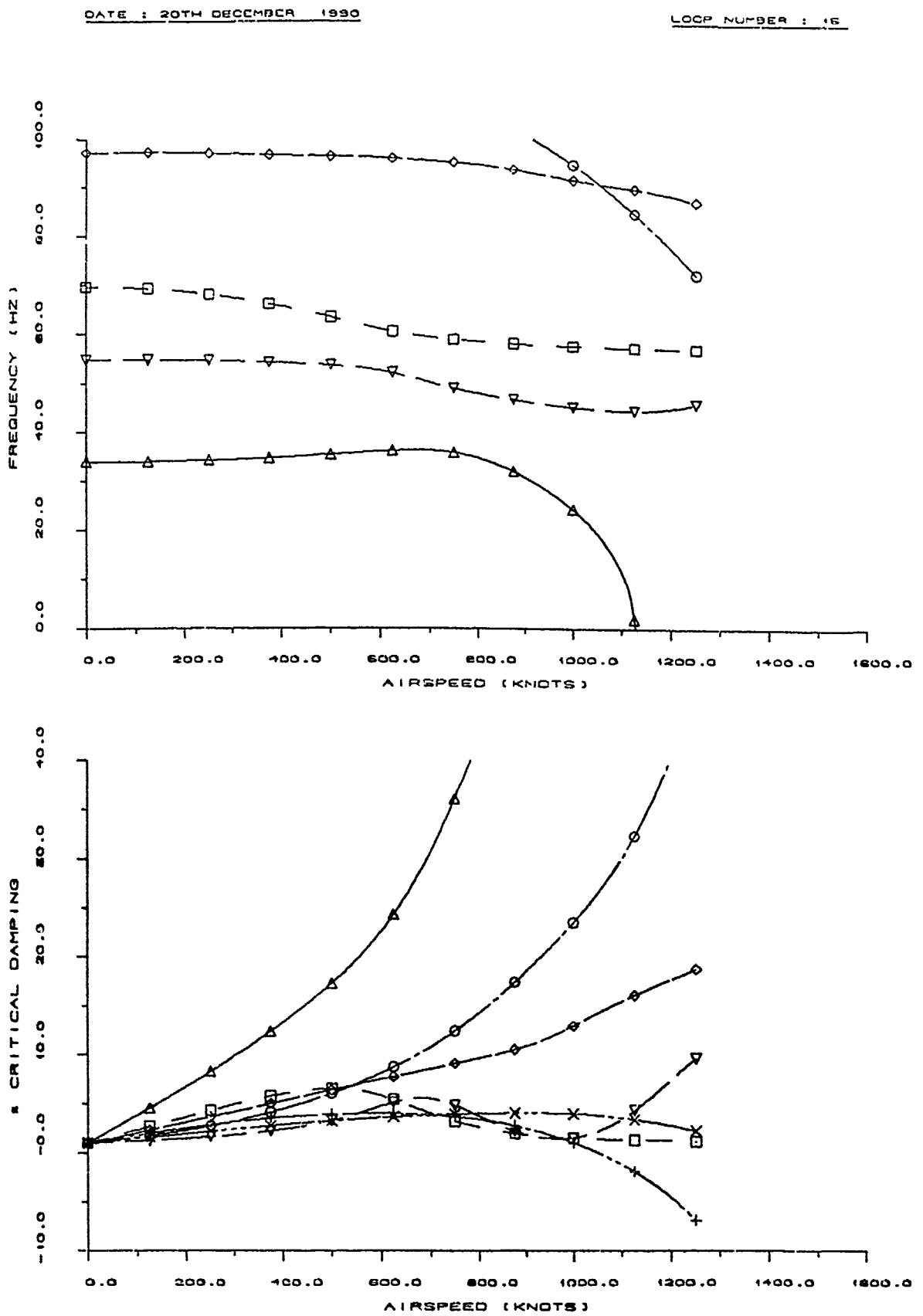

FREQUENCY/DAMPING PLOT

SPFDB FOREPLANE - 15 LOOPS FROM ENG. START SIZES

STRENGTH + FLUTTER + AEROEFFICIENCY (D024FP11)

FIG 6.20

7. FURTHER DEVELOPMENTS

The system is in a continous state of change, short and long term development plans are frequently made only to be modified by the new and higher priority requirements of the Stress Office. However having said that, development plans still have to be made and in this case are divided into two lists:- Present work and Long term.

7.1. Present Work

We are at present installing the following new facilities into ECLIPSE:-

- Optimisation for Flutter Speed and associated post processing analysis.
- Shear web post processing facility - incorporates several detail stressing requirements for the various types of shear webs and attachment flanges.
- Post processing of laminated plates incorporating variable strain allowables and the suppression of anti-clastic bending.
- Updating the "User Guide" and "Theoretical Manual" to reflect the new facilities.
- Improved restart and output facility coupled to NASTRAN PCOMP input format.
- Integration with NASTRAN 66 New Executive system.
- Integration with NASTRAN Data Base software.
- Quality Assurance of the new release.

7.2. Long Term Plans.

The following long term plans are not in any order of priority.

- Incorporation of an interactive "What If?" facility.
- Extend Flutter capability to include non structural mass and damping gradient.
- Add a Gust Response constraint.
- Add optimisation of laminated bending plates for stiffness.
- Combine basic strength, stiffness and fabrication constraints into one algorithm.
- Use existing ECLIPSE structure to adapt system to a multi-level optimisation facility (see fig 7.1).
- Improve the Pre-Processor to include Automated Idealisation using Data Generation Menus System coupled to Graphical I/O.

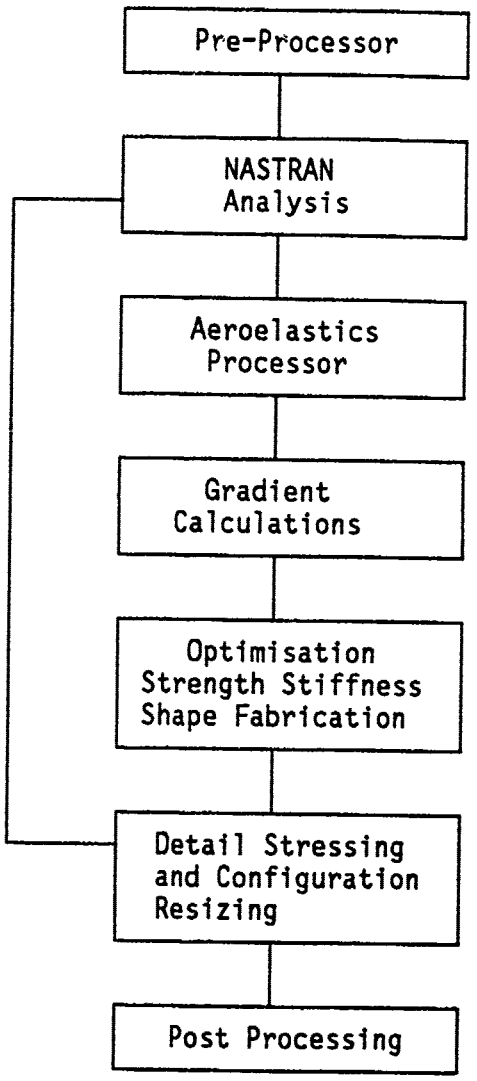

Fig. 7.1 - Multi-Level resizing System

8. CONCLUDING REMARKS

The three example cases given in this paper illustrate the succesful incorporation into ECLIPSE of a Detail Stressing and Flutter constraint. The Flutter capability needs further development to cater for Matched Aerodynamics, Non Structural Mass and Structural Damping. The facility requires evaluating by Flutter Analysts in order to improve the User Interface and generate additional Dynamic Aeroelastic constraints.

REFERENCES

Ref 1 A.K. Berry and R.I. Kerr — 'Minimum Weight of a Swept Back Wing Spar designed by Stiffness' Sir W.G. Armstrong Whitworth Research Report R.185 December 1952.

Ref 2 Dantzig G.B — 'Linear Programming and Extensions' Princeton University Press, Princeton New Jersey 1963.

Ref 3 G. Schneider, H. Krammer, H. Godel — MBB-FE2-S-PUB-0398 Preliminary Results Fin Optimisation. April 1990

ACKNOWLEDGEMENT

The Authors wish to thank British Aerospace for permision to publish this work.

MULTIDISCIPLINARY OPTIMIZATION STUDIES USING ASTROS

Alfred G. Striz
University of Oklahoma
Norman, Oklahoma 73019

Vipperla B. Venkayya
WRDC/FIBR
Wright-Patterson AFB, Ohio 45433

Abstract

The influences of the structural and aerodynamic modeling on flutter analysis and multidisciplinary optimization of fully built-up finite element wing models in an aeroelastic environment are not yet well understood. Therefore, the dynamic aeroelastic and optimization capabilities in the Automated STRuctural Optimization System (ASTROS) were used to evaluate the flutter behavior and the behavior of structural optimization with flutter constraints of various representative fully built-up finite element wing models in subsonic and supersonic flow. ASTROS was here used as a tool to calculate flutter speeds and frequencies and to minimize the weight of these wing models in subsonic and supersonic flow under given flutter and frequency constraints to determine the effect that these modeling factors have.

First, the performance of the flutter module was tested against results from other codes (MSC/NASTRAN, FASTEX) on a straight and uniform wing used by Rudisill and Bhatia and various other researchers for optimization and flutter analyses. Also, the optimization module was evaluated performing optimization with a flutter constraint. Results were compared against those reported in the literature for the same wing.

Then, fully built-up finite element models of various wings with different aspect ratios were investigated for the influence on the free vibration modes, the natural frequencies, the flutter characteristics, and the optimum weight of such modeling factors as finite element selection, structural grid refinement; number of selected modes, retention

of inplane and breathing modes; aerodynamic panel size and placement; splining of the aerodynamic grid to the structural grid, selection of extra points off the structural wing box for splining; solution procedures such as eigenvalue extraction routines, reduction schemes; selection of reduced frequency values; selection of the constraint retention parameter, etc. Knowledge of these influences as well as of the program behavior is important, since optimization can be made more efficient by the selection of reasonable initial models. Also, it is shown that modeling has an impact on the results of modal and flutter analyses. Since any optimization is only as good as the associated analyses, modeling errors can negatively impact a minimum weight optimization and can result in optimal designs that may be unreliable.

In the following, selected results are presented and the influences of modeling parameters on modal analysis, flutter analysis, and optimization are pointed out.

1. Introduction

In recent years, structural optimization as required and applied by the aerospace industry has expanded in scope to include such additional disciplines as static and dynamic aeroelasticity, composite materials, aeroelastic tailoring, etc. One of the more promising multidisciplinary codes presently under development is the Automated STRuctural Optimization System (ASTROS) [1-3]. In this computer code, static, dynamic, and frequency response finite element structural modules, subsonic and supersonic steady and unsteady aerodynamic modules, and an optimization module are combined and allow for either analysis or optimized design of given aircraft configurations. Interfering surface aerodynamics are incorporated to handle the aerodynamic modeling of combinations of wings, tails, canards, fuselages, and stores. Structures are represented by finite element models, constructed from rod, membrane, shear, plate, and other elements. Static and dynamic aeroelastic capabilities include trim, lift effectiveness, aileron effectiveness, gust response, and flutter analysis.

In the present paper, as part of an ongoing effort to gain a better understanding of the optimization process with aeroelastic constraints, the flutter analysis portion of ASTROS was used for various investigations of fully built-up finite element wing models in subsonic and supersonic flow to determine the influences of structural and aerodynamic modeling on flutter analysis as well as splining and, thus, to investigate the behavior of the

analyses modules of the code. Also, the optimization portion of ASTROS was used together with the normal modes and flutter module for various investigations of the same fully built-up finite element wing models to determine the influences of structural and aerodynamic modeling on optimization with flutter constraints and, thus, to investigate the behavior of the combined flutter and optimization modules of the code. This knowledge is incidental to the understanding of the dynamic behavior of wings during the optimization process. It will also result in better initial models and, thus, a more efficient optimization cycle.

First, the performance of the flutter analysis module was evaluated against results by other methods and codes such as the large scale finite element code MSC/NASTRAN [4] and the flutter analysis code FASTEX [5]. Similar comparisons for beam-type wing models were performed by Garner and French [6] and by Pendleton, French, and Noll [7] with good results. Also, the performance of the optimization module was evaluated against results reported in the literature. For both comparisons, the straight untapered wing (Figure 1), used by Rudisill and Bhatia [8,9], McIntosh and Ashley [10], Segenreich and McIntosh [11], and others for structural optimization with flutter constraints, was chosen since it represents one of the few models where all structural, material, and environmental data are given for aeroelastic analysis and optimization with flutter constraint.

It is well known that the normal modes response depends on the structural modeling and the non-structural mass distribution only, while flutter and optimization results depend on and vary with the quality of the structural and aerodynamic modeling and the splining connecting the structural and the aerodynamic representations. Thus, the main interest of this investigation was to determine the influences of the structural models, the aerodynamic models, and the splining on the free vibration frequencies and mode shapes, the flutter speeds, and the optimization behavior and minimum weights of fully-built-up wings.

For this investigation, the simple rectangular unswept wing shown in Figure 1 was initially used. Then, a set of test cases was selected consisting of a high aspect ratio swept and tapered wing, a medium aspect ratio straight wing with a tapered section toward the wing tip, and a low aspect ratio swept and tapered fighter-type wing (Figure 2). The straight wing and the high aspect ratio wing were evaluated at subsonic Mach numbers while the fighter wing was investigated for flutter at subsonic and supersonic speeds. These latter three wings were modified derivatives of the wings used in the investigation of the influence of modeling on normal modes and flutter analysis by Striz and Venkayya [12] and identical to the wings investigated by the same authors in Reference 13.

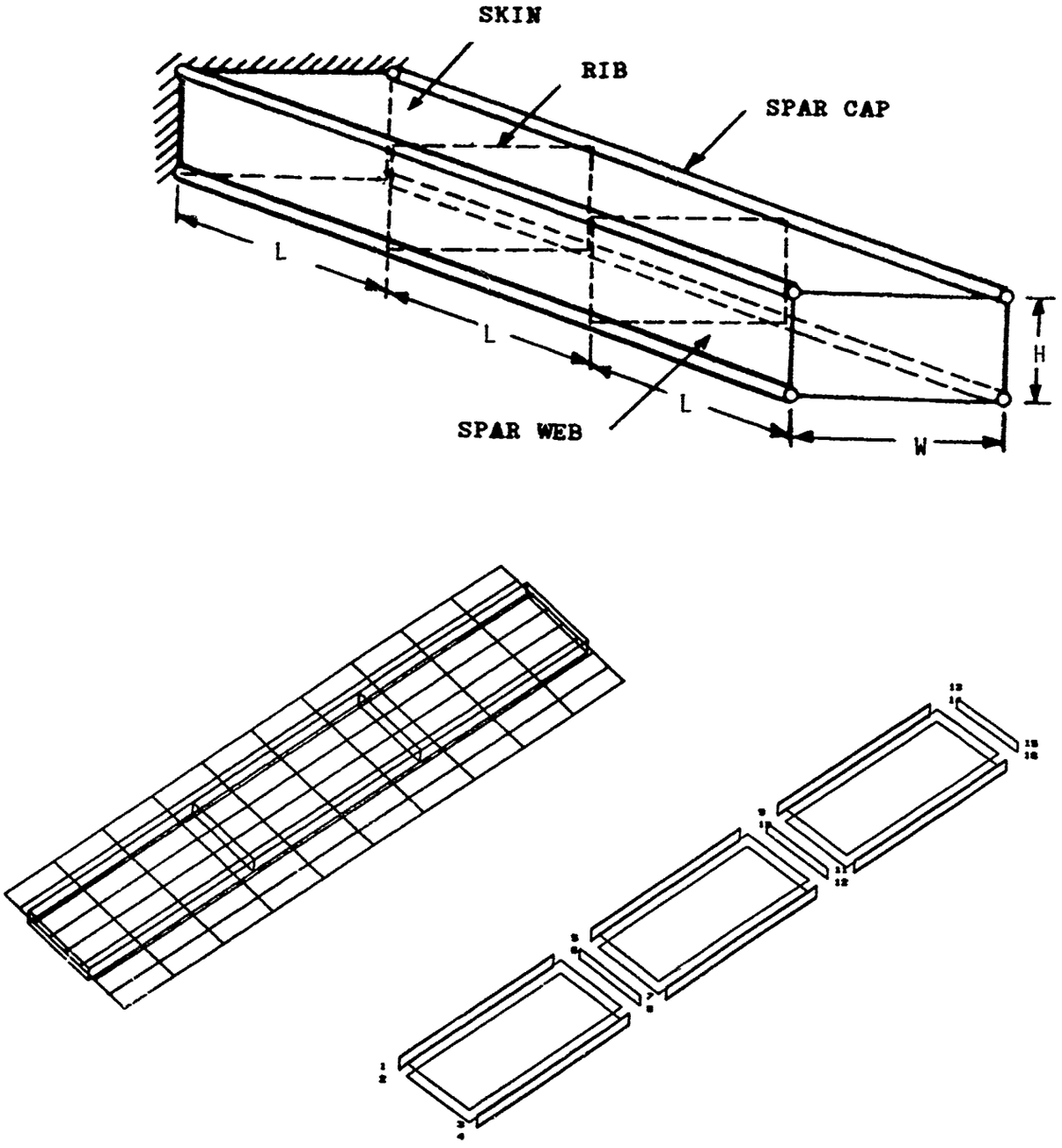

Figure 1. Wing Model of Reference 8

2. Background

The importance of this investigation can be seen from the following example: It is generally understood that membrane elements when used for spars and ribs overpredict the stiffness of a wing. Thus, when the wing used by Rudisill and Bhatia was modeled by the present authors by replacing the front and rear spar membrane elements with shear elements, the natural frequencies of the first three bending modes dropped from 10.5, 55.9, and 125.8 Hz to 6.3, 37.6, and 110.3 Hz, respectively. This kind of change in wing bending

frequencies can have a considerable impact on control surface performance and flutter. However, this example represents only a structural modeling change. In flutter analysis and optimization with aeroelastic constraints, the aerodynamic modeling also affects the results: the number, size, and distribution of the aerodynamic panels and the splining between the aerodynamic points and the structural grid. Since optimization is only as good as the associated analyses, it can, in some cases, compound and exaggerate errors arising from these. Thus, if modeling errors can have a considerable impact on the quality of the results of the associated analyses [12], optimization can be seriously jeopardized to the point where the resulting optimal design can be very unreliable. In the cited example, use of the stiffer membrane elements resulted in a 10% lower minimum weight design (38 lbs) as compared to the more realistic, less stiff shear elements (42 lbs). If flutter is the driving constraint, this could lead to the design of a structure that is potentially too weak. It is, therefore, essential that the initial designs used in optimization are feasible and modeled correctly especially when built-up finite element structural models are used rather than the previously more common beam models.

Thus, fully built-up finite element structural models for the four wings were evaluated for their flutter behavior and their performance in optimization with flutter constraint under the influence of such modeling factors as finite element selection, structural grid refinement; number of selected modes, retention of inplane and breathing modes, selection of upper frequency bounds; aerodynamic panel size and placement; selection of reduced frequencies for aerodynamic computations; splining of the aerodynamic grid to the structural grid; selection of extra points off the structural wing box (multi-point constraint or MPCs) for better mass distribution and aerodynamic splining; solution procedures such as eigenvalue extraction routines and reduction schemes; selection of optimization parameters; etc., and results are presented.

3. The Rudisill and Bhatia Wing Model

The finite element wing model used by Rudisill and Bhatia and later by other researchers (shown in the exploded view portion of Figure 1) represents one of the very few cases in the flutter optimization literature where all structural, material, and environmental data were given to allow for a direct comparison of results. It was, therefore, chosen in the present study for this same purpose.

However, three drawbacks of the model have to be pointed out: a) the aspect ratio

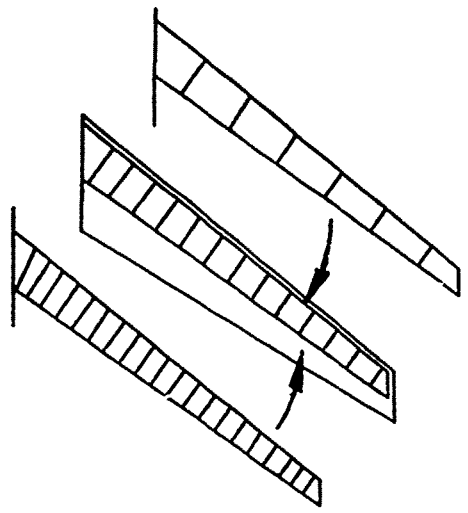

High Aspect Ratio Wing

Medium Aspect Ratio Wing

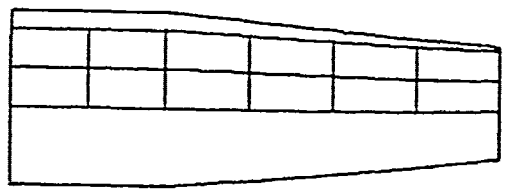

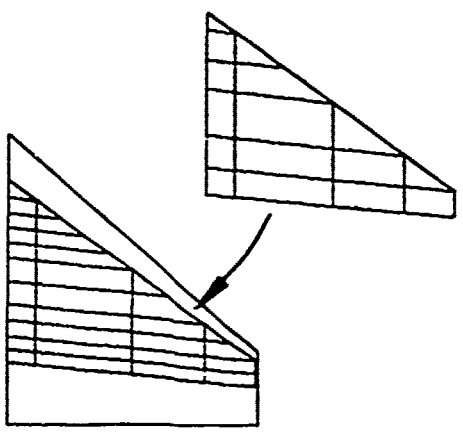

Low Aspect Ratio Wing

Figure 2. Wing Planforms Used for Modeling in Flutter Analysis

of the spar web elements in the model is 15, thus, too high for a reliable performance of the element, even in dynamic analysis; b) the spar webs are modeled by membrane elements rather than shear elements, which results in an unrealistically stiff structure; c) since no non-structural distributed mass was added to the model, the mass center of the wing coincides with the elastic axis, resulting in a close proximity of flutter speed and divergence speed as first suggested by Eastep [14]. Here, for the base model with skins,

ribs, and webs all modeled by membrane elements, the flutter speed for an input Mach number of M = 0.5566 and an altitude of h = 10,000 ft was calculated by ASTROS and MSC/NASTRAN as 10,881 in/sec and 10,500 in/sec, respectively, with divergence speeds of 11,900 in/sec and 11,500 in/sec, respectively. It has to be pointed out that MSC/NASTRAN no longer supports pure membrane elements, but uses QUAD4 elements instead. The flutter analysis code FASTEX computed a flutter speed of 10,525 in/sec, based on the ASTROS mode-shapes, but did not show a divergence branch in the root-locus plot. The flutter speed shown in Figure 3 of Reference 8 for the initial configuration was about 10,800 in/sec. When the optimized versions of the model as obtained in References 10 and 11 were analyzed for flutter, they were found to all encounter a divergence speed much lower than the speed used as a flutter constraint. It seems that none of these optimizations included the possibility of divergence as a flutter root with zero frequency. Thus, the size distributions of these optimized results seem to have been limited to flutter constraints only and would have resulted in designed wing models that considerably exceeded their divergence speeds.

First, in order to test the influence of the finite element selection on the natural frequencies, the mode shapes, and the flutter speed, the spar webs as well as the ribs were alternately modeled as shear elements and as membrane elements. The rest of the model was kept as in Reference 8. All not out-of-plane displacements were eliminated by Guyan reduction and aerodynamic MPCs were used. The results are presented in Table 1.

It can be seen that changing the ribs from membrane elements to shear elements did not seem to influence the natural frequencies at all, nor did it have any impact on the flutter speed. However, when the spar webs were changed from membranes to the more realistic shear elements, there was a significant drop in the first three bending frequencies (40%, 33%, and 12%, respectively), while the first three torsion frequencies dropped by only about 8% each. The flutter speed, at the same time, dropped by about 5%, indicating that the all-membrane model was non-conservative.

Then, to examine the influence of the number of aerodynamic boxes on the wing, various paneling schemes were chosen for the model with shear elements for spar webs: 6 spanwise x 4 chordwise, 6 x 9, 15 x 4, 15 x 9, 24 x 4, and 24 x 9. Results are presented in Table 2.

Here, the results for the cases with coarse (6 x 4 and 6 x 9) spanwise mesh distribu-

tion were almost identical (0.5%) as were those of the medium (15 x 4 and 15 x 9, difference 0.5%) and fine (24 x 4 and 24 x 9, difference 0.5%) spanwise distributions. Quadrupling the spanwise distribution increased the flutter speed somewhat (4%). These results seem to indicate that a reasonably coarse mesh, used to save computer time for quick preliminary analyses, can at least result in a conservative approximation to the flutter speed.

Table 1. Varying Element Types on Wing Model of Reference 8
Flutter Analysis

Ribs : Spars:	Membrane El. Membrane El.	Shear El. Membrane El.	Membrane El. Shear El.
Natural	10.50 B	10.50 B	6.26 B
Freqs.[Hz]	26.60 T	26.60 T	24.75 T
	55.86 B	55.85 B	37.57 B
(Bending)	79.12 T	79.12 T	71.77 T
(Torsion)	125.83 B	125.81 B	110.35 B
	134.42 T	134.42 T	122.65 T
Flutter Speed [in/sec]	10,881	10,881	10,400

Table 2 . Varying Aerodynamic Paneling Schemes on Modified Wing Model of Reference 8
Flutter Analysis

spanwise :	6	6	15	15	24	24
chordwise:	4	9	4	9	4	9
Flutter Speed [in/sec]	9,945	9,992	10,267	10,314	10,348	10,400

Varying the input Mach number from M = 0.5566 to 0.65 and, finally, to 0.717 for the all-membrane wing model with a 24 x 9 aerodynamic mesh, increased the flutter speed very slightly, from 10,881 in/sec to 10,943 in/sec to 11,010 in/sec, respectively. Then, a decrease in altitude from h = 10,000 ft at M = 0.717 to h = 4,500 ft (initial conditions from Reference 11) lowered the flutter speed as expected, in this case to 10,320 in/sec.

Finally, the free vibration mode shapes computed for the base wing model showed a considerable number of inplane, breathing, and stretching modes. It was considered advantageous to eliminate these from the flutter calculations to improve convergence and to omit false flutter points which occurred when the solution algorithm jumped between modes for this case (inplane modes). From the obtained results, it became clear, however, that only the inplane modes need to be eliminated, which is most easily done by Guyan reduction to only out-of-plane displacements. Omitting those breathing and stretching modes which had mostly out-of-plane displacements in addition to the inplane modes did not seem to change the flutter results by a noticeable amount. Almost identical results were obtained with MSC/NASTRAN.

Then, the same element variations were performed to test the influence of the finite element selection on the optimization (Table 3). All in-plane displacements were again removed from the analysis set by Guyan reduction and aerodynamic MPCs were used.

Here, too, changing the ribs from membrane elements to shear elements did not have any effect on the optimization. Then, when the spar webs were again changed from membranes to shear elements, there was a significant increase in the optimum weight due to the fact that the natural frequencies, especially for the bending modes, as well as the divergence and flutter speeds all dropped significantly, showing the all-membrane model to be non-conservative. When non-structural masses were added to the all-shear model, the minimum weight stayed essentially the same, but now the divergence and flutter speeds almost coincided for the optimized structure.

Here, too, the number of aerodynamic boxes on the wing model with shear elements for spar webs was varied similar to the flutter analysis: 6 spanwise boxes x 4 chordwise boxes, 6 x 9, 15 x 4, 15 x 9, 24 x 4, and 24 x 9 were used, respectively.

The results suggest that a reasonably coarse mesh, especially in chordwise direction, can be used to save computer time for preliminary optimization and design, since it seems to

Table 3. Varying Element Types on Wing of Reference 8
Optimization (9 Design Variables)

Rib Elements:	Membrane	Shear	Membrane	Shear	Shear/Mass
Spar Elements:	Membrane	Membrane	Shear	Shear	Shear/Mass
Init. Struc. Weight:	195.92	195.92	195.92	196.04	196.04
Opt. Struc. Weight:	37.69	37.69	41.76	41.79	41.68
Aeroelastic Mode:	Divergence No Flutter	Divergence No Flutter	Divergence Flut. Close	Divergence Flut. Close	Divergence Flutter

result in a conservative approximation to the minimum weight (Table 4). However, for this case, results with box aspect ratios of less than 1 failed to converge.

Table 4. Varying Aerodynamic Paneling Schemes on Modified Wing Model of Reference 8
Optimization

spanwise :	6	6	15	15	24	24
chordwise:	4	9	4	9	4	9
Init. Struc. Weight:	43.3	43.5	no con-	42.5	no con-	42.3
Opt. Struc. Weight:			vergence		vergence	

4. Three Wing Models with Different Aspect Ratios

The three wing models represent, in that order, a swept and tapered transport/bomber type wing of high aspect ratio, a straight and partially tapered light transport/combat aircraft type wing of medium aspect ratio, and a swept and tapered fighter type wing of low aspect ratio.

As pointed out earlier, a severe deficiency in many flutter analysis reports is the

absence of adequate details with respect to the structural and aerodynamic modeling to allow for a meaningful comparison with results obtained by other methods. Thus, for all structural and aerodynamic models used in the present investigation, all necessary dimensions and parameters are available in a report [15] to allow for such comparisons. Some selected structural and environmental data for these wings are given in Table 5.

Table 5. Environmental, Initial Geometrical, and Material Properties Model Data

HIGH ASPECT RATIO WING: (Transport Aircraft/Bomber, M = 0.87, h = 30,000 ft; M = 0.60, h = 5,000 ft)		
Variation:	Seven ribs, fourteen ribs, twenty-one ribs	
Thick-nesses:	Shear panels:	0.145" to 0.1" in ribs (for 14-rib); 0.2" to 0.1" in spars
	Membranes:	0.3" to 0.1" in skins
Areas:	Spar stiffeners:	0.15 in^2 (for 14-rib)
	Spar caps:	3.6 to 3.0 in^2
MEDIUM ASPECT RATIO WING: (Light Transport/Combat Aircraft, M = 0.58, h = 5,000 ft)		
Variations:	No MPCs, aerodynamic MPCs (14), mass MPCs (14), all MPCs (28); aerodynamic mesh variations; splining	
Thick-nesses:	Shear panels:	0.08" in spars/ribs
	Membranes:	0.06" in skins, 0.08"in ribs
Areas:	Spar stiffeners:	0.2 in^2
	Spar Caps:	1.0 in^2
LOW ASPECT RATIO WING: (Fighter, M = 0.85, h = 5,000 ft)		
Variation:	Five spars, ten spars; input Mach number (subsonic - supersonic);	
Thick-nesses:	Shear panels:	0.08"{I} / 0.12"{II} in ribs; 0.15 to 0.06" in spars (5-spar) 0.135 to 0.05" le/te, 0.075 to 0.03" int., (10-spar)
	Membranes:	0.25 to 0.04" in skins
Areas:	Spar caps:	2.0 to 1.0 in^2 {I} / 1.0 to 0.5 in^2 {II} (5-spar) 1.75 to 0.88 in^2 le/te, 1.0 to 0.5 in^2 int. (10-spar)
	Spar stiffeners:	0.05 in^2
Material for all wings is Aluminum: E = 10,000,000 lb/in^2, ν = 33, ϱ = 0.1 lb/in^3. All values decreasing from root to tip.		

The structural models for the three wings were built from rod, membrane, and shear elements to represent the wing boxes with spars, spar caps, spar stiffeners, ribs, and skins. Here, the rods corresponded to spar caps and spar stiffeners, the membranes were used for the skins, and the shear elements for the spar webs and the ribs of the wings.

a) High Aspect Ratio Wing

For the high aspect ratio wing, the structural weight was assumed to be 30% of the overall weight of the wing, with the other 70% distributed as non-structural masses at all nodal points. No MPCs were used. For the flutter analyses and optimizations, Guyan reduction was applied to retain out-of-plane displacements only.

For this wing, the influence of structural complexity in spanwise direction was evaluated. The original wing model consisted of a reasonable box with fourteen bays, showing good aspect ratios in most of the elements. Then, the wing was modeled in a simpler form with only seven bays and also subdivided into a larger number of bays (twenty-one) while keeping the total weight constant. The distribution of mass and stiffness on the wing was, thus, varied without significantly changing their values. The reasonable width to length ratio of the elements was herein exceeded, especially in the seven-bay model to determine how forgiving the structural modeling process is (Figure 3). In the optimization study, a flutter constraint of 14,000 in/sec was chosen together with a lower bound of 1 Hz on the lowest natural frequency. Also, the number of design variables was varied (13 and 26).

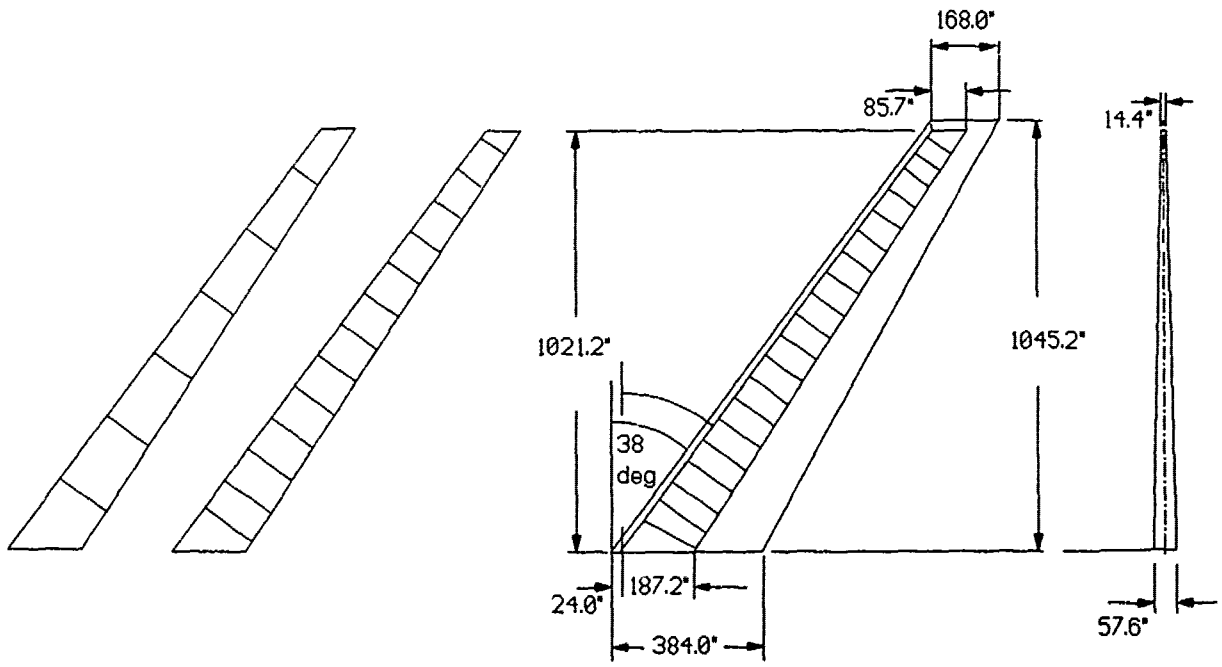

Figure 3. High Aspect Ratio Wing Model

From the results (Table 6), it seems that a spanwise increase in the complexity of the structural modeling has very little, if any, influence on the natural vibration and flutter behavior since it only accounts for a more uniform distribution of the mass and stiffness without changing their overall values. The flutter results show the expected increase as input Mach number and altitude are changed from M = 0.60 at 5,000 ft to M = 0.87 at 30,000 ft, but show very little differences between the three models for the same respective flight condition. These small existing differences can possibly be attributed to a slight deterioration in the quality of the aspect ratios of the panels for the seven and the twenty-one bay wings from those of the fourteen bay wing as well as to the way the wing root section is modeled between the three wings.

Table 6. Spanwise Structural Variation, High Aspect Ratio Wing
Flutter Analysis, Aero Mesh 7 x 5

# of Ribs:	Seven	Fourteen	Twenty-One
Natural	1.09 B	1.08 B	1.09 B
Freqs.[Hz]	4.04 B/T	3.99 B/T	4.05 B/T
	8.67 T	8.74 T	8.76 T
(Bending)	9.48 T/B	9.29 T/B	9.37 T/B
(Torsion)	15.24 T/B	15.43 T/B	15.51 T/B
	16.73 T/B	16.45 T/B	16.47 T/B
Flutter [M = 0.60]	14,607	14,721	14.972
Speed [in/sec] [M = 0.87]	20,756	20,719	20,938

For the optimization, the most reasonable fourteen bay wing seemed to show the most conservative results (Table 7) while the other two wings yielded lower minimum weights. This could be due to the stiffness distributions in the respective models, especially in the root area, or due to the somewhat excessive aspect ratios in some of the elements. Comparing the V-g plots (Figures 4a,b,c) for the three models before and after the design process, it can be seen that the optimization caused the first flutter mode to approach the constraint flutter speed. Here, all three cases show almost identical results. Finally, in all cases, an increase in the number of design variables resulted in a lower weight as expected since a finer discrete distribution of masses is possible.

Table 7. Spanwise Structural Variation, High Aspect Ratio Wing Optimization, Aero Mesh 7 x 5

# of Ribs:	Seven		Fourteen		Twenty-One	
# of Design Variables:	13	26	13	26	13	26
Init. Struct. Weight:	10206	10206	10205	10205	10205	10205
Opt. Struct. Weight:	6409	6341	6498	6448	6372	6352

b) Medium Aspect Ratio Wing

For all models of the medium aspect ratio wing (Figure 5), the structural weight was assumed to constitute about 30% of the overall weight of the wing, with the other 70% distributed as non-structural masses at all structural nodal points and MPCs. For the optimization, the flutter constraint chosen was 14,000 in/sec.

Here, the influence of the aerodynamic wing model complexity was evaluated as follows: The number of aerodynamic boxes on the wing was increased from an initially very coarse grid (5 spanwise by 5 chordwise) by increasing the number of spanwise subdivisions to 11 and 22. Then, the number of aerodynamic boxes on the wing was increased from the same coarse initial 5 x 5 grid by doubling the number of chordwise subdivisions. For most of the cases, the reasonable width to length ratio of the aerodynamic boxes was exceeded to determine how forgiving the aerodynamic modeling process is.

The results are presented here in comparison to a more reasonable spanwise and chordwise subdivision of 22 x 10 (Table 8). Similar to the results for the Rudisill and Bhatia wing model, the flutter speed changed little for all the different types of meshes. Here, as for the Rudisill and Bhatia wing, the models with a lower number of chordwise boxes showed slightly lower flutter speeds, while increasing the number of spanwise boxes raised the flutter speeds.

In the optimization, the models with less spanwise boxes showed slightly higher minimum weights with virtually no variation due to a change in the number of chordwise boxes.

a) 7 Ribs

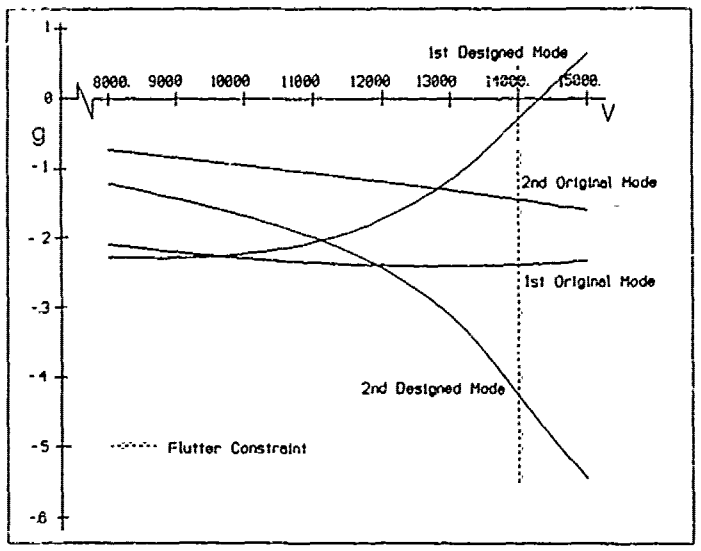

b) 14 Ribs

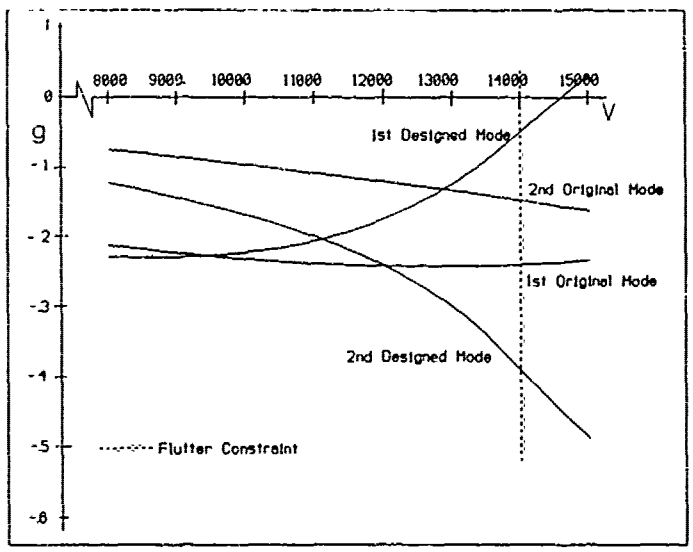

c) 21 Ribs

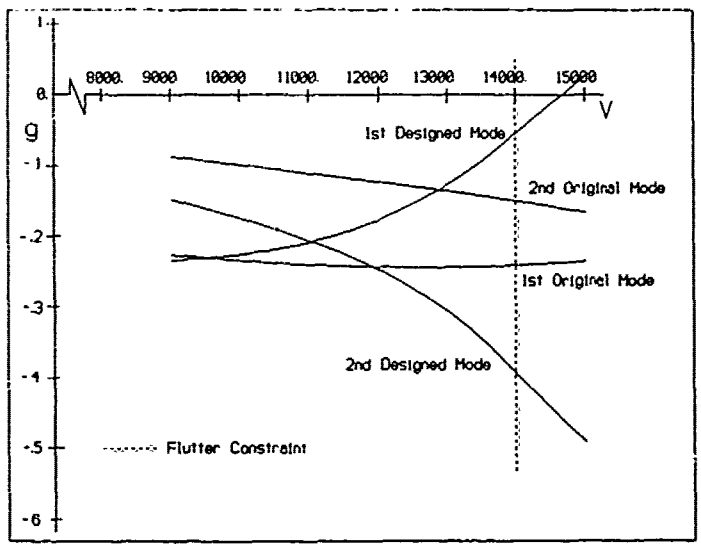

Figure 4. V-g Plots for High Aspect Ratio Wing Model: a) 7 Ribs, b) 14 Ribs, c) 21 Ribs 26 Design Variables

Table 8. Aerodynamic Mesh Variation, Medium Aspect Ratio Wing Flutter Analysis

Panel Mesh:	5 x 5	5 x 10	11 x 5	11 x 10	22 x 5	22 x 10
Flutter Speed [in/sec]	19,512	19,581	19,912	19,969	20,167	20,240

This seems to indicate that a coarse aerodynamic mesh can be used for preliminary design and will result in a conservative design (Table 9).

Table 9. Aerodynamic Mesh Variation, Medium Aspect Ratio Wing Optimization (31 Design Variables)

Panel Mesh:	5x5	5x10	11x5	11x10	22x5	22x10
Init. Struc. Weight:			576.8			
Opt. Struc. Weight:	177.7	177.3	170.6	168.6	167.5	166.5

Then, the use of multi-point constraints (MPCs) was evaluated. These MPCs add non-structural points rigidly splined to existing structural points for two purposes: to attach masses for better overall mass distribution and to add points to which the aerodynamic loads can be splined for better aerodynamic load distribution (Figure 5). They had been used in all above mentioned computations for the medium aspect ratio wing. Here, the splining and the mass points were omitted on a model with an aerodynamic mesh of 22 x 10. Only out-of-plane displacements were included in the analyses.

For all cases, the main flutter mode occurred with an average flutter frequency of 7.35 Hz and with flutter speeds varying between 22,800 to 20,200 in/sec. For the cases of no and all MPCs, additional crossovers of the flutter curve were found at lower speeds (15,500 and 12,200 in/sec, respectively) and at flutter frequencies of about 16.45 Hz. These represented a slowly crossing mode and a hump mode, respectively. Finally, for the no-MPC

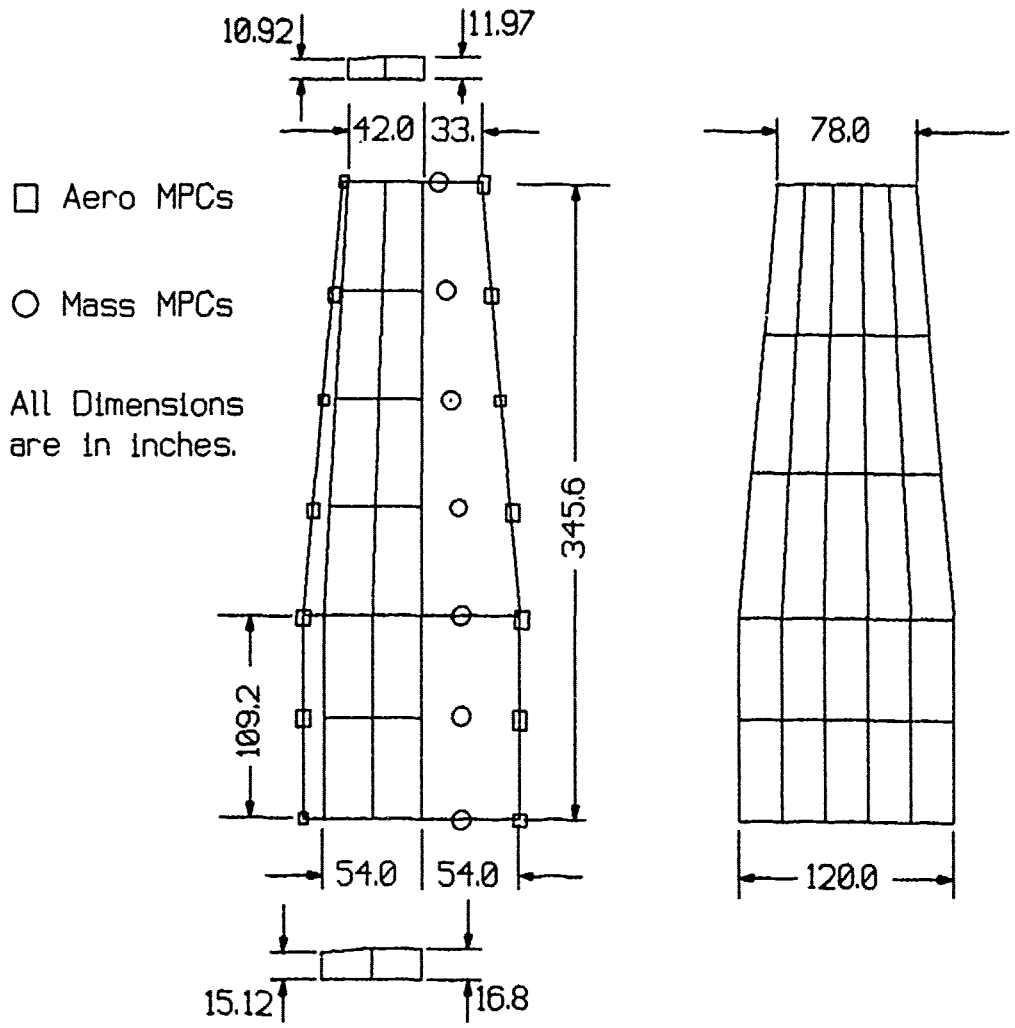

Figure 5. Medium Aspect Ratio Wing Model

case only, divergence was found at 24,200 in/sec. It seems from the results in Table 10 that the use of MPCs for better distribution of the non-structural mass away from just the structural wing box has the effect of lowering the natural frequencies slightly. Also, larger rotational moments are produced due to this offset. This effect, together with that of the MPCs used for splining the aerodynamic forces to a larger area than just the structural wing box, dropped the flutter speed for the lowest frequency flutter mode by about 12%. From the additional modes encountered with the no-MPC wing model, the use of MPCs seems indicated for a realistic flutter analysis, at least for wings which have the structural wing box located such that elastic axis and center of mass are in close proximity.

For the optimization, Guyan reduction to only out-of-plane displacements was used, while three different values of the constraint retention parameter EPS were applied: -0.02, -0.03, and -0.05, as well as two values for the upper frequency bound on the modal flutter

analyses: 50 Hz and 100 Hz. For this study only, the vertical spar stiffeners were eliminated and the ribs converted from shear to membrane elements to eliminate breathing modes.

In the optimization (Table 11), for a given combination of upper frequency limit and

Table 10. Use of MPCs, Medium Aspect Ratio Wing
Flutter Analysis

	Without MPCs	Aero MPCs	Mass MPCs	All MPCs
Natural	3.22 B	3.22 B	3.22 B	3.22 B
Freqs.[Hz]	16.40 B/T	16.40 B/T	16.31 B	16.31 B
	20.14 T	20.14 T	18.72 T	18.72 T
(Bending)	41.16 T	41.16 T	40.43 B/T	40.43 B/T
(Torsion)	48.35 T	48.35 T	45.01 T	45.01 T
(Breathing)	73.13 Br	73.13 Br	68.91 T	68.91 T
Flutter	15,563 (16.6 Hz) low			12,239 (16.5 Hz) hump
Speed	22,779 (7.3 Hz)	21,395 (7.4 Hz)	21,156 (7.3 Hz)	20,238 (7.4 Hz)
[in/sec]	24,220 divergence			

Table 11. Use of MPCs, Medium Aspect Ratio Wing Model, Optimization
I: EPS=-0.02; II: EPS=-0.03; III: EPS=-0.05
31 Design Variables

MPCs:		None		Aero		Mass		Aero+Mass	
Up. Freq. Bounds: [in Hz]		50	100	50	100	50	100	50	100
Init. Struc. Weight:					576.8				
Opt. Struc. Weight:	I	170.3	184.2	157.4	157.1	229.9	477.0	175.6	180.0
	II	179.1	184.2	157.4	157.1	229.9	477.0	175.3	175.6
	III	179.1	186.4	157.4	157.1	229.9	477.0	175.6	206.4

However, three drawbacks of the model have to be pointed out: a) the aspect ratio

constraint retention parameter EPS, the use of MPCs for better distribution of the non-structural mass away from just the structural wing box seems to have the effect of increasing the optimized weight coupled with a lowering of the flutter speed found in the accompanying analysis. This may be caused by the larger rotational moments produced by these offsets. The use of MPCs for splining the aerodynamic forces to a larger area than just the structural wing box had the opposite effect, i.e. the optimized weight was even lower than for the case with no MPCs. This was consistent with an increase in the flutter speed from the accompanying analysis. When the two sets of MPCs were combined, however, the minimum weight of the structure was comparable to that for the case of no MPCs. Thus, mass MPCs seem to be a necessity for obtaining a conservative weight in optimization, even though the lack of aerodynamic MPCs may result in too high a minimum weight. The results for the optimization do not show the same common trend that was encountered in the flutter analysis, i.e., that of the common lowest frequency flutter mode, since the optimization cannot distinguish between an important mode and one of less importance (e.g., a hump mode). V-g plots of the wing with all MPCs before and after the optimization (Figure 6) show that the first designed-mode flutter speed was almost identical to the constraint flutter speed as expected while the second designed mode represented a divergence mode, which is again not unexpected for such a straight wing. Next, an increase in the upper frequency limit, i.e. in the number of modes retained in the flutter analyses, resulted in an increase in the minimum weight for all but the aerodynamic splining results while the effect of a change in the constraint retention parameter had, for most cases, little influence. However, both of these parameters have to be chosen with care.

Finally, mention needs to be made of the effects of the choice of reduced frequencies on the flutter analysis and, especially, on the optimization. Due to the use of cubic splines in the Mach number/reduced frequency interpolation of the aerodynamic coefficients in ASTROS, the results of the computations can show large variations for only slightly different values of reduced frequencies. In the optimization, this can result in the minimum weights converging on different local optima for two identical models with only small differences between the two sets of reduced frequencies. Thus, extreme care has to taken in selecting the reduced frequencies. Useable optima can possibly be obtained in a statistical manner by running a number of cases with different sets of reduced frequencies and selecting an average value between the lowest weight of the lot representing the lowest weight obtainable in the optimization and the highest weight of the lot representing the most conservative design.

divergence speed as first suggested by Eastep [14]. Here, for the base model with skins,

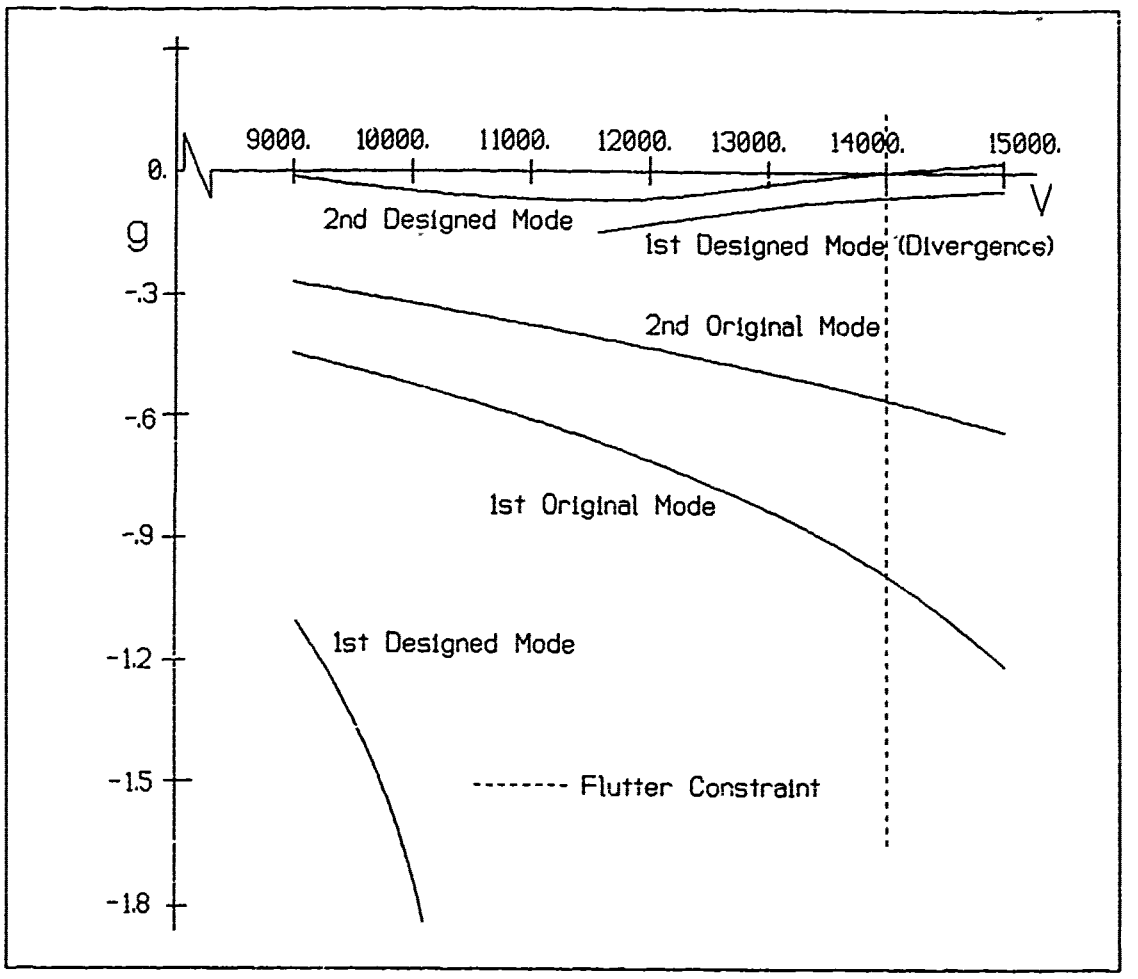

Figure 6. V-g Plot for Medium Aspect Ratio Wing Model: All MPCs, 50 Hz Upper Bound

Finally, various overlaps were investigated for the splining of the aerodynamic coefficients to the structural grid points. The inboard (straight) and outboard (tapered) sections of the wing were treated as separate aerodynamic surfaces. All previously mentioned results were obtained with the aerodynamic coefficients for each surface splined only to the respective underlying structure. Now, the coefficients from each surface were splined to the underlying structure plus to additional rows of structural nodal points on the structure underlying the respective other surface, resulting in an overlapping splining scheme.

The results (Table 12a) show a slight decrease in flutter speed as the aerodynamic forces are distributed more and more over the adjoining structural sections. As the inboard section is covered and only an increase in the distribution over the outboard section continues, the flutter speed shows a slight increase.

The optimum weights show very little variations for the different splining overlays

Here, the results for the cases with coarse (6 x 4 and 6 x 9) spanwise mesh distribu-

Table 12. Structural-Aerodynamic Interaction, Medium Aspect Ratio Wing Model
a) Flutter Analysis

Rows of Splining Overlap:	None	One	Two	Three	All
Flutter Speed [in/sec]	20,241	20,202	20,173	20,188	20,195

Structural-Aerodynamic Interaction, Medium Aspect Ratio Wing Model
b) Optimization

Init. Struc. Weight:			576.8		
Opt. Struc. Weight:	175.6	176.0	176.6	176.4	176.1

(Table 12b) but behave consistently, i.e., with an increase in flutter speed, the optimum weight decreases, and vice versa.

c) Low Aspect Ratio Wing:

For the low aspect ratio wing (Figure 7), non-structural mass in the amount of 2400 lbs was distributed over all nodal points and a mass of 200 lbs for a wing tip store with launcher was distributed over the wing tip points. No MPCs were used, since the wing box covers a large part of the projected wing area. An aerodynamic mesh of 15 x 15 boxes was chosen. For the optimization, an additional mesh of 5 x 5 was chosen and a flutter constraint of 25,000 in/sec was applied.

For this wing, the influence of structural complexity in chordwise direction was evaluated. Starting with a reasonable model for the wing box using five internal spars, the wing was then subdivided by adding five more spars while keeping the total weight constant. The influence of a more evenly distributed stiffness and mass arrangement was, thus, evaluated. Results for the subsonic case with M = 0.85 are presented in Table 13.

The results suggest that distributing mass and stiffness more evenly in chordwise

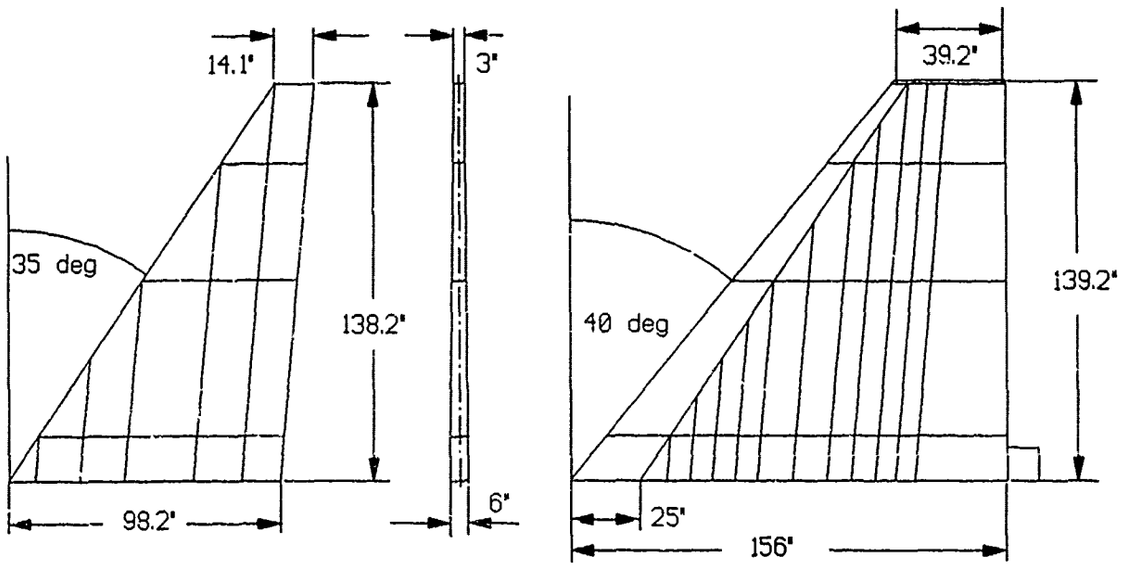

Figure 7. Low Aspect Ratio Wing Model

direction reduces the natural frequencies especially in the two lowest modes while also lowering the flutter speed slightly. Thus, the coarser model in chordwise direction seems to be non-conservative.

Table 13. Chordwise Structural Variation, Low Aspect Ratio Wing Model
Flutter Analysis, Aero-Mesh 15 x 15

Internal Spars:	Five	Ten
Natural Freqs.[Hz]	5.23 B	4.67 B
	21.18 B/T	18.29 B/T
	24.79 B/T	24.63 B/T
(Bending)	37.36 I	29.56 I
(Torsion)	37.78 B/T	37.81 B/T
(In-plane)	57.67 B/T	45.99 B/T
Flutter Speed [in/sec]	25,367	24,948

For the optimization, results for the subsonic case (M = 0.85) are presented in Table 14 for aerodynamic meshes of 5 x 5 and 15 x 15 boxes and for various numbers of design variables.

Table 14. Varying Spar Number on Low Aspect Ratio Wing Optimization
Aero Mesh a) 5 x 5 b) 15 x 15

# of Internal Spars:		Five		Ten	
# of Design Variables:		6	18	6	26
Init. Struc. Weight:	I	497.8		I 497.7	
	II	402.7			
Opt. Struc. Weight:	Ia	330.3	228.0	Ia 303.6	202.8
	Ib	352.6	237.0	Ib 328.5	208.6
	IIa	322.6	218.6		
	IIb	362.4	228.4		

The results suggest that distributing mass and stiffness more evenly in chordwise direction allows the optimization to optimize more members and, thus, leads to lower final weights. The same is, of course, true when the number of design variables is increased. It should be noted that the five spar wing with 18 design variables resulted in a lower weight than the ten spar wing with six design variables suggesting that it might be advantageous for the preliminary sizing of wings with flutter constraints to use a relatively simple model with a reasonably large number of design variables rather than go through the effort of creating a more complex model. Since the initial structure {I} of the five spar wing had somewhat oversized spar caps but undersized shear webs, both sets of values were adjusted in structure {II} to result in a 19.1% lighter wing with a more balanced size and mass distribution. However, this only resulted in a slightly lower overall weight in the optimization (less than 5% for the structural weight and less than 0.5% for the total weight of the wing). When the fine aerodynamic mesh was chosen (15 x 15) rather than the coarse (5 x 5), the resulting minimum weights were somewhat higher (generally less than 12% for the structural weight and less than 1.5% for the total weight of the wing). However, for preliminary sizing, the coarser mesh resulted in much shorter CPU times (for ten spar wing with 26 design variables, the CPU times were 0:12:06 for the 5 x 5 mesh and 1:28:55 for the 15 x 15 mesh on the WRDC/FDL VAX8650). Here, the sets of V-g plots with the first two initial and designed modes for the five and ten spars wing models (Figures 8a,b) did not agree quite as well as did those for the high aspect ratio wing with spanwise distribution variation. The difference between the five and ten spar models was larger in the second

a) 5 Spars

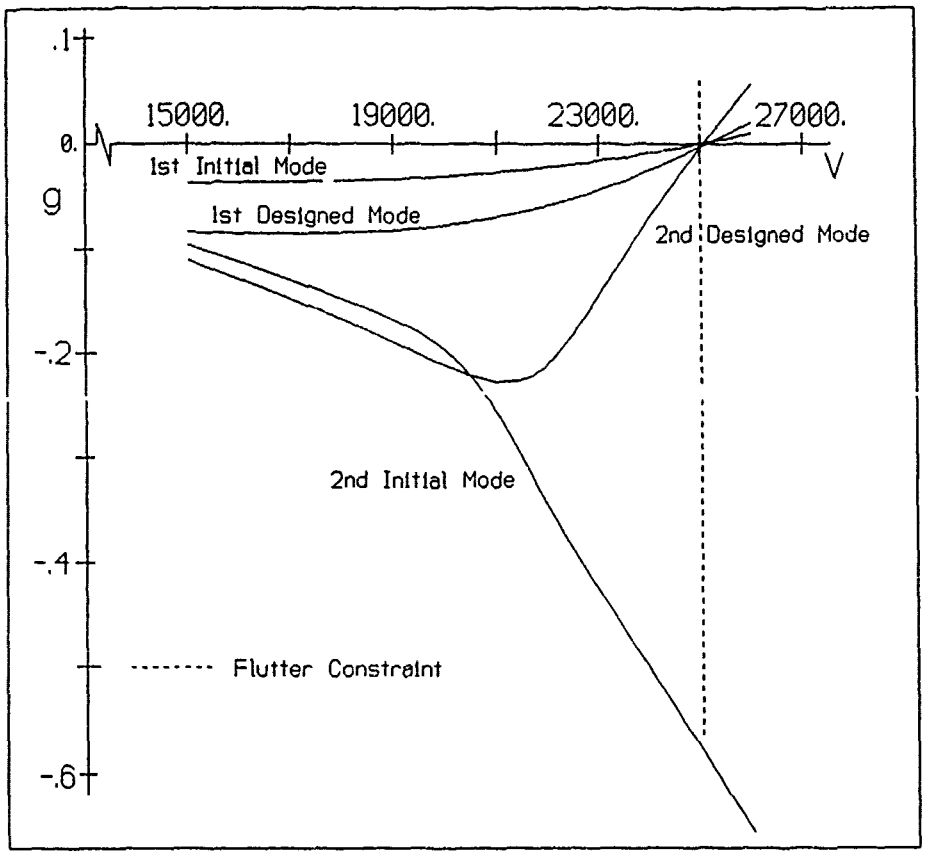

b) 10 Spars

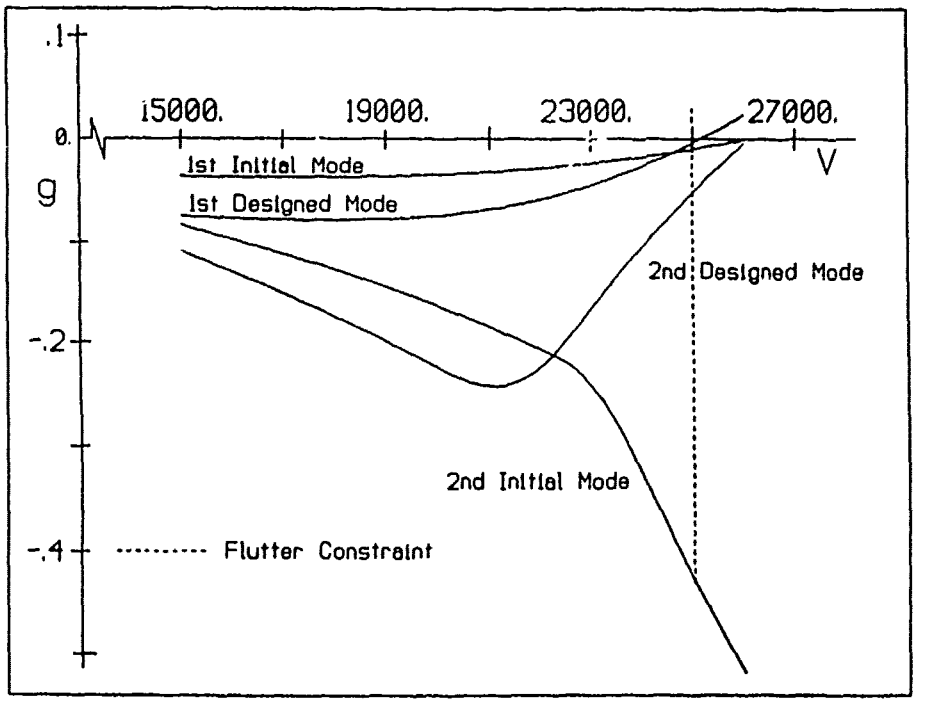

Figure 8. V-g Plots for Low Aspect Ratio Wing Model: a) 5 Spars, b) 10 Spars 15x15 Aero Mesh

mode which showed a considerably larger flutter speed for the ten spar model than for the five spar model. However, the trends agreed reasonably well.

Also, the influence of input Mach number on flutter speed was evaluated as the aerodynamic coefficients were calculated for subsonic (M = 0.5 - 0.85), transonic (M = 0.85 - 1.2), and supersonic speeds (M = 1.2 - 1.5). It has to be pointed out that the aerodynamic modules in ASTROS compute aerodynamic coefficients only by linear theory and, thus, do not account for the non-linearities of shock development in the transonic regime.

The results showed (Tables 15a and 15b) that, with an increase in input Mach number, the flutter speed decreased in the subsonic regime and increased in the supersonic regime. Reasonably converged (linear) results were obtainable up to M = 0.92 and above M = 1.2. At M = 0.95, 1.15, and 1.2, a lower speed hump mode emerged in addition to the regular flutter mode. For M = 1.1, no converged results could be obtained. Naturally, all the results above about M = 0.85 and below about M = 1.20 have to be treated with extreme care since they fall in the highly non-linear transonic regime.

5. Discussions and Recommendations

The influences of structural and aerodynamic modeling on flutter analysis and on optimization and the minimum weight design of built-up finite element wing models were investigated using the normal modes, flutter, and optimization modules of the Automated STRuctural Optimization System (ASTROS). This was done to gain a better understanding of the optimization process with dynamic aeroelastic, i.e. flutter, constraints. Several trends could be observed during the course of the modeling, the flutter analysis, and the optimization even though it is understood that, until many more cases have been evaluated, any set of analyses has to be regarded as more or less wing type and model specific.

A quick initial evaluation of a preliminary design with a reasonably coarse grid for both the structure and the aerodynamics will result in natural frequencies and modes that are close to those from a more detailed model, while this evaluation will also result in flutter speeds and optimum weights that are, for the most part, conservative. In the flutter analysis, the chordwise distribution needs more attention than the spanwise one in the structural modeling, while, for the aerodynamic modeling, the opposite seems indicated.

Table 15. Variation of Input Mach Number, Low Aspect Ratio Wing Model Flutter Analysis, 5-Spar, Aero Mesh 15 x 15

a) Initial Speed Selection [M] - Subsonic:	0.50	0.75	0.85	0.90	0.92	0.95
Flutter Speed [in/sec]	31,440	28,716	25,367	22,709	21,168	18,400 +hump

b) Initial Speed Selection [M] - Supersonic:	1.10	1.15	1.20	1.50
Flutter Speed [in/sec]	No Convergence	23,616 + hump	25,667 +hump	34,723

In the optimization, too, a finer chordwise structural distribution seems to yield a better pay-off in terms of a lower minimum weight while, for the aerodynamic modeling, a finer spanwise distribution seems preferable. In general, however, a good start is obtained for a conventional redesign process as well as for optimization.

The selection of the correct finite elements for modeling the structure is rather critical since, e.g., choosing membrane instead of shear elements for spars can result in non-conservative flutter speeds and minimum optimum weights. Further, care has to be taken when selecting the modes included in the optimization. In-plane modes as well as extensional modes of the vertical spar connecting rods can cause convergence problems and should be eliminated. For wings where chordwise bending modes are not expected, it is suggested to increase the frequency of the extensional modes by eliminating the connecting rods and converting the shear elements generally used for ribs to membrane elements. For fighter type wings with possible chordwise bending modes, the upper and lower wing surfaces can be connected by MPCs instead. Finally, the number of modes retained for modal flutter analysis during the course of an optimization can affect the computed

optimum weights as can the selection of the constraint retention parameter. Thus, these two parameters have to be carefully chosen.

The use of mass MPCs is advised for a more realistic mass distribution, and that of aerodynamic MPCs for a better aerodynamic force distribution. However, the use of aerodynamic MPCs can lower the minimum weights in a non-conservative fashion. Depending on the model, the omission of all MPCs can also result in increased flutter speeds and lower minimum weights and can be non-conservative as well.

Using overlaps in the splining of multiple spanwise aerodynamic surfaces seems to be mostly conservative and to have little influence on the flutter speed and the minimum weights.

Reduced frequencies sets have to be chosen with care until a more rugged interpolation scheme for the aerodynamic coefficients is incorporated in ASTROS. The constraint retention parameter, on the other hand, seems to have little influence on the optimization for most cases.

An issue of interest has resurfaced during the course of these analyses and, to some extent, the optimizations. In most cases, when a model was evaluated for flutter at subsonic speeds, a supersonic flutter speed resulted. The opposite also can occur: a subsonic flutter speed resulting from a supersonic analysis. This problem, the two-way crossing over the transonic regime, is presently being addressed in a parametric study. Initial results for a fighter wing in flutter analysis showed convergence of the (linear) aerodynamics in ASTROS up to about M = 0.95 and from M = 1.15 with reasonable results obtainable up to M = 0.92 and from M = 1.2. As expected, the flutter speed decreased as the transonic dip was approached and increased above the transonic regime.

Future work will include investigations into the influence of how the splining of the aerodynamic forces to the structure affects the optimization, into the effect of input Mach number on optimized weight, and into the use of move limits in optimization. Optimization with strength, static aeroelastic, and flutter constraints is being performed at present to evaluate the behavior of representative wings in a true multi-disciplinary optimization environment and to allow for a more general understanding of the modeling influences on such optimization.

Acknowledgments

The authors would like to acknowledge Mark French and Victoria Tischler of the Flight Dynamics Laboratory, Wright Research and Development Center, Wright-Patterson AFB, Ohio, as well as Frank Eastep of the University of Dayton, Dayton, Ohio, for helpful technical discussions and computational support.

REFERENCES

1. Johnson, E.H., and Venkayya, V.B., "Automated Structural Optimization System (ASTROS), Vol. I: Theoretical Manual", AFWAL-TR-88-3028/I, Air Force Wright Aeronautical Laboratories, December 1988.

2. Neill, D.J., Johnson, E.H., and Herendeen, D.L., "Automated Structural Optimization System (ASTROS), Vol. II: User's Manual", AFWAL-TR-88-3028/II, Air Force Wright Aeronautical Laboratories, April 1988.

3. Johnson, E.H., and Neill, D.J., "Automated Structural Optimization System (ASTROS), Vol. III: Applications Manual", AFWAL-TR-88-3028/III, Air Force Wright Aeronautical Laboratories, December 1988.

4. Rodden, W.P., Editor, MSC/NASTRAN Handbook for Aeroelastic Analysis, The MacNeal-Schwendler Corporation, Los Angeles, California, 1987.

5. Taylor, R.F., Miller, K.L., and Brockman, R.A., "A Procedure for Flutter Analysis of FASTOP-3 Compatible Mathematical Models", AFWAL-TR-81-3063, Air Force Wright Aeronautical Laboratories, August 1981.

6. Garner, G., and French, M., "A Comparison of Supersonic Flutter Predictions for a Straight Wing", AFWAL-TM-88-176-FIBR, Air Force Wright Aeronautical Laboratories, May 1988.

7. Pendleton, E., French, M., and Noll, T., "A Comparison of Flutter Analyses for a 45° Swept Model", AIAA-87-2886, presented at the AIAA/AHS/ASEE Aircraft Design, Systems and Operations Meeting, St. Louis, Missouri, September 1987.

8. Rudisill, C.S., and Bhatia, K.G., "Optimization of Complex Structures to Satisfy Flutter Requirements", AIAA Journal, Vol. 9, No. 8, August 1971, pp. 1487-1491.

9. Rudisill, C.S., and Bhatia, K.G., "Second Derivatives of the Flutter Velocity and the Optimization of Aircraft Structures", AIAA-Journal, Vol. 10, No. 12, December 1972, pp. 1569-1572.

10. McIntosh, S.C. Jr., and Ashley, H., "On the Optimization of Discrete Structures with Aeroelastic Constraints", Computer and Structures, Vol. 8, No. 3/4, 1978, pg. 411-419.

11. Segenreich, S.A., and McIntosh, S.C., "Weight Minimization of Structures for Fixed Flutter Speed Via an Optimality Criterion", AIAA-75-0779, AIAA/ASME/SAE 16th Structures, Structural Dynamics, and Materials Conference, Denver, Colorado, May 27-29, 1975.

12. Striz, A.G., and Venkayya, V.B., "Influence of Structural and Aerodynamic Modeling on Flutter Analysis", AIAA-90-0954-CP, Proceedings, 31st AIAA/ASME/ASCE/AHS/ ACS Structures, Structural Dynamics and Materials Conference, Long Beach, California, April 1990, pp. 110-118.

13. Striz, A.G., and Venkayya, V.B., "Influence of Structural and Aerodynamic Modeling on Optimization with Flutter Constraint", presented at the USAF/NASA Symposium on Recent Advances in Multidisciplinary Analysis and Optimization, San Francisco, California, September 1990.

14. Eastep, F.E., Private Communication.

15. Striz, A.G., "Realistic Structural and Aerodynamic Wing Models for Flutter Analysis and Structural Optimization", OU-AME-TR-90-110, University of Oklahoma, Norman, Oklahoma, January 1990 (updated January 1991).

Design of a Fighter Aircraft Vertical Tail for Enhanced Buffet Environment Survivability

Dale M. Pitt, Senior Technical Specialist

and

Robert W. Scanlon, Senior Engineer
McDonnell Aircraft Company
McDonnell Douglas Corporation
St. Louis, MO 63116 US

ABSTRACT

A method developed for multidisciplinary design of aircraft primary surfaces to include buffet fatigue life improvements is presented. The method is a multistep procedure. (1) Measured buffet pressures are used as the source of excitation. These pressures excite the primary structural modes of the tail and result in high dynamic strains. (2) The ASTROS multidisciplinary code is used to either raise or lower the primary modal frequencies. (3) A NASTRAN random analysis is used to determine the buffet dynamic strains. (4) A subsequent fatigue analysis is used to compute the change in fatigue life. The process was demonstrated on a generic vertical tail.

INTRODUCTION

Present day and future fighter aircraft are being designed for increased agility and maneuverability. These aircraft are being flown at the extreme points of their flight envelopes. Severe environmental effects are being felt by the aircraft empennage from the operational time spent at these high angles of attack. At these flight conditions the aircraft stabilator and vertical tails are subjected to buffet pressures. Buffet is often caused by high-energy vortices, generated upstream, which burst and impact the empennage with turbulent flow. This is illustrated in Figure 1. These turbulent pressures excite the primary vibratory modes of the structure, resulting in high cyclic strain levels and subsequent fatigue failure. This problem is particularly acute for lifting surfaces.

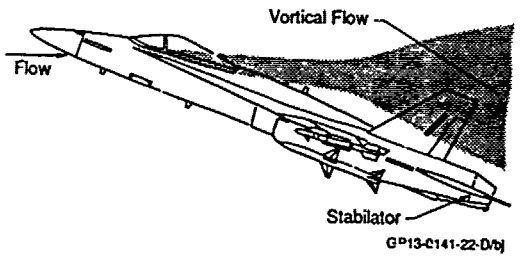

Figure 1. Example of Fighter Aircraft at High Angle-of-Attack Experiencing Buffering Flow on the Empennage

The standard design practice for fighter aircraft vertical tails calls for them to be flutter free and to withstand the maneuvering loads for the life of the aircraft. Traditionally the aircraft maneuvering and static loads are used for structural sizing of the tails for fatigue and strength, while the flutter free requirement generally sizes the tails for stiffness. Buffet considerations historically have not had a significant impact on the preliminary design of aircraft structure. Yet, for modern fighter aircraft buffet has been found to be one of the major design drivers. Increased emphasis on cost effectiveness and minimum time to design requires a change in design philosophy from sequential sizing of structure, to a technique that simultaneously addresses all design phases at once. Design techniques which account for physical design constraints imposed by a variety of disciplines are increasingly being employed at an earlier stage in the design process. Formalisms of these multidisciplinary techniques, as proposed in Reference 1, may speed the integration of the various design disciplines for future aircraft designs.

The recent availability of structural optimization codes, coupled with existing finite element technology, has provided the analyst with a means to address the multidisciplinary aspects of structural design. The objective of structural design is to minimize the weight while still maintaining structural integrity and avoiding aeroelastic problems such as buffet and flutter. Buffet constraints, which may be in the form of dynamic response levels or fatigue damage resulting from the cyclic application of those levels, cannot be directly imposed on current design. Ideally, fatigue life constraints should be imposed at various locations of a structure during the optimization-type design studies.

BACKGROUND/OBJECTIVE

The goal of this study was to use structural optimization techniques to increase the fatigue life of an empennage surface in a buffeting environment. In particular, this paper addresses the vertical tail buffet/fatigue life requirements at the preliminary design stage. A generic fighter vertical tail is designed to improve buffet life with no significant degradation in the existing flutter and static loads margin. An existing multidisciplinary optimization code, ASTROS (Automated Structural Optimization System) was used for the design, Reference 2. The method was to indirectly effect an improvement in fatigue life by changing the dynamic properties of the entire structure. Specifically, shifting the primary structural frequencies away from the peak buffet forcing frequencies was expected to lower the structure's responses and thereby improve fatigue life.

The method was indirect in that the dynamic properties were modified by designing primary structure.

Studies performed demonstrate the interrelation between the choice of design variables, the frequency shifts due to changing the dynamic properties, and the resulting fatigue life change. The complex relationships due to the dependence of the dynamic properties on the changing design variables do not lend themselves to a direct algorithmic approach to controlling buffet by changing the dynamic properties of the structure.

DESCRIPTION OF STRUCTURE

The generic vertical tail selected for this study was of conventional design for a modern fighter aircraft, consisting of a stationary mounted fin and hinged rudder. The fin torque box is covered with carbon/epoxy skins which are mechanically fastened to eight aluminum spars. The root attachment is through stub frames at the forward six spars. The leading edge and tip internal structure are nonstructural honeycomb material. The rudder is attached to the fin through a series of hinges, the lower one of which contains a drive mechanism attached to the fin-mounted actuator.

The finite element model (FEM) of the generic fighter tail is shown in Figure 2. The skins are modeled as composite quadrilateral bending plates. The spar and rib caps are extensional rods, while the webs are quad plates. The root attachment and fin/rudder interface are simulated with spring elements. The rudder is simulated by bending bars whose properties represent the dynamic characteristics of the control surface. A summary of the model construction is given in Table 1.

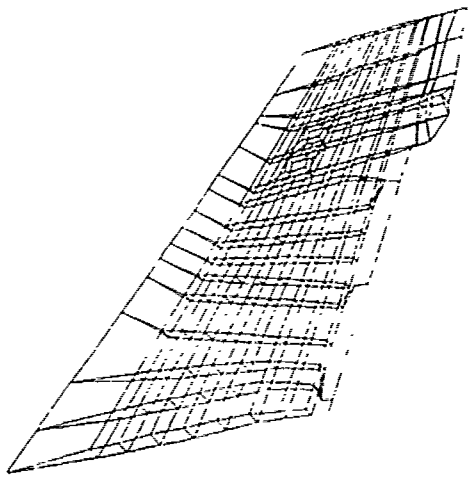

GP13-0141-2E-D

Figure 2. Finite Element Mode of Generic Vertical Tail

The dynamic modal properties of the tail are shown in Figure 3. The first four modes are : 1st bending (1B), 1st torsion (1T), rudder rotation (RR), and second bending (2B). The natural frequencies for modes 1T and RR are very close in the 45-50 Hz range, and are sometimes difficult to separate in an analyses. Modes 1B and 1T combine for flutter, and modes 3 and 4 also combine for a flutter mechanism.

TABLE 1. DETAILS OF THE FINITE ELEMENT MODEL

Gnd Points	394
Elements	976
Beams	20
Shear	11
Conrod	344
Elas1	6
Elas2	1
Quad4	524
Bar	29
Tria3	11

GP13-0141-19-D/bj

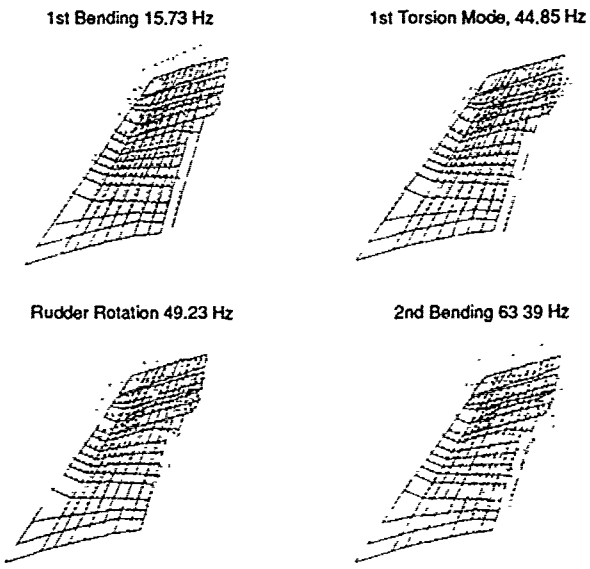

GP13-0141-27-bj

Figure 3. Generic Vertical Tail Mode Shapes

Buffet pressures, in the form of differential pressures across the tail surface, were measured in a wind tunnel at 9 locations on both sides of a rigid model tail. The measurements were made using a grid of three spanwise and three chordwise locations. The measurements were made at two aircraft angle of attacks known to be critical from a fatigue standpoint. Although the two conditions correspond to high angles of attack, where a typical fighter spends little of its service time, previous studies have indicated that certain critical flight regimes make a significant contribution to fatigue damage far in excess of the proportion of total time spent at those conditions. The two conditions used in this study were identified as being members of the critical flight regime set. These unsteady pressures, scaled to aircraft size, were used as the forcing functions in a NASTRAN "random analysis." The resulting responses were used to estimate fatigue for the baseline tail.

For fatigue calculations, the tail was assumed to spend equal amount of time at both angle of attacks. The measured buffet pressures were found to be unimodal, with peaks at approximately 22 Hz and 42 Hz for the two conditions, as illustrated in Figure 4. These conditions are referred to as the Mode 1 and Mode 2 conditions, respectively, due to

the primary structural modes which are predominantly excited by the buffet pressures i.e., mode 1 excites 1B at 15 Hz and mode 2 excites 1T at 45 Hz.

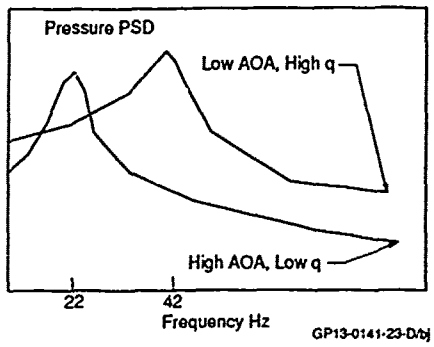

Figure 4. Generic Vertical Tail Buffet Pressures

APPROACH

Fatigue calculations were performed at three different structural locations on the tail to demonstrate the generality of the method. Figure 5 show the three locations which will be referred to as location A, B, and C. Two point were chosen at the root, one forward and one aft, and one at the control structure interface. Experience has shown these to generally be hot spots for buffet fatigue crack initiation. During the design process the geometric and material properties at these points remained fixed. By fixing the properties, the improvement in fatigue life at these three points will be due to changes in tail response levels, not due to local "beef-ups."

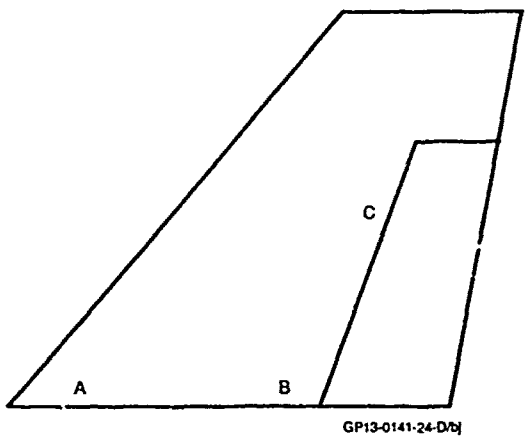

Figure 5. Locations for Fatigue Life Calculations

The initial design technique started with shifting the modal frequencies of the primary vibratory modes of the structure using the frequency constraint capabilities of ASTROS. It was assumed, that the structural frequencies could be moved away from the peak forcing frequencies of the buffet pressures, and yield lower vertical tail responses assuming no increase in the system transfer function magnitude at the primary modal frequencies. ASTROS produced changes in the design variables required to satisfy the frequency constraints. These changes in design variables were used to update the new finite element model (FEM) of the tail. A NASTRAN buffet analysis was performed using the new FEM at each of the two angles of attack.

Fatigue life was computed at locations A, B, and C using the NASTRAN random buffet strain responses. The responses, in the form of power spectral densities, or PSDs, were obtained from NASTRAN using methods documented in Reference 3. Two buffet analyses at the two angles of attack were performed for each tail design. The response PSDs were converted to the time domain, using the assumption that the instantaneous time-history values followed a Gaussian probability distribution. The resulting time-histories were detected for peaks and valleys to yield a fatigue spectrum for a given flight condition. These methods are documented in Reference 4. The spectra for the two flight conditions were combined assuming a 50-50 relative distribution of time spent in each flight regime. The resulting overall fatigue spectrum was input to the standard MCAIR crack initiation code to yield fatigue life at a particular location. This process was repeated for each location, yielding three fatigue life estimates for each designed configuration.

The fatigue lives of each designed configuration were normalized by the corresponding values for the baseline tail to yield a relative improvement factor. The logarithm of this ratio was then used for comparison purposes, with a unit value representing an order of magnitude change in the fatigue life. A negative value represented a reduction in life, while a positive value represented the desired increase in fatigue life. Based on the fatigue life calculations at the three locations, a decision was made on new frequency constraints to impose through ASTROS. This overall approach is pictorially shown in Figure 6.

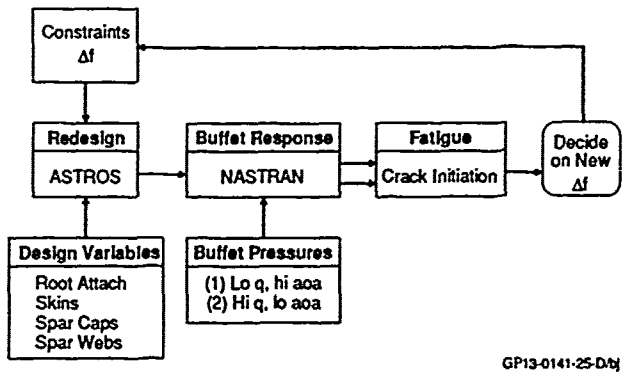

Figure 6. Redesign Methodology Flow Chart

The decision of where to move the frequencies was originally thought to be straight-forward. Intuitively, it seemed that moving the structure's frequencies away from the frequencies at which the unimodal buffet pressures peaked would lower the responses, and therefore increase the fatigue life. However, this reasoning assumes that slight shifts in the structural frequencies do not result in changes in the magnitudes of the transfer functions at those frequencies. This would be amenable to implementation

the most conservative design.

using optimization, with fixed-magnitude transfer function peaks shifted minimally along the frequency axis until changes in response levels yield acceptable fatigue lives.

Initial studies indicated that shifting the frequencies of the lower modes did change the magnitudes of the transfer functions. In fact, the magnitudes increased in many instances, resulting in higher buffet responses even though the modes were being excited at lower forcing function levels. Consequently, a different approach was adopted. It was decided to try to gain a better understanding of the interplay between the design variables and shifted frequencies by a random search of the design space. In other words, various different combinations of shifting frequencies and including design variable subsets were analyzed to obtain designs for desirable fatigue life improvements at the three locations. The best cases were repeated using flutter and strength constraints with the original frequency constraints for a multidisciplinary design of the vertical tail. The new tail was in turn checked for fatigue life improvements.

ANALYTICAL RESULTS

The design model consisted of the set of elements which are allowed to vary during the optimization process. For this study, the design variables were broken into four subsets. These subsets were comprised of: 1) the root attachment stiffness, 2) the torque box skin thicknesses, 3) the spar cap cross sectional areas, and 4) the spar web thicknesses. Table 2 is a list of design variables used in this study. One or more of these subsets were enabled, or turned "on," during the various designs. Upper and lower bounds of 0.1 and 10.0 were imposed on all the design variables. Since ASTROS does not allow discrete changes in material type during optimization, these bounds can be thought to represent a combination of a change in geometry and a material change.

TABLE 2. LIST OF DESIGN VARIABLES

Root Springs:	6	Elas2
Skin Thicknesses:	196	Quads
Spar Cap Areas:	220	Rods
Spar Web Areas:	110	Quads

GP13-0141-20-L

Two types of constraints were considered: normal modes and flutter. The normal modes constraints were used to provide the desired shift in modal frequencies to effect a change in buffet fatigue life. The flutter constraint was to maintain the original baseline configuration's speed. The objective function was the weight of the design variables. This is the only option available in ASTROS. Thus, ASTROS was always changing design variables to satisfy constraints and minimize the weight of the design variables. This tended to change the design variables more than was required to satisfy the constraints.

A number of ASTROS runs were made using various combinations of design variables and design constraints. Fatigue calculations were performed for each of the designs. The fatigue analysis results were summarized using ID3, a code which classifies a set of data by synthesizing a decision tree. The decision tree captures meaningful relationships between the objects in a data set and the values of the attributes used to characterize these objects. In ID3, the attributes are selected using information theory to be nodes of the tree, with the values that each attribute can take on representing the branches emanating from each node. The leafs of the tree are the unique classes associated with a particular set of values from each attribute, found by following the appropriate branches through to the leaf. The tree is created, or "trained," using examples composed of one value for each attribute and an associated class. This method is described in Reference 5.

The attributes and classes used in this study were:

ATTRIBUTES:

Location	(L), with values {A, B, C}
Mode 1 frequency shift	(M1), with values {-1, 0 1}
Mode 2 frequency shift	(M2), with values {-1, 0,1}
Root design variables	(R), with values {off, on}
Skin design variables	(S), with values {off, on}
Caps design variables	(C), with values {off, on}
Webs design variables	(W), with values {off, on}

CLASSES: { -2, -1, 0, 1, 2 }

where each class represents the logarithm of the fractional change in the fatigue life.

The results of the initial analyses with only normal modes constraints are shown in Figure 7. The tree was obtained from ID3, based on 66 training examples from 22 analyses and 3 locations. Note that the ID3 tree has only 19 leaf nodes, indicating that only essential attributes were retained along each path. The following rules can be inferred from the data, as represented in the ID3 tree:

- If the webs are "off," the skins are "off," and the root springs are "on" in conjunction with moving mode 2 down 1 Hz, then the fatigue life at location A will increase.

- If the skins are "off," the webs are "on" in conjunction with moving mode 1 down 1 Hz, then the fatigue life at location B will increase.

- If the skins are "on" in conjunction with moving mode 1 down 1 Hz, then the fatigue life at location C will increase.

- If the skins are "on" then the fatigue life at location B will decrease.

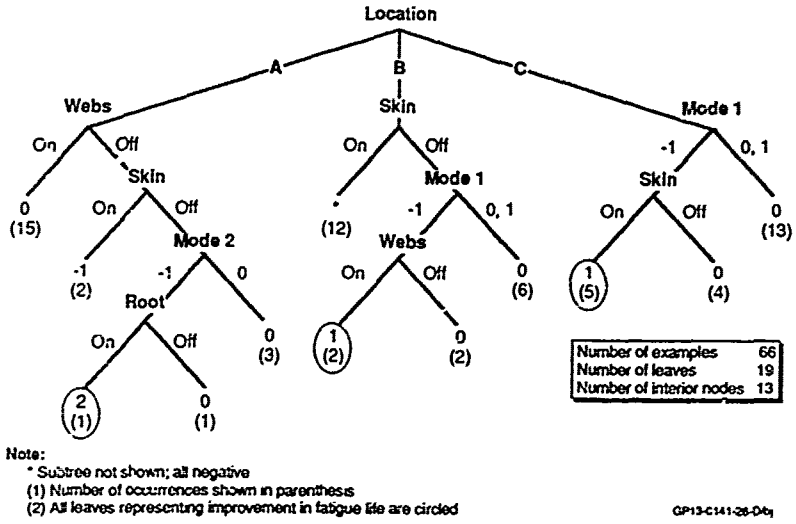

Figure 7. Tree of Design Variables and Constraint Effects on Fatigue Life

- If the webs are "off" and the skins are "on," then the fatigue life at location A will decrease.

- Else no significant change in fatigue life can be obtained at any location.

NOTE: "on" and "off" refer to the specific design variable set being enabled or disabled during a design study.

It is evident from studying the decision tree that there are conflicting requirements to improve the fatigue life at all three locations simultaneously. In particular, including the skins as design variables always resulted in decreases in fatigue life at locations A and B, but was required to obtain a fatigue life increase at location C. Table 3, shows the results of the analyses which yielded the greatest improvements at the three locations. It can be seen that improving the fatigue life significantly at one location often resulted in a minimal increase or even decrease in the life at the other locations. It should not be concluded from this that it is impossible to improve the fatigue endurance at many structural locations using optimization methods. Rather, it is an indication that trying to do so by indirect means (shifting frequencies in this case) is difficult to control and will inevitably lead to design requirement conflicts.

TABLE 3. COMPARISON OF FATIGUE LIFE IMPROVEMENT FOR BEST REDESIGNS

Redesign Parameters							Life Improvement Factor (LIF) at Each Location			
R	S	C	W	M1	M2		A	B	C	Comments
√				-1			89	0.4	0.5	Best LIF for Location A
			√	-1			0.4	8.0	0.6	Best LIF for Location B
√	√		√	-1	+1		0.5	0	9.5	Best LIF for Location C

Note:
1. Redesign parameter codes are: R = include root attachment design variables, S = include skin design variables, C = include caps design variables, W = include webs design variables, M1 = move mode 1 specified Hz, M2 = move mode 2 specified Hz

GP13-0141-21-04j

The changes to the webs for a normal mode constraint, for mode 2 lowered 1 Hz is shown in Figure 8. The change to the webs for the same normal modes constraint, flutter constraint, and static stress constraint is shown in Figure 9. It should be noted that the changes in the structure are widely different and that they yield different fatigue life results. These figures demonstrate the difficulty of using nonbuffet constraints to try to improve buffet fatigue life.

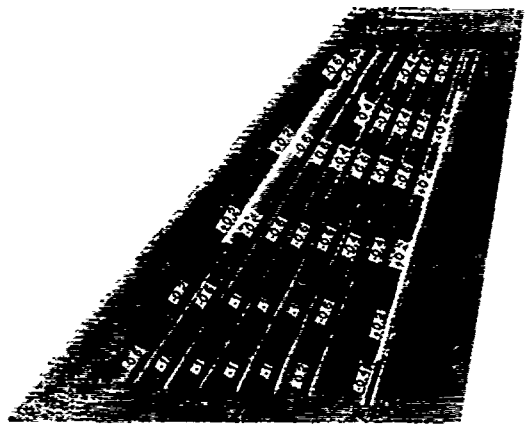

GP13-0141-25-0j

Figure 8. Log of Fractional Changes to the Webs of the Generic Vertical Tail for a Normal Modes Constraint of Moving Mode 2 Down 1 Hz

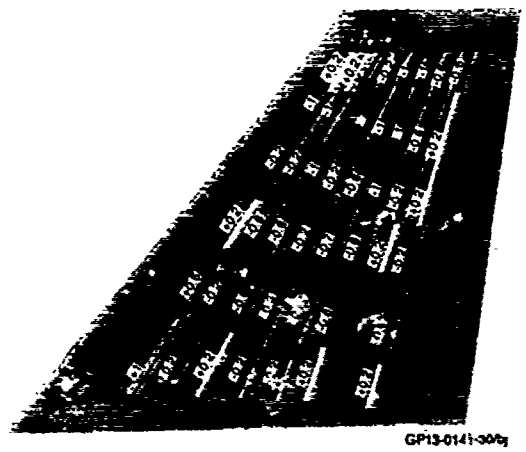

GP13-0141-30-0j

Figure 9. Log of Fractional Changes to the Webs of the Generic Vertical Tail for a Normal Modes Constraint of Moving Mode 2 Down 1 Hz Conjunction With a Flutter and Static Stress Constraints

The results suggest that distributing mass and stiffness more evenly in chordwise

SUMMARY/CONCLUSIONS

The goal of the study was to demonstrate a design technique to increase the fatigue life of a generic vertical tail in a buffet environment. The ASTROS structural optimization software was used to design a generic vertical tail, subjected to frequency, flutter and stress constraints. Buffet pressures, measured in a wind tunnel and scaled to the full aircraft, were used with NASTRAN random analysis technique to calculate the buffet response of the generic vertical tail. A separate external FORTRAN program processed the NASTRAN data for fatigue life calculations at three selected points. An external decision tree program was used to determine the best selection of design variables and design constraints for an improved fatigue life.

This was the first attempt to use multidisciplinary techniques including buffet considerations to design an empennage surface. Due to the limitations of existing optimization software, an indirect method was used to effect changes in fatigue life due to buffet excitation. This indirect method of shifting the natural frequencies of the structure to avoid the forcing frequencies proved to be an ineffective way to improve fatigue life. It is clear from this study that buffet responses and the resulting fatigue damage must be included directly in the design formulation as constraints which need to be satisfied at critical structure locations.

Aeroelastic optimization of a lifting surfaces might be applicable for transport type aircraft; but for fighter aircraft, buffet considerations are mandatory. Further work is required to address the multidisciplinary design of the vertical tail for buffet fatigue life constraints, flutter constraints and maneuvering loads constraints.

REFERENCES

1. Sobieszcanski-Sobieski, J., On The Sensitivity of Complex, Internally Coupled Systems, NASA TM-100537, Jan. 1988.

2. Johnson, E. H., and Venkayya, V. B., Automated Structural Optimization System (ASTROS), AFWAl-TR-3 028, Volume 1 - Theoretical Manual, Dec 1988.

3. Ferman, M. A., Patel, S. R., Zimmerman, N. H., and Gerstenkorn, G., A Unified Approach to Buffet Response of Fighter Aircraft Empennage, Distributed at 70th Meeting of the Structures and Materials Panel, "Aircraft Dynamic Loads Due to Flow Separation," 2-4 April 1990, Sorrento, Italy, Agard No. 17.

4. Harbison, S. T., Perez, R., et al., NADC Report NADC-90071-60, Development of Technique for Incorporating Buffet Loads in Fatigue Design Spectra, Mar 1990.

5. Quinlan, J. R., "Induction of Decision Trees," Machine Learning I:81-106, Kluwer Academic Publishers, Boston, 1986.

FIRST APPROACH TO AN INTEGRATED FIN DESIGN

G. Schneider
Dr. J. Krammer
H.R.E.M Hörnlein

DEUTSCHE AEROSPACE
Messerschmitt-Bölkow-Blohm GmbH.
Airplane Division
P.O. Box 801160, D-8000 Munich 80

SUMMARY

The present paper is focused on findings and results of an integrated design optimisation study for an aircraft fin. The basic flightmechanics design requirement for a vertical fin is to provide a specified control power inside the whole flight envelope with a minimum weight structure.

A method proposed by Dr. Sobieski using implicit function theorem presents a practical way of performing the sensitivity analyses of internally coupled systems. This method has been applied on our MBB fin sample problem. The definition of state variables and independent design variables will be discussed in detail.

Normally a fin design procedure contains a large number of design variables from different disciplines. For keeping our test problem handy, only a limited set of design variables has been treated. Three basic aerodynamic design parameters (taper ratio, aspect ratio and surface area) have been chosen for the sensitivity analysis. This aerodynamic sensitivity analysis has been performed by the finite difference method.

The cross coupling terms aerodynamic/structure have been analysed by our structure analysis and optimisation program LAGRANGE. The necessary finite element models of the structure have been generated in the same way as the aerodynamic model for the finite difference method. Aerodynamic and structure partial sensitivities have been inserted to the total system sensitivity equations. This system has been solved and total sensitivityies will be discussed in their physical meaning.

The applied method based on implicit function theorem has proven its capability to provide a transparent method with clear defined discipline interfaces which are essential to monitor a complex system.

LIST OF SYMBOLS

b	Spanwidth
C_β	Side force coefficient
CR	Root chord
CT	Tip chord
F_A	Aerodynamic function
F_S	Structural function
P_y	Side force
$p = P/q \cdot \beta$	Unit laterai load
q	Dynamic pressure
S	Surface area
$\underline{t}$	Vector of element sizing variables
T_x, T_y, T_z	Linear transformation functions
x_T, y_T, z_T	Transformed structure coordinates
W	Structure weight
x, y, z	Structure coordinates
$\underline{x}$	Vector of independent design variables
y_A	Vector of aerodynamic state variables
y_S	Vector of structural state variables
β	Side slip angle
η	Aeroelastic efficiency coefficient
λ	Taper ratio
Λ	Aspect ratio

1. INTRODUCTION

The AGARD Workshop topic "Integrated design analysis and optimisation" addresses an essential part in the development history of each aerospace project. A successful project is always the integration of a lot of different design procedures and each individual part is optimised under certain design constraints aiming for required physical target values.

The growing complexity of modern aerospace projects and the large amount of design parameters were only possible by the extensive use of computer aided design procedures. The field of computer aided engineering is still growing and design engineers have to decide how to handle these new generation of design procedures. The question is, which parts of the design loop can be automated, where are the monitor stations and who will decide what is going right or wrong.

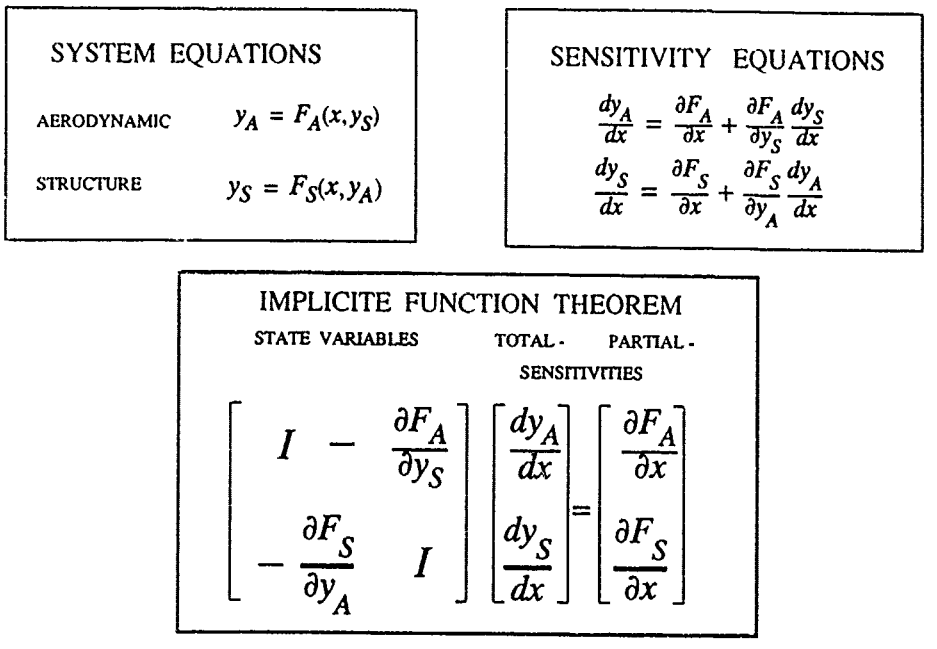

FIG. 1 SENSITIVITY OF A COUPLED SYSTEM

The important question of the specialist is always how transparent are complex automated design procedures. An answer to this question, we found in an AIAA paper of J. Sobieski given in 1988, see Ref. 1 and 2.

In these papers, a method is presented for computing sensitivity derivatives with respect to independent design variables. The method entails two alternative algorithms. The first is based on the classical implicit function theorem and the second develops the system sensitivity equations in a form using the partial sensitivity derivatives.

Each integrated design procedure must be based on an agreed method of data exchange and data handling. Different partial disciplines must be integrated to a higher level system.

The original intention of the AGARD activities using the MBB fin was the integration of structure and aerodynamic design procedures. In a first step, the structure analysis and optimisation procedures for a basic fin geometry were tested by different partners. The results obtained using different structural optimisation programs gave an impression of the sensitivity of different analysis design tools.

In a second step the structure analysis and an aerodynamic analysis will be performed together to provide the input for an integrated design sensitivity analysis.

A mathematical formulation of this sensitivity analysis for our MBB fin problem be derived by three steps.

First we need the system of equations which represents the engineering disciplines of aerodynamics and structure. These equations formulate the physical relations between the independent design variables x and the dependent state variables y_A and y_S.

Secondly we derive the sensitivity equations by using the chain rule. The third s is a reordering of these equations. Th. new form will give us the necessary form for the application of the method of partial sensitivity derivatives. All equations mentioned above are given in Fig. 1.

A similar method of coupling the aerodynamic and structure design work is presented in Ref. 3.

2. INTEGRATED FIN DESIGN EQUATIONS

After having defined the general method for the fin design sensitivity analysis, we must establish the basic equations. In our first approach we will concentrate our attention to characteristic design parameter which can be analysed by already available computer programs. It was our intention to apply the proposed method and to find out what kind of computer software is still missing to cover our requirements.

The main design requirement for a control surface like a fin is to provide enough lateral control power inside the whole flight envelope. Limiting cases are given by a low speed high incidence condition and a high speed lateral control requirement .

For our design study we have chosen the high speed case with a required aeroelastic efficiency η and a definition of the aerodynamic planform. The possible sideload for flightmechanics investigations can be derived by the following equation:

$$P_y = q \cdot c_\beta \cdot \beta \cdot \eta \cdot S$$

Normally the fin volume is an important design parameter, but in our case we have considered a constant distance of the fin center of pressure to the aircraft center of gravity.

The unit lateral control force p per side slip angle β and dynamic pressure q is given in the following equation:

$$p = P_y / q \cdot \beta \quad \text{or} \quad p = c_\beta \cdot \eta \cdot S$$

The design requirement can be formulated now, providing a unit lateral control force equal or greater than a target value at a minimum structure weight.

The unit side load p depends on the aerodynamic derivative c_β, on the surface area S and the aeroelastic efficiency η, a reduction factor for the aerodynamic derivative due to structure deformations.

The definition of the state variables for our fin example is obvious, because the problem is limited to a minimum of three disciplines: flightmechanics, aerodynamics and structure analysis. The aeroelastic analysis will be treated as part of the structure analysis. For each discipline we have selected only one state variable. The flightmechanics state variable is the unit load p, the aerodynamic state variable is defined by c_β and the structure analysis will be represented by the state variable η. Other state variables could be for example, flutter speed and aerodynamic drag.

A fin design has usually a large variety of design variables. Aerodynamic design variables are the surface area S, the aspect ratio Λ, the taper ratio λ, the sweep angle and the profil shape.

Much more design variables we have in our structure model. To get a reasonable number of design variables we assume that the structure design concept is fixed and our design variables are a selected set of element sizes $\underline{t}$ of our finite element model.

For our first approach to an integrated design analysis we have selected three aerodynamic design variables, taper ratio λ, aspect ratio Λ and surface area S. Structure design variables are a set of element sizes $\underline{t}$ which were already selected for the first optimisation exercise. After the selection of state variables and design variables for our fin problem we can formulate the system sensitivity equations. The method from Fig. 1 applied to our fin example give us the following equation system.

STATE VARIABLES — TOTAL DERIVATIVES — PARTIAL SENSITIVITIES

$$\begin{bmatrix} I - \frac{\partial p}{\partial c_\beta} - \frac{\partial p}{\partial \eta} \\ -\frac{\partial c_\beta}{\partial p} \; I - \frac{\partial c_\beta}{\partial \eta} \\ -\frac{\partial \eta}{\partial p} - \frac{\partial \eta}{\partial c_\beta} \; I \end{bmatrix} \begin{bmatrix} \frac{dp}{d\lambda} & \frac{dp}{d\Lambda} & \frac{dp}{dS} & \frac{dp}{d\underline{t}} \\ \frac{dc_\beta}{d\lambda} & \frac{dc_\beta}{d\Lambda} & \frac{dc_\beta}{dS} & \frac{dc_\beta}{d\underline{t}} \\ \frac{d\eta}{d\lambda} & \frac{d\eta}{d\Lambda} & \frac{d\eta}{dS} & \frac{d\eta}{d\underline{t}} \end{bmatrix} = \begin{bmatrix} \frac{\partial p}{\partial \lambda} & \frac{\partial p}{\partial \Lambda} & \frac{\partial p}{\partial S} & \frac{\partial p}{\partial \underline{t}} \\ \frac{\partial c_\beta}{\partial \lambda} & \frac{\partial c_\beta}{\partial \Lambda} & \frac{\partial c_\beta}{\partial S} & \frac{\partial c_\beta}{\partial \underline{t}} \\ \frac{\partial \eta}{\partial \lambda} & \frac{\partial \eta}{\partial \Lambda} & \frac{\partial \eta}{\partial S} & \frac{\partial \eta}{\partial \underline{t}} \end{bmatrix}$$

DESIGN VARIABLES	λ	Λ	S	$\underline{t}$

FIG. 2 SYSTEM SENSITIVITY EQUATIONS

The coefficients of the equations are the negative partial derivatives of the state variables, p, c_β and η. The unknown terms on the left side are the total derivatives of state variables and design variables. The partial derivatives of the state variables and design variables which will be provided by the individual disciplines are on the right hand side of the system sensitivity equations. For each design variables we will receive one columne of partial derivatives on the right side and we will receive the corresponding solution of total derivatives on the left hand side by solving the equation system.

The formulation of the state variable equations for our fin example in an analytical form would be very difficult. In a more generalised form we have the following equations:

FLIGHTMECHANICS	$p = c_\beta \cdot \eta \cdot S$
AERODYNAMICS	$c_\beta = f_A(\lambda, \Lambda)$
STRUCTURE / AEROELASTICS	$\eta = f_S(\lambda, \Lambda, S, t)$

The first equation for p is the relation between the different state variables and it is easy to derive the partial sensitivities. The second equation for c_β is independent of p and the partial sensitivities are zero. The third equation for η is also independent of the other state variables and the partial sensitivities are zero too.
The internal coupling of the system is given by the first equation. The state variables c_β and η are not internally coupled.

$$\begin{bmatrix} 1 & \frac{\partial p}{\partial c_\beta} = \eta S & \frac{\partial p}{\partial \eta} = c_\beta S \\ \frac{\partial c_\beta}{\partial p} = 0 & 1 & \frac{\partial c_\beta}{\partial \eta} = 0 \\ \frac{\partial \eta}{\partial p} = 0 & \frac{\partial \eta}{\partial c_\beta} = 0 & 1 \end{bmatrix}$$

FIG. 3 LEFT HAND SIDE OF THE EQUATION SYSTEM

3. PARTIAL DISCIPLINE SENSITIVITY ANALYSIS

The right hand side of our total system sensitivity equation represents partial state variable sensitivities with respect to the independent design variables. Each discipline which will contribute to the analysis is able to prepare its partial sensitivities independently, see Fig. 4.

BY FINITE DIFFERENCE METHOD $\frac{\Delta y}{\Delta x} \Rightarrow \frac{\partial y}{\partial x}$

STATE VARIABLE \ DESIGN VARIABLE	$\frac{\partial \cdot}{\partial \lambda}$	$\frac{\partial \cdot}{\partial \Lambda}$	$\frac{\partial \cdot}{\partial S}$	$\frac{\partial \cdot}{\partial t}$
FLIGHTMECHANICS $p = c_p \eta \cdot S$	0	0	$c_\beta \cdot \eta$	0
AERODYNAMICS $c_\beta = f_A(\lambda,\Lambda)$	$\frac{\Delta c_\beta}{\Delta \lambda}$	$\frac{\Delta c_\beta}{\Delta \Lambda}$	0	0
STRUCTURE / AEROELASTICS $\eta = f_S(\lambda,\Lambda,S,t)$	$\frac{\Delta \eta}{\Delta \lambda}$	$\frac{\Delta \eta}{\Delta \Lambda}$	$\frac{\Delta \eta}{\Delta S}$	$\frac{\partial \eta}{\partial t}$

FIG. 4 PARTIAL DISCIPLINE SENSITIVITIES

Looking to the first line which represents flightmechanics state variable p, the only partial derivative which can be derived analytically, is that with respect to the surface area S. The unit lateral load p has no direct relation to the other design variables.

The contribution of aerodynamics state variable c_β to the partial sensitivity analysis is limited to the design variables taper ratio and aspect ratio. The aerodynamic lift coefficient is independent of the surface area S and, of course, of all structure element sizing variables. An analytical derivation of these partial sensitivities is dependent on the applied method. For some cases with a rather simple geometry, one can find an analytical method to derive the sensitivity of the lift coefficients with respect to taper ratio and aspect ratio.

But for an arbitrary configuration numerical methods are in use and an analytical gradient is not available or even not possible to derive. A practical way to compute sensitivity derivatives is the finite difference technique. The panel method calculation will be repeated for a slightly changed design parameter. About the range of design parameter changes, the user must decide carefully because if the change is to small the numerical uncertainties may become important.
If the difference is to large, nonlinearities may cause significant errors. The range in which accuracy of finite differencing is acceptable becomes problem dependent and the specialist who has to provide the contributing data must have a deeper understanding about the off-design behaviour of his problem and a knowledge of design limitations. During the design phase very often a lot of effort is spent on trade-off-studies and this work is very similar to a sensitivity analysis by finite difference procedure. Therefore one can state, that integrated design analysis is the collection of various trade-off studies from different disciplines to get a total trade-off design analysis with an agreed set of design variables. For our sensitivity analysis using the finite difference method, we have chosen a 10% perturbation magnitude on the aerodynamic design variables.

The aeroelastic state variable η has partial sensitivities with respect to all design variables. The aerodynamic design variables have an impact on the aeroelastic efficiency which will be analysed by the finite difference method. The partial sensitivities with respect to structure design variables can be derived with analytical methods. Such a method is already in use in the MBB LAGRANGE program system for optimisation purpose.

After these general comments of the partial sensitivity analysis, more details about this step toward an integrated design analysis are presented in the following chapters.

The finite difference method, applied on different disciplines, requires a software package which can generate the different computer models with respect to a common set of design variable changes.

One part of the required software is a transformation procedure which describes the relations between new aerodynamic design geometry and initial aerodynamic input. Taper ratio, aspect ratio and surface area can be transformed by linear equations to geometry parameters, like root chord, tip chord and spanwidth. These geometry parameters are needed for the generation of the aerodynamic and structure model inputs.

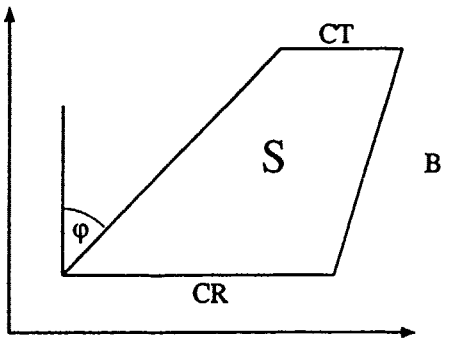

GEOMETRY PARAMETER	
ROOT CHORD	$CR = \frac{2}{1+\lambda}\sqrt{\frac{S}{\Lambda}}$
TIP CHORD	$CR = \frac{2\lambda}{1+\lambda}\sqrt{\frac{S}{\Lambda}}$
SPANWIDTH	$B = \sqrt{S\Lambda}$

FIG. 5 AERODYNAMIC GEOMETRY RELATIONS

A decision has to be made about the rate of percentage change of independent design variables. A 10 percent increase of the shape design variables seemed to be reasonable and the fin geometry parameter for the sensitivity analysis are given in the following Table 1.

A physical impression of design variable changes is given in a plot of all aerodynamic shape models in Fig. 6.

	INITIAL DESIGN	$\lambda+0.1\lambda$	$\Lambda+0.1\Lambda$	$S+0.1S$
λ	.3671	.4038	.3671	.3671
Λ	1.1907	1.1907	1.3098	1.1907
S	4.7090	4.7090	4.7090	5.1799
CR	2909.6	2833.0	2773.9	3051.6
CT	1068.0	1144.0	1018.3	1120.1
B	2368.0	2368.0	2483.5	2483.6

TABLE 1 MODEL DATA FOR FINITE DIFFERENCE PROCEDURE

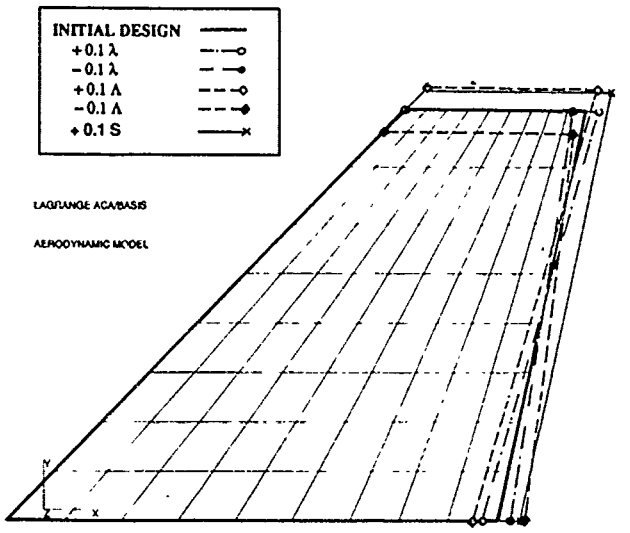

FIG. 6 AERODYNAMIC SHAPE DIFFERENCIES

The results of the aerodynamic sensitivity analysis have been derived from several Woodward panel method runs. The finite differencies of lift coefficients due to changes of design variables are presented in Table 2.

	+0.1 λ	−0.1 λ	+0.1 Λ	-0.1 Λ	+0.1 S
Δ	+.0367	-.0367	+.1191	-.1191	+.471
Δc_β	.00010	-.00012	.00133	-.00151	0.
$\frac{\Delta c_\beta}{\Delta \cdot}$	.00272	.00327	.01117	.01268	0.
$\frac{\Delta c_\beta}{c_\beta}$	.0032	-.0038	.0426	-.0484	0.

TABLE 2 AERODYNAMIC PARTIAL DERIVATIVES

A 10 percent increase in taper ratio gives only a .3 percent increase in lift. But a 10 percent increase in aspect ratio gives a 4.3 percent increase in lift. The contribution of aerodynamic sensitivities can be derived from these values for the total system sensitivity analysis.

According to the aerodynamic shape parameter changes, the structure model grid system must be changed in the same manner. Normally a finite element model is developed for a specified structural concept which is valid also for limited geometry changes. We have assumed in our structure generation that a 10 percent change of shape would not change the structure quality. The structure model generation for this design study consists of a "zooming" of the grid point system according to shape parameter changes.

A linear transformation based on the same geometry parameter of the aerodynamics models, produced the grid point coordinates of the finite element models for the structure sensivity analysis.

LINEAR TRANSFORMATION OF F.E.M. GRID SYSTEM

$$x_T = T_x(x,y,z)$$
$$y_T = T_y(x,y,z)$$
$$z_T = T_z(x,y,z)$$

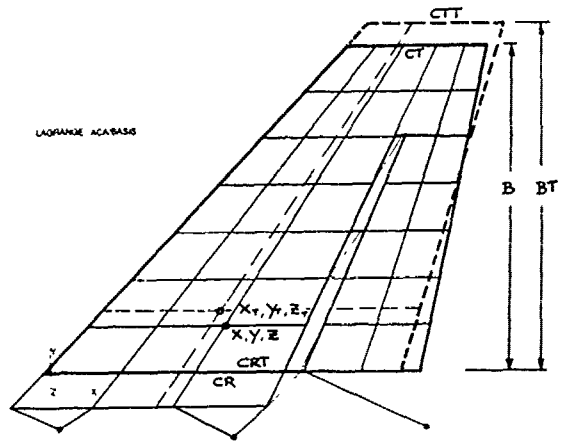

FIG. 7 STRUCTURE MODEL GENERATION

The structure sensitivity analysis has been performed with the MBB LAGRANGE structure optimisation program. The partial derivatives for the aerodynamic design variables are analysed for the initial structure. The partial sensitivities of the state variable η with respect to the structure element sizes are available inside the LAGRANGE program as a vector. The number of elements of this vector depends on the number of structure design variables. The structure sensitivity analysis provides also the structure weight derivatives, which are essential for the optimisation toward minimum weight structure.

The structure and aeroelastic partial derivatives with respect to the aerodynamic design variables derived from the initial design are shown in Table 3.

DESIGN VARIABLE		PARAMETER					VARIABLES
		+0.1 λ	−0.1 λ	+0.1 Λ	−0.1 Λ	S	t
INITIAL SENSITIVITY ANALYSIS	$\Delta\eta$	-.01988	.01940	-.06349	.06280	-.00845	available inside LAGRANGE
	ΔW	-1.23	1.31	-1.12	1.37	9.43	
STRUCTURE OPTIMUM SENSITIVITY ANALYSIS	$\Delta\eta_{opt}$	-.00046	.0121	-.00492	.0446	.00205	
	ΔW_{opt}	3.77	-3.14	10.02	-7.00	12.82	

TABLE 3 STRUCTURE PARTIAL DERIVATIVES

The 10 percent increase of taper ratio has caused a reduction of approximately 2 percent efficiency and 1.23 kg structure weight. The design variable with the strongest influence to the aeroelastic efficiency is the aspect ratio. A 10 percent increase of aspect ratio would cause a 6.3 percent decrease in aeroelastic efficiency. The partial derivative for the surface area increase presents a small reduction of 1 percent in efficiency and a considerable weight penalty. To check the linearity of the derivatives we have also analysed the structure derivatives for a shape variable decrease by 10 percent. Table 3 shows that the differencies between the plus and minus data are small enough to consider the derivatives as linear. At that point of our integrated fin design study we have not yet formulated the influence of the structure element design variables. How strong is the influence of the element sizing variables? A possibility is the use of the already existing structure optimisation module. Therefore we performed for the aerodynamic design variable sensitivity analysis also a structure optimisation to overcome the loss of structure efficiency. We have stated the requirement of 0.8 efficiency on fin lift and a 0.5 efficiency on rudder lift for all aerodynamic design variables. After a structure weight optimisation we have got partial weight sensitivities which are given in Table 3 for comparison. The efficiency changes are inside the convergence requirement of the optimisation, but the weight derivatives have given an indication about the summation of structure element sensitivities. Structure weight increase is linear related to element size increase. Looking to the influence of a 10 percent aspect ratio increase which has caused a 6 percent reduction of efficiency for the initial design, a structure optimisation with a 0.8 efficiency design constraint would produce an increase of 10 kg structure weight.

All these structure optimisation runs were performed with the LAGRANGE program using the optimisation modul CONLIN which was developed by Prof. C. Fleury. In our first report [4] we have presented results obtained with an other optimisation modul called RQP. D. Thomson from BAe who is also working with our MBB fin example has shown optimisation results produced with the ECLIPSE optimisation package. A description of the ECLIPSE and a presentation of fin optimisation results is given in Ref. 5. A total structure weight history of different optimisation runs are plotted in Fig. 8.

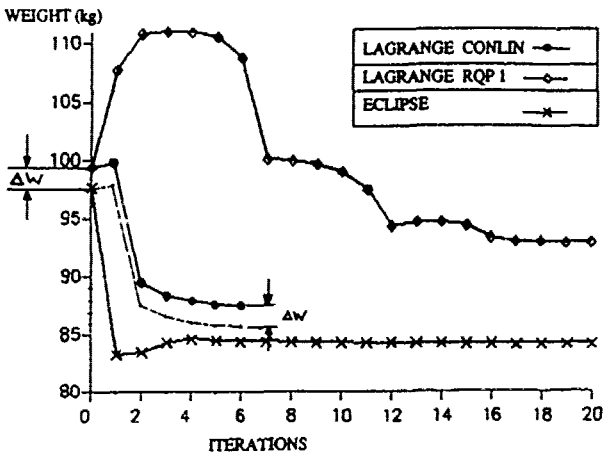

FIG. 8 INITIAL STRUCTURE WEIGHT OPTIMISATION HISTORY

The RQP optimisation modul is a higher order optimisation modul which has used the partial derivatives and the slope or second order derivatives. We have found applications where this modul worked very efficient.
But in this case, the comparison with the ECLIPSE results were not very satisfactory. Because of this very precise way of going on, RQP method takes too long to find the way down to minimum weight and easily it gets lost in local minima. In comparison to this procedure, the CONLIN modul works more global and very efficient. The structure weight goes down quickly to a minimum. The reason for the little difference between LAGRANGE and ECLIPSE final weight is a difference in finite element stiffness matrices and a small difference Δw already in initial design weight.

The achieved flutter speed during the different iteration steps is plotted in Fig. 9.

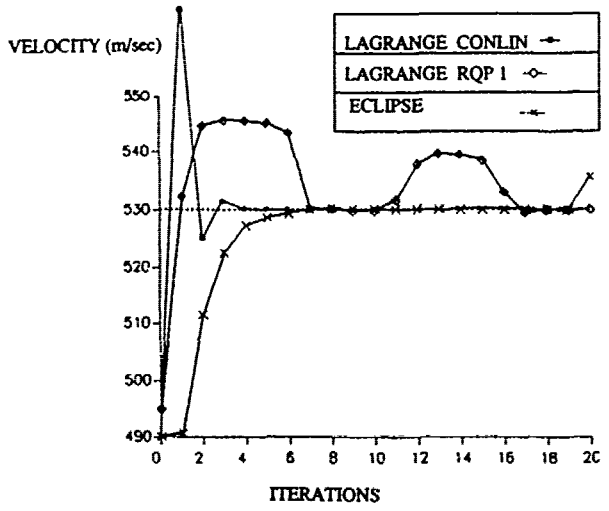

FIG. 9 FLUTTER VELOCITY OPTIMISATION HISTORY

The CONLIN modul shows a remarkable convergence behaviour and after four iterations the design is nearly developed.

An efficient optimisation needs an optimisation modul which has the best tuning to the given problem. We have also found test examples where the CONLIN did not work satisfactory, because the problem object function must have had a mathematical character which was contradictory to the CONLIN modul philosophy. We have assumed that in this fin study the structure optimisation by CONLIN modul will treat the modified fin structures in an equivalent way, inside the selected range of finite differencies.

4. TOTAL SYSTEM SENSITIVITY ANALYSIS

After having prepared all necessary partial sensitivities of state variables we can formulate the total system sensitivity equations. Because of the limitation to three state variables, our equation system is only a 3 x 3 problem. The equation system is given in Fig. 10. The left hand side with its state variable derivatives coupling terms only in the first line.

STATE VARIABLE SENSITIVITIES TOTAL SENSITIVITIES PARTIAL SENSITIVITIES

$$\begin{vmatrix} 1-\eta S- & c_\beta S & \\ 0 & 1 & 0 \\ 0 & 0 & 1 \end{vmatrix} \begin{vmatrix} \frac{dp}{d\lambda} & \frac{dp}{d\Lambda} & \frac{dp}{dS} & \frac{dp}{dt} \\ \frac{dc_\beta}{d\lambda} & \frac{dc_\beta}{d\Lambda} & \frac{dc_\beta}{dS} & \frac{dc_\beta}{dt} \\ \frac{d\eta}{d\lambda} & \frac{d\eta}{d\Lambda} & \frac{d\eta}{dS} & \frac{d\eta}{dt} \end{vmatrix} = \begin{vmatrix} 0 & 0 & c_\beta\eta & 0 \\ \frac{\Delta c_\beta}{\Delta\lambda} & \frac{\Delta c_\beta}{\Delta\Lambda} & 0 & 0 \\ \frac{\Delta\eta}{\Delta\lambda} & \frac{\Delta\eta}{\Delta\Lambda} & \frac{\Delta\eta}{\Delta S} & \frac{\Delta\eta}{\Delta t} \end{vmatrix}$$

FIG. 10 FIN SAMPLE SENSITIVITY EQUATIONS

The second and third line is decoupled and the equation system can be easily solved by hand. The solution for the total derivatives of the state variable p is presented in Fig. 11. Looking to this solution one can argue, that this solution can be written down straight away. This argument is right, but it shows also the transparency of the whole method, which is very important for complex problems.

1.LINE

$$\frac{dp}{d\lambda} = \eta \cdot S \cdot \frac{\Delta c_\beta}{\Delta\lambda} + c_\beta \cdot S \cdot \frac{\Delta\eta}{\Delta\lambda}$$

$$\frac{dp}{d\Lambda} = \eta \cdot S \cdot \frac{\Delta c_\beta}{\Delta\Lambda} + c_\beta \cdot S \cdot \frac{\Delta\eta}{\Delta\Lambda}$$

$$\frac{dp}{dS} = c_\beta \cdot \eta + c_\beta \cdot S \cdot \frac{\Delta\eta}{\Delta S}$$

$$\frac{dp}{dt} = c_\beta \cdot S \cdot \frac{\Delta\eta}{\Delta t}$$

2.LINE $\frac{dc_\beta}{d\lambda} = \frac{\Delta c_\beta}{\Delta\lambda}$

3.LINE $\frac{d\eta}{d\lambda} = \frac{\Delta\eta}{\Delta\lambda}$

FIG. 11 SOLUTION OF FIN SENSITIVITY EQUATIONS

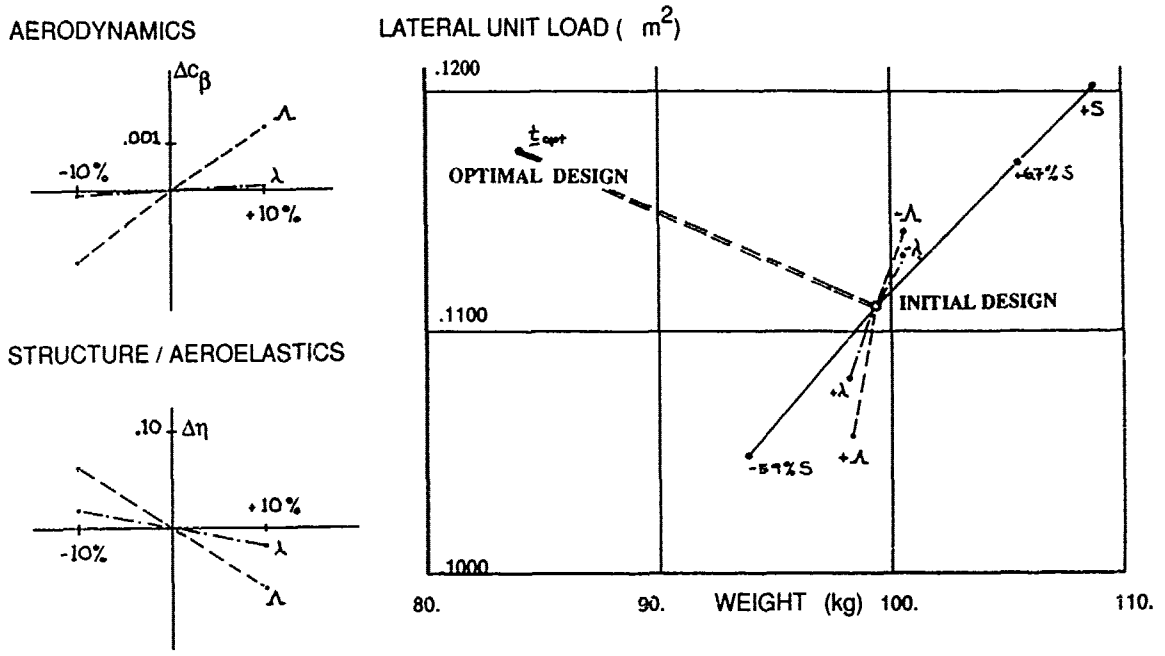

FIG. 12 INITIAL PARTIAL SENSITIVITY ANALYSIS

After we have formulated the total derivatives we would need an optimisation modul which performs the necessary steps with other design variables, than structure element sizing. This modul we do not have in the moment.

But we will continue our discussion of partial sensitivities in their physical meaning for our integrated design problem.

The initial fin design was the basis for our sensitivity analysis and after the structure optimisation we have found the minimum weight solution for the initial aerodynamic shape. For this configuration we have got a lateral load p_o and a structure weight w_o which will be now the reference values for further design studies. The integrated design study allows additional aerodynamic design variables, and we want to find out, if there might be solutions with an higher p and the same weight w_o or solutions with a lower weight w and the same lateral load p_o.

From the partial sensitivities, shown in Table 3 we can see the influence of design variable changes to state variable c_β and η, and the impact on structure weight w. With these informations we can derive increments of the lateral load p with respect to the structure weight w, see Fig. 12.

The state variable p is plotted for all finite difference sensitivities of design variables λ, Λ, S and for the optimised element sizes $\underline{t}$. The strong impact of element sizes to structure weight is obvious.

To gain more knowledge about the influence of structure optimisation, we performed for each aerodynamic partial sensitivity model a structure optimisation with an aeroelastic fin efficiency requirement of 80 percent. Additional static design loads were introduced to the structure optimisation. Flutter requirement were excluded because of work limitations. The new partial sensitivities for the optimised structure are presented in Fig. 13.

A comparison with Fig. 12 shows that the partial sensitivities of λ and Λ have changed their direction completely, but the partial sensitivities of the surface area S seems quite similar. The best integrated design solution we have got with a 10 percent reduction of aspect ratio. In this case the lateral unit load will be slightly increased and the weight is reduced by 7.5 percent. These examples shows already that state variables are coupled and with parametric studies it will be very time consuming to find an optimum solution.

Therefore we need an optimisation modul which will be provided for each iteration step by the appropriate models for structure and aerodynamics, to perform the sensitivity analysis. Because of the large amount of analyses the discipline participants must be very careful with the selection of the models. If the models are too complex, the costs for computation time will be out of a realistic project budget.

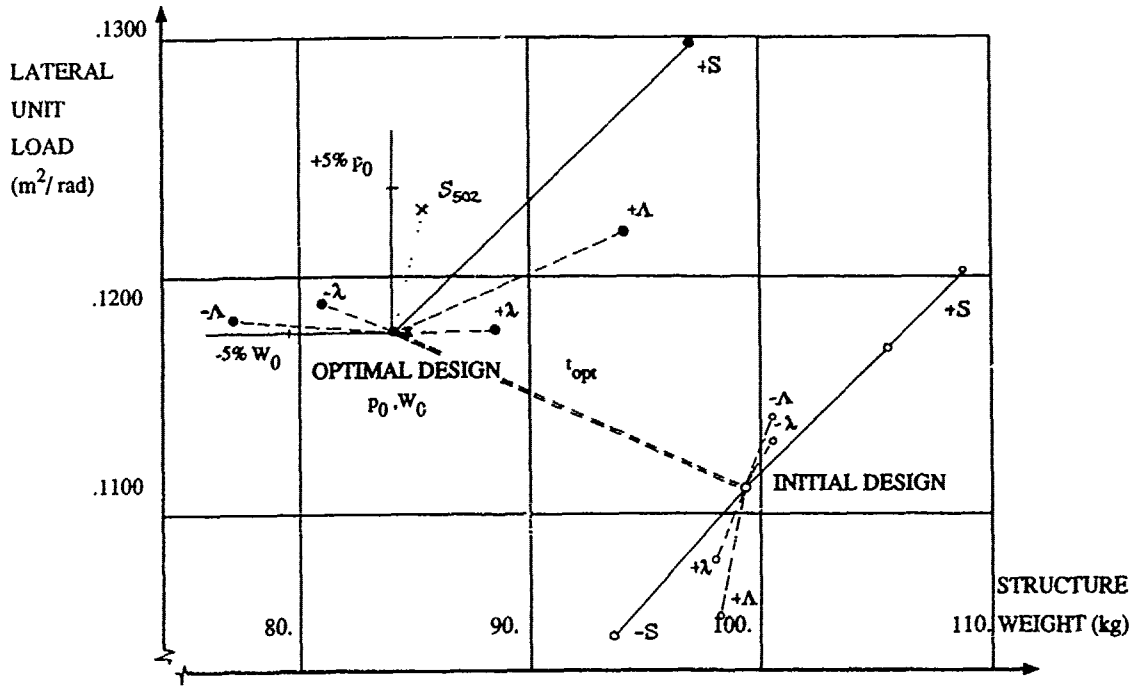

FIG. 13 SUMMARY OF PARTIAL SENSITIVITIES

5. FIRST STEP TO AN INTEGRATED DESIGN

In Fig. 13 we have seen that from the optimum initial design the most effective increase of lateral lift we would get from an increased surface area. Therefore we performed an additional study for two fin designs with the following design philosophy. One design will have a reduced structure efficiency and an increased surface area and the other one will have an increased structure efficiency and reduced surface area. The scaled design variables are shown in Table 4.

	AERODYNAMICS		STRUCTURE	
	c_β	S	η_{Fin}	η_{Rudder}
INITIAL DESIGN	.03121	4.709	.80	.50
SMALL AREA	.03121	4.433	.85	.531
INCREASED AREA	.03121	5.024	.75	.469

TABLE 4 SURFACE AREA VERSUS STRUCTURE EFFICIENCY

We expected a clear answer, but we were at very surprised when we looked at the results after the optimisation. The design with the higher efficiency did not have the expected weight penalty and the solution was very close to initial design optimisation. Remarkable is the linearity of the starting points for the different surface area cases.

The second design, called S 502 with lower structure efficiency requirement and increased surface area has an increase of 4.2% in lateral lift and the weight increase is very close to the first design.

This little exercise has shown the possibilities of improvements of an initial design by increasing the number of design variables.

6. CONCLUSIONS

The application of the implicit function theorem on our little fin example was a first test case to study a new method and to understand the way to go. The method has proved to be a helpful tool to integrate partial disciplines to a total system optimisation.

During the application of the partial discipline sensitivity analyses, we noticed that those investigation have been common knowledge in the past as off-design studies during the design phase of a project.

Whilst in the past the interactions in between different disciplines were defined as design constraints, this method provides the possibility of state variables which allows a larger number of design variables which might be free to change for a longer periode inside the design phase.

A proper definition of state variables is very important for the interdisciplinary understanding and it supports the transparency of the whole design problem.

Each discipline must decide the partial complexity of their sensitivity analysis. For the handling of the total

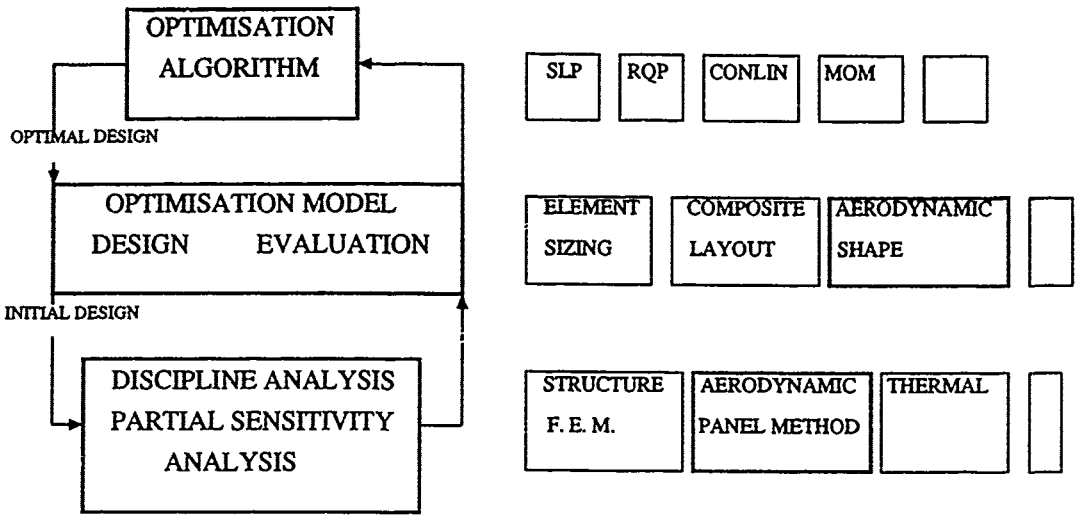

FIG. 14 ARCHITECTURE FOR GENERAL OPTIMISATION

system optimisation, modifications of existing software are necessary to meet the requirements of an integrated design optimisation. A rough scheme of such a modular software like MBB-LAGRANGE is shown in Fig. 14.

REFERENCES

[1] J. SOBIESKI
Sensitivity of Complex, Internally Coupled System;
AIAA Journal, Vol. 28, No. 1,
January 1990

[2] J. SOBIESKI
Everything influences everything else: A math that can help
AIAA, SDM-Conference, Long Beach, Ca. 1990

[3] R. T. HAFTKA, B. et al. GROSSMAN, W. M. EPPARD, P. J. KAO and D. M. POLEN
Efficient Optimisation of integrated Aerodynamic-Structural Design;
International Journal for Numerical Methods in Engineering, Vol. 28, 593-607 (1989)

[4] G. SCHNEIDER, H. KRAMMER, H. GÖDEL
Preliminary Results Fin Optimisation;
MBB-FE2-S-PUB-0398
70th SMP Meeting, April 1990, Sorrento, Italy

[5] D. THOMPSON
GARTEUR Action Group on Structural Optimisation - ECLIPSE
BAe-WSO-RP-GEN-SON-000816,
02/11/90

A FIN OPTIMISATION STUDY

G. POLLANO

ALENIA AERITALIA & SELENIA
DEFENCE AIRCRAFT GROUP
41, CORSO MARCHE
10146 TORINO
ITALY

SUMMARY

This paper details the ALENIA activities performed in order to optimise the design of a fin, proposed by MBB in a AGARD Sub-committee, using the in-house optimisation program S.O.S. (Structural Optimisation System). A series of different optimisation studies using stress, efficiency & flutter constraints was carried out. In addition comparisons between these results and optimisations having frequency separation and displacements as constraints, were done.

INTRODUCTION

Structural Optimisation has become increasingly important due to demands for better performance and greater efficiency and so can no longer be seen as an academic luxury. Alenia has, over the past six years, developed its own optimisation program called S.O.S (Structural Optimisation System) which is capable of optimising structures with static, dynamic, aeroelastic, flutter and manufacturing constraints.

The mathematical formulation has not been described here. A wide bibliography, comprising of two AGARD conference proceedings [1,2], details this complex aspect. Emphasis has been placed on the application of the program, i.e. on the results themselves, not on how they have been obtained, thus leaving out any "computer" considerations such as c.p.u. time, memory required and organisation of the code. Although the object of this optimisation refers to a realistic configuration it has a number of characteristics that make it "ideal"; it is almost completely defined and, where not, assumptions can easily be made. Furthermore these definitions do not change midway through the project. These characteristics are very difficult to find in a "real life" project. The number of iterations performed for the various optimisations in the present study is well beyond that required for usual analysis. This is due to the fact that the model never leaves the computer and so it can remain isolated from worldly constraints such as manufacturability which would make a mockery of theoretical optimum results calculated to great precision. Our desire to examine closely the problem and to highlight the programs behaviour only exasperated the number of iterations to be carried out.

PROBLEM SURVEY

The main data of the problem is summarized here.
The overall fin geometry is shown in fig.1. It has an area of 5.46 msq., a leading edge sweep angle of 45° and a profile NACA 66006 with a thickness to chord ratio of 6%.

Five design load cases with different centres of pressure are given for strength design of the structure:
1) Max. Sideforce Mach 0.9 80KN,
2) Max. Sideforce Mach 1.8 80KN,
3) Max. Sideforce and Rudder Setting Mach 0.9 40KN,
4) Max. Sideforce and Rudder Setting Mach 1.8 80KN,
5) Max. Rudder Loading Mach 1.8 40KN.

AEROELASTIC REQUIREMENTS
Sideslip efficiency 0.8, Mach 1.8/750Kts
Rudder efficiency 0.5, Mach 1.8/750Kts
Flutter requirement: Mach 1.2/S.L. Vf greater than 530 m/s.

STRUCTURAL MODEL
A MSC/NASTRAN finite element model based on a coarse mesh, has been used for structure analysis and optimisation, see fig.2. The fin structure is coupled to a generalized rear fuselage stiffness matrix (Genel) at the attachment points. The fin box has one shear pick-up point (forward), one bending attachment on two points (rearward) and it is coupled with the rudder by three hinges. The structure itself is modelled by CQUAD4 and CTRIA3 elements, composite materials being modelled by one card for every layer. The fibre orientations are shown in fig.3 .

PROGRAM DETAILS

The Alenia program S.O.S., can optimise shells and rods in a structure subjected to the following constraints:
Fully Stressed Design,
Buckling,
Flutter,
Frequency Separation,
Displacement,
Aeroelastic Efficiency,
Rate of Roll.
S.O.S. works in conjunction with the MSC/NASTRAN finite element modelling program and the format of the information to be input is the same. It requires the user to write a number of small files detailing the various sorts of optimisation to be carried out and any other files to be called. The

MSC/NASTRAN Bulk Data is now split into three sections:

1. A file containing Executive and Case control decks,
2. A geometry file,
3. A property file.

Panels in the geometry file are divided up into groups which are to be subjected to the same limiting conditions. This means that alterations to a standard MSC/NASTRAN Bulk Data can be done in quiet a short time regardless of the size of the problem.
The property file is changed at the end of each iteration with the insertion of the new optimised properties and the output model is fully compatible with the usual procedures for the analysis and check.

S.O.S uses optimality criteria to optimise the structure. The final structure depends on a function giving the gradient of the change in structural behaviour for a change in the physical structure, and on the Lagrangian Multiplier Lambda. One of these multipliers exists for each constraint being optimised. It gives an indication of the deviation from the target values for that particular constraint.

Fully Stressed Design and Buckling are treated as side constraints by S.O.S.. This is because they can be dealt with by simple explicit functions without introducing more complicated methods. A new version of the buckling program which allows the optimisation of the layers of each bay, the bay loads being fixed, will only be introduced in the next version as it needs information about the stacking sequence of the plies of each bay.

A wide range of information from each of the optimisation modules can be given upon request by the user. Data may also be extracted from the database if further details of the optimisation procedure are desired.

The change allowed in the properties in any one iteration can be altered by changing the step size. The larger the step size the smaller this change will be. This enables us to progress with the optimisation at different speeds to avoid local minima and so on.

Further details can be found in the S.O.S theoretical manual [3].

THE OPTIMISATION

Manufacturing constraints for the composite impose a minimum total thickness of 2 mm for the surface skins with no single ply being allowed to have more than 2/3^{rds} of the total. We considered, also, that the minimum gauge for a single layer is .125 mm and that, for a symmetric laminate distribution over the thickness, two layers of the same fibre orientation are necessary.

S.O.S carries out optimisation using MSC/NASTRAN CQUAD4 & PSHELL cards and as the bending effect of the faces is not taken into account (i.e. they are considered to be membranes) we took them to have four plies, each with a minimum gauge of 0.25 mm (2 X .125mm). This means that the thickness of each ply can only be a multiple of 0.25 mm. The first runs show this step increase to be too large as any optimisation effects end up being effectively masked as the structure jumps from one set of properties to another. Since the purpose of this study is to show the design capabilities of various optimisation programs, we decided that it would be more beneficial to take .25mm as the minimum thickness for the ply and to impose no further restrictions. This of course means that the optimised structure is not manufacturable but it does show the mathematical possibilities for this structure. Only the CFC face panels were optimised, notwithstanding the fact that valuable weight savings could have been made in other parts of the fin, particularly in the GFC face panels at the tip. The reason for this was that CFC was the only property to have well defined constraints for the various types of optimisation to be carried out. This also had the advantage of allowing us to carry out the optimisation in a quicker manner due to the reduced number of design variables and side constraints.

Technological constraints

As a first step to understanding the structure and the problem we faced, we decided to determine the properties of the structure and the amounts by which it violated its various constraints. We then decided to see the minimum optimisable weight for the structure when the panels of the fin were all set to their minimum values of .25mm, and finally the mass breakdown shown in the diagram below was done to show the weights of the various components.

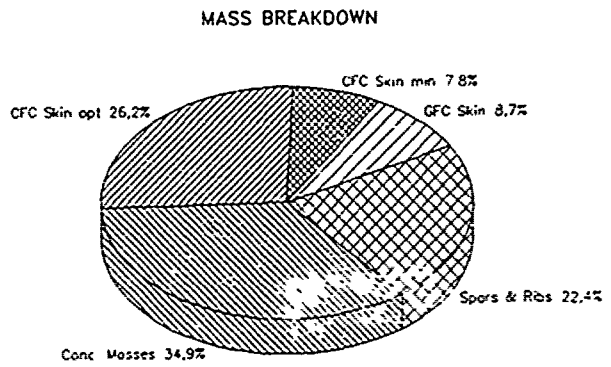

Initial Structure : Mass 153.7

The various properties of the initial and the minimum possible structures are shown below along with the extent by which they violate the constraints. (Violations are in per cent)

(target)	Initial Structure (actual)	Minimum Structure (actual)
Mass	153.70	113.31
FSD (max)	11.7	74.1
Flutter (530)	6.8 (494.1)	31.4 (363.4)
Eff. AE. (0.8)	2.9 (.777)	24.1 (.608)
Eff. Rud. (0.5)	O.K. (.523)	52.6 (.237)
Buckling (max)	72.0	91.1

The so called "Initial Structure" was the starting point for all the optimisation studies reported on here.

Fully Stressed Design

This was the first of the optimisation runs to be carried out and it is the most basic. The result is a minimum weight structure to withstand all the tensile and compressing forces (buckling not included) and is comprised of panels which are either fully stressed or at the minimum allowed value.

Almost all of the panels end up being at their minimum design constraint thickness of 0.25mm. Those that are not, are at the places where higher stress concentrations occur, either at the hinge between the rudder and the fin or at the rearward bending attachment of the fin fuselage connection. The plies that were affected most were those acting in the near vertical directions of the 0° and -45° plies.

Details of the iterations are shown below. It can be seen that the structure was quickly reduced to dimensions very near to the optimimum. The scaled weight, however, is very slow to be reduced and, in fact, the optimisation was terminated before full convergence was achieved.

Iteration	Scaled Mass Kg	Panel Label	Actual Mass Kg.
0	174.12	3022	153.70
1	179.86	3022	118.03
2	149.75	3019	117.50
3	136.32	3019	117.74
4	129.44	3019	117.83
5	125.00	3019	117.91
6	122.74	3016	117.94
7	121.90	3016	117.94
8	121.39	3016	117.94
9	120.97	3016	117.94
10	120.60	3016	117.94
11	120.29	3016	117.95
12	120.00	3016	117.95
13	119.74	3016	117.95
14	119.51	3016	117.95
15	119.31	3016	117.95
16	119.14	3016	117.95

Fully Stressed Design and Flutter

The flutter constraint has been included in S.O.S. in a similar way to the displacement constraints [4]. To this end, the stiffness and mass matrices for the modal base, used to solve the flutter equation and to obtain the derivatives of the flutter speed, are computed for each design variable. In the present flutter optimisation and analysis the first five normal modes are taken as a base and the above matrices are updated at each iteration. The divergence speed constraint can follow the same way, provided a modal base fully representative of the structure flexibility. At the moment any attempt to experience this constraint has been carried out.

The flutter optimisation allows the user to select a number of parameters which enable him to guide the program where to look for flutter. This is important as a change in the flutter coupling modes or a large change in the structure due to some other constraint can have a large effect on the flutter velocity. In the event of flutter not occurring in the range specified by the user an appropriate message is given and a restart of the optimisation can be carried out with the new input data.

The optimisation,which history is shown below and in Table 1 later on in the report, led to a steady reduction in the mass towards the optimum.

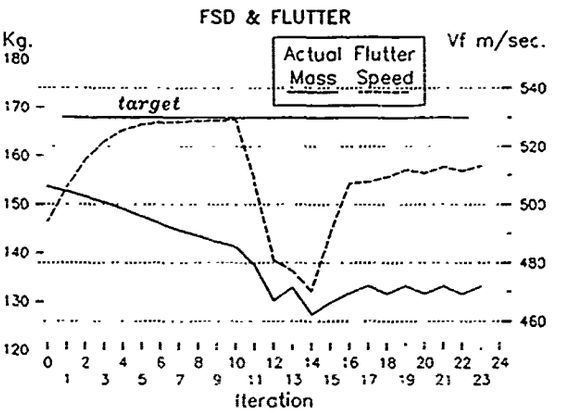

The flutter speed was increased steadily to its constraint value. When reached, the program concentrated on reducing weight and this was accompanied by a reduction in the flutter velocity to a value below the initial level. A slow optimisation involving increasing the flutter speed and toying with the weight then ensued.

In the optimisation of the fin with constraints of FSD and flutter the optimum oscillated between two different structures with different stiffnesses, and different modes generating flutter while the flutter velocity was slowly increased towards its constraint value. To reach the non-violated optimum design the program should be allowed continue in this manner until the constraints are satisfied. The problem that was encountered arises when the structure is in a critical position between two different flutter couplings. A slight change in the structure and it changes to the other coupling. A change in the step size would serve to make more clear this border between one coupling and the other but it would not positively affect the optimisation. Looking at the mode shapes the primary flutter is a classical bending-torsion coupling (first and second modes). (fig.4) While optimising, due to the reduction in weight and stiffness, a second type of flutter arose : a coupling of tip modes with the participation of the rudder mode; this new coupling, already present in the original structure, although at a higher speed gives a miid flutter. In the present analysis no structural damping has been included.

Fully Stressed Design and Efficiency

As was stated earlier in this report S.O.S. has the capacity to optimise a structure with constraints of various efficiencies. The constraints imposed on the fin for this study were an Aeroelastic efficiency of 0.8 and a Rudder efficiency of 0.5. The Aerodynamic Influence Coefficient matrix for the fin and rudder surface at Mach 1.8 was obtained with

the aid of SUPNLR, a program written by NLR. A number of other matrices were needed for the force efficiency optimisation:
(a) a matrix whose columns contain the deflections of the aerodynamic surface (e.g. Rudder or Fin)
(b) an integration vector necessary for the calculation of efficiency (this can either be provided by the user or generated by S.O.S.)
The optimisation can be seen to move at a very slow rate, initially reaching the constraint values and then concentrating on reducing mass (details shown in Table 2). The final structure has a maximum violation of less than 1%. Further iterations at a slow speed would succeed in reducing this.

Fully Stressed Design and Buckling

This optimisation was dealing with a constraint which initially was greatly violated. The end result, achieved in only seven iterations, is a fully converged structure not violating any constraint imposed. Unfortunately, to achieve this, the weight had to be increased substantially (details are shown in the follwing table).
The buckling run requires the definition by the user of the bays and type of constraint on the panel to be enforced. We decided to take the conservative approach due to the lack of more precise information. This meant that each panel was defined as a bay simply supported on the spars and ribs.

Iteration	Scaled Mass	Panel Violated	Actual Mass
0	549.1	51	153.7
1	237.8	26	190.3
2	199.4	26	191.9
3	193.6	63	192.2
4	192.3	84	192.2
5	192.2	104	192.2
6	192.2	104	192.2
7	192.2	20	192.2

FSD, Fin Efficiency & Flutter

The structure was optimised in only seven iterations to a final structure with a maximum violation of less than 1%. A discussion as to why the optimisation proceeded in this quick manner is carried out later in this report. Details are shown in Table 3.

Fully Stressed Design, Flutter and Buckling

This optimisation resulted in a structure much the same as that for buckling only. The effect of the flutter optimisation is minimal as the optimised buckling structure already satisfies the flutter constraint. Details are shown in Table 4.

Fully Stressed Design, Flutter, Efficiency and Buckling

This optimisation run, imposing all the required constraints, except those material thickness specifications mentioned earlier, is very similar to the Fully Stressed Design and Buckling optimisation described earlier. The structure required to withstand buckling alone is one that automatically fulfils the flutter and efficiency constraints and it is almost as if they are not constraints at all having been satisfied from iteration one on.
While the total weights of these two structures are the same it was noted that the individual panels were not the same in every case. This can be explained by the fact that the small effect of the other constraints has led to a slightly different structure with load paths that differ.

The optimisation itself was very quick to carry out. Each iteration took longer but the structure had fully converged with negligible violations in only eight iterations using a relatively small step size. Details are shown below.

ALL CONSTRAINTS IMPOSED

It.	Flutter mode	Flutter freq. Hz	Flutter speed m/s	Initial frequency of five different modes Hz					Fin Eff.	Rudd. Eff.	Scaled Mass	Mass Kg
0	2	20.09	494.11	9.10	30.65	45.11	56.06	71.59	.7771	.5229	174.36	153.70
1	4	59.44	575.54	9.90	32.23	42.05	63.74	69.58	.8502	.6201	227.61	198.56
2	4	59.14	589.32	9.90	32.26	42.31	63.94	69.59	.8512	.6215	206.20	198.85
3	2	23.39	688.54	9.89	32.24	42.46	63.98	69.54	.8510	.6210	200.66	197.88
4	3	56.39	558.49	9.79	32.10	42.23	64.03	68.23	.8488	.6161	205.83	191.81
5	3	56.44	558.84	9.79	32.10	42.24	64.02	68.28	.8490	.6163	194.66	192.11
6	3	56.45	558.87	9.79	32.09	42.24	64.02	68.28	.8490	.6163	192.66	192.18
7	3	56.45	558.87	9.79	32.09	42.24	64.01	68.28	.8490	.6164	192.29	192.20
8	3	56.45	558.86	9.79	32.09	42.24	64.01	68.28	.8490	.6164	192.21	192.20

Aeroelastic Vs. Stiffness Constraints

A series of runs were carried out using frequency separation as a design constraint as an alternative to the use of flutter speed. The advantage of this substitute constraint is that it avoids all the aerodynamic aspects of the problem and the solution of the flutter equation. A relationship between the two was established by drawing a graph and from this the frequency separation between the two first modes corresponding to the flutter velocity constraint was found.

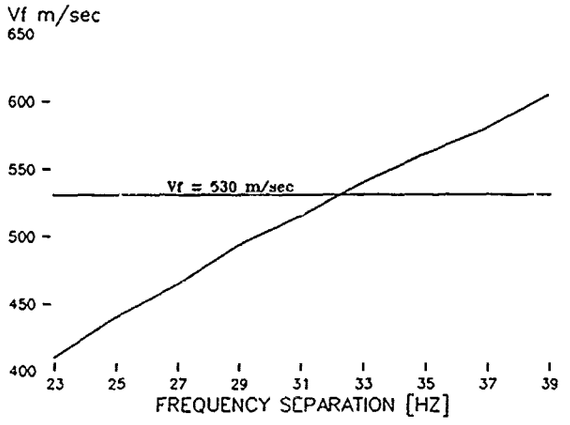

This method, however, was found not to be very representative for the present structure as the frequency separation was only constrained between the first two modes while flutter also occurred at higher modes.
It can be noted from Table 5 that the frequency separation of the optimised flutter structure is about 1Hz less than those requested from the above curve. This is due to the fact that advantage can be taken from the change in mode shapes. Where no account is taken of this, as with frequency constraints, we are effectively over optimising.

As an alternative to the optimisation of the fin with efficiency constraints it was decided to compare the results with an optimisation using displacement constraints. A relationship between the two constraints was established from the graph shown below.

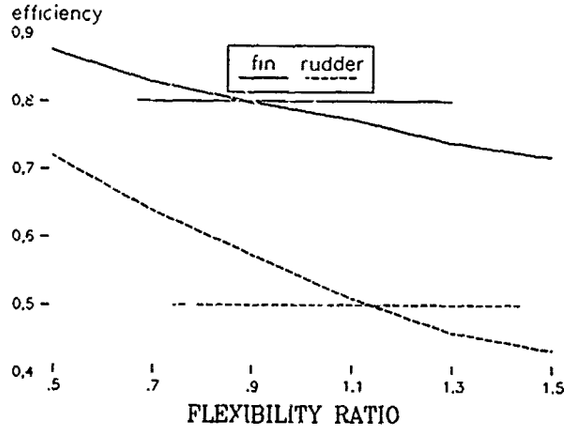

This graph has been obtained from the initial structure by means of a factorisation of the stiffness matrix. This flexibility ratio was multiplied by the original displacement (found using Multi Point Constraint cards) to give us the maximum torsion limiting displacements.

The results of this method, however, were found to differ a great deal with the displacement method which had an optimised weight of 153.3 Kg compared with the efficiency result of 127.5 Kg. The reason for this is that imposing displacement constraints necessarily meant imposing a deformed shape constraint. The efficiency runs didn't have this additional restriction and so were free to find a different deformation geometry under load, resulting in a considerably lighter structure.

DISCUSSION

It can be seen looking at the tables of results for the various optimisations that the more constraints imposed the faster convergence was reached. In those instances where buckling is present this fact can be explained by the fact that its requirements are so different and its influence so large that the other constraints have little effect and we are basically left with a buckling only optimisation. Where buckling is not a constraint however, the optimisation still turns out to be considerably faster in terms of iterations done.
The equations that dictate the new values for the optimised properties are affected by each of the constraints. The level of this effect depends on lambda: a parameter that gives an indication of how close to the constraint value this property is, and a gradient which gives the rate of change of the constraint violation for a change in the property. Lambda is affected by the presence of other constraints and it therefore makes allowances for the fact that where there is more than one constraint acting on a particular property the effect of each constraint is summed. This means that in the case where both of the design constraints, as was the case in the FSD, Flutter and Aeroelastic efficiency optimisation, desire a structure to be trimmed their effects will be summed and the structure may be affected by a greater amount than if they were optimising one by one. It must be remembered that the step size parameter continues to exercise its influence throughout all of this and so the combined change is less than the sum of two individual changes. All of the constraints have equal weightings and so in the case where two constraints try to impose opposing directions for the property being optimised that one furthest from its optimum will be dominant.

CONCLUSIONS

The following graph summarizes the weights of each structure optimised by imposing the combinations of constraints studied.

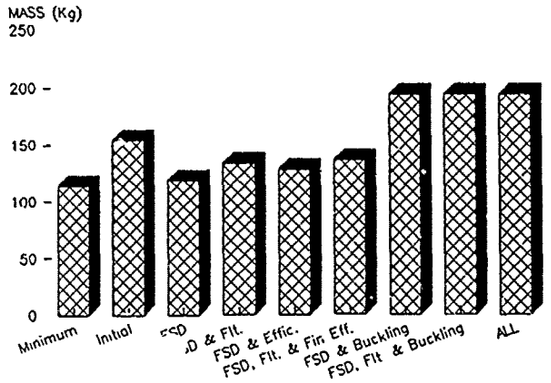

All optimisation runs other than buckling resulted in a lighter structure satisfying the violated constraints. Buckling, on the other hand, needs a considerable amount of mass to be satisfied, regardless of what other constraints are imposed. Greater confidence in the post buckling behaviour of the carbon fibre composites, would allow profitable mass saving, either by buckling critical load scaling up or by post buckling analysis.

In the above optimisations the weight was the objective function to be minimised, and, unless a non feasible design is chosen[1], the constraints must be satisfied. Sometimes, however, it is possible to reduce the importance of some of the constraints and save more mass. This means a new objective function, capable of dealing with various kinds of parameters with non homogeneous units, and defining the best compromise among multidisciplinary constraints. But a multidisciplinary, omnicomprehensive optimisation code is a chimera. As hinted in the introduction, it would be very difficult to gather all necessary data ready for the optimisation runs. A large project generates and updates data following each disciplines time schedules, although integrated in upper level planning.

Furthermore, the specialised codes, used in each department, are rarely able to be integrated into a general purpose code with ease.

The above considerations do not mean a stop in the optimisation development. For the present projects, these problems already exist, and are solved by a trade off work. The optimisation will improve these solutions, for instance, being applied at two levels. One more general, considering multidisciplinary aspects of the project but with coarse details, aimed to assess the constraints for subsequent second level optimisations, to be carried out by means of the state of the art codes, available for each discipline.

Acknowledgements

The author wishes to thank Colin MURPHY for running the optimisation jobs, discussing the results and for his help in writing this paper.

BIBLIOGRAPHY

1. Venkayya, V.B., Khot, N.S. and Berke, L., "Application of Optimality Criteria Approaches to Automated Design of Large Practical Structures", in "Second Symposium on Structural Optimisation", AGARD CP 123, April 1973, paper 3
2. Taig, I.C. and Kerr R.I., "Optimisation of Aircraft Structures with Multiple Stiffness Requirements", in "Second Symposium on Structural Optimisation", AGARD CP 123, April 1973, paper 16
3. Sistema di Ottimizzazione Strutturale (S.O.S.) Manuale Teorico, Doc. nr. 99/rt/t820f/902012
4. Mantegazza, P. & Ricci, S., "Studio di Metodologie Numeriche per la Introduzione del Vincolo di Flutter nel Sistema di Ottimizzazione Strutturale (S.O.S.)". Politecnico di Milano, Novembre 1986
5. Morris, A.J., "Foundations of Structural Optimisation: A Unified Approach", John Wiley & Sons Ltd., (ISBN 0 471 10200 8), 1982

1 The optimality criteria, while reaching the optimum, may pass through the non feasible domain.

TABLE 1 : FSD AND FLUTTER

It.	Flt. mode	Flutter frequency Hz	Flutter speed m/s (530.)	Initial frequency of five different modes Hz					Lambda	Mass Kg.
				Hz1	Hz2	Hz3	Hz4	Hz5		
0	2	20.09	494.11	9.10	30.65	45.11	56.06	71.59	2.205+02	153.7
1	2	20.39	505.89	9.13	30.98	45.56	56.67	71.79	1.769+02	152.8
2	2	20.61	515.24	9.10	31.25	45.87	57.06	71.91	1.382+02	151.7
3	2	20.75	521.84	9.09	31.47	46.04	57.39	71.93	1.076+02	150.5
4	2	20.82	525.73	9.06	31.63	46.09	57.61	71.86	8.878+01	149.1
5	2	20.84	527.58	9.02	31.75	46.05	57.75	71.72	8.066+01	147.5
6	2	20.83	528.32	8.98	31.83	45.96	57.86	71.53	7.877+01	146.0
7	2	20.80	528.67	8.94	31.89	45.81	57.95	71.32	7.909+01	144.7
8	2	20.78	528.90	8.91	31.94	45.62	58.03	71.09	7.977+01	143.5
9[2]	2	20.75	529.11	8.88	31.98	45.41	58.11	70.85	8.027+01	142.36
10	2	20.72	529.27	8.86	32.02	45.17	58.18	70.61	7.616+01	141.37
11	4	61.17	507.60	8.73	32.05	43.80	58.21	69.41	2.667+00	137.63
12	2	19.22	481.01	8.46	31.15	41.86	56.66	67.03	1.537+01	130.29
13[3]	4	59.62	477.33	8.59	31.66	42.00	57.92	67.41	9.845+00	132.91
14	2	18.85	470.22	8.35	30.84	41.32	56.72	65.75	4.946+01	127.37
15	2	19.43	490.40	8.52	31.24	42.07	57.57	66.61	3.807+01	129.79
16	2	19.87	507.38	8.59	31.54	42.60	58.11	67.29	2.657+01	131.77
17	4	59.96	507.89	8.62	31.73	42.88	58.41	67.72	7.317+00	133.22
18	2	19.89	509.38	8.55	31.55	42.70	58.09	67.31	2.520+01	131.70
19	4	59.98	511.91	8.59	31.74	42.95	58.38	67.72	5.697+00	133.16
20	4	19.90	510.78	8.53	31.57	42.70	58.07	67.27	2.418+01	131.68
21	4	59.97	512.89	8.58	31.75	42.93	58.36	67.66	5.392+00	133.11
22	2	19.90	511.74	8.52	31.58	42.67	58.05	67.21	2.344+01	131.66
23	4	59.95	513.32	8.58	31.75	42.90	58.33	67.60	5.285+00	133.06

TABLE 2 : FSD, FIN & RUDDER EFFICIENCY

It.	Aeroelastic Efficiency Target=0.8	Force Efficiency Target=0.5	Lambda from Fin Eff.	Lambda from Rudd. Eff.	Scaled Mass Kg.	Actual Mass Kg.
0	.7771	.5229	3.579+01	0.0	174.12	153.70
1	.7876	.5275	2.483+01	0.0	164.81	152.60
2	.7948	.5285	n/a	n/a	157.97	151.09
3	.7984	.5259	1.077+02	0.0	153.83	149.18
4	.7993	.5210	9.099+01	0.0	151.66	147.07
5	.7992	.5152	8.839+01	0.0	149.80	145.00
6	.7989	.5095	8.871+01	0.0	147.37	143.07
7	.7987	.5038	7.776+01	9.65+00	144.99	141.28
8	.7987	.5002	5.983+01	2.510+01	142.94	139.73
9	.7987	.4993	5.450+01	3.082+01	141.43	138.45
10	.7986	.4990	5.258+01	3.387+01	140.04	137.35
11	.7985	.4990	n/a	n/a	138.65	136.38
12	.7865	.4921	5.091+01	4.690+01	139.64	129.57
13[2]	.7935	.5010	4.022+01	4.329+01	135.92	129.41
14	.7962	.5030	3.235+01	4.323+01	134.51	128.84
15	.7966	.5029	2.855+01	4.400+01	134.47	128.31
16	.7968	.5027	2.620+01	4.451+01	133.60	127.96
17	.7963	.5027	2.577+01	4.454+01	132.89	127.75
18	.7961	.5029	2.541+01	4.444+01	132.20	127.63
19	.7962	.5031	2.485+01	4.438+01	131.57	127.57
20	.7961	.5035	2.497+01	4.401+01	131.08	127.55
21	.7960	.5036	2.493+01	4.385+01	129.76	127.53
22	.7963	.5037	2.445+01	4.381+01	129.32	127.54
23	.7963	.5038	2.436+01	4.368+01	129.01	127.51
24	.7963	.5039	2.432+01	4.363+01	128.78	127.49
25	.7963	.5040	2.443+01	4.351+01	128.43	127.49
26	.7962	.5040	2.449+01	4.343+01	128.25	127.49

2 Step size changed from 16 to 4, increasing the speed of optimisation.

3 Step size changed from 4 to 16, reducing speed of optimisation.

TABLE 3 : FSD, FIN EFFICIENCY AND FLUTTER

Iteration	Flutter mode	Flutter freq. Hz	Flutter speed m/s	Initial frequency of five different modes Hz					Fin Eff.	Scaled mass	Mass Kg
				Hz1	Hz2	Hz3	Hz4	Hz5			
0	2	20.09	494.11	9.10	30.65	45.11	56.06	71.59	.7771	174.36	153.7
1	2	20.26	500.56	9.19	31.66	45.29	58.08	70.19	.7918	147.90	139.7
2	2	20.61	514.48	9.25	31.96	45.61	58.64	70.50	.7960	145.08	140.8
3	2	20.53	522.27	9.14	32.31	43.90	58.95	68.93	.7988	138.86	136.8
4	2	20.65	528.31	9.14	32.42	43.93	59.05	69.05	.7977	137.77	137.3
5	2	20.66	529.77	9.13	32.45	43.84	59.00	69.02	.8000	137.33	137.3
6	2	20.63	529.83	9.11	32.45	43.71	58.92	68.94	.8000	137.09	137.0
7	4	60.95	527.14	9.09	32.44	43.57	58.83	68.86	.8000	137.58	136.8

TABLE 4 : FSD, FLUTTER AND BUCKLING

Iteration	Flutter mode	Flutter freq. Hz	Flutter speed m/s	Initial frequency of five different modes Hz					Lambda	Mass Kg
				Hz1	Hz2	Hz3	Hz4	Hz5		
0	2	20.09	494.11	9.10	30.65	45.11	56.06	71.59	2.209+02	153.7
1	4	59.45	575.54	9.90	32.24	42.05	63.74	69.58	--	198.5
2	4	59.17	589.10	9.89	32.26	42.31	63.94	69.57	--	198.8
3	4	60.08	541.83	9.85	32.04	42.80	63.31	69.75	4.095-01	187.0
4	4	60.06	529.28	9.81	31.93	43.00	62.95	69.76	2.321+01	181.7
5	3	56.38	561.41	9.79	32.09	42.32	64.00	68.29	--	191.7
6	3	56.46	561.08	9.79	32.09	42.33	64.01	68.34	--	192.1
7	3	56.48	561.06	9.79	32.09	42.34	64.02	68.35	--	192.2
8	-	-	561.07	9.79	32.09	42.34	64.02	68.35	--	192.2
9	3	58.49	561.07	9.79	32.09	42.34	64.02	68.35	--	192.2

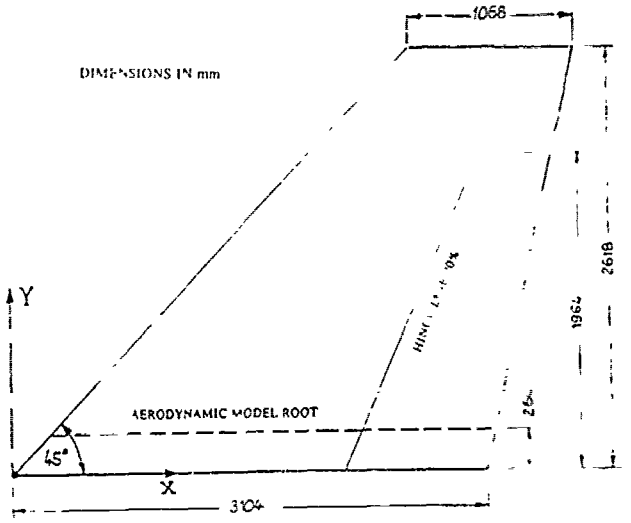

Fig.1 OVERALL GEOMETRY

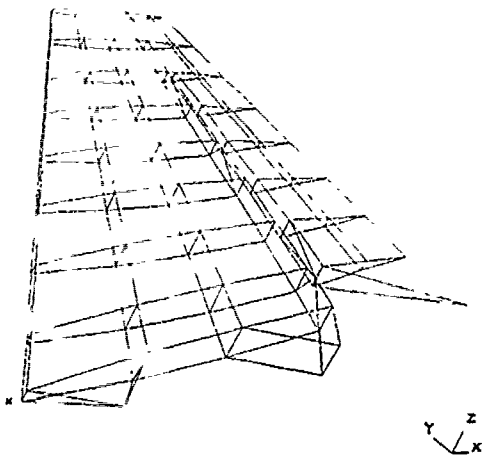

Fig.2 FINITE ELEMENT MODEL

	Orientation	Fin Element ID's	Rudder Element ID's
CFC UPPER FACE	0°	11-28	81-90
	45°	1011-1028	1081-1090
	90°	2011-2028	---
	-45°	3011-3028	3081-3090
CFC LOWER FACE	0°	51-68	101-110
	45°	1051-1068	1101-1110
	90°	2051-2068	---
	-45°	3051-3068	3101-3110

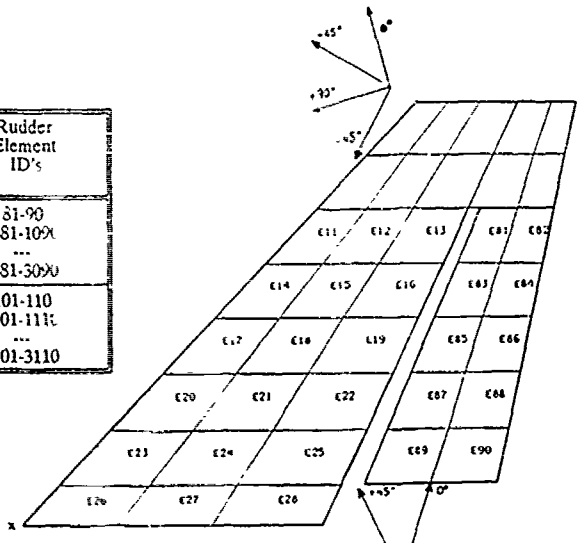

Fig 3 Panel Numbering & Fibre Orientations

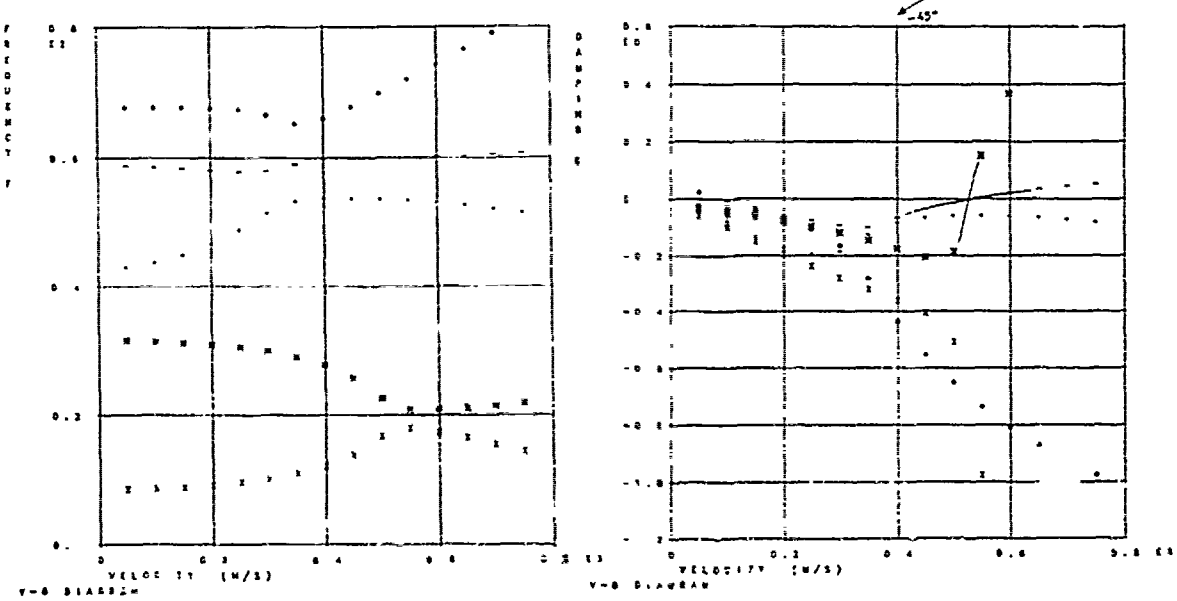

Fig 4 V-G Plots : FSD & Flutter after iteration 21

All dimensions in μm (x10^{-6}m)

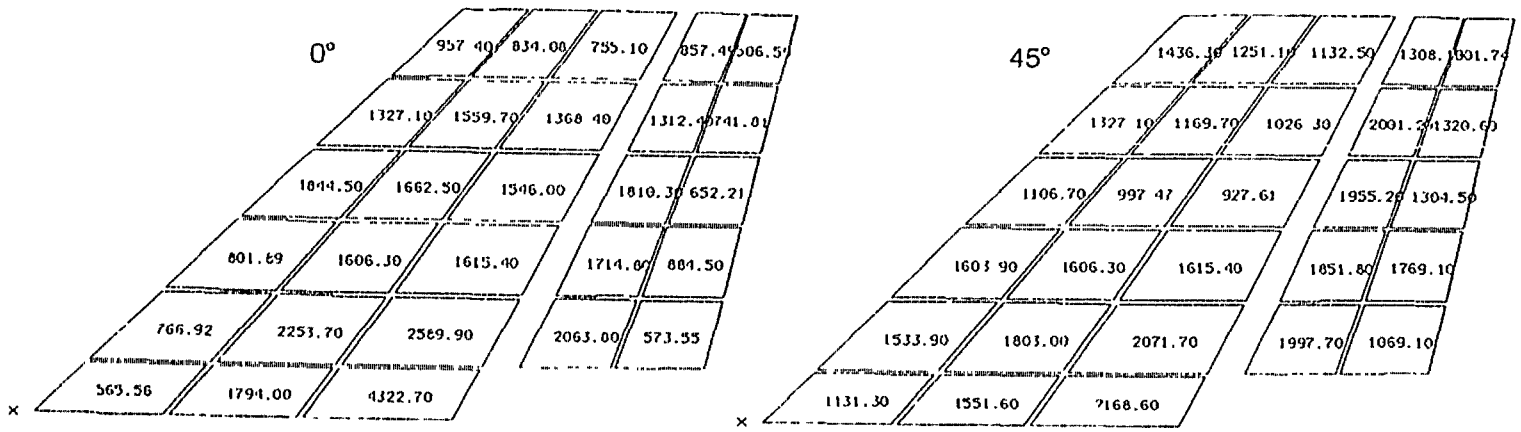

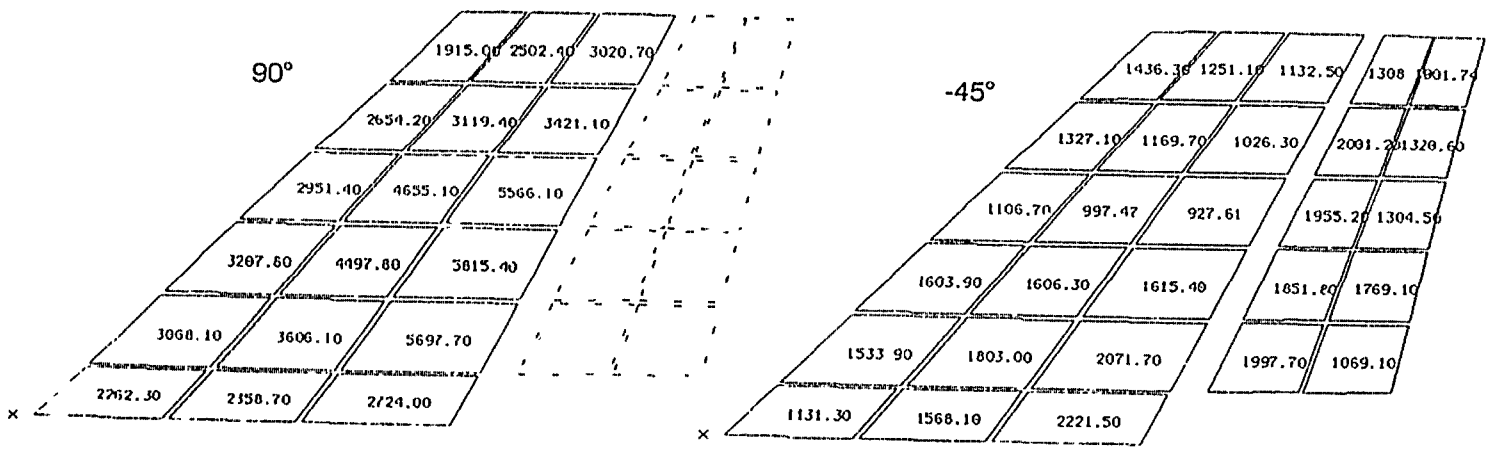

Fig.5 Thickness of Panels - All Constraints after 8 Iterations

SIMULTANEOUS STRESS AND FLUTTER OPTIMIZATION FOR THE WING OF A TRANSPORT AIRCRAFT EQUIPPED WITH FOUR ENGINES

J M D Snee
British Aerospace
Commercial Aircraft Ltd.
Airbus Division
Filton House
Bristol BS 99 7 AR
England

H. Zimmermann
D. Schierenbeck
P. Heinze
EF 24
Deutsche Airbus GmbH
Hünefeldstr. 1-5
D-2800 Bremen

1. INTRODUCTION

This contribution is based on an international cooperation in a four engine transport aircraft project incorporating a common wing design. BAe Filton has the overall wing responsibility and DA Bremen the overall responsibility for aeroelastics in this project.

The main objective of this work is to demonstrate the benefits of interdisciplinary optimization techniques to a modern aircraft design.

The optimization task therefore has an interdisciplinary character.
BAe has defined static constraints, dimensioning load cases, allowable stresses, design variables and their bounds and has prepared the optimization results with its own program (ECLIPSE, Stress Ratio Method).
DA has defined aeroelastic constraints and, using DA's own new software (SimOpt) has prepared wing design solutions.

Description of the Optimization Project

The optimization related to a four engine transport aircraft series equipped with a common wing. The series comprises two aircraft differing in fuselage length by approx. 4 m but with the same maximum take-off weight.

Wing commonality in terms of optimization means that all the significant aeroelastic and static constraints are taken into account in order to achieve a weight-optimized but also valid design proposal. In effect, this means that critical flutter situations of both aircraft types dependent on the fuel and load conditions as well as the dimensioning static load cases in combination with the stress allowables must be introduced into a mathematical optimization model and the weight-optimized solution must be sought with the aid of various optimization techniques.

BAE CONTRIBUTIONS

2. WING ANALYSIS

A basic requirement for structural optimization of an aircraft wing, is to create a single finite element (F.E.) model which adequatuely repesents the strength and stiffness characteristics of the wing structure. This enables wing structural optimisation for both static and aeroelastic design requirements, simultaneously.
The model must accurately represent the distribution of stiffness, as this controls the load path and the dynamics, whilst the stress must be calculated accurately enough for comparison with structural allowables in the desired areas. In the idealisation used for the wing F.E. model, it is reasonable not to directly represent the manholes and skin pocketting in skins, but to choose effective panel thicknesses and allow for the change in load paths.
Similarly, panel thicknesses and beam areas are modified to simulate the effects of cutouts/reinforcements in spars. Clearly the "optimum" effective sizes for panels and beams which result from structural optimization ought to be translated to correct panel thicknesses and beam areas.

Skin/stringers on the top surface are generally subject to compressive loads and could possibly suffer from panel buckling which could reduces their allowable stresses. These allowables are size dependent, i.e. they change with skin thickness and stringer area. During the optimization process, skin/stringers are resized and, therefore, would be associated with a new set of stress allowables. At present these features are under development and not included in this work.

3. THE FINITE ELEMENT MODEL OF THE WING

The MSC/NASTRAN finite element suite is used to model the wing for the purpose of optimization, see fig. 1.

The wing skins are modelled using the 4 noded CQUAD4 plate elements.
Membrane and bending actions are modelled (with no coupling) and the elements have constant thickness. The finite element nodes are placed on the mid-skin line so that element offsets are not used.

The front/rear spars and ribs are idealised as a combination of CQUA4 plate elements representing the webs and 2 noded CROD beam elements representing spar caps. Plate elements have constant thickness and model membrane and bending behaviour whilst the beams have end load carrying capability.

The coarseness of the finite element mesh dictates that not every stringer can be modelled. Beam elements are used to represent two, three or four stringers with a corresponding increase in element properties.

The secondary structure such as the fix leading edge, although included in the finite element model for its structural contribution, is not considered to be of interest in the optimization process. A coarse mesh of these areas is generally employed.

In order to restrain the model the NASTRAN SPC (single point constraint) cards are used, whilst loads are applied via NASTRAN RBE3 elements positioned in the plane of each rib. The design load cases considered for this optimization exercise are presented in Table. 1

4. THE ECLIPSE DESIGN OPTIMIZATION SYSTEM

A detailed description of the ECLIPSE optimization system, can be found in the theory and user manuals [1, 2]. In Table 2, a summary description of the ECLIPSE optimization system is provided.

5. Design Optimization Data

5.1 Static and Manufacturing Constraints

The stress allowables and design variable groupings for top and bottom skins and front spar web are represented in figures 2. 3. and 4. respectively. It should be noted that for this structural optimization development only a small number of design variable groupings were considered. In addition, the stringer area was assumed constant and the panel to stringer relationships were not enforced. For manufacturing considerations, gauge limits of minimum 1.5 mm and maximum 48 mm were assumed.

6. ECLIPSE STATIC STRUCTURAL OPTIMIZATION RESULTS

The static structural optimization results are presented in figures 5-8. Figures 5 and 6 show the distribution of initial and optimum thicknesses for the top and bottom skin panels. These panels are situated at every third rib bay adjacent to the front spar. As a result of optimisation, the top surface thicknesses have increased inboard of rib 7 and decreased outboard of rib 7 (fig. 5).

For the bottom surface, the thicknesses at the root and between ribs 19 and 34 have increased, whereas between ribs 4 and 16 and at the tip they have decreased.

For the front spar webs the thicknesses have consistently decreased throughout the whole spar (fig. 7).

The total weight history presented in figure 8, shows a 7% decrease for ECLIPSE. The final optimized weight for SIMOPT gives an 8% decrease.

It should be noted that the following assumptions are reflected in these results:

- o Very coarse design variable groupings.
- o A limited number of load cases is considered for design optimization of top skin panels and front spar webs.
- o Only static design constraints (stress allowables) are considered.

There are some detailed differences in the results of ECLIPSE and SIMOPT which require further investigation. A possible source of discrepancy is that ECLIPSE uses fully stressing whereas SIMOPT uses mathematical programming techniques.

DA CONTRIBUTION

7. DESCRIPTION OF THE THEORETICAL MODELS

Semi-models with symmetric and antisymmetric boundary conditions in the symmetry plane were used for dynamic considerations. With the exception of the forward fuselage section, high-resolution was achieved for all components by the FE method. Condensation and assembling of the residual structure matrices were effected with the NASTRAN Superelement method.

Mass models allocated to the stiffness models basically represent a connection of structural and non-structural degrees of freedom provided with 6 * 6 mass matrices. This coupling is represented by special elements of the NASTRAN FE code without introducing additional stiffenings.

The unsteady airloads were calculated by the NASTRAN Doublet-Lattice method with taking into account the full interference of the lifting surfaces. The engines were represented by through-flow cylinder. This representation is backed up by DA research results.

An FE model of the wing, fixed at the wing rib, was used for determination of stresses and their gradients.

8. DEFINITION OF THE MATHEMATIC OPTIMIZATION MODEL

The top and bottom surface as well as the front spar of the wing, broken down into 21 design variables, were released for optimization. The stress optimization model was defined by seven dimensioning load cases and a total of 5072 stress constraints (principal stresses) (see Fig. 36).

The aeroelastic optimization model covers critical symmetric and antisymmetric flutter modes for each of the two aircraft variants. Such problems arise at both aircraft when they have high payloads and full tanks. To ensure freedom from flutter upon alteration of the trim tank contents, it was additionally required that damping should be monitored for 50% of its fuel level and the empty condition. This resulted in 24 aeroelastic constraints.

The symmetrical flutter problem is due to frequency coupling of the degrees of freedom for vertical movement of the outboard engines with the related twisting of the outer wings and wing bending in combination with two-nodal fuselage bending. The antimetric situation is determined by frequency coupling of the three-nodal bending of the wing and wing bending in plane in combination with lateral movement of the outboard engines and lateral bending of the rear fuselage including fin bending. Fulfillment of the flutter safety requirements led to the definition of damping constraints. To this end, an area of allowable damping was defined at the point v-d; M = 0.84 for the flutter modes to be monitored.

Damping constraints can be applied at various speed values of points for a flutter mode. This offers the advantage of being able to influence the entire curve progression for damping. Whereas, the flutter speed constraint only to influence the flutter speed.

9. DESCRIPTION OF THE OPTIMIZATION METHODS APPLIED

Three methods which are generally acknowledged as suitable for the solution of comprehensive optimization tasks were used (table 32).
To keep the efficiency of the methods comparable for our example, optimization modules have been kept constant in combination with the one-dimensional search. A further point to note is that the methods have been applied to utilize the advantages of simultaneous optimization.

The direct algorithm "Modified Method of Feasible Direction" is installed in NASTRAN version 66 and is considered to be very robust.

SCP (Sequential Convex Programming) was made known by Fleury. In this case, it has been used to the effect that a constraint function with hyperbolic progression versus the design variables has a linear progression versus the inverse variables.
For the convex approximation problem the objective function and the constraint functions are approximated with increase design variables by a Taylor series if the components of the gradient have a negative sign, otherwise the direct design variables are used.
This estimation provides values which are very accurate to exact.
We considered this method to be very promising since the optimization problem to be solved involved numerous stress constraints where the hyperbolic relationship between function value and variable is very distinct.

In contrast, the SQP method (Sequential Programming Method) uses only direct design variables. To use the advantages offered by SCP, we inverted externally. The estimation of constraints is linear and the objective function is approached quadratically. There are different forms of this method which is used for the solution of major optimization tasks.

10. THE SIMOPT PROGRAM: SIMULTANEOUS OPTIMIZATION UNDER STATIC AND AEROELASTIC CONSTRAINTS

A structural optimization program used with a minimum of expenditure for development activities in the industry must satisfy the following requirements:

- Extensive compatibility with NASTRAN:

  All element types are accepted.

  All presentation forms of coordinate systems and grids are recognized.

  No limitations of model size in terms of the number of elements or grids.

- Independent FE models from the individual disciplines

  In each model, the physical units can be selected in the manner most suitable for the discipline.

  Each discipline uses their own designations (ID's) for grids and elements.

  The models coming from the various disciplines relate to the subquantity of the overall structure which is required for specific requirements: e.g. for stress constraints on the wing, the model describes the wing box and for flutter constraints it describes the symmetric and antisymmetric semi-model of the overall aircraft.
  FE discretizations can be adapted to the respective needs of the problem.
  However, it is important to ensure that the elements of the design vector are related to physically the same parts of the structure.

- Extensibility by further types of constraint.

- Interchangeability of the modules.

SimOpt is written in the interpretative command language CLIST. It uses the existing programs NASTRAN, ADSOPT and PkGrad which have already been used successfully for flutter optimization. Development expenditure for SimOpt has therefore been minimized.

The task of SimOpt concentrates on allocation of files, calling of program modules, data transfer between these and control of the overall process.

The interface programs used to implement data transfer and normalize constraints and gradients are written in FORTRAN (normalization, see Fig. 31, 37).

ADSOPT executes the mathematic optimization task. It is the control program which calls and supplies the sub-routine ADS of G. N. Vanderplaats with parameters.

ADS provides a wide range of optimization procedures.

NASTRAN is used both for static and for dynamic computations.

Regarding static constraints, NASTRAN computes stresses and deformations and determines the corresponding gradients. NASTRAN permits the introduction of

principal stresses

normal stresses

shear stresses

buckling stresses

displacements

as constraints which are thus available to SimOpt.

For flutter constraints, NASTRAN provides the generalized stiffness, mass and air load matrices and their derivative matrices.

PkGrad carries out the flutter computation, the reanalysis and the gradient computation.

Constraints which can be processed are

flutter speed

modal damping

control surface

effectiveness

dynamic divergence pressure

This concept meets the requirements for a practice-oriented optimization tool.

The FE tools used for structural optimization are the same as those used for conventional project work so that the call for NASTRAN compatibility is satisfied.
The interchangeability of individual modules is facilitated by the consistent separation of physical components - which are realized by NASTRAN and PkGrad - and the mathematical optimization - for which ADS is used.

Regarding ADSOPT, constraints are not provided in physical units but in their normalized form. As a result of this, individual disciplines can use different models and further types of constraint can be introduced without modification of existing modules.

11. SEQUENTIAL STRESS AND FLUTTER OPTIMIZATION

Computation with Stress Constraints

Using the strategy of Sequential Convex Programming (SCP) and the modified method of feasible directions for determination of the search direction, an optimization was performed with 5072 stress constraints. Direct design variables were selected.

The objective function of the optimal design was -767 kg. Its design vector provided reductions for 17 design variables while reinforcements were assigned to design variables 1, 5, 16 and 17 (Fig. 41).

Design variables 1 and 5 relate to areas in the top and bottom surface at the wing root rib. Design variables 16 and 17 relate to the front spar, namely the inner half of the area between the engines.

Optimization with Flutter Constraints

The result of the stress optimization served as the basis for an optimization with flutter constraints only. To avoid mode tracking problems, the elements of the initial design were set to 1 except where the stress optimizations had allocated a higher value. The lower bounds of the design variables prevented a reduction of the elements of the design vector below the level of the stress design.

The method selected was the same as that for the optimization with stress constraints.

Compared to the design made with stress constraints only, the optimization with flutter constraints provided the following reinforcements:

- in the top surface in the area of the outer pylon connection.
- the front spar with the exception of the outer wing area, specially the outer half between the engines; i.e. design variables 18 and 19.

The bottom surface remains practically unchanged.

These reinforcements yielded an objective function value of
- 418 kg, which is 349 kg more than with the stress optimization.

Reductions are not possible due to the limitation of the design space.

Fig. 41 to 42 show the development of the objective function, the design variables and selected constraints for both computations.

12. SIMULTANEOUS STRESS AND FLUTTER OPTIMIZATION

5072 stress constraints and 24 flutter constraints were simultaneously considered in the following computations. Three different methods were tried out.

No strategy was used for the first computation. The modified method of feasible directions (MMFD) was used directly. In the following computation, Sequential Quadratic Programming (SQP) was used as strategy for MMFD. The last computation was carried out with Sequential Convex Programming and MMFD.

Application of the Modified Method of Feasible Directions Without Using a Strategy

This computation was performed with inverse design variables because the stress constraints are nearly linear in the inverse variables.

The process satisfied the stress constraints relatively quickly but could not influence one of the total of six violated flutter constraints. A second flutter constraint which was not originally critical was violated in the course of the optimization and could not be corrected in the further process.

The computation was stopped after 23 function calls. The objective function amounted to 2550 kg so that it must be considered unattractive. The relative CPU requirement of 0.4 was relatively low.

Sequential Quadratic Programming (SQP)

Sequential Quadratic Programming was used as strategy for MMFD in this computation. Since - as has already been pointed out - SQP approximates the objective function quadratically and the constraints linearly, inverse variables were also used in this way.

In the course of the computation, the stress and flutter constraints progressed continuously into the allowable area. However, progress was relatively slow compared to the pure stress or pure flutter optimization.

The computation was stopped after 50 function calls. The objective function with six violated constraints amounted to 79 kg. The relative CPU time was 1.0.

Sequential Convex Programming (SCP)

This computation was made with the SCP strategy. Direct design variables were used for the calculation.

The process had satisfied the constraints after 9 function calls, the value of the objective function having risen to 298 kg. In the following steps, design variables 2, 12, and 15 were reduced and design variables 17, 18 and 19 simultaneously increased.
The value of the objective function had dropped to -587 kg after 60 function calls while all constraints remained fulfilled.

A comparison of the results of the simultaneous and sequential optimization (see Fig. 38) shows that the essential differences relate to the design of the front spar.

The simultaneous optimization process produces an area between the fuselage and inboard engine that is approximately half as thick. The inner half of the area between the engines is approx. 30% thicker after simultaneous optimization while the outer half is approx. 20 % thinner in this case. The thickness of the outer wing is approximately the same in both cases.

In terms of the objective function, the difference between the two methods is 151 kg in favour of the simultaneous computation.

Fig. 43 to 44 show the progression of the objective function, the design variables and selected constraints for simultaneous optimization computations.

13. CONCLUSION

The main task defined in the beginning was achieved with an appearent 587 kg weight saving per wing, on the idealized structure.
The application of ECLIPSE and SimOpt on the Optimization with stress constraints only, lead to close results in terms of the objective function.

The optimization computations have shown that simultaneous consideration of stress and flutter constraints with SimOpt offers advantages with regard to the target function value. These weight savings are due to load transfer effects inside the structure at constant external loads.

Reinforcements required to satisfy flutter constraints lead to stress reductions in other parts of the structure where material reductions are then allowed. The material becomes optimally with the fulfillment of flutter and stress constraints.

The suitability of the different optimization methods was found to vary. the most favourable results having been obtained with the SCP method. This method should be further refined for interdisciplinary optimization projects in future to achieve a better consideration of the mathematical properties of the different constraint types in approximations.

REFERENCES

1. ECLIPSE User Guide,
   Structural Analysis Group, Stress Office
   Warton, BAe (Military Aircrafr) Limited,
   Warton Aerodrome, Preston, Lancashire
   PR4 1 AX.

2. ECLIPSE Theoretical Manual,
   Report No. BAe-WSO-RP-GEN-SON-000828
   BAe (Military Aircraft) Limited, Warton
   Aerodrome, Preston, Lancashire PR4 1AX.

3. Turner, M.J. "Optimization of Structures to Satisfy Flutter Requirements" AIAA Journal, Vol. 7 No. 5, May 1969

4. Rudisill, C.S., Bhatia, "Optimization of Complex Structures to Satisfy Flutter Requirements". AIAA Journal, Vol. 9 Nr. 8, Aug. 1971

5. Vanderplaats, G.N., "ADS-A Fortran Program for Automated Design Synthesis" ADS Users Manual 1987 EDQ. Santa Barbara, CA, USA

6. Heinze, Schierenbeck, Niemann "Structural Optimization in View of Aeroelastic Constraints" Beitrag zum European Forum on Aeroelastic and Structural Dynamics", 1989.

7. Vanderplaats, G.N. "Numerical Optimization Techniques for Engineering Design". N.Y. Mac Graw Hill. 1984.

8. C. Fleury, (1989-2): "CONLIN, and efficient dual optimizer based on convex approximation concepts", in Structural Optimization 1, S. 81-89, 1989.

9. Sobieszczenski-Sobieski, J. "Multidisciplinary Optimization for Engineering Systems: Achievements and Potential" in Optimization, Methods and Applications. Possibilities and Limitations ed. H.W. Bergmann, Springer 1989.

10. Zimmermann, Schierenbeck "Strukturoptimierung für Transporterflügel", DLR Conference 1989, Hamburg.

flutter coupling modes of a large change in the rudder surface at Mach

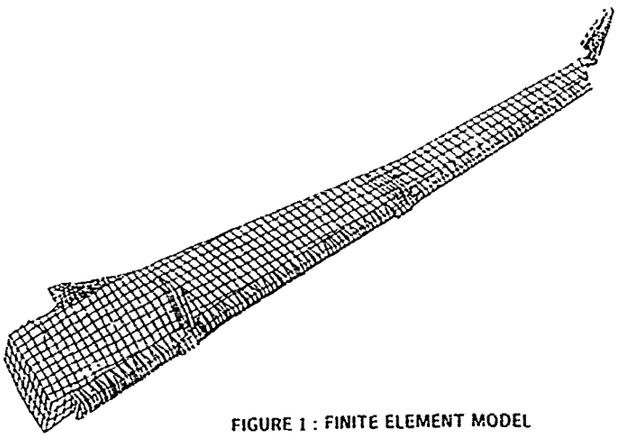

FIGURE 1 : FINITE ELEMENT MODEL

STATIC CONSTRAINTS & DESIGN VARIABLE LINKING

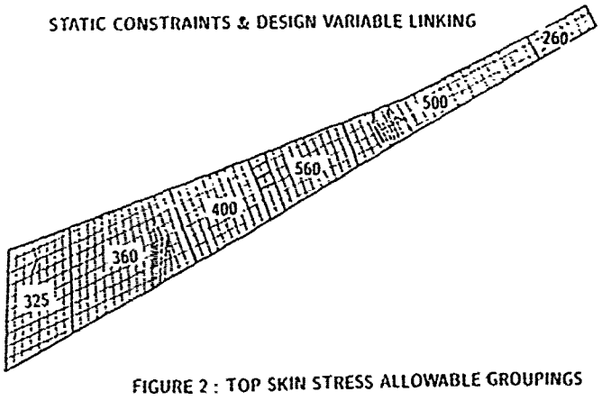

FIGURE 2 : TOP SKIN STRESS ALLOWABLE GROUPINGS

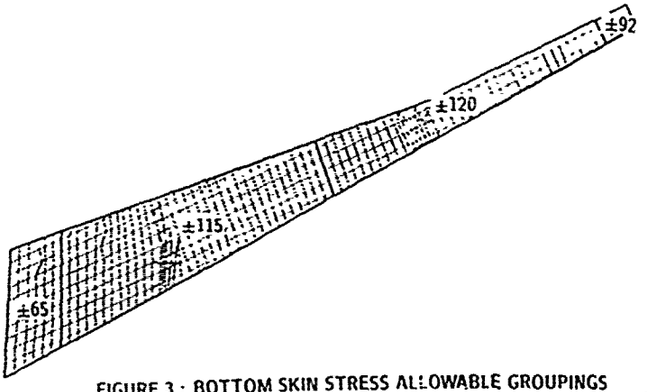

FIGURE 3 : BOTTOM SKIN STRESS ALLOWABLE GROUPINGS

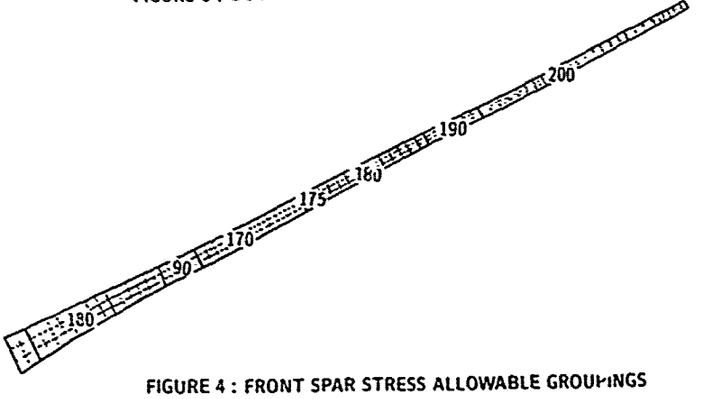

FIGURE 4 : FRONT SPAR STRESS ALLOWABLE GROUPINGS

Normalization

$$G^N = -\frac{\left(D^{current} - D^{requested}\right)}{\max\left(ABS(D^{requested}), 0.01\right)}$$

Table 31 Aeroelastics Constraints

Strategy	Optimizer	Line Search	Inv. DV
Direct	MMFD	polynom.	yes
SCP	MMFD	polynom	no
SQP	MMFD	polynom.	yes

Table 32 Applied Optimization Schemes

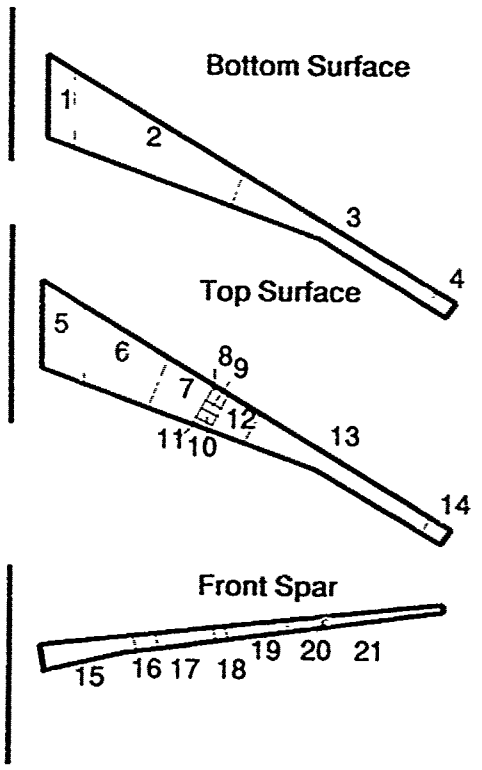

Fig. 36 Design Variable Definition

7 load cases with corresponding stress allowables, 5072 stress constraints

Normalization

$$G^N_{max} = \frac{\sigma^{current}}{ABS\left(\sigma^{allowable}\right)} - 1\ sign\left(\sigma^{allowable}\right)$$

$$G^N_{min} = 1\ sign\left(\sigma^{allowable}\right) - \frac{\left(\sigma^{current}\right)}{ABS\left(\sigma^{allowable}\right)}$$

Fig. 37 Statics Constraints

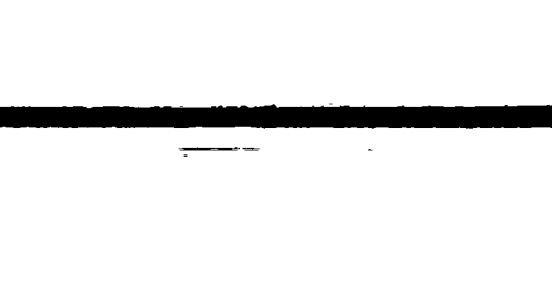

Fig. 38 Comparison of Final Front Spar Design of Sequential and Simultaneous Optimization

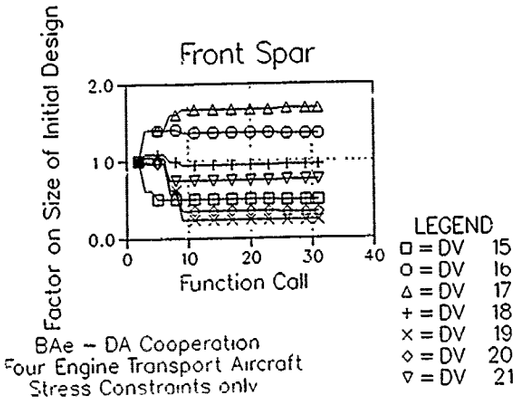

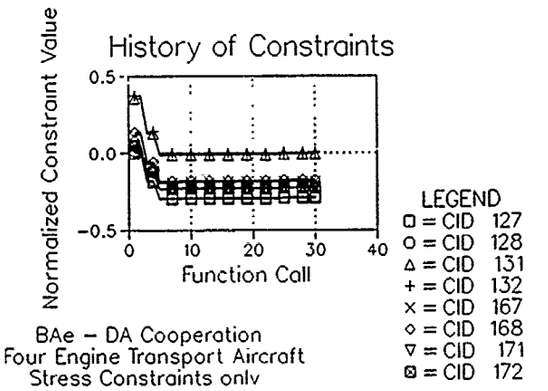

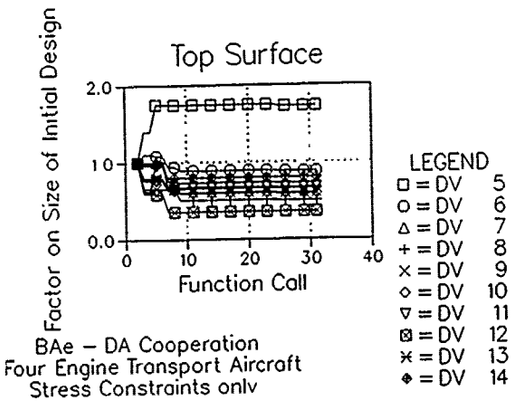

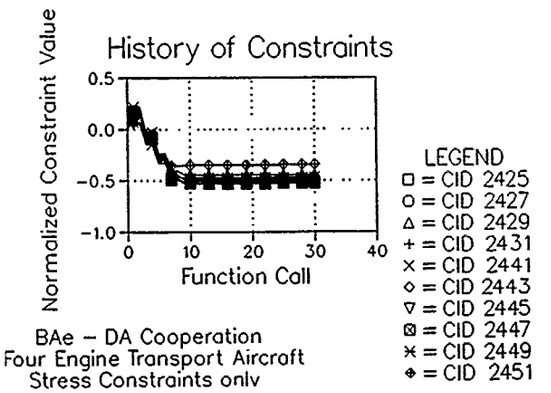

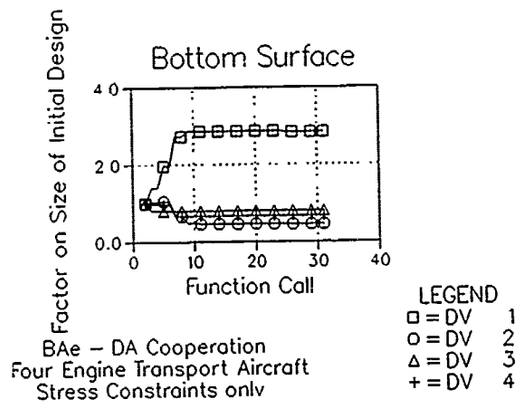

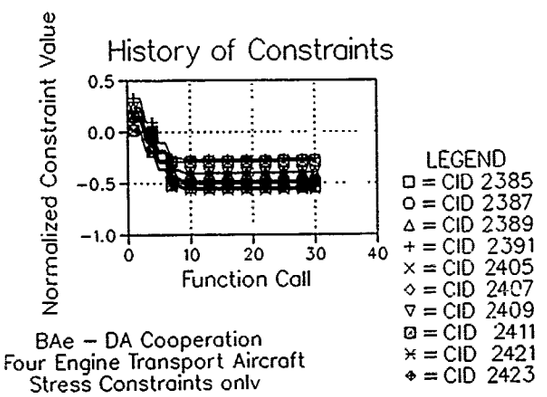

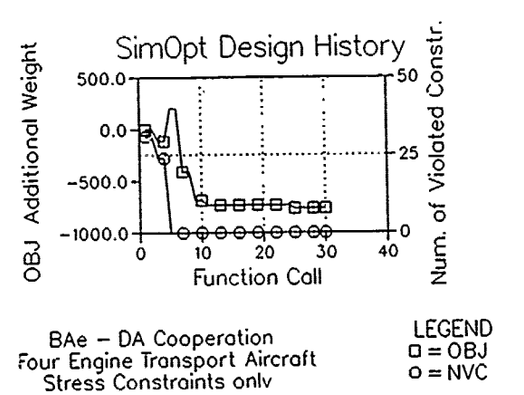

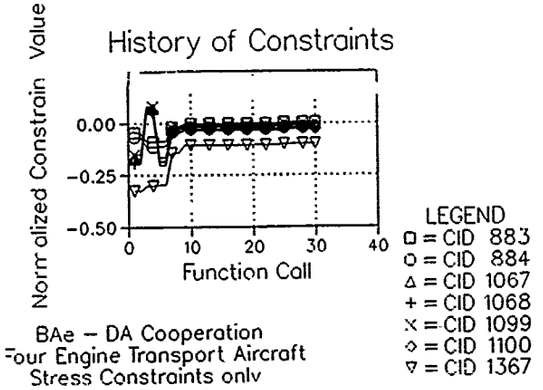

Fig. 41 Optimization with Stress Constraints only

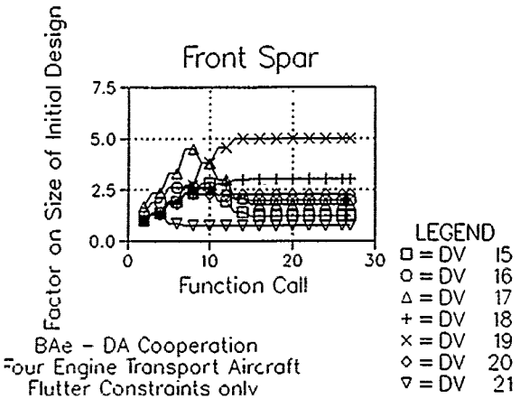

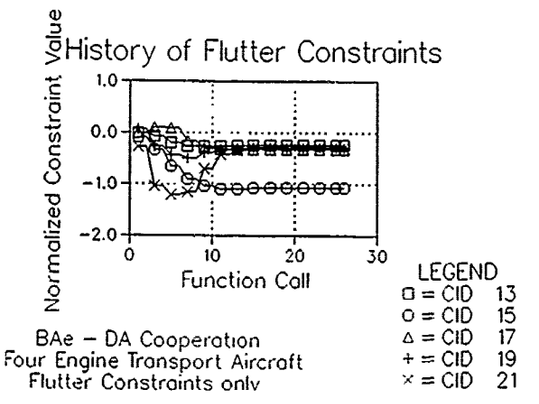

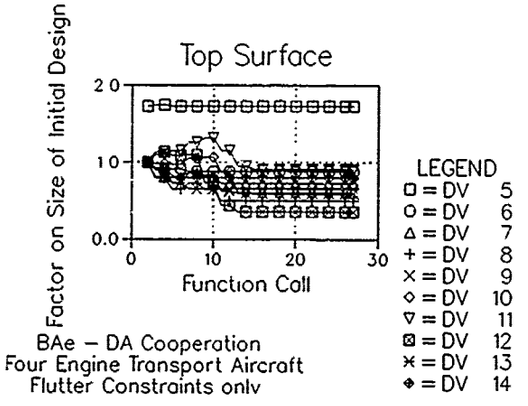

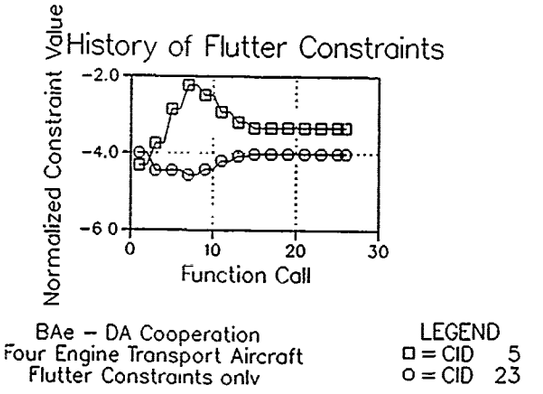

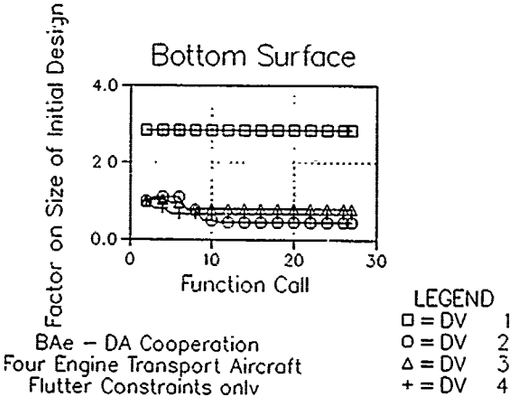

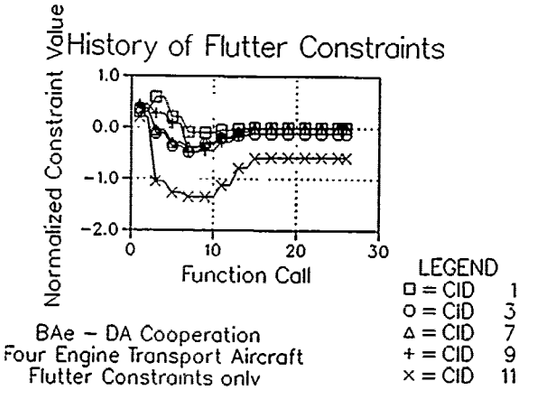

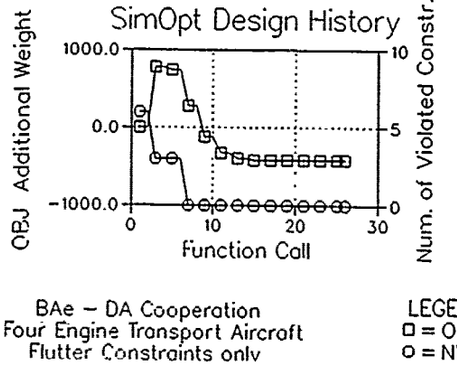

Fig. 42 Optimization with Flutter Constraints only

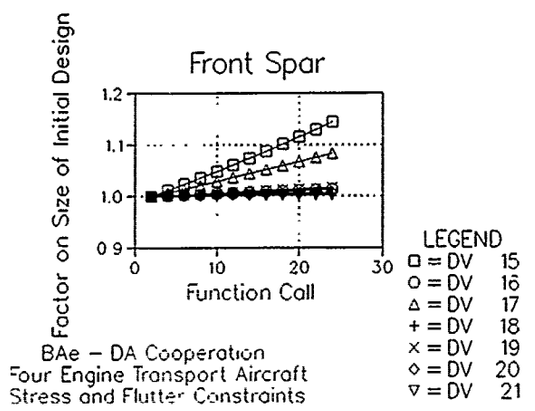

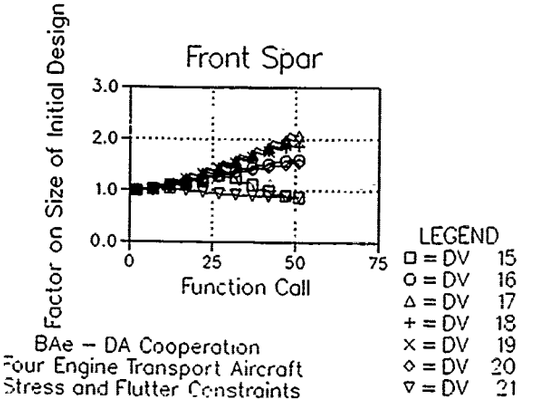

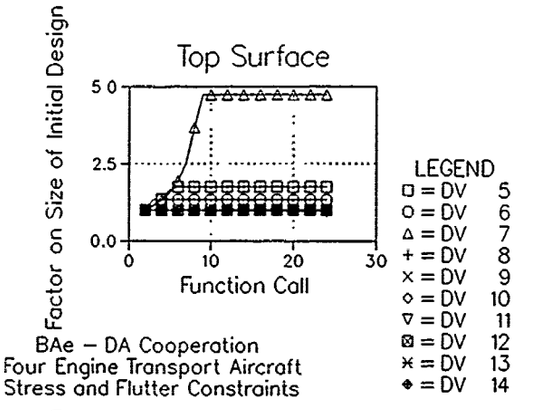

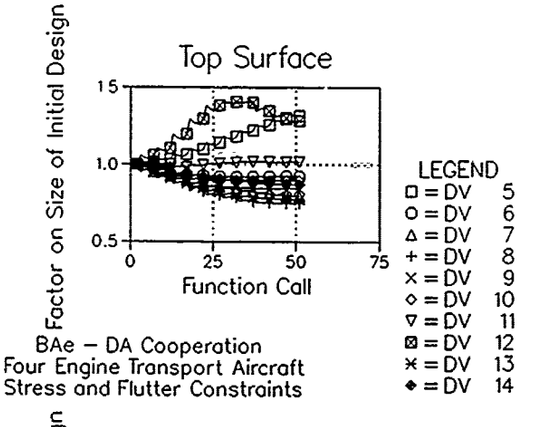

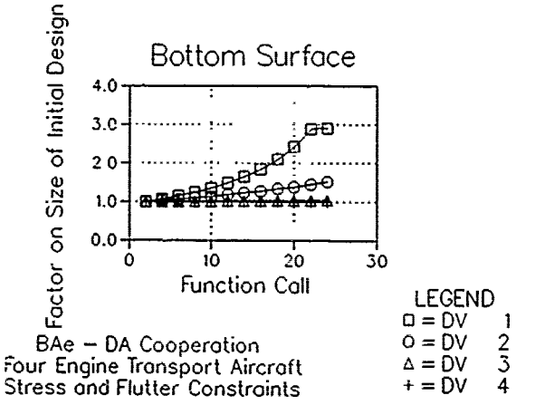

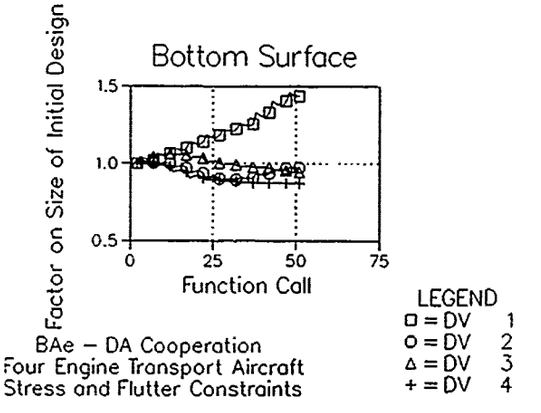

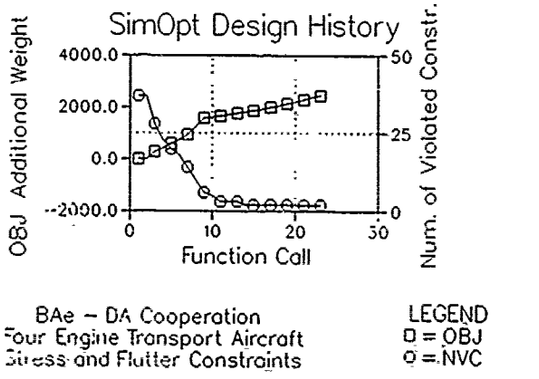

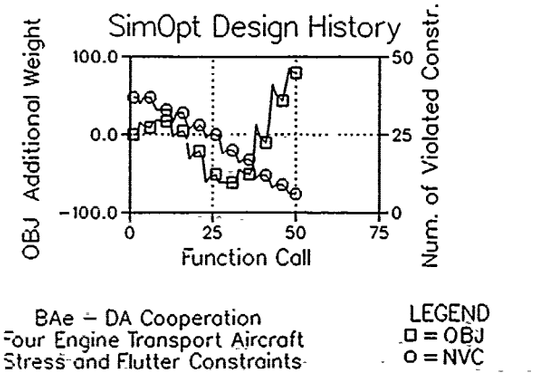

Fig. 43 Simultaneous Optimization with Stress and Flutter Constraints using MMFD direct (left) and SQP (right)

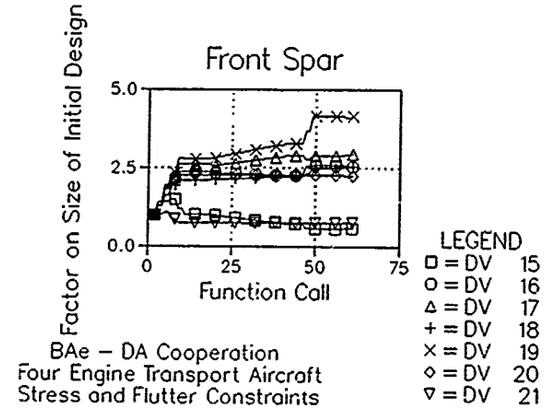

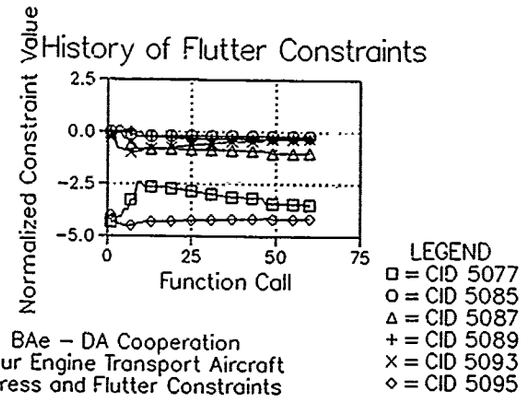

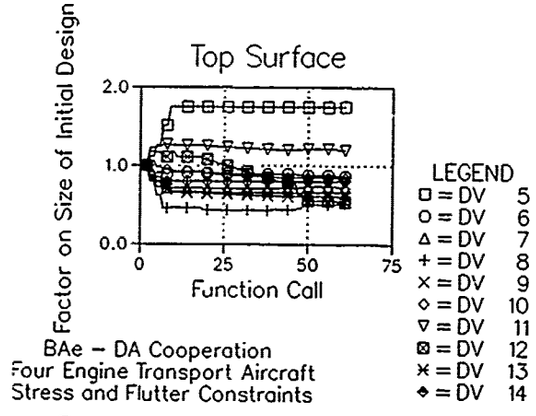

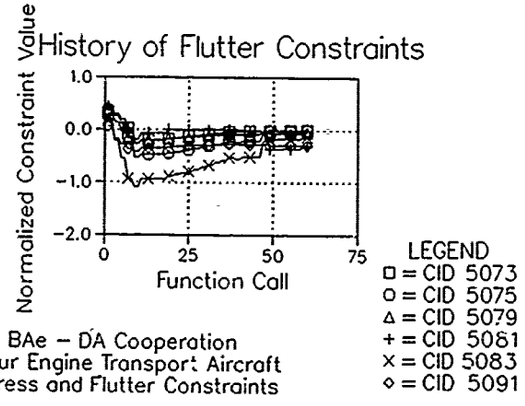

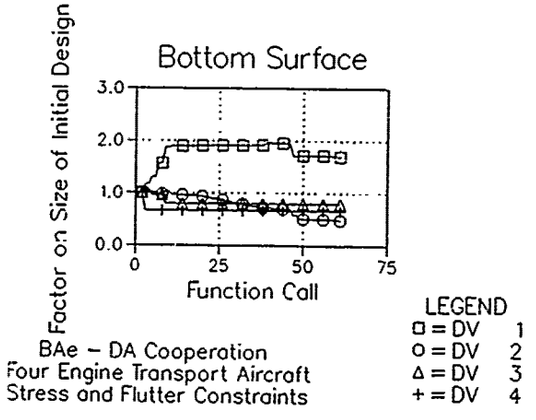

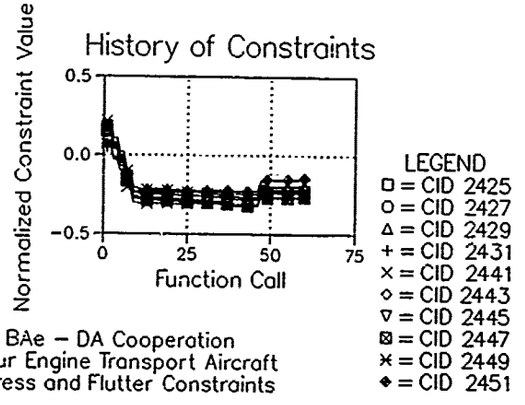

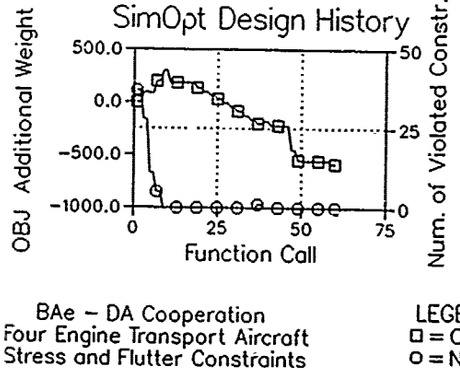

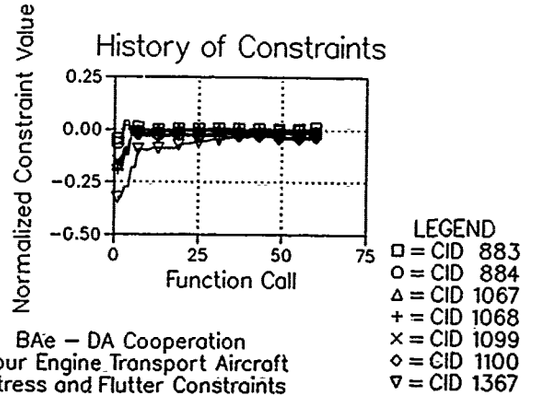

Fig. 44 Simultaneous Optimization with Stress and Flutter Constraints using SCP

STRUCTURAL OPTIMIZATION OF AIRCRAFT PRACTICE AND TRENDS

by

C. Cornuault, C. Petiau, B. Coiffier and A. Paret
Dassault-Aviation
78 quai M. Dassault
92214 St Cloud
France

ABSTRACT

After a general presentation of the CATIA-ELFINI tool, developed by DASSAULT, where C.A.D., structural analysis and optimization are fully embedded, we focus on a detailed description of the optimization algorithm. We show the special features of optimization with composite materials.

We present the new organization of design resulting from use of optimization technics.

We present the application of our optimization technics on the case of the MBB-FIN.

We recall technics neighbouring optimization as model adjustment and computation with uncertain data.

We conclude by presenting further developments.

1 - INTRODUCTION

The structural optimization technics is a routine process at Dassault since the late seventies. It has been applied for all project from Mirage 2000 to Rafale.

In the past, design of structure was achieved with the "fully stress design" process (F.S.D.) made of iterations of drawing and analyses with reinforcement where the structure is not sufficiently strong and lightening when there are strength margins. Yet with only strength of material constraints on metallic structure it has been demonstrated (see reference 1) that this approach was neither optimum (maximization of stresses is not equivalent to weight minimization) nor efficient for design process. Practically designer is completely unable to intuitate any solution when constraints due to flexibility are involved such as eigen frequencies, aerodistorsion, flutter, and with ply disposal of composite materials.

Therefore we consider that, to-day, the use of mathematical optimization tool is compulsory for the design of aircraft.

We have built the structural optimization tool inside the Dassault software CATIA-ELFINI, it includes :

- the well-known C.A.D. tool CATIA, which gives us geometry and mesh generation
- static finite element analysis for linear and non linear problems
- static aeroelasticity, calculation and management of loads
- linear dynamics : eigen modes calculation, harmonic and transient responses
- non linear dynamics : impact and crash analysis, landing gear and aircraft interaction
- unsteady aeroelasticity, flutter, coupling with flight control system
- fatigue and crack propagation analyses
- heat transfer and thermo elastic coupling
- acoustic and elastoacoustic coupling.

The optimization monitor covers most of theses branches.

The system works on request either in a interactive or in a batch mode, and use a common data base managed automatically.

Some of the main common characteristics of branches are :

- topological dialogue for mesh and every data generation. All properties as connectivities between nodes and elements, geometry connection with CATIA surface element characteristics, etc.., are described by block of constant properties in a space of indices referring node and element. The process leads to very clean meshes for all types of structure from the whole aircraft meshes to tridimensional analyse of fitting details (plates 1 and 2)

GENERAL MESH OF COMBAT AIRCRAFT

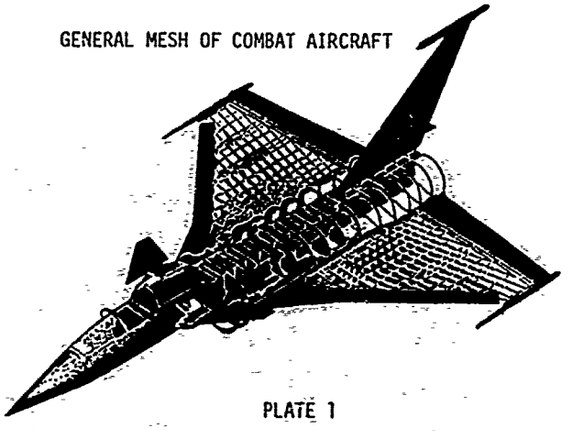

PLATE 1

LANDING GEAR FITTING ANALYSIS

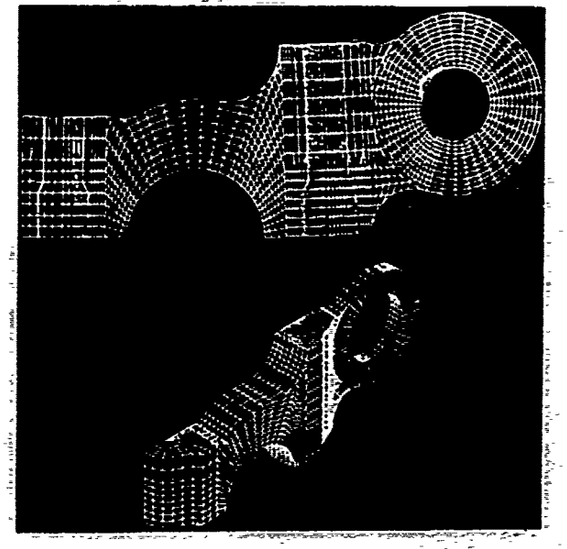

PLATE 2

- very wide possibilities of visualization of inputs and outputs, a lot of "wire frame" and "pixel" type of picture for displacement stresses, failure criteria and for optimization design variable, active constraints and safety margin plot (see § 2 Final Touches)

- advanced mathematical solution : the solution of linear problems is run by a very powerful variant of the Frontal Gauss method, which makes relatively trifling the computer time for classical linear problems (about 1' of CPU on IBM 3090-VF for a complete aircraft calculation, see plate 1).

For 3D massive problems (plate 2) the use of conjugate gradient technics allows to keep the same level of performance, taking into account the contact non linearities.

For geometric non linear problems (membrane effects, post-buckling, snap through, etc...) an original algorithm called "preconditioned B.F.G.S. with exact line search" has been developed (Ref. 3 and 4). This algorithm benefits directly from the biquadratic character of total potential. It can handle the most severe snap-through conditions (see plate 3 : calculation of post buckling of curved stiffened panel in carbon epoxy material).

We must underline the strong practical interest of the post buckling analysis, which allows to design thin composite skin buckling before ultimate load.

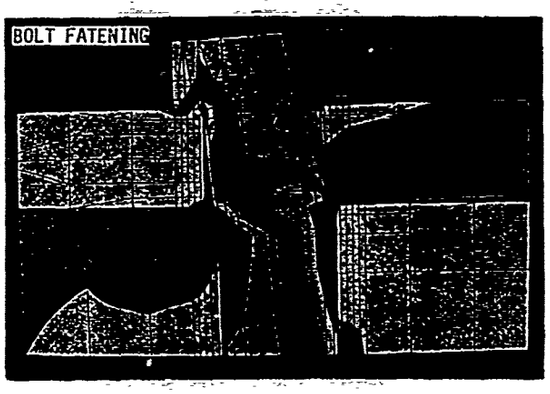

PLATE 3

We are going to present a more detailed view of :
- the optimization technics which is mainly used to set the general dimensioning of the structure. It is supported by F.E. models of the whole aircraft which are elaborated only from the rough definition of external shape and internal architecture, the result of this optimization being the starting point of detail drawing,
- the checking analyses which comes with detail drawings,
- the organization for drawing and analysis which results from necessities of composite design and present possibilities of computer tools.

2 - THE OPTIMIZATION METHOD

We have described it in several papers (Ref. 1 and 2) ; now we present the operational tool as it was used for "Rafale" design ; the organization is iterative with the flow-chart below.

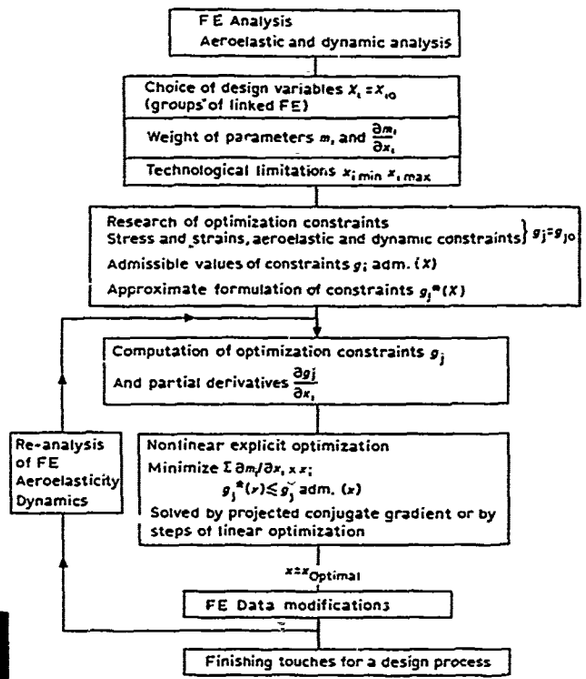

- Cost function

The current goal in optimization is weight minimization. Nevertheless, in some cases, weight can be taken as a constraint, the objective being maximization of safety margin.

- Design variables

The characterization of the optimization design variables is made on groups of Finite Elements (plate 4). The choice of these variables partly takes into account manufacturing constraints and tooling rules for metallic material.

OPTIMIZATION OF CARBON EPOXY WING

UPPER PANEL OPTIMUM LAY UP

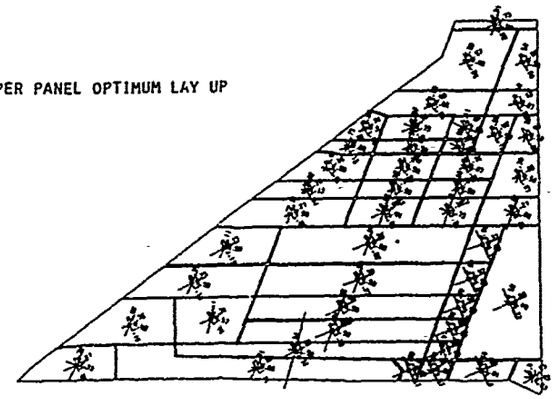

LOWER PANEL OPTIMUM LAY UP

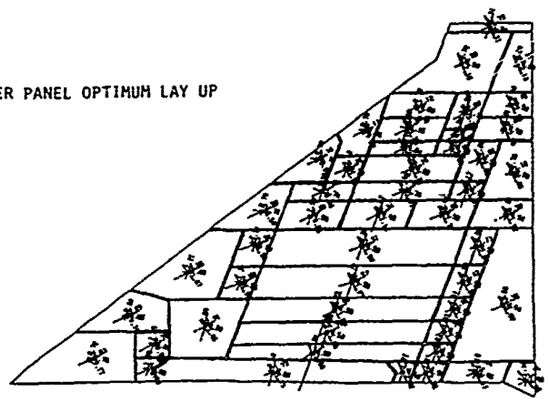

PLATE 4

For a composite material, the design variables are the number of plies in each direction for each group.

The number of design variables often reaches 500, which can act simultaneously over several analysis models.

STRUCTURAL OPTIMIZATION

FINITE ELEMENT ANALYSIS

Displacement computation :

$$X = [K]^{-1} F$$

Strength, stress computation :

$$\sigma = \left[\frac{\partial \sigma}{\partial X}\right] X$$

OPTIMIZATION CONSTRAINT DERIVATION

Displacement derivation :

$$\Delta X = - [K]^{-1} [[\Delta K] X - \Delta F]$$

Strength, stress derivation :

$$\Delta \sigma = - \left[\frac{\partial \sigma}{\partial X}\right] [K]^{-1} [[\Delta K] X - \Delta F] \quad (1)$$

$$\Delta \sigma = - \left[[K]^{-1} \left[\frac{\partial \sigma}{\partial X}\right]^{t}\right]^{t} [[\Delta K] X - \Delta F] \quad (2)$$

(1) number of resolutions equal number of load cases

(2) number of resolutions equal number of constraint operators

TABLE 1

- Constraints and "sensitivities"

Constraints inequations come from the different analysis branches of ELFINI, we can consider simultaneously :

. Various failure criteria (including composite materials), computed from static stresses for all the dimensioning cases of loads
. Local buckling criteria
. Limited displacements
. Aeroelastic variation of aerodynamic derivatives
. Dynamic natural frequencies
. Flutter speed and aeroelastic dynamic damping
. Various technological constraints (as minimum values of design variables, and limitations of the thickness variation between adjacent design variables).

The constraints considered during the same optimization can come from several analysis models (ex : symmetric and anti-symmetric F.E. aircraft model, local buckling analysis by Rayleigh-Ritz method, local refined F.E. analysis , different external store configurations for dynamic and flutter, variation of shape due to control surface deflections, etc.).

We call "sensitivities" the derivatives of constraints in function of design variables. The principle of ELFINI optimization is to compute these derivatives by a correct mathematical process. It can easily be demonstrated, (see table 1 and references 1 and 2) that the computation of derivatives of static stresses, displacements, and aeroelastic coefficients is equivalent to solutions with "dummy" case of loads.

The number of this dummy case of loads is :

- number of loading case x number of design variables if formula 1 of table 1 is used
- number of constraints if formula 2 is used.

For practical problems this number of dummy case of load reaches currently several thousands, and their resolution does the main part of computer cost of optimization.

When constraints are eigenvalue or are directly related to eigenvalue (e.g. eigen frequency, linear buckling load, divergence or flutter speed, aeroelasticity damping) the cost of their derivation is neglectible (see tables 2 and 3 and references 1 and 2). But we must underline that these derivations need a far more accurate calculation of eigenvectors than those needed for eigenvalue analysis only. Within the same range of ideas, we have noticed that it was very difficult to compute with proper accuracy derivations of solution of problems treated with the classical modal basis reduction (e.g. dynamic response, aeroelasticity), practically it would be necessary to compute the correct mathematical derivative of vectors. This is mainly why we have developed an approach of static aeroelasticity without basis troncature effect (see ref. 1), it leads to a mathematically exact and low cost calculation of derivatives.

DERIVATION OF EIGEN VALUES

ANALYSIS

- eigen modes : V_i
- eigen values : ω_i

$$[[K] - \omega_i^2 [M]] V_i = 0$$

SENSIVITY ANALYSIS OF EIGEN VALUES

$$\Delta [V_i^t [[K] - \omega_i^2 [M]] V_i] = 0$$

$$2 V_i^t [[K] - \omega_i^2 [M]] \Delta V_i +$$
$$V_i^t [[\Delta K] - \omega_i^2 [\Delta M]] +$$
$$\Delta\omega_i^2 V_i^t [M]] V_i = 0$$

$$\Delta\omega_i = \frac{V_i^t [[\Delta K] - \omega_i^2 [\Delta M]] V_i}{2 \omega_i V_i^t [M] V_i}$$

TABLE 2

- Mathematical optimization

Starting from the analysis and derivation of constraints, we use an explicit non linear approximation of the constraints in terms of the design variables, mainly the formulation in inverse variables. Taking as new variables inverses of design variables, it leads to minimize an homographic function (weight) subject to linear inequations. This problem is easily solved by projected conjugate gradient algorithm. The cost of the mathematical optimization step is low.

The mathematical optimization step gives a prediction of the optimum, from which we start new iterations.

The number of iterations, needed to get the global convergence, ranges from 3 to 5 (see plate 4).

The cost of all the iterations of optimization ranges about 8 to 15 times the cost of the analysis.

- Final touches

Generally the theoretical optimum obtained from the optimization algorithm needs some modifications, since it does not often represent a realistic design. Starting from the table of constraints derivatives, the final touches consist in examining interactively the effect of small modifications, directly given by the designer during the drawing. The program instantaneously shows the picture of new safety margin and violated constraints (see plate 6).

We can also interactively rerun the mathematical optimization step after changing assigned value of constraints.

3 - SPECIAL FEATURES OF OPTIMIZATION WITH COMPOSITE MATERIAL

The organization described above is well suited for a composite material with the addition of following specificities.

- Failure criteria analysis and derivation

Inside the optimization loop we use failure criteria of the "Tsaï-Hill" family as :

$$C = \sqrt{\left(\frac{\sigma_x^2}{\sigma_{xad}^2} + S_1 * \frac{\sigma_y^2}{\sigma_{yad}^2} + S_2 * \frac{\tau_{xy}^2}{\tau_{xyad}^2} - S_3 * \frac{\sigma_x \sigma_y}{\sigma_{xad}^2}\right)}$$

with

σ_x , σ_y and τ_{xy} : stress tensor components

σ_{xad} , σ_{yad} , τ_{xyad} and $S_i = 0$ or 1 : criteria parameters

Arguments of criteria are adapted to each situation (eg : tension, compression, bending, holed panel, etc...), by calibration on more sophisticated criteria and on test results.

Due to the fact that, at a given point, the final failure mode is not known beforehand, it is necessary to handle constraints on all potential failure modes simultaneously.

This is achieved at a relatively low cost if the derivation is performed in two steps :

- compute strain tensor and its derivative by formula 1 of table 1 (3 components common to all plies with membrane assumption),
- starting from strain tensor and material Hook law, calculate ply by ply failure criteria and their derivatives.

- Local buckling criteria

Even if optimization can handle directly global buckling, for management and cost effectiveness it is generally preferable to calculate and to derivate local buckling criteria with the following post-processing analysis :

- On the general finite element model, calculation and derivation of stress flows of structural meshes,
- Local buckling load factors and their derivatives calculation by a Rayleigh Ritz method (see table 3).

Sizes of meshes for local buckling analyses are independent from their representation in the global F.E. model, and they can be tuned to be suited to the actual stiffening.

LOCAL BUCKLING ANALYSIS

BY RAYLEIGH-RITZ METHOD

RAYLEIGH-RITZ MODEL

External load fluxes : $\Phi = \begin{vmatrix} \Phi_{x0} \\ \Phi_{y0} \\ \Phi_{xy0} \end{vmatrix} = \rho \Phi_0$

Normal deflection :

$w = \sum a_{mn} x^i . x^j . L(x,y) \qquad V = \begin{vmatrix} a_{11} \\ \cdots \\ a_{mn} \end{vmatrix}$

BUCKLING FACTORS

Buckling initiation : $W_1 = W_2$

W_1 = Bending elastic energy
W_2 = Membrane work of external loads ($W_2 = \rho U_2$)

$W_1 = \rho U_2$

$\min \rho = W_1 / U_2 \iff \partial W_1/\partial V - \rho \, \partial U_2/\partial V = 0$

$[K - \rho G] V = 0$

DERIVATION OF BUCKLING FACTORS

$$\rho = - \frac{V^t . K(\lambda) . V}{V^t . G(\Phi) . V}$$

$$\frac{\partial \rho}{\partial \lambda} = - \frac{V^t . \partial K/\partial \lambda . V}{V^t . G(\Phi) . V} + \rho \frac{V^t . \partial G/\partial \Phi . \partial \Phi/\partial \lambda . V}{V^t . G(\Phi) . V}$$

TABLE 3

In the optimization loop, stacking sequences are not taken into account (assumption of material homogeneity through panel thickness), this for the sake of algorithm simplicity, and due to difficulties to express lays covering and stacking constraints in drawing.

The order of buckling modes can change between iterations ; this can cause a non convergence of iterations if all potential buckling modes are not controled simultaneously (see reference 2).

Design constraints

These constraints express the fact that results of optimization must correspond to a real drawing of composite panel, which must be made of stacked layers with special rules for easy manufacturing.

Design constraints are handled at two levels :

- Inside the optimization loop, as by placing constraints checking a minimum number or a given minimum proportion of plies in each direction, or a maximum slope of thickness (constraints corresponding to linear inequalities on design variable),
- After mathematical convergence, by automatic thicknesses rounding off to get a whole number of plies, and by a special half interactive program which transforms the stacking of plies by area, which are the rough output of optimization, into a proper cut out of layers.

4 - EXAMPLE OF APPLICATION OF OPTIMIZATION OF CARBON EPOXY STRUCTURE

We present two significant examples of optimization calculation of carbon epoxy parts for a combat aircraft.

- Optimization of a combat aircraft wing

We resume here the configuration of the optimization of a carbon epoxy Delta Wing box, corresponding to the mesh presented on plate 2, with the design variable patch of plate 4.

We had used two analysis models for static and aeroelasticity with the survey of flutter on three external load configurations.

	MODEL 1	MODEL 2
F.E. models	wing model with a representation of other part of the aircraft by super element technique (3544 DOF) symmetric and antisymmetric analysis	complete plane 13003 DOF symmetric and antisymmetric analysis
Design Variable	476 Design Variable (Number of plies in 4 directions)	
Static cases of loads	24 cases of loads combined from symmetric and antisymmetric	0
Failure criteria	476 failure criteria equivalent "Tsaï-Hill criteria"	
Buckling criteria	144 critical buckling factor issued from 77 local buckling analyses of composite plates by Rayleigh Ritz method	0
Static aeroelastic constraint	0	7 control surface efficiencies and minimal roll speed
Flutter		5 flutter speeds and 60 aeroelastic dampings corresponding to 3 external load configuration
Technological constraint	374 constraints on composite lay-up (thickness shape, maximum and minimum ratio between each ply direction)	

On plate 5, we present the history of convergence in weight. Drawing constraints and flutter constraints have been successively introduced later in order to see their influence. The optimum values of design variables are presented plate 4.

We present on the table above weight sensitivities of wing panels to typical project hypothesis obtained by optimization.

OPTIMIZATION OF CARBON EPOXY WING
HISTORY OF CONVERGENCE

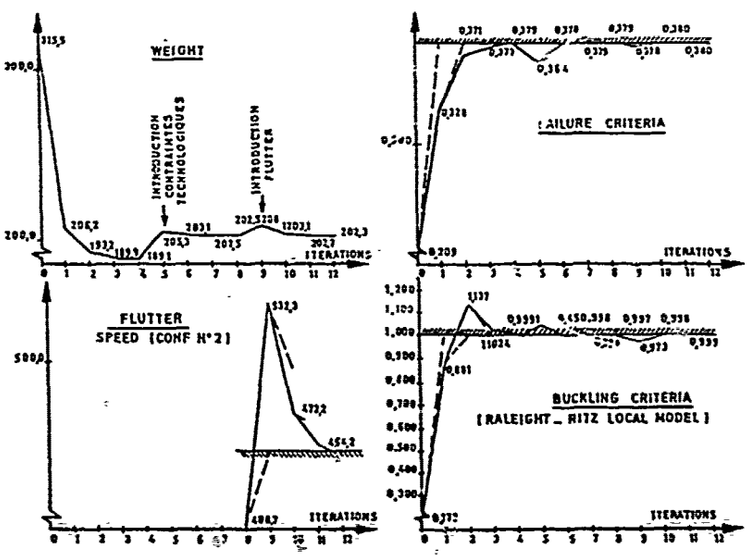

PLATE 5

	Design Hypothesis	weight (ratio)
1	Composite material Strength of material constraints only, rough from computer optimization	1.
2	+ Aeroelasticity constraint	1.19
3	+ Aeroelasticity + Technological constraints	1.25
4	Weight from final detailed drawing (review by checking analyses)	1.36
5	Aluminium alloys solution Strength of material + Aeroelasticity (comparable with 3)	2.10

HSB-fin preliminary design optimization

- Finite Element model (Plate 6)

A finite element model has been built with our ELFINI tool, from the Nastran data.

We got a slightly different model (more refined) and we had to make hypotheses for the attachments to the fuselage. Moreover it can be noticed that no definition of internal stiffeners exist.

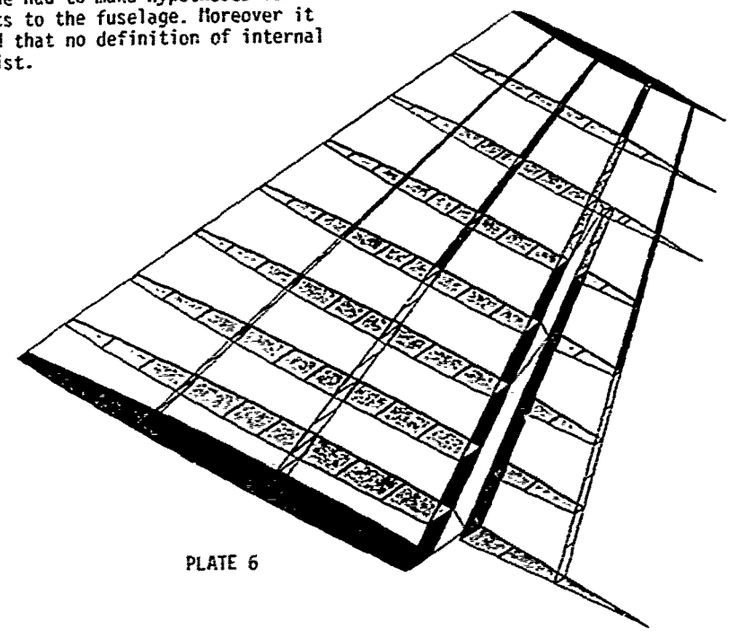

PLATE 6

- Loads

The data provided consist in a pressure case given by a torque and the center of pressure.

In order to have precise and realistic load cases, we have generated aerodynamic load cases at Mach 0.9 with slideslip effect ($\beta = 6.1^{\circ}$) and rudder deflection ($d = 8.5^{\circ}$).

- Design variables (Plate 7)

The design variables are the number of plies in each direction of the four classical direction, with the zero degree one parallel to a spar.

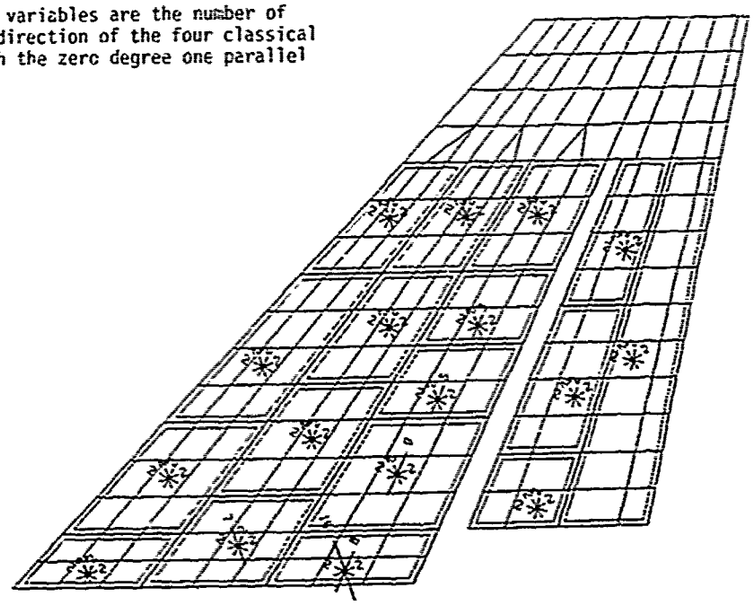

PLATE 7

Constraints

Strength constraints were introduced as strain failure criteria and buckling criteria, as well as static aeroelastic constraints and flutter constraints.

Running of the optimization

Starting from an arbitrary design (fixed values of the design variables), the optimization was run in several steps taking into account progressively failure criteria, buckling criteria, static aeroelasticity constraints and finally flutter speed constraints (Plate 8).

It must be noticed that, in the initial configuration of the fin, flutter was not a critical phenomenon. For the sake of demonstration, additional masses were put at the top of the fin to have significative flutter constraints.

These results can be considered as a preliminary design. Our optimization tool has shown the principal effects and sensivities of the various kinds of constraints. It is a starting point for further analyses with a more detailed definition (panels stiffening for example).

68 design variable	(number of plies in 4 direction)

3 static cases of load	• sideslipe beta=6.1 deg • rudder deflection d=8.5 deg • pressure 2 t/m2

Failure Criteria	23 strains (direction 0 deg) 123 quadratic criteria	< 0.003 < 1
Buckling Criteria	141 failure buckling factors issued from 71 local analysis	< 1
Static Aeroelastic Constraint	Fy efficiency for sideslipe Mz efficiency for rudder deflection	> 0.9 > 0.85
Flutter	3 flutter speeds 6 aeroelastic dampings	> 700 m/s

5 - CHECKING ANALYSIS

It must be understood that, if optimization tool is essential to reach rationally a good general drawing, the result must be justified in detail with more complex analyses than those which can be handled inside the optimization loop. The most typical of these checking analyses are the following :

- Effect of local loads (e.g. fuel tank pressures, vibration, thermal load, etc.)
- Local fatigue analysis
- Damage tolerance analysis
- Detailed local analysis of holed composite panel (e.g. point stress analysis)
- Post buckling analysis

Design constraints corresponding to these details checking analyses have been simplified to be handled by general optimization. These simplified assumptions must be validated by local checking analysis.

Effects of calibration of these constraints can be examined with Lagrange multiplier of active constraints (handled interactively by "Final Touches" modules) or by replay of Mathematical optimization step.

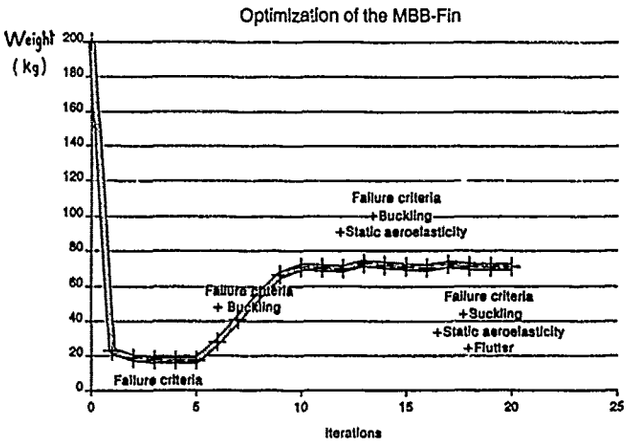

PLATE 8

6 - ORGANIZATION OF DESIGN PROCESS

Now we have the following organization for design of composite structures, from the preliminary project to the delivery of manufacturing drawings :

- . Start from a CATIA drawing of only external shape and a brief definition of internal architecture
- . Elaborate, by CATIA-MESH, a first simple general F.E. mesh of the whole aircraft (10-30000 D.O.F.) with approximate cross sections and thicknesses (see plate 2). The model is adjusted with simple cases of load
- . Static aeroelasticity and loads, which give the envelope cases of loads and show the latent problems of aeroelasticity
- . Examination of internal load fields and stresses for selection of "strength of material" constraints in optimization
- . Dynamic modes computation with the various external store configurations, flutter problem recognition
- . First run of optimization
- . Drawings of the structure supported by :
  - interactive test of authoritative modifications of results of optimization to make drawing easier, this with the final touches module,
  - changes and additions of constraints,
  - critical examination of "cost of requirements", directly obtained from "Lagrange multipliers" of optimization. It allows to appreciate the influence of safety margin on certain criteria (e.g. : composite materials),
  - detail checking analyses supported by methods described above in § 5. They are performed taking proper boundary conditions in the Finite Element model of the whole aircraft via a super Element technics. Detail checking analyses must validate the simplified criteria used for mathematical optimization ; otherwise optimization must be replayed with calibrated criteria.

Although a single run of optimization in production last no more than a few C.P.U. hours, for the Rafale design the optimization job have remained inside the computer more than six months, in order to examine detail analysis effects, the influence of the choice of constraints and alternative designs.

7 - NEIGHBOUR OF OPTIMIZATION : IDENTIFICATION AND COMPUTATION WITH UNCERTAIN DATA

The solution of these problems can be considered thanks to possibilities of elaboration of sensitivity table.

- Model adjustement

A typical example of these technics is the adjustement of F.E. dynamic model to measured natural modes ; the unknowns are design variables of local thickness and mass, modal deformation and frequencies ; the modal equation appears as an equality constraint, the objective is to minimize a "distance" from measured to computed mode ; the method don't need the knowledge of connection between computed and measured modes.

- Computation with uncertain data

Sometimes, at the start of any problems, we have an imprecise knowledge of data ; the idea of computation with uncertain data is to search the "worst" point in the uncertain design variable space.

The problem is solved by two approaches :

- . find the "worst" possible point by minimization of a safety margin function inside the authorized space of design variable variations,
- . if it exists a possibility of failure, compute the probability of failure, starting from probability density of design variables.

Now we have started to apply these ideas on flutter and vibro-acoustic analysis of preliminary projects.

8 - FURTHER LEVELS OF OPTIMIZATION

The general tendency is to introduce progressively all the "arguments" of structural design in the optimization loop.

The next steps of development follows :

- Optimization with "bending" design variables

It doesn't give rise to any theoretical difficulties ; the relative complication comes from the non linear dependance of stiffness, neutral surface and constraints on design variables, which complicates program writing.

- Optimization with post-buckling analysis

It is one of the most important lack of the present operational optimization. Now we get round the difficulty, by an empiric adjustment of the load level of linear buckling ; we only verify results of optimization by post-buckling analysis.

The correct solution is not a lot more intricate than that of bending case ; it can easily be demonstrated that the derivation cost is almost that of linear problem ("dummy" cases of load at the final equilibrium state).

- Shape optimization

It is needed by a lot of practical problems of varying difficulty (shape of stiffeners, pressurised vessels, fitting, etc.).

The main difficulty is to express design variables and "topological" constraints.

For the above problems, many authors and ourselves have elaborated specimen programs running on academic cases, but to have a really operational tool, it is necessary to introduce geometric design variables and the associated "topological" constraints at the level of CAD system, this need important investments.

- Optimization in heat transfer problems

One of the necessity of Hermes project has been to put thermal analysis at same level of sophistication as structural analysis ; immediately after we have met the need for a thermal optimization tool.

The general arrangement of thermal optimization is the same as in structural optimization, the complications are in the transient and highly non linear character of thermal problems.

Fortunately it can be demonstrated that temperature derivation needs the solution of the same differential linear equation system for all design variables and, integrated at the same time as the analysis, it doesn't need additional factorization. Therefore the cost of derivatives is relatively lower than that of static elasticity problem.

Jointly we develop heat transfer identification process and also computation with uncertain data, particularly needed by the random or badly known character of a lot of data.

- Multidisciplinary interactions

For a combat aircraft, the idea should be to optimize at the same time : structure, cut out of control surfaces, actuators and hydraulic power, parameters of electrical flight control system, and aerodynamic shape.

For the moment this state of grace is not yet reached, but tendency is to apply optimization to each discipline and to proceed in relation to the other matters by "fixed point method" or by simplification of interactions. So starting from Lagrange multipliers issued from the optimization of each discipline, it is possible to "condense" their interactions ; for instance, as far as structure is concerned, we can easily give the weight cost of requirements of other disciplines (exchange rate between structure weight and roll speed, profile relative thickness, etc.).

9 - CONCLUSION

The tendency would be to include more and more detailed analyses inside the mathematical optimization loop. This evolution is hindered by the difficulties of the task.

The tool described above represents the achievement of the first level of structural optimization, where geometry is given and mass and stiffness matrices are linear functions of design variables.

Significant progress is not easy. It corresponds to including inside optimization :
- "bending" design variables
- non linear and post-buckling analysis, rules of effective width
- stacking order of plies and constraints on layers cut out of composite material
- shape optimization, which is also implicitly necessary in the above functionalities.

Independently from their theoretical difficulty these developments need a higher level of integration of F.E. optimization with C.A.D. ; in particular the architecture of C.A.D. system must support the description of design variables and of drawing constraints.

Another promising field of research is to use technics of artificial intelligence to pilot the design, it seems to be one mean to manage optimization with discontinuous evolution of design variables. Presently we have started the development of this technics at the level of check sizing of carbon fiber panels. It rests on a knowledge basis composed of rules, referring technological constraints and methods of calculations.

REFERENCES

1 - C. PETIAU & G. LECINA
Elements finis et optimisation des structures aéronautiques
Agard conference proceeding N° 280
"the use of computer as a design tool" - Munich 1978.

2 - G. LECINA & C. PETIAU
Optimization of aircraft structure
Fundations of structure optimization approach
Edited by A.J. Morris - 1982 Hohn Waley & Sons Ltd

3 - C. PETIAU & C. CORNUAULT
Efficient algorithms for post-buckling computation
6th international symposium on computing methods in applied science and engineering - Versailles 1983.

4 - C. PETIAU & C. CORNUAULT
Algorithmes efficaces pour le calcul des équilibres en post-flambement
3ème colloque : tendances actuelles en calcul des structures
Edited by J.P. Grellier et J.M. Campel - Editions Pluralis Paris.

5 - C. PETIAU & M. DE LAVIGNE
Analyse aéroélastique et identification des charges en vol
Agard conferences proceeding N° 375
"operational loads data" - Sienne 1984.

REPORT DOCUMENTATION PAGE

1. Recipient's Reference	2. Originator's Reference	3. Further Reference	4. Security Classification of Document
	AGARD-R-784	ISBN 92-835-0653-7	UNCLASSIFIED

5. Originator Advisory Group for Aerospace Research and Development
North Atlantic Treaty Organization
7 rue Ancelle, 92200 Neuilly sur Seine, France

6. Title INTEGRATED DESIGN ANALYSIS AND OPTIMISATION OF AIRCRAFT STRUCTURES

7. Presented at the 72nd Meeting of the AGARD Structures and Materials Panel, held in Bath, United Kingdom 29th April—3rd May 1991.

8. Author(s)/Editor(s)	9. Date
Various	February 1992
10. Author's/Editor's Address	**11. Pages**
Various	212

12. Distribution Statement This document is distributed in accordance with AGARD policies and regulations, which are outlined on the back covers of all AGARD publications.

13. Keywords/Descriptors

Aircraft	Structural design
Design	Airframes
Aeroelasticity	Weight — mass
Computer programs	Active control
Optimization	Composite materials

14. Abstract

At its 72nd Meeting, the Structures and Materials Panel held a Workshop to address the role of integrated design analysis and optimisation of aircraft structures in order to review and evaluate modern computer codes, and the methodologies for their use.

The Workshop provided a very useful forum for the exchange of information which is reflected in the papers presented in this Report.

Papers presented at the 72nd Meeting of the Structures and Materials Panel held in Bath, United Kingdom, 29th April—3rd May 1991.

AGARD Report 784 Advisory Group for Aerospace Research and Development, NATO INTEGRATED DESIGN ANALYSIS AND OPTIMISATION OF AIRCRAFT STRUCTURES Published February 1992 212 pages At its 72nd Meeting, the Structures and Materials Panel held a Workshop to address the role of integrated design analysis and optimisation of aircraft structures in order to review and evaluate modern computer codes, and the methodologies for their use. The Workshop provided a very useful forum for the exchange of information which is reflected in the papers presented in this Report. P.T.O.	AGARD-R-784 Aircraft Design Aeroelasticity Computer programs Optimization Structural design Airframes Weight — mass Active control Composite materials	AGARD Report 784 Advisory Group for Aerospace Research and Development, NATO INTEGRATED DESIGN ANALYSIS AND OPTIMISATION OF AIRCRAFT STRUCTURES Published February 1992 212 pages At its 72nd Meeting, the Structures and Materials Panel held a Workshop to address the role of integrated design analysis and optimisation of aircraft structures in order to review and evaluate modern computer codes, and the methodologies for their use. The Workshop provided a very useful forum for the exchange of information which is reflected in the papers presented in this Report. P.T.O.	AGARD-R-784 Aircraft Design Aeroelasticity Computer programs Optimization Structural design Airframes Weight — mass Active control Composite materials
AGARD Report 784 Advisory Group for Aerospace Research and Development, NATO INTEGRATED DESIGN ANALYSIS AND OPTIMISATION OF AIRCRAFT STRUCTURES Published February 1992 212 pages At its 72nd Meeting, the Structures and Materials Panel held a Workshop to address the role of integrated design analysis and optimisation of aircraft structures in order to review and evaluate modern computer codes, and the methodologies for their use. The Workshop provided a very useful forum for the exchange of information which is reflected in the papers presented in this Report. P.T.O.	AGARD-R-784 Aircraft Design Aeroelasticity Computer programs Optimization Structural design Airframes Weight — mass Active control Composite materials	AGARD Report 784 Advisory Group for Aerospace Research and Development, NATO INTEGRATED DESIGN ANALYSIS AND OPTIMISATION OF AIRCRAFT STRUCTURES Published February 1992 212 pages At its 72nd Meeting, the Structures and Materials Panel held a Workshop to address the role of integrated design analysis and optimisation of aircraft structures in order to review and evaluate modern computer codes, and the methodologies for their use. The Workshop provided a very useful forum for the exchange of information which is reflected in the papers presented in this Report. P.T.O.	AGARD-R-784 Aircraft Design Aeroelasticity Computer programs Optimization Structural design Airframes Weight — mass Active control Composite materials

Papers presented at the 72nd Meeting of the Structures and Materials Panel held in Bath, United Kingdom, 29th April—3rd May 1991.

ISBN 92-835-0653-7

Papers presented at the 72nd Meeting of the Structures and Materials Panel held in Bath, United Kingdom, 29th April—3rd May 1991.

ISBN 92-835-0653-7

Papers presented at the 72nd Meeting of the Structures and Materials Panel held in Bath, United Kingdom, 29th April—3rd May 1991.

ISBN 92-835-0653-7

Papers presented at the 72nd Meeting of the Structures and Materials Panel held in Bath, United Kingdom, 29th April—3rd May 1991.

ISBN 92-835-0653-7

AGARD

NATO OTAN

7 RUE ANCELLE · 92200 NEUILLY-SUR-SEINE

FRANCE

Téléphone (1)47.38.57.00 · Télex 610 176
Télécopie (1)47.38.57.99

DIFFUSION DES PUBLICATIONS
AGARD NON CLASSIFIEES

L'AGARD ne détient pas de stocks de ses publications, dans un but de distribution générale à l'adresse ci-dessus. La diffusion initiale des publications de l'AGARD est effectuée auprès des pays membres de cette organisation par l'intermédiaire des Centres Nationaux de Distribution suivants. A l'exception des Etats-Unis, ces centres disposent parfois d'exemplaires additionnels, dans les cas contraire, on peut se procurer ces exemplaires sous forme de microfiches ou de microcopies auprès des Agences de Vente dont la liste suite.

CENTRES DE DIFFUSION NATIONAUX

ALLEMAGNE
Fachinformationszentrum,
Karlsruhe
D-7514 Eggenstein-Leopoldshafen 2

BELGIQUE
Coordonnateur AGARD-VSL
Etat-Major de la Force Aérienne
Quartier Reine Elisabeth
Rue d'Evere, 1140 Bruxelles

CANADA
Directeur du Service des Renseignements Scientifiques
Ministère de la Défense Nationale
Ottawa, Ontario K1A 0K2

DANEMARK
Danish Defence Research Board
Ved Idraetsparken 4
2100 Copenhagen Ø

ESPAGNE
INTA (AGARD Publications)
Pintor Rosales 34
28008 Madrid

ETATS-UNIS
National Aeronautics and Space Administration
Langley Research Center
M/S 180
Hampton, Virginia 23665

FRANCE
O.N.E.R.A. (Direction)
29, Avenue de la Division Leclerc
92320, Châtillon sous Bagneux

GRECE
Hellenic Air Force
Air War College
Scientific and Technical Library
Dekelia Air Force Base
Dekelia, Athens TGA 1010

ISLANDE
Director of Aviation
c/o Flugrad
Reykjavik

ITALIE
Aeronautica Militare
Ufficio del Delegato Nazionale all'AGARD
Aeroporto Pratica di Mare
00040 Pomezia (Roma)

LUXEMBOURG
Voir Belgique

NORVEGE
Norwegian Defence Research Establishment
Attn: Biblioteket
P.O. Box 25
N-2007 Kjeller

PAYS-BAS
Netherlands Delegation to AGARD
National Aerospace Laboratory NLR
Kluyverweg 1
2629 HS Delft

PORTUGAL
Portuguese National Coordinator to AGARD
Gabinete de Estudos e Programas
CLAFA
Base de Alfragide
Alfragide
2700 Amadora

ROYAUME UNI
Defence Research Information Centre
Kentigern House
65 Brown Street
Glasgow G2 8EX

TURQUIE
Millî Savunma Başkanlığı (MSB)
ARGE Daire Başkanlığı (ARGE)
Ankara

LE CENTRE NATIONAL DE DISTRIBUTION DES ETATS-UNIS (NASA) NE DETIENT PAS DE STOCKS DES PUBLICATIONS AGARD ET LES DEMANDES D'EXEMPLAIRES DOIVENT ETRE ADRESSEES DIRECTEMENT AU SERVICE NATIONAL TECHNIQUE DE L'INFORMATION (NTIS) DONT L'ADRESSE SUIT.

AGENCES DE VENTE

National Technical Information Service
(NTIS)
5285 Port Royal Road
Springfield, Virginia 22161
Etats-Unis

ESA/Information Retrieval Service
European Space Agency
10, rue Mario Nikis
75015 Paris
France

The British Library
Document Supply Division
Boston Spa, Wetherby
West Yorkshire LS23 7BQ
Royaume Uni

Les demandes de microfiches ou de photocopies de documents AGARD (y compris les demandes faites auprès du NTIS) doivent comporter la dénomination AGARD, ainsi que le numéro de série de l'AGARD (par exemple AGARD-AG-315). Des informations analogues, telles que le titre et la date de publication sont souhaitables. Veuiller noter qu'il y a lieu de spécifier AGARD-R-nnn et AGARD-AR-nnn lors de la commande de rapports AGARD et des rapports consultatifs AGARD respectivement. Des références bibliographiques complètes ainsi que des résumés des publications AGARD figurent dans les journaux suivants:

Scientifique and Technical Aerospace Reports (STAR)
publié par la NASA Scientific and Technical
Information Division
NASA Headquarters (NTT)
Washington D.C. 20546
Etats-Unis

Government Reports Announcements and Index (GRA&I)
publié par le National Technical Information Service
Springfield
Virginia 22161
Etats-Unis

(accessible également en mode interactif dans la base de données bibliographiques en ligne du NTIS, et sur CD-ROM)

Imprimé par Specialised Printing Services Limited
40 Chigwell Lane, Loughton, Essex IG10 3TZ